THE UNIVERSITY OF MICHIGAN RESEARCH INSTITUTE
ANN ARBOR, MICHIGAN

FINAL REPORT

FOR

THEORETICAL AND EXPERIMENTAL INVESTIGATION OF LARGE-SIGNAL TRAVELING-WAVE TUBES

Electron Physics Laboratory
Department of Electrical Engineering

By: G. T. Konrad
R. W. Larson
J. G. Meeker
J. E. Rowe
H. Sobol
J. W. Ward
C. P. Wen

Approved by: J. E. Rowe
J. E. Rowe, Director
Electron Physics Laboratory

Project 2750

CONTRACT NO. AF30(602)-1845
DEPARTMENT OF THE AIR FORCE
PROJECT NO. 5573, TASK NO. 55253
PLACED BY: THE ROME AIR DEVELOPMENT CENTER
GRIFFISS AIR FORCE BASE, NEW YORK

August, 1960

ABSTRACT

Analysis of Linear and Nonlinear O-Type Systems

The nonlinear O-type backward-wave oscillator is analyzed using the large-signal traveling-wave amplifier equations. These equations have been modified by simply introducing a change in the sign of the circuit impedance to account for backward energy flow on the circuit. Starting conditions are calculated as a function of the r-f level at the output of the device for a range of operating parameters. Efficiency is calculated as a function of the ratio of stream current to minimum starting current.

An analysis of the Crestatron beating-wave amplifier is presented and the small-signal gain is calculated as a function of the various circuit and stream parameters.

The integral equation and differential equation methods of analysis of the large-signal traveling-wave amplifier are compared and the equivalence is rigorously proven. Also the equivalence of the space-charge models of Tien and Rowe is shown. Radial variations of the circuit field in a traveling-wave tube with a large-diameter beam are accounted for in a simple manner and the effect on efficiency is calculated.

A small-signal analysis of the interaction between a premodulated electron stream and a propagating structure is developed and various calculations are made to show the effect on interaction length and gain. Equations are developed to calculate the optimum predrift length for a premodulated beam in either the growing-wave tube or the beating-wave tube.

Phase Focusing in Traveling-Wave Tubes

The basic limitation on the efficiency of O-type devices is that the beam slows down as it gives up energy to the r-f wave and finally falls out of synchronism with the traveling r-f wave on the circuit. A general analysis (nonlinear) of the phase focusing of electron bunches in growing-wave devices and beating-wave devices is presented and several possibilities are considered. These are (1) prebunching of the electron stream, (2) tapering of the circuit phase velocity, and (3) variation of the d-c voltage gradient along the electron stream. Calculations are presented for all of these methods and a discussion of important physical points pertaining to each is given.

X-Band Traveling-Wave Amplifiers

Design and experimental information on several models of an X-band traveling-wave amplifier is presented and discussed. The tube employs coaxial-cavity matches and coupled-helix attenuators. Detailed gain, VSWR and power output data are given.

Experimental Study of Crestatrons

A detailed experimental investigation has been carried out on a series of S-band Crestatron amplifiers of both the cw and pulsed type. These tubes utilize coupled-helix couplers and do not require attenuators. Small-signal gain, large-signal gain, power output and efficiency curves are presented for both these types of tubes as a function of various operating parameters. Some correlation with theory is presented.

Analysis of Modulated O-Type Devices

A general analysis of the beam-modulated traveling-wave tube is given. The modulations are signals applied to the beam in addition to the carrier signal. Modulations are considered both at frequencies very much lower and also at those comparable to the carrier frequency. Large- and small-signal carrier levels are studied. The analysis includes effects on C, QC, b, d and the initial wave amplitudes. Recommendations for the design of traveling-wave tubes for low modulation frequency applications are given. The high-frequency analysis is used to analyze the longitudinal-beam parametric amplifier. The upper and lower sidebands around the pump fundamental are considered. Lower gain and more noise than found by previous theories is predicted.

Disk and Helically Loaded Coaxial and Waveguide TWA Structures

The various field analyses that have been made on disk and helically loaded waveguide structures for high-power traveling-wave amplifiers are reviewed and various comparisions are made. In particular the various analyses are applied to gain an understanding of the operation of the helically loaded coaxial line structure.

UHF Crestatron

The design of a high-pulsed-power Crestatron to operate in the uhf frequency range is presented. This tube utilizes a single-filar helical line r-f structure and coupled-helix couplers designed to cover the 300-900-mc frequency range. The electron gun employs a hollow beam and is magnetically focused. Design considerations are discussed as well as small-signal gain measurements for three tubes.

TABLE OF CONTENTS

Title	Page
ABSTRACT	iii
LIST OF TABLES	ix
LIST OF ILLUSTRATIONS	x
PERSONNEL	xvii
LIST OF PUBLICATIONS	xix
I. GENERAL INTRODUCTION	1
II. ANALYSIS OF LINEAR AND NONLINEAR O-TYPE SYSTEMS	2
A. Nonlinear O-Type Backward-Wave Oscillators	2
1. Backward-Wave Circuits	2
2. Nonlinear Backward-Wave Equations	6
3. Efficiency Calculations	13
4. Conclusions	18
B. Beating-Wave Amplifier (Crestatron)	18
1. Introduction	18
2. Gain Equation	20
3. Small-Signal Gain	24
4. Maximum Gain vs. C and QC	27
5. Large-Signal Results	28
6. Conclusions	30
C. Comparison of Integral and Differential Equation Analyses of the Traveling-Wave Tube	30
1. Introduction	30
2. Equivalence of Integral and Differential Equation Approaches	31
3. Space-Charge Expressions	37
4. Efficiency Calculations	38
5. Radial Electric Field Variations	40
6. Conclusions	47
D. Effect of a Beam Premodulation	48
1. Velocity Modulation	48
2. Determination of Optimum Drift Length	49
3. Discussion of Linear Analysis Results	53
E. General Large-Signal Traveling-Wave Amplifier Calculations	54
1. Introduction	54
2. General Design Procedure	54
3. Power Output and Bandwidth	55
4. Effect of Circuit Loss	56
5. N-Beam Analysis	56

TABLE OF CONTENTS (cont.)

Title	Page
III. PHASE FOCUSING IN TRAVELING-WAVE TUBES	57
A. Limitation on Conversion Efficiency in O-Type Devices	57
B. Methods of Phase Focusing	58
C. The Basic Large-Signal Traveling-Wave Amplifier Equations	59
D. Prebunched Beam Studies	61
E. The Variable-Pitch Helix Program	68
1. Digital Computer Solutions	71
2. Analog Computer Analysis	73
3. Pitch Optimization by Computer	75
F. D-C Gradient Program	75
IV. X-BAND TRAVELING-WAVE AMPLIFIERS	77
A. Introduction	77
B. Experimental Investigation of the X-Band Amplifier	78
C. Electron Gun Performance	79
D. R-F Matching and Attenuation	80
E. Small-Signal and Saturation Gain	80
F. Saturation Power	85
G. Oscillation	85
H. Conclusion	85
V . EXPERIMENTAL STUDY OF CRESTATRONS	89
A. Objectives of the Program	89
B. Electron Guns	90
C. Slow-Wave Structure	91
D. Couplers and Attenuators	98
E. Collector Designs	98

TABLE OF CONTENTS (cont.)

Title	Page
F. CW Operation of the Crestatron	102
G. Pulsed Operation of the Crestatron	109
H. Conclusions	112
VI. ANALYSIS OF MODULATED O-TYPE DEVICES	120
A. Introduction	120
B. Low Modulation Frequencies - Calculations of the Modulation Device Functions	121
C. Low Modulation Frequencies - Using the Modulation Device Functions	143
D. High Modulation Frequencies - General Analysis	148
E. High Modulation Frequencies, Longitudinal-Beam Parametric Amplifier	153
F. Conclusion	160
VII. DISK AND HELICALLY LOADED COAXIAL AND WAVEGUIDE TWA STRUCTURES	161
A. Introduction	161
B. Filter Theory Approach	165
C. Perturbation Technique	167
D. Developed Structures, Altered Geometry	168
E. First Limiting Case - Enclosed Helicoid	168
1. "Wrapped" Rectangular Guide	168
2. Exact Helicoid Solutions	170
F. Second Limiting Case - Disk Structure	174
G. "Exact" Helicoid	187
H. Modifications, Conclusions	190
VIII. UHF CRESTATRON	192
A. Introduction	192
B. Principles of Crestatron Operation	192

TABLE OF CONTENTS (concl.)

Title	Page
C. General Design Considerations	194
D. Helix Design and Cold Test Measurements	197
E. Helix-Impedance Measurement	202
F. Hollow-Beam Gun	203
G. Tube Design	208
H. R-F Transitions	209
I. Experimental Results	211
IX. GENERAL CONCLUSIONS	220

LIST OF TABLES

Table		Page
IV.1	X-Band Amplifier Parameters	78
V.1	Design Objectives	89
V.2	Crestatron Dimensions	91
VIII.1	Uhf Helix Parameters	198
VIII.2	Summary of Electrical Design Parameters	208
VIII.3	Uhf Coupler Dimensions	211

LIST OF ILLUSTRATIONS

Figure		Page
II.1	Equivalent Circuits for Forward-Wave and Backward-Wave Devices.	5
II.2	R-F Voltage Amplitude vs. Distance. ($C = 0.1$, $QC = 0$, $d = 0$, $b = 1.9$)	11
II.3	Indication of Proximity to an Oscillation Condition.	12
II.4	Efficiency vs. I_o/I_s with b Adjusted for Oscillation. ($B = 1.0$, $d = 0$)	15
II.5	CN_s and b vs. I_o/I_s with b Adjusted for Oscillation. ($B = 1.0$, $d = 0$)	16
II.6	Gain vs. Length. ($C = 0.1$, $QC = 0.25$, $d = 0$, $b_{x_1=o} = 2.57$)	25
II.7	Maximum Gain vs. $b-b_{x_1=o}$ with Space Charge as the Parameter. ($C = 0.2$, $d = 0$)	29
II.8	Space-Charge-Field Weighting Function.	39
II.9	Saturation Efficiency vs. Injection Velocity Parameter. ($QC = 0.25$, $d = 0$)	41
II.10	Device Length at Saturation vs. Stream Diameter. ($\psi = -30$ db, $d = 0$)	42
II.11	Field Reduction Factor and Efficiency Reduction vs. Stream Diameter. ($C = 0.1$, $QC = 0.125$, $d = 0$, $a'/b' = 2$)	46
III.1	Saturation Tube Length. ($C = 0.1$, $B = 1.0$, $b = 2.0$)	63
III.2	Efficiency and Gain vs. Drive Level. ($C = 0.1$, $B = 1.0$, $QC = 0$)	65
III.3	Velocity vs. Phase.	66
III.4	Velocity vs. Phase.	67
III.5	Velocity vs. Phase.	69
III.6	Efficiency and Gain vs. Drive Level. ($C = 0.1$, $B = 1.0$, $QC = 0.25$)	70

LIST OF ILLUSTRATIONS (cont.)

Figure		Page
III.7	Effect of One Shift of Pitch on Saturation Amplitude. (C = 0.1, QC = 0, d = 0, A_o = 0.0225)	72
III.8	Phase Velocity vs. Helix Length. (C = 0.1, Assumed Constant Throughout; QC = 0; b = 0 at Input; A_o = Normalized Input)	74
III.9	Effect of d-c Gradient on Saturation Amplitude. (C = 0.1, QC = 0, d = 0, A_o = 0.0225)	76
IV.1	VSWR of Input and Output Couplers vs. Frequency for TWA-X-3-1.	81
IV.2	Cold Insertion Loss (db) vs. Frequency Including Attenuators and Couplers.	82
IV.3	Small-Signal Gain (db) vs. Frequency for TWA-X-3-1.	83
IV.4	TWA X-4-5 Gain vs. Frequency.	84
IV.5	Power Output vs. Power Input. (Helix Voltage Adjusted for Maximum Power Output at Each Frequency) TWA X-3-1.	86
IV.6	TWA X-4-5 Power Output vs. Power Input. (Two Attenuators and I_c = 3.8 ma).	87
IV.7	TWA X-4-5 Power Output vs. Power Input. (Three Attenuators I_c = 5.0 ma)	88
V.1	Cross Section of Crestatron R-F Structure and Vacuum Envelope.	92
V.2	Phase Velocity as a Function of Frequency for Shielded (b/a' = 1.6) and Unshielded (b/a' = ∞) S-Band Crestatron Helices.	94
V.3	Helix Impedance vs. Frequency for S-Band Crestatron Helices. Shielded and Unshielded Cases. (a'/b' = 1.4)	95
V.4	Dielectric Loading Factor as a Function of Frequency for the Unshielded S-Band Crestatron.	96

LIST OF ILLUSTRATIONS (cont.)

Figure		Page
V.5	Helix Loss in db Per Inch as a Function of Frequency for the S-Band Crestatron.	97
V.6	VSWR for Two Types of Couplers Used with the S-Band Crestatrons.	99
V.7	Typical Coupler Loss and Directivity of S-Band Crestatron Coupled-Helix Couplers.	100
V.8	Early Models of the cw S-Band Crestatron.	101
V.9	Small-Signal Gain vs. Frequency for S-8-3 Crestatron. Drive Level $\cong$ 100 mw; 3.0 kmc, C = 0.095, QC = 0.185, P $\cong$ 0.60.	103
V.10	Power Output vs. Power Input for the S-8-3 Crestatron at 3.0 kmc.	104
V.11	Saturation Efficiency vs. ψ(Input Signal Level in db Relative to CI_oV_o) with b as the Parameter for the S-8-3 Crestatron at 3.0 kmc.	106
V.12	Variable Length S-Band Crestatron and Coupled Carriage.	107
V.13	Small-Signal Gain vs. R-F Interaction Length for S-10-4 Crestatron. ($b/a' = \infty$, Freq. = 3.0 kmc)	108
V.14	Small-Signal Gain vs. Frequency for the S-10-4 Crestatron with Voltage as a Parameter for Shielded and Unshielded Helices. (Length = 3.0 inches, Drive Level $\cong$ 10 mw)	110
V.15	Maximum Saturation Efficiency vs. Operating Voltage for the S-10-4 Crestatron. Interaction Length = 3.25 inches.	111
V.16	Small-Signal Gain as a Function of b for the S-12-1 Pulsed Crestatron. Interaction Length = 2.42 inches, R-F Duty Cycle = 0.001.	113
V.17	Saturation Gain for the S-12-1 Pulsed Crestatron at 2.4 kmc. Interaction Length = 2.42 inches, R-F Duty Cycle = 0.001.	114
V.18	Saturation Gain for the S-12-1 Pulsed Crestatron at 3.3 kmc. Interaction Length = 2.42 inches, R-F Duty Cycle = 0.001.	115

LIST OF ILLUSTRATIONS (cont.)

Figure		Page
V.19	Saturation Gain as a Function of ψ(Input Signal Level in db Relative to CI_oV_o) with b as the Parameter for the S-12-1 Pulsed Crestatron. Interaction Length = 2.42 inches. (C = 0.11, QC = 0.25, $b_{x_1=o}$ = 2.57, B = 1.1, d = 0.02)	116
V.20	Saturation Efficiency vs. Input Signal Level Relative to CI_oV_o for the S-12-1 Pulsed Crestatron. Injection Velocity is the Parameter Length = 2.42 inches. (C = 0.12, QC = 0.20, $b_{x_1=o}$, B = 0.88, d = 0.02)	117
V.21	Saturation Gain for the S-12-1 Pulsed Crestatron at 2.7 kmc. Interaction Length = 2.42 inches, R-F Duty Cycle = 0.001.	118
VI.1	Small-Signal Propagation Constants for TWA with Modulated Beam Potential. (C_o = 0.10, QC_o = 0.250, b_o = 1.0, d_o = 0, ΔI = 0)	125
VI.2	Small-Signal Propagation Constants for TWA with Modulated Beam Current. (C_o = 0.10, QC_o = 0.250, b_o = 1.0, ΔV = 0)	126
VI.3	Variation of the Phase and Magnitude of "A" During Beam-Potential Modulation. (C_o = 0.10, ΔI = 0, b_o Adjusted for Maximum Gain)	128
VI.4	Variation of the Phase and Magnitude of "A" During Beam-Current Modulation. (C_o = 0.10, ΔV = 0, b_o Adjusted for Maximum Gain)	129
VI.5	Phase Modulation Device Function for Beam-Potential Modulation. (C_o = 0.10, ΔI = 0, b_o Adjusted for Maximum Gain)	131
VI.6	Amplitude-Modulation Device Functions for Beam-Potential Modulation. (C_o = 0.10, ΔI = 0, b_o Adjusted for Maximum Gain)	132
VI.7	Phase-Modulation Device Functions for Beam-Current Modulation. (C_o = 0.10, ΔV = 0, b_o Adjusted for Maximum Gain)	133
VI.8	Amplitude-Modulation Device Functions for Beam-Current Modulation. (C_o = 0.10, ΔV = 0, b_o Adjusted for Maximum Gain)	134

LIST OF ILLUSTRATIONS (cont.)

Figure		Page
VI.9	Modulation Device Functions for Crestatron with Beam-Potential Modulation. (C_o = 0.10. d_o = 0, QC_o = 0, b_o = 2.4, $b_{o,x_1=o}$ = 2.1)	135
VI.10	Modulation Device Functions for Crestatron with Beam-Current Modulation. (C_o = 0.10, d_o = 0, QC_o = 0, b_o = 2.4, $b_{o,x_1=o}$ = 2.1)	136
VI.11	Variation of Phase and Amplitude During Beam-Potential Modulation. (C_o = 0.10, QC_o = 0, d_o = 0, b_o = 0.1525, ΔI = 0, y = 3.4)	138
VI.12	Phase-Modulation Device Function During Beam-Potential Modulation, Large-Signal Calculation. (C_o = 0.10, QC_o = 0.250, d_o = 0, b_o = 1.0, B = 1.0, a'/b' = 2.0)	143
VI.13	Amplitude-Modulation Device Function During Beam-Potential Modulation, Large-Signal Calculation. (C_o = 0.10, QC_o = 0.250, d_o = 0, b_o = 1.0, B = 1.0 a'/b' = 2.0)	144
VI.14	Modulation Device Functions During Beam-Current Modulation, Large-Signal Calcuation. (C_o = 0.10, QC_o = 0, d_o = 0, b_o = 0.1525, ΔV = 0)	145
VI.15	Longitudinal-Beam Parametric-Amplifier Propagation Constants as Functions of the Pump Amplitude (a' = b' = 1.0)	157
VI.16	Longitudinal-Beam Parametric-Amplifier Propagation Constants as Functions of the Pump Amplitude. (a' = 0.697, b' = 0.513)	158
VII.1	Some Possible Slow-Wave Structures with Helical or Cylindrical Geometry.	162
VII.2	Equivalent Filters for Disk-Loaded Waveguide with Angularly Symmetric Field.	166
VII.3	Phase Velocity vs. ka for Various R-F Structures.	175
VII.4	Normalized Slot Area Admittance Parameter, a, vs. $\beta_o a$ with Ratio of Disk Hole Radius to Shield Radius as Parameter.	180

LIST OF ILLUSTRATIONS (cont.)

Figure		Page
VII.5	Beam Area Admittance vs. γa with Ratio of Rod Radius to Disk Hole Radius as Parameter.	181
VII.6	$\frac{\text{Rod Radius}}{\text{Disk Hole Radius}}$ vs. $\frac{\text{Shield Radius}}{\text{Disk Hole Radius}}$ with $\frac{v}{c}$ and $\frac{\text{Shield Radius}}{\text{Beam Area Gap}}$ as Parameters.	184
VII.7	Impedance Function, F, vs. γa with Rod Radius/Disk Hole Radius as the Parameter.	186
VIII.1	$b_{x_1=0}$ vs. C with QC as a Parameter and b vs. C with 1+Cb as a Parameter.	196
VIII.2	Measured Phase Velocity vs. Frequency.	199
VIII.3	Calculated Ratio of Phase to Group Velocity for Sheath Helix with External Shield.	200
VIII.4	Measured and Calculated Impedance, $E_z^2/2\beta^2 P$, for Unshielded Helix.	204
VIII.5	Schematic Drawing of a Hollow-Beam Electron Gun.	205
VIII.6	Uhf Hollow-Beam Gun.	206
VIII.7	Perveance and Beam Current vs. Beam Voltage for uhf Crestatron Hollow-Beam Gun.	207
VIII.8	Uhf Coupler.	210
VIII.9	Measured VSWR with Helix Terminated in Matched Load.	212
VIII.10	Experimental Test Setup.	213
VIII.11	5-10 kw uhf Crestatron.	215
VIII.12	Uhf Crestatron and Coupled-Helix Couplers.	216
VIII.13	Small-Signal Gain vs. Frequency for uhf Crestatron with Voltage as Parameter. Length = 7.5 inches. (Drive Level $\cong$ 60 Watts, 4μ sec. Pulse at 250 pps.)	217

LIST OF ILLUSTRATIONS (concl.)

Figure		Page
VIII.14	Small-Signal Gain vs. Beam Voltage for uhf Crestatron for Shielded and Unshielded Helices. (Frequency = 650 mc, Pulse Length = 4μ sec., pps. 250)	218
VIII.15	Power Output vs. Drive Level for uhf Crestatron. (Frequency = 650 mc, V_o = 8.5 kv, I_o = 3.5 amps., 4μ sec. Pulses, 250 pps.)	219

PERSONNEL

Scientific and Engineering Personnel		Time Worked in Man Months*
J. Black	Professors of Electrical Engineering	1.45
W. Dow		1.33
G. Hok		.23
J. Rowe		5.22
L. Flanigan	Assistant Research Engineer	12.24
J. Fox		8.72
G. Konrad		6.06
H. Krage		16.67
R. Larson		8.55
R. Martin		.42
N. Masnari		.56
J. Meeker		25.24
L. Paul		13.02
J. Pua		21.24
H. Sobol		16.06
J. Ward		12.71
C. Wen		8.30
Y. Lim	Assistant Research Mathematician	4.45
H. Detweiler	Research Assistants	1.85
R. Ohtomo		10.64
L. Stafford		4.12
R. Lee	Assistants in Research D	9.84
J. Loh		.89
J. Mason		.34
A. Pajas		.33
C. Rhee		.23
J. Spratt		1.52
D. Terry		.37
T. Tseng		1.40
C. Watkins		2.17
W. Bowen	Technicians	20.49
K. Knopf		1.30
K. McCrath		3.23
J. Murphy		19.89
J. Van Natter		4.55
D. Williams		6.84

Service Personnel		
V. Burris	Administrative Assistant	6.51
T. Knopf	Shop Foreman	4.26

PERSONNEL (concl.)

		Time Worked in Man Months*
M. Ellicott	Instrument Makers	.37
E. Kayser		7.27
G. Post		2.91
M. Prince		22.70
H. Sanford		2.56
M. Tobias		4.73
R. Casterline	Group Leader	7.15
R. Kepler	Machinist	4.40
P. Woodhead	Technical Illustrator	4.82
G. Beauchamp	Draftsman	5.36
K. Bilotta	Secretaries	.12
J. Corkin		.91
M. Collins		2.63
R. Demsetz		2.07
B. Fleming		.10
P. Foerster		3.79
Y. Igl		.22
J. Johnston		6.30
J. Marsh		2.10
A. Rowe		.09

* Time Worked is based on 172 hours per month.

LIST OF PUBLICATIONS

Journal Articles

1. J. E. Rowe, "Analysis of Nonlinear O-Type Backward-Wave Oscillators", Proceedings of the Symposium on Electronic Waveguides, Microwave Research Inst. Symposia Series, vol. VIII, Polytechnic Press; 1958.

2. J. E. Rowe, H. Sobol, "General Design Procedure for High-Efficiency Traveling-Wave Amplifiers", Trans. PGED-IRE, vol. ED-5, No. 4, pp. 288-301; October, 1958.

3. J. E. Rowe, "Theory of the Crestatron: A Forward-Wave Amplifier", Proc. IRE, vol. 47, No. 4, pp. 536-545; April, 1959.

4. W. G. Dow, J. E. Rowe, "General Aspects of Beating-Wave Amplification", Proc. IRE, vol. 48, No. 1, p. 115; January, 1960.

5. J. E. Rowe, "One-Dimensional Traveling-Wave Tube Analyses and the Effect of Radial Electric Field Variations", Trans. PGED-IRE, vol. ED-7, No. 1, pp. 16-22; January, 1960.

6. H. Sobol, "Extension of Longitudinal-Beam Parametric-Amplifier Theory", Proc. IRE, vol. 48, No. 4, p. 792; April, 1960.

7. H. Sobol, J. E. Rowe, "Theoretical Power Output and Bandwidth of Traveling-Wave Amplifiers", Trans. PGED-IRE, vol. ED-7, No. 2, pp. 84-94; April, 1960.

8. H. Sobol, J. E. Rowe, "Analysis of Modulated Traveling-Wave Devices and Beam-Type Parametric Amplifiers", (To be published in the British Journal of Electronics and Control).

9. J. E. Rowe, H. Sobol, "Start-Oscillation Conditions in Modulated and Unmodulated O-Type Oscillators", (To be published in the Trans. PGED-IRE).

10. J. E. Rowe, G. T. Konrad, H. W. Krage, "Experiments on a Series of S-Band Crestatrons, (To be published in the Trans. of the A.I.E.E.).

Technical Reports

1. J. E. Rowe, H. Sobol, "General Design Procedure for High-Efficiency Traveling-Wave Amplifiers", Tech. Rpt. No. 24 Parts I and II; February, 1958.

2. J. E. Rowe, "Analysis of Nonlinear O-Type Backward-Wave Oscillators", Tech. Rpt. No. 25; June, 1958.

3. J. E. Rowe, "Theory of the Crestatron: A Forward-Wave Amplifier", Tech. Rpt. No. 27; September, 1958.

4. J. E. Rowe, "One-Dimensional Traveling-Wave Tube Analyses and the Effect of Radial Electric Field Variations", Tech. Rpt. No. 30; July, 1959.

5. H. Sobol, "Extension of Longitudinal-Beam Parametric-Amplifier Theory", Tech. Rpt. No. 31; September, 1959.

6. H. Sobol, J. E. Rowe, "Theoretical Power Output and Bandwidth of Traveling-Wave Amplifiers", Tech. Rpt. No. 32; August, 1959.

7. H. Sobol, "Modulation Characteristics of O-Type Electron-Stream Devices", Tech. Rpt. No. 33; October, 1959.

8. J. E. Rowe, H. Sobol, "Start-Oscillation Conditions in Modulated and Unmodulated O-Type Oscillators", Tech. Rpt. No. 35; February, 1960.

9. H. Krage, "High-Power Coupled-Helix Attenuators", Tech. Rpt. No. 36, March, 1960.

THEORETICAL AND EXPERIMENTAL INVESTIGATION OF LARGE-SIGNAL TRAVELING-WAVE TUBES

I. GENERAL INTRODUCTION

The purpose of this study was to investigate both theoretically and experimentally the detail operation of large-signal traveling-wave amplifiers. In particular such topics as efficiency improvement by phase focusing, modulation characteristics, high-power r-f structures and backward-wave oscillator efficiency were to be investigated. All of these studies plus many others were to be directed towards determining methods for predicting and improving the operating characteristics of high-power (peak and average) traveling-wave tubes.

A number of the studies initiated during the contract period were completed and technical reports have been issued and numerous journal articles were published. A complete listing of the technical reports prepared and the journal articles published is given in the front of this report.

The following sections of this final report contain a summary of some of the most interesting and significant problems studied. Many of the items have already been reported in journal articles or will soon be published; hence only a summary of the important aspects and conclusions

II. ANALYSIS OF LINEAR AND NONLINEAR O-TYPE SYSTEMS (J. E. Rowe)

A. Nonlinear O-Type Backward-Wave Oscillators

1. Backward-Wave Circuits. A nonlinear analysis of the O-type backward-wave oscillator has been made using the modified large-signal traveling-wave amplifier equations, which account for finite values of C, QC and d. The derived equations apply equally well to both the backward-wave amplifier and oscillator. The purpose of this investigation is to determine the theoretical limitations on efficiency as a function of the operating parameters.

In backward-wave interaction as well as in forward-wave interaction it is required that the circuit wave and the electron stream be in approximate synchronism. This requirement results in a voltage-tunable device in the case of backward-wave interaction, since the r-f circuit must be dispersive in order to obtain oppositely directed phase and group velocities. The phase and group velocities of periodic structures are written as

$$v_p = \frac{\omega}{\beta} \tag{II.1}$$

and

$$v_g = \frac{v_p}{1 - \frac{\omega}{v_p}\frac{dv_p}{d\omega}} \quad . \tag{II.2}$$

A negative group velocity requires that the circuit exhibit negative dispersion; i.e., the denominator must remain negative.

Any r-f propagating circuit that satisfies the requirement of oppositely directed phase and group velocities for at least one space

harmonic component of the total field can be used as a backward-wave device circuit. These space harmonics exist in all periodic structures, as indicated by the periodic nature of the boundary conditions. The fields can be expressed over all periods of the r-f structure in terms of their values over one period through the use of Floquet's theorem. Helical waveguides and interdigital lines have found widest application in oscillators of the O-type. Interdigital lines and vane-type structures are frequently used in M-type backward-wave oscillators.

It is well known that these circuits can be represented by an equivalent circuit in the form of an L-C transmission line (low-pass filter) when operating in the fundamental forward-wave mode. In this embodiment of the equivalent circuit the inductance and any series circuit loss are represented by the series elements and the capacitance by a shunt element. The equation for the voltage along the line as a function of distance and time is a linear second-order partial differential equation containing driving terms when an electron stream is present. It is known that this type of circuit has a phase shift per section which increases with frequency due to the series inductance. In the nondispersive region where it is usually operated the phase velocity is independent of frequency and is given by $v_o = 1/\sqrt{LC}$.

Usually the differential equation for the circuit voltage in a backward-wave device is found by simply changing the sign of the circuit impedance to account for backward energy flow. The equivalent circuit may be drawn by interchanging the positions of the series inductance and the shunt capacitance to give a high-pass type of circuit with a phase shift per section characteristic which decreases with frequency. The phase velocity for this circuit is an increasing function of frequency and is given by $v_o = -\omega^2 \sqrt{LC}$. A differential equation

of fourth order in time and second order in the distance for the voltage along the line can be derived for this circuit. This equation can be reduced to a second-order equation if a time variation of exp $j\omega t$ is introduced. The presence of an electron stream also adds driving terms to the circuit equation.

The forms of the two equivalent circuits are shown in Fig. II.1 and the differential equation used both for the nonlinear forward-wave amplifier and for the backward-wave device is given below. In those terms preceded by a double sign the upper sign refers to the forward-wave device and the lower sign to the backward-wave device. The backward-wave device equations apply equally well to the oscillator and the amplifier.

$$\frac{\partial^2 V(z,t)}{\partial t^2} - v_o^2 \frac{\partial^2 V(z,t)}{\partial z^2} + 2\omega C d \frac{\partial V(z,t)}{\partial t} = \pm v_o Z_o \frac{\partial^2 \rho(z,t)}{\partial t^2}$$

$$\pm 2\omega C d Z_o v_o \frac{\partial \rho(z,t)}{\partial t} . \qquad \text{(II.3)}$$

The symbols used in the above and subsequent equations are defined in a list of symbols at the end of the report.

While it is intuitively satisfying the backward-wave equivalent circuit cannot be realized in terms of a smooth circuit but only in terms of lumped parameters to give the desired, oppositely directed phase and group velocities. This form of the circuit also leads to difficulties in attaching physical significance to the circuit elements. It is generally most satisfying simply to change the sign of the circuit impedance.

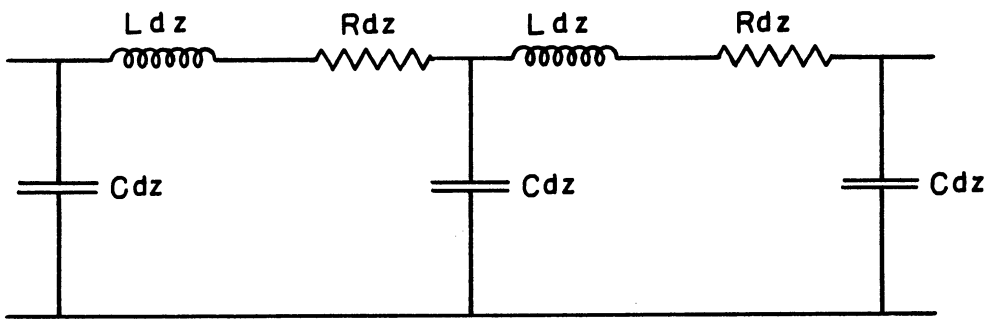

L = HENRYS / METER

R = OHMS / METER

C = FARADS / METER

$$v_0 = \frac{1}{\sqrt{LC}}$$

$$Z_0 = \sqrt{\frac{Z}{Y}}$$

a. FORWARD-WAVE CIRCUIT.

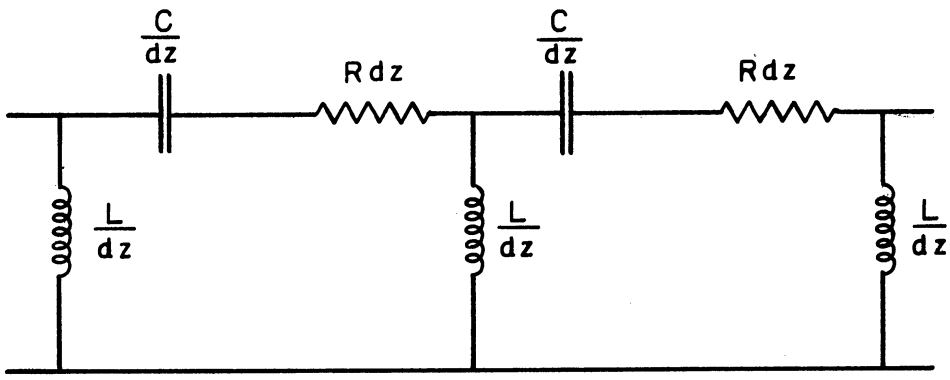

L = HENRYS · METER

R = OHMS / METER

C = FARADS · METER

$$v_0 = -\omega^2\sqrt{LC}$$

$$Z_0 = \sqrt{\frac{Z}{Y}}$$

b. BACKWARD-WAVE CIRCUIT.

FIG. II.1 EQUIVALENT CIRCUITS FOR FORWARD-WAVE AND BACKWARD-WAVE DEVICES.

2. Nonlinear Backward-Wave Equations. In this section the nonlinear backward-wave device equations will be presented rather than derived since they can be developed in a simple manner from the nonlinear forward-wave amplifier equations. The circuit equation used for the nonlinear backward-wave analysis is that given in Eq. II.3 with the lower signs. The normalized variables used in the analysis are defined below.

$$y \triangleq \frac{C\omega z}{u_o} = 2\pi C N_s \quad , \tag{II.4}$$

$$\Phi_o \triangleq \omega t_o \quad , \tag{II.5}$$

$$\theta(y) \triangleq \frac{y}{C} - \omega t - \Phi(y,\Phi_o) \quad , \tag{II.6}$$

$$u_t(y,\Phi_o) \triangleq u_o \left[1+2Cu(y,\Phi_o)\right] \quad , \tag{II.7}$$

$$V(y,\Phi) \triangleq \mathrm{Re}\left[\frac{Z_o I_o}{C} A(y)\, e^{-j\Phi}\right] \quad , \tag{II.8}$$

By a procedure similar to that used in obtaining the forward-wave equations the following set of working equations is obtained for backward-wave O-type devices.

$$\frac{\partial\Phi(y,\Phi_o)}{\partial y} + \frac{d\theta(y)}{dy} = \frac{2u(y,\Phi_o)}{1+2Cu(y,\Phi_o)} \quad , \tag{II.9}$$

$$\frac{d^2A(y)}{dy^2} - A(y)\left[\left(\frac{1}{C} - \frac{d\theta(y)}{dy}\right)^2 - \frac{(1+Cb)^2}{C^2}\right]$$

$$= \pm \frac{(1+Cb)}{\pi C}\left[\int_0^{2\pi} \frac{\cos\Phi(y,\Phi_o')d\Phi_o'}{1+2Cu(y,\Phi_o')}\right.$$

$$\left. + 2Cd\int_0^{2\pi} \frac{\sin\Phi(y,\Phi_o')d\Phi_o'}{1+2Cu(y,\Phi_o')}\right] , \quad \text{(II.10)}$$

$$A(y)\left[\frac{d^2\theta(y)}{dy^2} - \frac{2d}{C}(1+Cb)^2\right] + 2\frac{dA(y)}{dy}\left(\frac{d\theta(y)}{dy} - \frac{1}{C}\right)$$

$$= \pm \frac{(1+Cb)}{\pi C}\left[\int_0^{2\pi} \frac{\sin\Phi(y,\Phi_o')d\Phi_o'}{1+2Cu(y,\Phi_o')}\right.$$

$$\left. - 2Cd\int_0^{2\pi} \frac{\cos\Phi(y,\Phi_o')d\Phi_o'}{1+2Cu(y,\Phi_o')}\right] \quad \text{(II.11)}$$

and

$$\frac{\partial u(y,\Phi_o)}{\partial y}\left[1+2Cu(y,\Phi_o)\right] = A(y)\left[1-C\frac{d\theta(y)}{dy}\right]\sin\Phi(y,\Phi_o)$$

$$- C\frac{dA(y)}{dy}\cos\Phi(y,\Phi_o) + \frac{1}{1+Cb}\left(\frac{\omega_p}{\omega C}\right)^2\int_0^{2\pi}\frac{F(\Phi-\Phi')d\Phi_o'}{1+2Cu(y,\Phi_o')} . \quad \text{(II.12)}$$

The independent variables appearing in the equations are y, the distance along the tube in normalized units, and the entrance phase Φ_o of the electrons relative to the r-f wave at the input to the tube. The

dependent variables are $A(y)$, the normalized r-f voltage amplitude along the structure; $\theta(y)$, the phase lag across the amplifier at any y; $\Phi(y,\Phi_o)$, the phase of the displacement component of an electron that entered the helix at the moment Φ_o relative to the r-f wave; and $u(y,\Phi_o)$, the a-c velocity parameter of an electron at any point y.

The upper signs preceding the terms on the right-hand side of Eqs. II.10 and II.11 refer to the forward-wave device and the lower signs refer to the backward-wave device.

The assumptions made in the derivation of the above equations are:

1. The electric field, electron velocity and current are assumed to be functions only of distance along the tube and time and not functions of the radial dimension.

2. A solid model of the electron stream is assumed in developing the space-charge field expression. The equivalence of this method and the method used by Tien and Walker in obtaining a space-charge field expression can be shown.

3. The structure impedance is assumed to be only at the fundamental backward space harmonic.

4. Rectilinear electron flow is assumed so that the electrons have no transverse motion.

5. Nonrelativistic mechanics is used.

The boundary conditions to be used in the nonlinear backward-wave device analysis are very similar to those used in solving the forward-wave amplifier equations. The r-f structure is assumed to be matched to its characteristic impedance over its entire length and the problem is handled as an initial value problem rather than a boundary value problem. The dependent variables and their derivatives are specified at

state so that all the electrons at $y = 0$ have a zero a-c velocity and the same average velocity. The electrons are assumed to enter equally spaced over one period of the r-f wave at the input; therefore their initial phase positions are given. An initial value A_o of the r-f signal is assumed and if there is no circuit loss, $dA(y)/dy$ at the input is zero. The initial phase lag is of course zero and its derivative $d\theta(y)/dy$, the apparent phase constant of the total wave at the input, is found from the small-signal solutions as in the forward-wave amplifier theory.

The nonlinear backward equations can be solved by assuming specific values of the injection velocity b and the amplitude of the circuit voltage at $y = O(A_o)$ for any set of C, QC and d. Then the equations are integrated numerically using the appropriate difference equation formulation consistent with accuracy and stability of the system until the circuit voltage goes through a minimum in the case of a backward-wave amplifier or goes through zero in the case of an oscillator. The number of representative electrons which have to be used in finding the solutions depends critically upon the value of the space-charge parameter, increasing as QC becomes quite large (around 0.5). As the collector end of the tube is approached, i.e., as the circuit field becomes very small, electrons begin to overtake one another and a maximum in the fundamental component of stream current is reached as in the forward-wave amplifier.

It is apparent that in a backward-wave oscillator that is relatively short (CN approximately 0.3) the effect of crossing electron flight lines is not as important as in the forward-wave amplifier where the typical circuit lengths are quite great, since crossing occurs first in a backward-wave oscillator very near the collector end where the circuit voltage is small and decreasing approximately as a cosine

function. Overtaking of electrons does not result in an abrupt change in the slope of the voltage vs. distance curve. Of course in the backward-wave amplifier where long structures would be used overtaking of electrons, resulting in multi-valued velocities, would be important as in the forward-wave amplifier. In the event that electron trajectory crossings are not of great importance the Eulerian formulation of the equations could be used and hence the hydrodynamical form of the continuity equation is appropriate. This would result in a somewhat simpler set of equations to be solved and the effects of space charge could be more easily included.

In order to determine the combination of b and CN that leads to an oscillation condition several trials are required. The sensitivity of the start-oscillation conditions to the value of A_o at constant b for a particular set of C, QC and d is shown in Fig. II.2 where oscillation occurred for A_o equal to 0.68 and 0.685 but not for 0.67 and 0.69.

A detailed study of the variation of the phase lag across the amplifier $\theta(y)$ vs. y is useful in determining the direction of the change necessary in b or A_o when in the neighborhood of an oscillation condition. The behavior of $\theta(y)$ in the neighborhood of an oscillation condition is illustrated in Fig. II.3. This dependence is general for any set of circuit and stream parameters. It is seen that a nearly linear relationship of $\theta(y)$ vs. y is obtained at the oscillation condition. This is also true when the values of b and A_o are far from a start-oscillation condition and hence one must be near the optimum combination of b and A_o to use the criterion illustrated in the above figure. As the ratio of stream current to minimum starting current is increased, the oscillation condition is more difficult to locate and it is necessary to examine a plot of the CN to the minimum value of A(y)

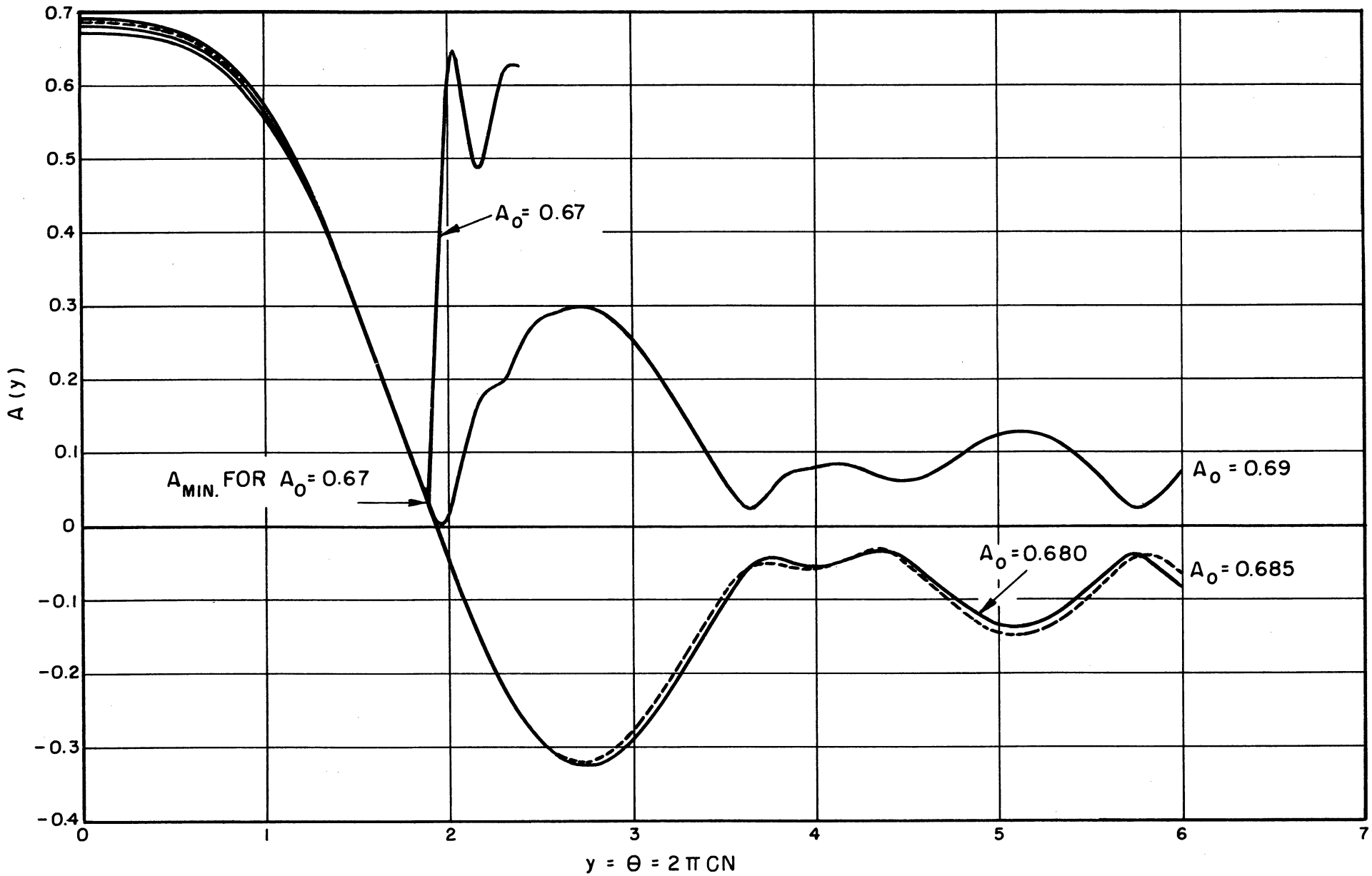

FIG. II.2 R-F VOLTAGE AMPLITUDE VS. DISTANCE. (C = 0.1, QC = 0, d = 0, b = 1.9)

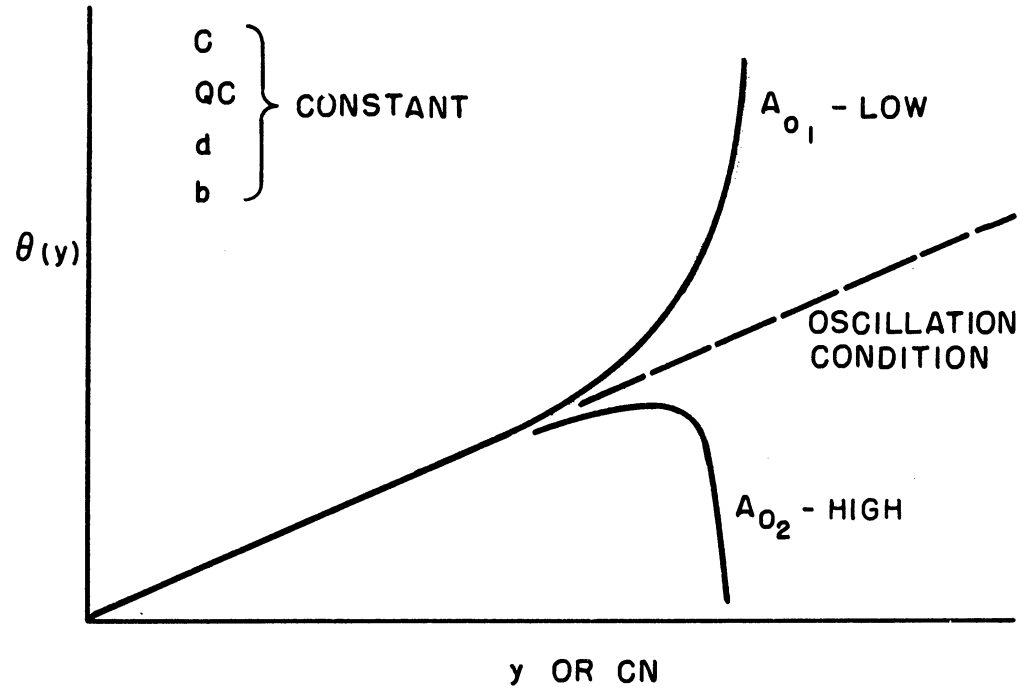

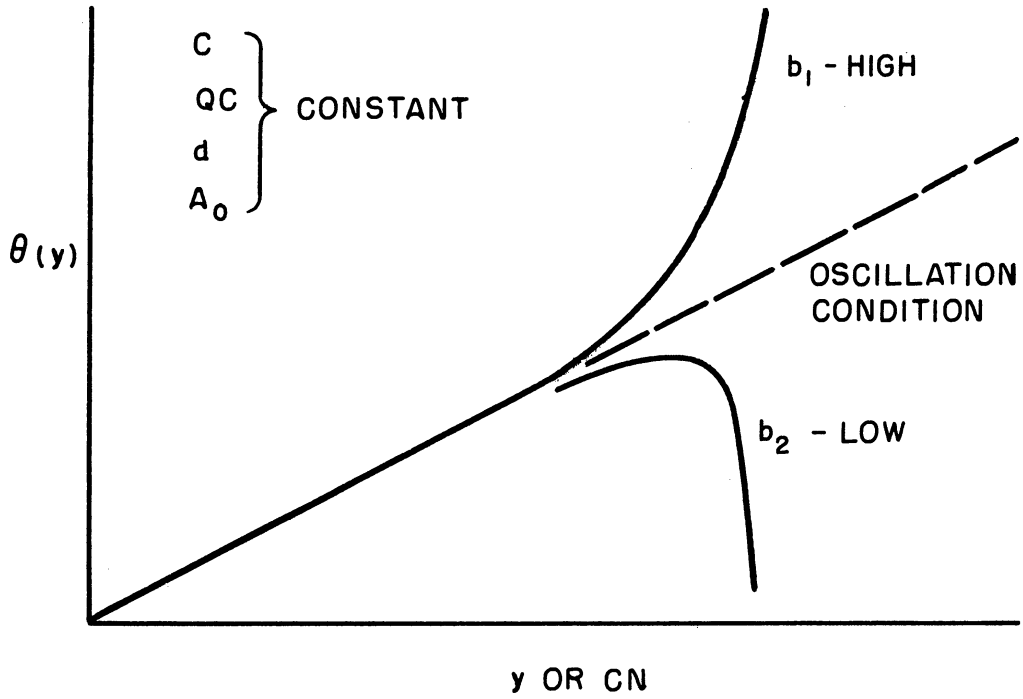

FIG. II.3 INDICATION OF PROXIMITY TO AN OSCILLATION CONDITION.

vs. A_o as well as the above plot in order to determine the oscillation conditions.

3. Efficiency Calculations. The CN length and value of b required for lowest-order start-oscillation condition may be determined by assuming an arbitrarily small value of the signal level A_o at $z = 0$ and then varying b for any particular set of C, QC and d.

As the value of b is increased from that corresponding to the lowest start-oscillation current, larger values of A_o are required to produce oscillation. The efficiency increases approximately linearly with increasing b at constant C, QC and d. The point at which the circuit voltage A(y) goes through zero occurs at a larger value of CN_s in general, which signifies an increase in the stream current above the minimum start-oscillation value. For moderate values of C the length N is nearly independent of the stream current, so that CN varies as the one-third power of the current. If this relationship is true for C's as large as 0.1 the ratio of stream current to minimum starting current can be expressed as

$$\frac{I_o}{I_s} = \left(\frac{CN}{(CN)I_s}\right)^3 , \qquad \text{(II.13)}$$

where I_o = stream current and

I_s = minimum start-oscillation current.

The efficiency is calculated using the following well-known relation:

$$\eta = 2CA_o^2 , \qquad \text{(II.14)}$$

where A_o is the normalized value of the r-f voltage at the gun end of the device.

A composite plot of efficiency vs. I_o/I_s is shown in Fig. II.4 for representative values of C and QC where circuit loss is neglected. The efficiency is seen to increase with increasing stream current up to a value of I_o/I_s of 1.8 and then levels off for all values of C and QC investigated. Increasing C produces an increased efficiency but increasing the space-charge parameter results in a decreasing efficiency. An increase of C from 0.05 to 0.10 results in an approximate doubling of the efficiency. For the case of C = 0.05 and QC = 0.25 a start-oscillation condition was found at $I_o/I_s = 4.3$.

The values of CN_s and b as functions of I_o/I_s corresponding to the data in Fig. II.4 are shown in Fig. II.5. It is seen that as the value of I_o/I_s is increased the value of b approaches a limiting value. These higher-current oscillation conditions indicate increasing output and are extremely difficult to locate since for large values of b the tube is relatively long and behaves much like a long line in the sense that the oscillation condition is very sensitive to the value of A_o. The value of CN at start oscillation is seen to increase smoothly as I_o/I_s is increased and probably becomes asymptotic to some limiting value at high stream currents.

Very high-order oscillation conditions have been observed in the calculations when the circuit voltage goes through zero to negative values and then increases to cross the zero axis again. This occurs at very large values of CN and these oscillation conditions would correspond to 80 to 100 times the minimum start-oscillation current.

Solutions were also found that decreased to a nonzero minimum and then increased and went through subsequent maxima and minima, one of which was zero. When C = 0.2 and QC = 0 it was found that the CN_s length decreased as b was increased (up to b = 2.3), indicating that for

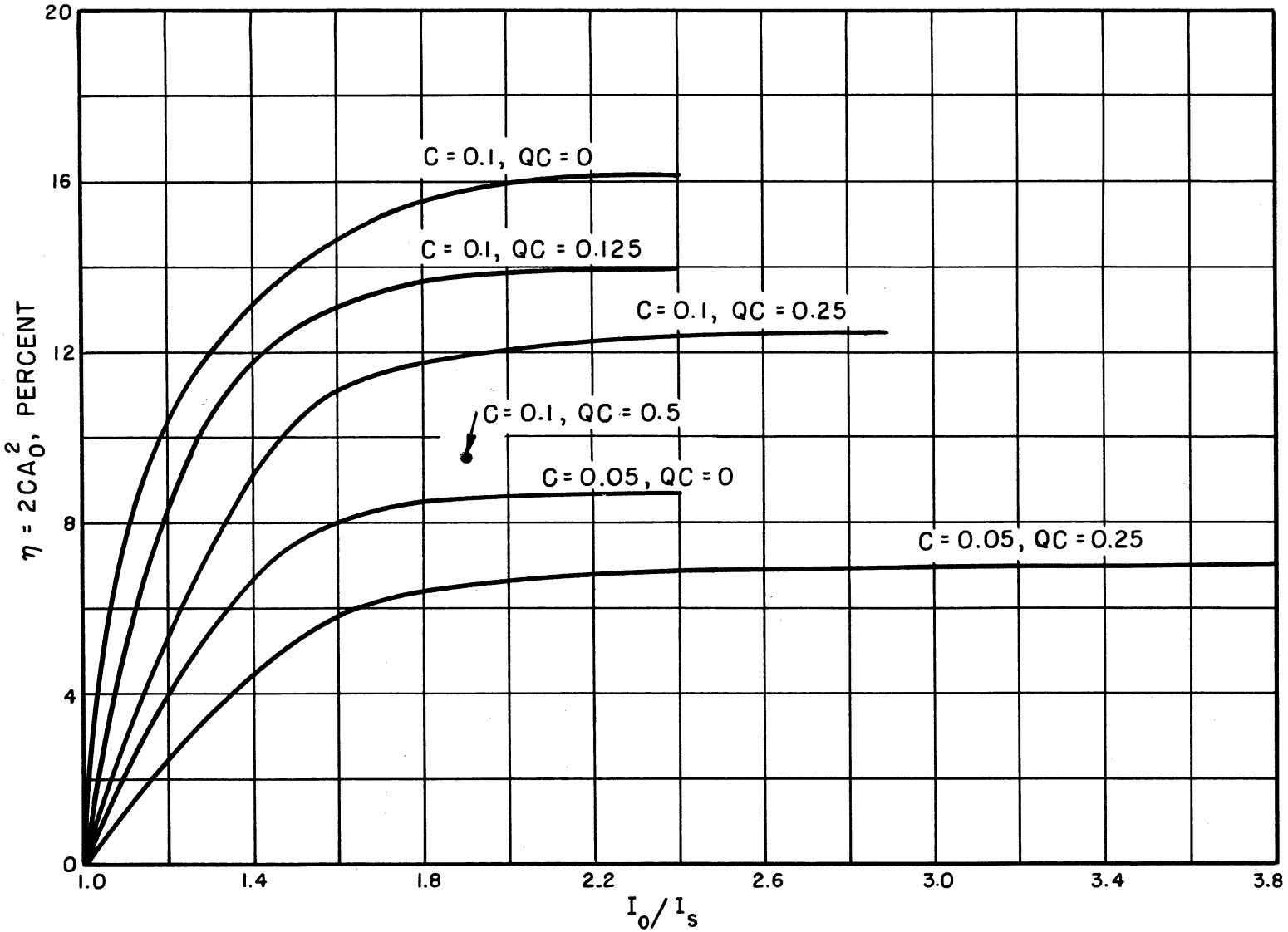

FIG. II.4 EFFICIENCY VS. I_0/I_s WITH b ADJUSTED FOR OSCILLATION.
(B = 1.0, d = 0)

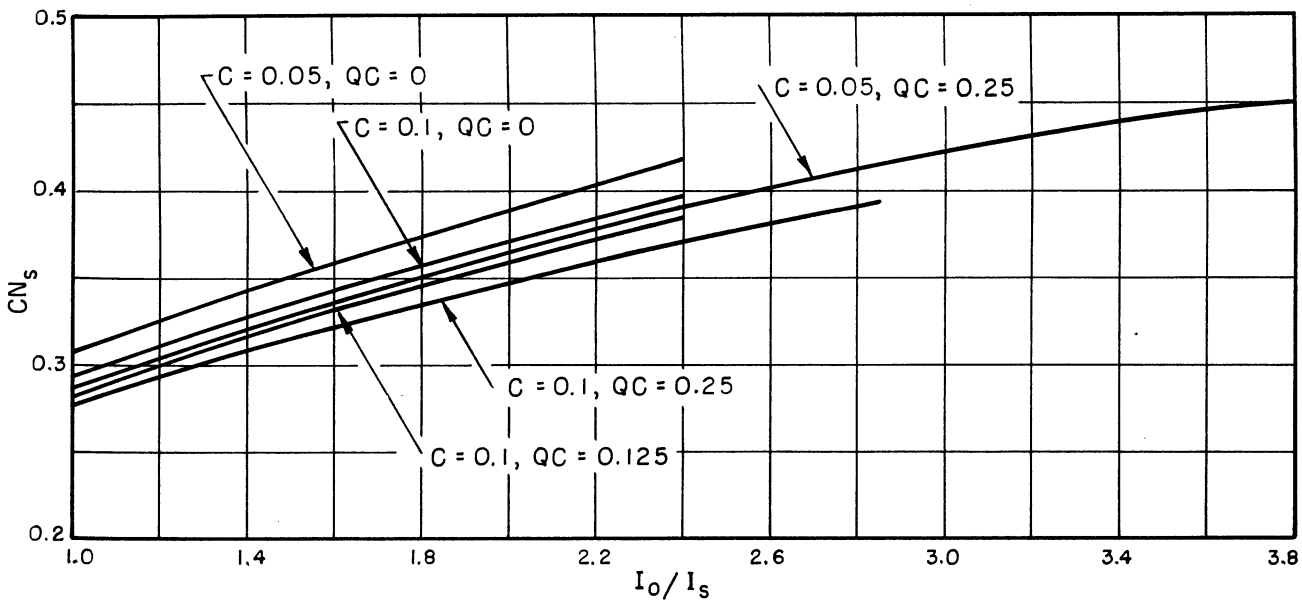

a. CN_s VS. I_o/I_s

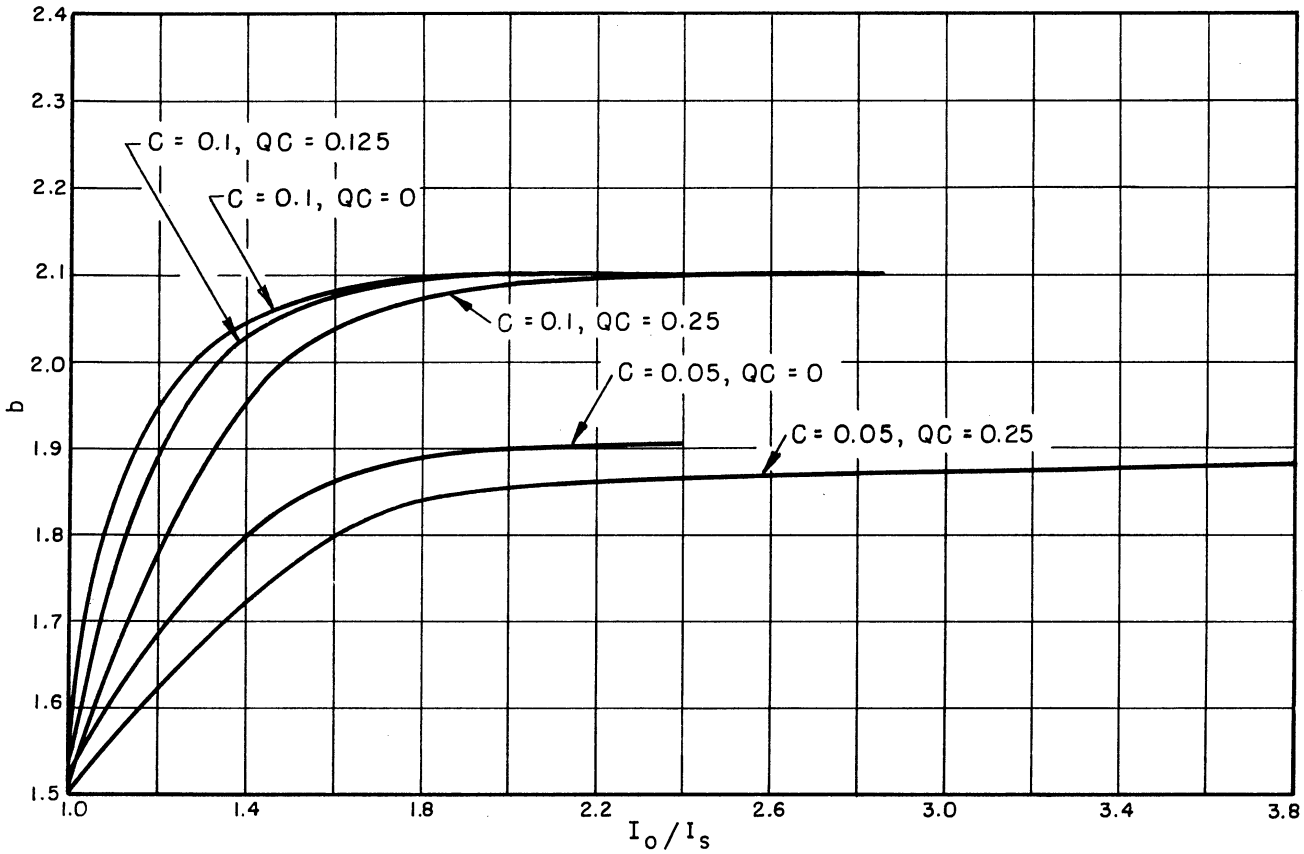

b. b VS. I_o/I_s

FIG. II.5 CN_s AND b VS. I_o/I_s WITH b ADJUSTED FOR OSCILLATION.
(B = 1.0, d = 0)

this large a value of C the length is not independent of the value of current and hence the cube relationship cannot be used.

When C is small, say up to 0.1, it can be determined from a Fourier analysis of the electron velocity variation with distance that the average stream velocity changes slowly with distance and is not significantly reduced at the collector end compared to its initial value. Thus it is seen that the number of stream or circuit wavelengths in a given length is independent of I_o, u_o being relatively constant. The efficiency for C = 0.2 is not appreciably increased over the values obtained when C = 0.1. Values of C = 0.2 are very difficult to achieve practically and for this reason extensive calculations were not carried out for this high value of the gain parameter.

The value of the ratio of fundamental current to d-c current in the stream depends on the level of oscillation generally increasing as the value of b and hence I_o/I_s is increased. For oscillation levels above the lowest oscillation condition it varies from 1.2 to 1.4, depending upon the values of C and QC. This is approximately midway between the values of 1 and 2 respectively used by Grow and Watkins[1] in computing efficiency from a linear theory. A value of the stream diameter B = 1 was used in the calculations, which corresponds to a fairly large beam; hence the efficiency results should probably be modified to account for variation of the circuit field across the stream.

The efficiency results calculated here are in good agreement with the efficiency data of Putz and Luebke[2] as reported by Grow and Watkins.

---

1. Grow, R., Watkins, D. A., "Backward-Wave Oscillator Efficiency", Proc. IRE, vol. 43, pp. 848-856; July, 1955.

2. Putz, J. L., Luebke, W. R., "High-Power S-Band Backward-Wave Oscillator", Tech. Rpt. No. 182-1, Stanford University Electronics Laboratory; February, 1956.

Their experimental values of efficiency indicate a spread of data for η/C vs. $\omega_q/\omega C$ between 1.0 and 2.0 with a clustering around 1.5. These experimental data correspond to operating efficiencies around 8-10 percent and values of QC between 0.2 and 0.6.

Dr. W. Veith of the Siemens and Halske Company of Munich, Germany, has obtained experimental data on efficiency vs. stream current that verified the nature of the efficiency curves shown in Fig. II.4. The efficiency values were lower due to a much lower circuit impedance and hence very small value of C. These results may be seen in "Das Carcinotron, ein Elektrisch Durchstimmbarer Generator für Mikrowellen", Fernmeldetechnische Zeitschrift, Bd. 7 (1954); pp. 23-27.

4. Conclusions. The nonlinear backward-wave oscillator equations were presented as modifications of the nonlinear forward-wave device equations and their method of solution was discussed. The start-oscillation values of CN and b were calculated for small values of output and found to check the small-signal calculations quite well. Efficiency and CN for values of I_o/I_s greater than one were calculated for a wide range of C and QC and the results were found to agree well with published experimental results on backward-wave oscillator efficiency.

B. Beating-Wave Amplification (Crestatron)

1. Introduction. It is well known that the operation of backward-wave devices, both O-type and M-type, depends on an interference phenomenon resulting from the beating between waves propagating along an r-f structure. It can also be shown that in forward-wave devices such as the traveling-wave amplifier gain can occur due to the beating of waves traveling on the r-f structure, providing that the length is correct. The magnitude of this gain for any given set of circuit and

operating parameters is determined by the relative injection velocity b rather than by the length of the tube as in the case of the conventional traveling-wave amplifier.

A voltage gain is produced in the Crestatron by a beating between the three forward waves propagating on the slow-wave structure. The device is operated with a beam velocity such that $b > b_{x_1=0}$ and hence there are no growing waves. The gain is achieved by adjusting the tube length to the proper value such that all the waves, one of which is out of phase with the others at the input, add together to give an r-f voltage greater than that at the input. Hence there is not voltage gain in the sense of that produced by growing waves but there is gain if the tube is considered to be a two-port network. The amount of gain is determined by the value of b and decreases as the beam velocity is raised above that at which growing waves cease to exist. The gain characteristics of the Crestatron can be calculated from the small-signal theory and these calculations also give information on the CN bandwidth achievable in the device.

The large-signal theory of traveling-wave amplifiers[3] has been used to calculate the nonlinear performance of the Crestatron in terms of the gain achievable and the expected operating efficiency. Ample experimental evidence[4] has been offered to verify the theory and indicate that high efficiency is obtained with short length and moderate gains.

---

3. Rowe, J. E., "A Large-Signal Analysis of the Traveling-Wave Amplifier: Theory and General Results", Trans. PGED-IRE, ED-3, No. 1, pp. 39-56; January, 1956.

4. Caldwell, J. J., and Hoch, O. L., "Large-Signal Behavior of High Power Traveling-Wave Amplifiers", Trans. PGED-IRE, ED-3, pp. 6-18; January, 1956.

2. Gain Equation. The three forward waves propagating on a traveling-wave tube r-f structure are known to vary in the following manner[5]:

$$e^{-\Gamma z} = e^{-j\beta_e z} \cdot e^{\beta_e C\delta z} \quad , \qquad \text{(II.15)}$$

where β_e is the stream phase constant. The normalized voltage V_z/V at any point along the r-f structure may be written in terms of the amplitudes of the three waves, neglecting space charge, as

$$\frac{V_z}{V} = e^{-j\frac{\theta}{C}} \left[\frac{V_1}{V} e^{\delta_1 \theta} + \frac{V_2}{V} e^{\delta_2 \theta} + \frac{V_3}{V} e^{\delta_3 \theta} \right] \quad , \qquad \text{(II.16)}$$

where $\delta_i = x_i + jy_i$, $i = 1,2,3$;

V_i/V = normalized voltage amplitude of each wave,

$\theta \triangleq \beta C z = 2\pi C N$,

N = structure length in wavelengths, and

C = gain parameter.

From the small-signal theory of the traveling-wave tube, the following expressions for the r-f convection current and velocity are obtained by retaining terms proportional to C:

$$\frac{(1+jC\delta_1)}{\delta_1} V_1 + \frac{(1+jC\delta_2)}{\delta_2} V_2 + \frac{(1+jC\delta_3)}{\delta_3} V_3 = \left(\frac{ju_o C}{\eta}\right) \tilde{v} \quad , \qquad \text{(II.17)}$$

and

$$\frac{(1+jC\delta_1)}{\delta_1^2} V_1 + \frac{(1+jC\delta_2)}{\delta_2^2} V_2 + \frac{(1+jC\delta_3)}{\delta_3^2} V_3 = \left(\frac{-2V_o C^2}{I_o}\right) \tilde{i} \quad , \qquad \text{(II.18)}$$

---

5. Pierce, J. R., Traveling-Wave Tubes, D. Van Nostrand Co., New York; 1950.

where η = e/m, charge-to-mass ratio of the electron,

$\tilde{v}$ = r-f velocity in the stream,

$\tilde{i}$ = r-f convection current in the stream,

V_o = d-c stream voltage, and

I_o = d-c stream current.

If an unmodulated stream is injected at z = 0 and an r-f signal level V is applied to the r-f structure at that point, the boundary conditions require that the right-hand sides of Eqs. II.17 and II.18 be zero and that

$$V = V_1 + V_2 + V_3 \quad . \tag{II.19}$$

Equations II.17, II.18 and II.19 may be solved simultaneously to give the normalized amplitudes of the individual waves. The general result is shown below.

$$\frac{V_i}{V} = \left[1 + \frac{1+jC\delta_i}{1+jC\delta_{i+1}}\left(\frac{\delta_{i+1}}{\delta_i}\right)^2 \frac{\delta_{i+2}-\delta_i}{\delta_{i+1}-\delta_{i+2}} + \frac{1+jC\delta_i}{1+jC\delta_{i+2}}\left(\frac{\delta_{i+2}}{\delta_i}\right)^2 \frac{\delta_i-\delta_{i+1}}{\delta_{i+1}-\delta_{i+2}}\right]^{-1} \tag{II.20}$$

where $\delta_i \equiv \delta_{i+3}$.

Equation II.20 gives the total voltage associated with each wave and in the absence of space charge also gives the circuit voltage. The effect of passive modes or space charge is to reduce the circuit voltage from the value predicted by Eq. II.20. The ratio of the circuit voltage to the total voltage is found from the ratio of the second term on the right-hand side of the following familiar quartic determinantal equation to the total right-hand side[6] of Eq. II.20:

6. Ibid., p. 113, Eq. 7.13 with corrections.

$$\delta^2 = \frac{(1+jC\delta)^2\,[1+C(b-jd)]}{\left[-b+jd+j\delta+C\left(jbd - \frac{b^2}{2} + \frac{d^2}{2} - \frac{\delta^2}{2}\right)\right]} - 4QC(1+jC\delta)^2 \quad . \qquad \text{(II.21)}$$

The general result for the circuit component of voltage is

$$\frac{V_{ci}}{V_i} = 1 + 4QC\,\frac{(1+jC\delta_i)^2}{\delta_i^2} \quad . \qquad \text{(II.22)}$$

Equations II.20 and II.22 have been obtained by Brewer and Birdsall[7].

Thus the voltage along the r-f structure may be written in general, including the effects of finite C and space charge QC, as

$$\frac{V_z}{V} = e^{-j\frac{\theta}{C}} \sum_{i=1}^{3} \left(\frac{V_i}{V}\right)\left(\frac{V_{ci}}{V_i}\right) e^{\delta_i\theta} \quad , \qquad \text{(II.23)}$$

where $\delta_i \equiv \delta_{i+3}$.

When C is small and the effect of passive modes or space charge is negligible, Eqs. II.20 and II.22 reduce to the following familiar form:

$$\frac{V_i}{V} = \frac{\delta_i^2}{(\delta_i-\delta_{i+1})\cdot(\delta_i-\delta_{i+2})} \qquad \text{(II.24)}$$

and

$$\frac{V_{ci}}{V_i} = 1 \quad . \qquad \text{(II.25)}$$

---

7. Brewer, G. R., and Birdsall, C. K., "Normalized Propagation Constants for a Traveling-Wave Tube for Finite Values of C," Tech. Memo. No. 331, Hughes Research and Development Laboratories, Culver City, California; October, 1953.

The voltage gain is written as

$$G_{db} = 10 \log \left(\frac{V_z V_z^*}{V V^*} \right) = 10 \log \left| \left(\frac{V_z}{V} \right)^2 \right| . \qquad \text{(II.26)}$$

It is important to note that, unlike conventional standing waves on a transmission line, each wave sees the r-f structure characteristic impedance at all points along the line.

The gain that occurs when the velocity parameter b is greater than that for which the growth constant of the growing wave is zero is, as mentioned before, due to a beating effect between the three small-signal waves which are set up at the input and propagate along the r-f structure. The interaction is primarily between the circuit wave and the slow space-charge wave. It will be seen later that the fast space-charge wave is excited to a negligible extent. This is the same basic mode of operation as in the backward-wave device of both the traveling-wave tube and crossed-field types. As the three waves travel along the structure the phase relationship between the r-f current in the beam and the r-f field on the circuit changes and at certain points along the circuit the phase is such that energy is transferred to the circuit. At the same time there are certain regions along the tube where the phase relationship between the beam current and the circuit field is such that energy is fed from the circuit back to the beam. The gain in this mode of operation depends upon the relative injection velocity b for any given set of tube parameters rather than on the length as in the case of the conventional traveling-wave tube.

The Crestatron is inherently more efficient than the backward-wave devices which operate on the same principle because the modulation in the stream and the field on the circuit producing the modulation travel

in the same direction, whereas in the backward-wave device the modulation in the beam and the circuit field travel in opposite directions. In the backward-wave device the circuit field is strongest where the modulation is weakest and vice versa.

Mathematically speaking all the energy is abstracted from the beam at the input since in satisfying the boundary conditions energy is put into setting up the three circuit waves. Then the circuit length is simply adjusted so that at the end of the tube the wave energies all add in phase. It should be recalled that in this region of operation the propagation constants are purely imaginary, giving rise to real voltage amplitudes, and at the input one voltage component is 180 degrees out of phase with the other two.

3. Small-Signal Gain. It was pointed out above that the normalized voltage amplitudes are purely real since the propagation constants are purely imaginary when $b > b_{x_1=0}$. For fixed values of C, QC, and d the gain may be calculated from Eqs. II.20 and II.26 as a function of θ for particular values of b. A typical gain curve is shown in Fig. II.6. The above gain equations are valid for all values of b and it is seen from the figures that the normal exponential gain is obtained when $x_1 \neq 0$. The gain curve was plotted over a range of 6π radians to indicate its repetitive nature.

When the loss parameter is zero all maxima of the gain curve are approximately equal (the slight variations and lack of periodicity will be explained later), but when $d \neq 0$ the first maximum will be highest and subsequent peaks will generally be lower. This merely emphasizes the fact that when circuit loss is significant the Crestatron length should be chosen so as to operate on the first maximum of the gain curve.

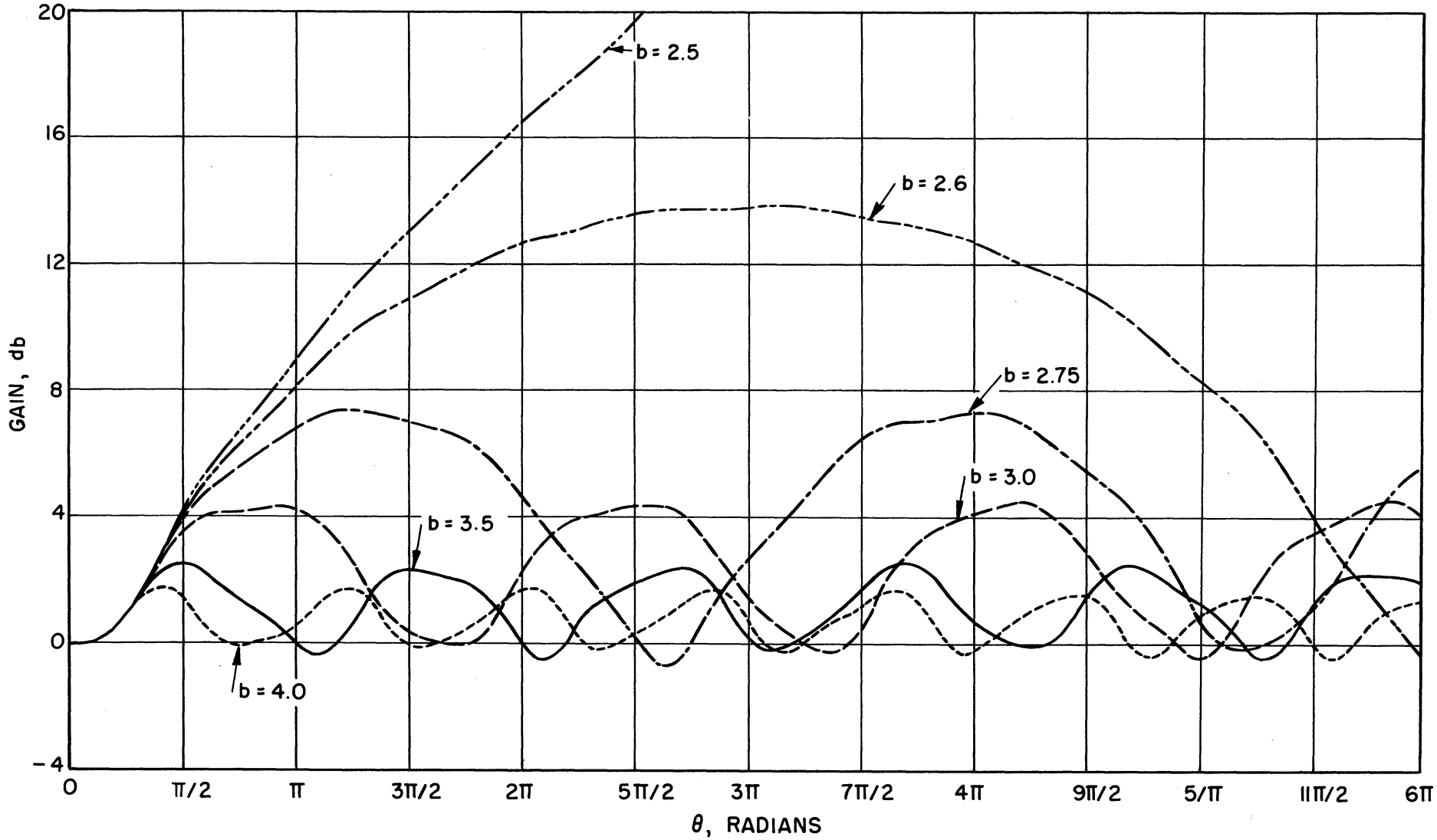

FIG.II.6 GAIN VS. LENGTH. ($C = 0.1$, $QC = 0.25$, $d = 0$, $b_{x_1 = 0} = 2.57$)

It is seen from the gain curves that for fixed b and variable θ the curves are nonperiodic within the interval 6π and exhibit periodic undulations in amplitude. The explanation of this phenomenon is contained in Eq. II.23 for the voltage amplitude vs. distance. The lack of periodicity with 2π and the undulating peak amplitudes are a result of the product of $\exp(-j\ \theta/C)$ and $\exp(\delta_i\theta)$, where each represents a vector rotating about the origin as a function of θ. The rate of rotation of the first vector is related to $1/C$, which is typically between 5 and 20, and the rate of rotation of the second is determined by δ_i, which varies between 1 and 3. The first, then, perturbs the second as a modulation and the fact that δ_i is nonintegral in general means that it is not periodic with 2π. It may be that θ must travel through $2m\pi$ radians with m very large before a periodicity is apparent, if ever.

The above phenomenon indicates that there is something more than a simple beating effect occurring between the waves. In fact there is a continual slipping of one wave with respect to the others along the tube. This process accounts for the fact that there is or may be a net interchange of energy between the beam and the circuit in a device of infinite length. It is interesting to examine the condition necessary for the gain curve to be periodic with period $2m\pi$ and also the condition required for the peak amplitudes to be constant. In fact these two conditions would result in a gain curve that is exactly reproduced every 2π radians.

Under very restricted conditions a simplified expression for the gain of the Crestatron may be obtained from Eq. II.23. When $C \to 0$, $QC = 0$, $d = 0$, and b is sufficiently large that the propagation constants are purely imaginary, it can be determined that the δ_i's are given approximately by

$$\delta_1 \approx -j/b^{1/2} \quad ,$$

$$\delta_2 \approx -jb \quad ,$$

and

$$\delta_3 \approx j/b^{1/2} \quad . \tag{II.27}$$

Substitution of Eq. II.27 into Eq. II.23 yields for the gain, after some simplification,

$$\left|\frac{V_z}{V}\right|^2 = \left(\frac{1}{1-b^3}\right)^2 \left[1 + b^6 + (b^3-1)\sin^2\frac{\theta}{b^{1/2}} - 2b^3\left\{\cos\theta b\cos\frac{\theta}{b^{1/2}} + b^{3/2}\sin\theta b\sin\frac{\theta}{b^{1/2}}\right\}\right] \quad . \tag{II.28}$$

Since b is usually greater than 2.5, Eq. II.28 can be further simplified to

$$\left|\frac{V_z}{V}\right|^2 = 1 + \frac{1}{b^3}\left[\sin^2\frac{\theta}{b^{1/2}} - 2\cos\theta b\cos\frac{\theta}{b^{1/2}} + b^{3/2}\sin\theta b\sin\frac{\theta}{b^{1/2}}\right] . \tag{II.29}$$

A useful expression for predicting the value of CN at the first maximum of the gain curve is

$$CN = \frac{0.25}{(\Delta b)^{1/2}} \quad , \tag{II.30}$$

where $\Delta b \triangleq b - b_{x_1=0}$.

4. Maximum Gain vs. C and QC. It was pointed out earlier that the voltages in the Crestatron are purely real and at the input one voltage is 180 degrees out of phase with the other two. Thus the

maximum gain will occur when the three waves all add in phase.

A typical maximum-gain curve for C = 0.2 is shown in Fig. II.7. The gain decreases with increasing voltage and for very high voltage approaches zero asymptotically. As would be expected the gain increases with C and decreases as QC is increased. The effect of loss on the circuit is also seen to reduce the gain. The greatest gain occurs for a b slightly larger than that for which growing waves cease to exist. There is a smooth transition from the region of exponentially growing waves to the region in which the gain is a result of the beating of the three waves.

Typical Crestatron lengths are in the vicinity of CN $\approx$ 0.4 to 0.5 and loss calculations show that the signal decreases at the approximate rate of 24 db per unit d with no stream present. The effect of circuit loss is to reduce the gain at only one-half the rate when the stream is present as compared with the rate of decrease of the signal in the absence of the stream. This compares favorably with the one-third figure for conventional traveling-wave tubes.

5. Large-Signal Results. The large-signal performance of the Crestatron amplifier has been evaluated using the large-signal theory of the traveling-wave amplifier[8]. Large-signal gain, phase shift and efficiency have been calculated for a wide range of parameters. The significant conclusion reached from these calculations is that the Crestatron offers a characteristic high saturation efficiency with a very short interaction length. The price paid for these desirable

---

8. Rowe, J. E., "Theory of the Crestatron: A Forward-Wave Amplifier", Proc. IRE, vol. 47, No. 4, pp. 536-545; April, 1959.

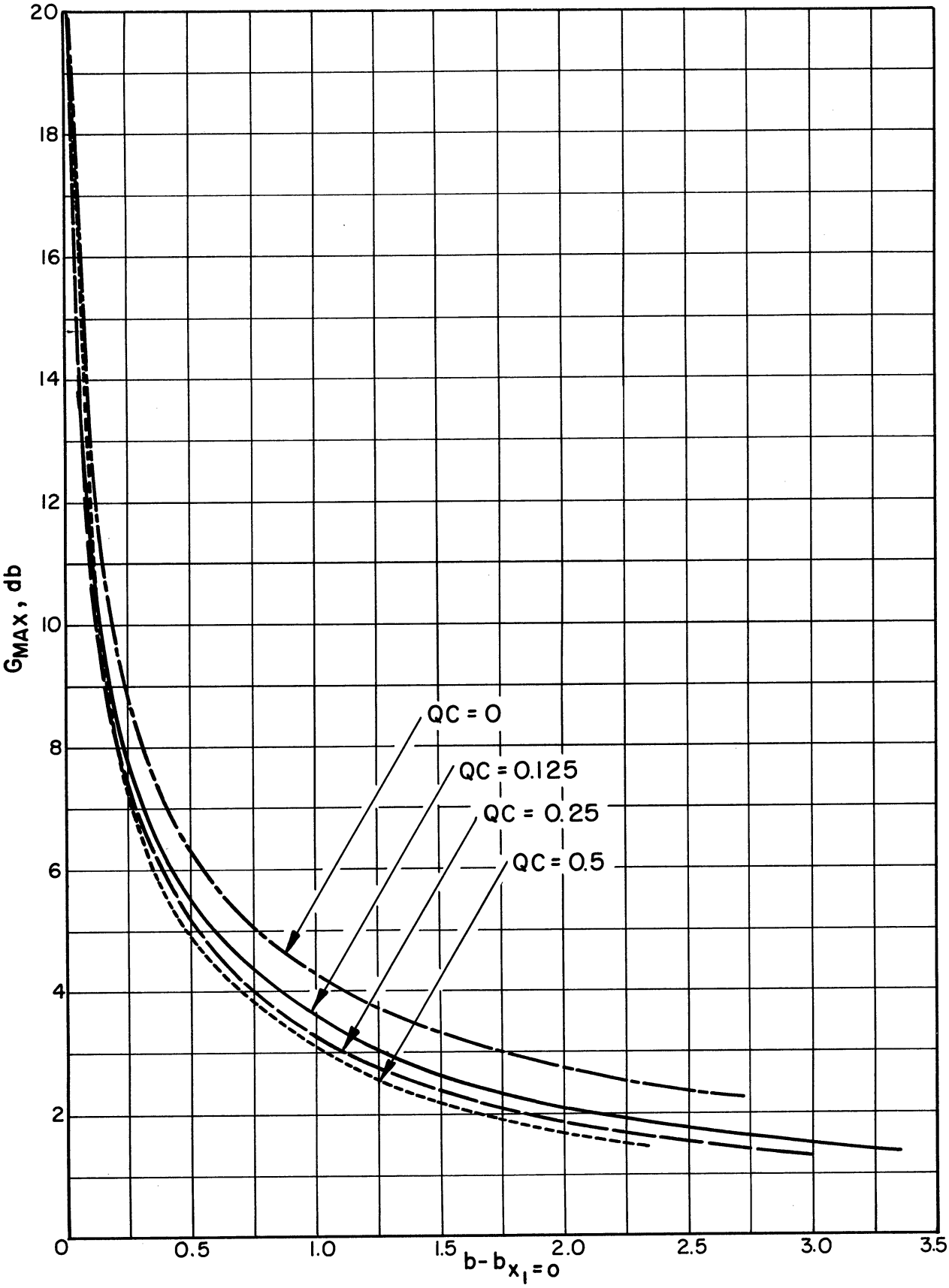

FIG. II.7 MAXIMUM GAIN VS. $b - b_{x_1=0}$ WITH SPACE CHARGE AS THE PARAMETER. (C = 0.2, d = 0)

characteristics is that the gain is moderate. Gain is maximized by utilizing high circuit impedance and high-perveance electron guns.

A great deal of experimental information has been obtained on several S-band tubes and this information will be presented in a later section of this report.

6. Conclusions. A new type of forward-wave amplifier device has been developed and analyzed with both a linear and a nonlinear theory. The Crestatron operates on the basis of gain being produced by a beating between the three forward waves set up at the input of the traveling-wave amplifier operating at a high voltage so that there are no growing waves. The gains achievable are moderate and increase with increasing C but decrease with increasing QC. The gain also decreases as the injection velocity as measured by "b" is increased.

Nonlinear calculations indicate the same type of behavior as both the voltage and drive level are increased, and it has been shown that the saturation power output increased with the drive level. The saturation efficiency is high for this type of operation and the CN bandwidth can be as large as ± 50 percent.

The chief advantage of the Crestatron over the conventional traveling-wave amplifier is that its length is quite short for reasonable gains (4 to 6 wavelengths), which means that the focusing magnet can be of minimum length and weight and under certain conditions may even be eliminated.

C. Comparison of Integral and Differential Equation Analyses of the Traveling-Wave Tube

1. Introduction. Basically two different methods of analysis have been used in analyzing the large-signal traveling-wave amplifier.

These are the integral equation methods of Poulter[9] and Tien[10] and the differential equation methods of Nordsieck[11] and Rowe[12]. It can be shown that these two methods are equivalent and give the same results regardless of the value of the gain parameter C. The results of calculations agree well with various experiments. This equivalence has been discussed recently in a journal paper[13]. A summary discussion will be presented here.

2. Equivalence of Integral and Differential Equation Approaches. It will be shown that Tien's large-C equations are in fact Rowe's earlier equations. Rowe writes a second-order differential equation for the voltage on the helix A(y). The solution of this equation for the voltage along the line must include all the components as required by the boundary conditions. Poulter and Tien prefer to write the total helix voltage in terms of the sum of two components $a_1(y)$ and $a_2(y)$, which are convolutions of the space charge with a "cold" forward and backward wave, respectively, on the helix. These components satisfy first-order differential equations. These two waves have no separate physical existence and nothing new is added when the total voltage is separated into the forward and backward components.

---

9. Poulter, H. C., "Large Signal Theory of the Traveling-Wave Tube", Electronics Res. Lab., Stanford University, Stanford, California, Tech. Rept. No. 73; January, 1954.

10. Tien, P. K., "A Large Signal Theory of Traveling-Wave Amplifiers", Bell Sys. Tech. J., vol. 35, pp. 349-374; March, 1956.

11. Nordsieck, A., "Theory of the Large-Signal Behavior of Traveling-Wave Amplifiers", Proc. IRE, vol. 41, pp. 630-637; May, 1953.

12. Rowe, J. E., "A Large-Signal Analysis of the Traveling-Wave Amplifier: Theory and General Results, IRE Trans. on Electron Devices, vol. ED-3, pp. 39-57; January, 1956.

13. Rowe, J. E., "One-Dimensional Traveling-Wave Tube Analyses and the Effect of Radial Electric Field Variations", Trans. PGED-IRE, vol. ED-7, No. 1, pp. 16-21; January, 1960.

Rowe's definition of the voltage is given by

$$V(y,\Phi) = \frac{Z_o I_o}{4C} [A_1(y) \cos \Phi - A_2(y) \sin \Phi] \quad , \qquad (II.31)$$

where $y = C\omega z/v_o = 2\pi C N_g$, and

$\Phi(y,\Phi_o) = y/C - \omega t$.

Tien's definition of the voltage along the structure is given by

$$V(y,\Phi) = F(y,\Phi) + B(y,\Phi) = \frac{Z_o I_o}{4C} \{[a_1(y) + b_1(y)] \cos \Phi$$

$$- [a_2(y) + b_2(y)] \sin \Phi\} \quad , \qquad (II.32)$$

where $F(y,\Phi)$ and $B(y,\Phi)$ represent, respectively, the voltages of the forward and backward waves on the cold helix. Tien's definition of normalized distance along the structure is

$$y = C\omega z/u_o = 2\pi C N_s \quad . \qquad (II.33)$$

This difference in definitions of the normalized distance will result in the presence of an additional factor $(1+Cb)$, which makes no essential difference in the final form. The parameter b is a measure of the injection velocity and is defined as $b = (u_o - v_o)/Cv_o$.

After introduction of the conservation of charge and considerable mathematical manipulations, Tien finds the following relationships between his dependent variables:

$$b_1(y) = \frac{-C}{2(1+Cb)} \frac{d}{dy} [a_2(y) + b_2(y)] \quad , \qquad (II.34)$$

$$b_2(y) = \frac{C}{2(1+Cb)} \frac{d}{dy} [a_1(y) + b_1(y)] \quad , \qquad (II.35)$$

$$\frac{da_1(y)}{dy} = \frac{-2}{\pi} \int_0^{2\pi} \frac{\sin \Phi(y,\Phi_o) d\Phi_o}{1+Cw(y,\Phi_o)} \quad , \tag{II.36}$$

and

$$\frac{da_2(y)}{dy} = \frac{-2}{\pi} \int_0^{2\pi} \frac{\cos \Phi(y,\Phi_o) d\Phi_o}{1+Cw(y,\Phi_o)} \quad , \tag{II.37}$$

In order to facilitate comparison the following definitions are made.

Let

$$A_1(y) = a_1(y) + b_1(y) \quad , \tag{II.38}$$

and

$$A_2(y) = a_2(y) + b_2(y) \quad . \tag{II.39}$$

Substituting Eqs. II.38 and II.39 into Eqs. II.34 and II.35 yields

$$b_1(y) = \frac{-C}{2(1+Cb)} \frac{dA_2(y)}{dy} \quad , \tag{II.40}$$

and

$$b_2(y) = \frac{C}{2(1+Cb)} \frac{dA_1(y)}{dy} \quad . \tag{II.41}$$

If Eqs. II.40 and II.41 are substituted into Eqs. II.38 and II.39 the following relationships are found for $a_1(y)$ and $a_2(y)$

$$a_1(y) = A_1(y) + \frac{C}{2(1+Cb)} \frac{dA_2(y)}{dy} \quad , \tag{II.42}$$

and

$$a_2(y) = A_2(y) - \frac{C}{2(1+Cb)} \frac{dA_1(y)}{dy} \quad . \tag{II.43}$$

The final step is to differentiate Eqs. II.42 and II.43 with respect to y and then substitute into Eqs. II.36 and II.37. The following equations result

$$\frac{dA_1(y)}{dy} + \frac{C}{2(1+Cb)} \frac{d^2A_2(y)}{dy^2} = -\frac{2}{\pi} \int_0^{2\pi} \frac{\sin \Phi(y,\Phi_o)d\Phi_o)}{1+Cw(y,\Phi_o)} \quad , \qquad \text{(II.44)}$$

and

$$\frac{dA_2(y)}{dy} - \frac{C}{2(1+Cb)} \frac{d^2A_1(y)}{dy^2} = -\frac{2}{\pi} \int_0^{2\pi} \frac{\cos \Phi(y,\Phi_o)d\Phi_o}{1+Cw(y,\Phi_o)} \quad . \qquad \text{(II.45)}$$

The other two working equations of Tien are presented without derivation for later comparison with Rowe's equations,

$$\frac{d\Phi(y,\Phi_o)}{dy} - b = \frac{w(y,\Phi_o)}{1+Cw(y,\Phi_o)} \quad , \qquad \text{(II.46)}$$

and

$$2[1+Cw(y,\Phi_o)] \frac{dw(y,\Phi_o)}{dy} = (1+Cb)\ [a_1(y) \sin \Phi + a_2(y) \cos \Phi]$$

$$- \frac{C}{2} \left[\frac{da_1(y)}{dy} \cos \Phi - \frac{da_2(y)}{dy} \sin \Phi\right] + \frac{C^2}{4(1+Cb)} \left[\frac{d^2a_1(y)}{dy^2} \sin \Phi\right.$$

$$\left. + \frac{d^2a_2(y)}{dy^2} \cos \Phi\right] - \frac{2e}{u_o m\omega C^2} E_s \quad . \qquad \text{(II.47)}$$

To facilitate comparison the working equations obtained by Rowe are presented without derivation. The four equations are obtained in a straight-forward manner from the circuit equation, the simplified Lorentz force equation and the continuity equation. They are

$$\frac{d\Phi(y,\Phi_o)}{dy} \quad \frac{v(y,\Phi)}{1+Cv(y,\Phi_o)} \quad , \tag{II.48}$$

$$\frac{C}{2} \frac{d^2a_1(y)}{dy^2} - \frac{da_2(y)}{dy} - \bar{d}a_2(y) = \frac{2}{\pi}\left[\int_o^{2\pi} \frac{\cos n\Phi(y,\Phi_o')d\Phi_o'}{1+Cv(y,\Phi_o')} + 2C\,\bar{d} \int_o^{2\pi} \frac{\sin n\Phi(y,\Phi_o')d\Phi_o'}{1+Cv(y,\Phi_o')} \right] , \tag{II.49}$$

$$\frac{C}{2} \frac{d^2a_2(y)}{dy^2} + \frac{da_1(y)}{dy} + \bar{d}a_1(y) = -\frac{2}{\pi}\left[\int_o^{2\pi} \frac{\sin n\Phi(y,\Phi_o')d\Phi_o'}{1+Cv(y,\Phi_o')} - 2C\,\bar{d} \int_o^{2\pi} \frac{\cos n\Phi(y,\Phi_o')d\Phi_o'}{1+Cv(y,\Phi_o')} \right] , \tag{II.50}$$

and

$$\frac{\partial}{\partial y}[1+Cv(y,\Phi_o)]^2 = C(1+Cb)^2 \left[\left(a_2(y) - C\frac{da_1(y)}{dy}\right)\cos\Phi(y,\Phi_o) + \left(a_1(y) + C\frac{da_2(y)}{dy}\right)\sin\Phi(y,\Phi_o) + \frac{4}{(1+Cb)}\left(\frac{\omega_p}{\omega C}\right)^2 \int_o^{2\pi} \frac{F(\Phi-\Phi')d\Phi_o'}{1+Cv(y,\Phi_o')} \right] , \tag{II.51}$$

where the variables and parameters are as defined previously and $\bar{d}$ is the loss parameter. These equations are valid for large C, circuit loss, and space-charge effects. Equation II.18 relates two of the

dependent variables, whereas Eq. II.49 and II.50 come from the circuit equation. Equation II.51 is the force equation and contains the space-charge field expression.

Except for the factor (1+Cb), which was discussed previously, the circuit equations of Tien are exactly Rowe's equations if the loss parameter and the space-charge parameters are placed equal to zero. It should be pointed out that no additional assumptions were made in proving the equivalence. The equivalence of the other working equations is readily apparent after appropriate transformation of variables as defined above. The b in Eq. II.46 arises because of a slightly different definition of $\Phi(y,\Phi_o)$. The similarity of the space-charge expressions used by Rowe and Tien will be discussed later.

In solving the equations both authors apply four boundary conditions at the input plane in lieu of three conditions at the input plane and one additional condition at the output plane of the circuit. These conditions are on the entering electron velocity, phase constant of the r-f wave, initial r-f voltage amplitude and rate of change of the voltage amplitude. Small-signal conditions are assumed to exist at the input to the device. These conditions guarantee that there is no backward wave at the input plane. The output of the circuit is terminated so that there is a reflection in the presence of the stream which exactly cancels the backward traveling wave produced by the modulated electron stream. The lack of synchronism of the backward traveling wave with the stream precludes any significant interaction between them even when C is large. This equivalence of the circuit equations has also been investigated by Gould[14].

---

14. Private communication.

Poulter uses an integral equation method similar to, but not identical to Tien's. The equivalence of his method to that of Rowe's has been shown by comparing numerical solutions for the same set of parameters. The results are virtually identical.

3. Space-Charge Expressions. It remains now to discuss the similarity of the space-charge equation formulations used by the authors. Tien[15] uses in his large-signal calculations a space-charge model consisting of infinitely thin charge disks distributed in a conducting cylinder, which replaces the helix. He computes the force between the disks as a function of their separation and obtains a space-charge weighting function which depends on the electron distribution in space (z). On the other hand, Poulter's and Rowe's space-charge expressions and weighting functions are based on the electron distribution in phase space. These are related, since the dependent variable giving the electron phase position is a function of z, $\Phi(y,\Phi_o)$.

The expansion of the space-charge field components in a Fourier series in time at a constant z plane assumes that the change in amplitude of the waves is small during any one cycle. The space-charge field pattern for the nearest neighboring cycle will be very like its own, but the one further away may be very different. The distribution of electrons in space for constant time is very nearly the same as their distribution in time for a small interval of y, providing that the gain per wavelength is small even for relatively large a-c velocities, since it is the closely spaced electrons about Φ which are important in

15. Tien, P. K., Walker, L. R., and Wolontis, V. M., "A Large Signal Theory of Traveling-Wave Amplifiers", Proc. IRE, vol. 43, pp. 260-277; March, 1955.

evaluating the space-charge force at Φ. The influence of space charge does not extend further than two or three cycles in either direction.

After obtaining a space-charge weighting function, Tien approximates it by an exponential function of the following type

$$\exp\left(-k|\Phi-\Phi'|\right) \quad , \qquad \text{(II.52)}$$

where k varies between 1 and 5. The particular value of k depends upon the ratio of the stream to helix diameters. The approximate form for the space-charge field weighting function used by Tien gives the following relationship between his k and Rowe's space-charge range parameter B, which expresses the range of effectiveness of the space-charge in terms of the stream diameter.

$$B = \frac{2}{k} \quad \text{(using Tien's approximate form)} \quad . \qquad \text{(II.53)}$$

A comparison of Tien's and Rowe's space-charge weighting functions is shown in Fig. II.8. It is seen from Rowe's calculations that the weighting function is not highly dependent upon the ratio of helix and stream radii. From the figure it is also seen that the correspondence between k and B is that

$$Bk = 1.25 \quad . \qquad \text{(II.54)}$$

This difference in the proportionality constant arises from the approximation made by Tien in computing the weighting function. Hence, it is seen that the two methods of accounting for space-charge forces give essentially the same results.

4. Efficiency Calculations. It has been shown that the large-signal equations of Rowe and Tien are equivalent and that the space-charge weighting functions are essentially the same. Hence it is interesting to compare the results of large-signal calculations for specific values of the various operating parameters. Unfortunately in some earlier calculations of the author an error in sign in the space-charge expression

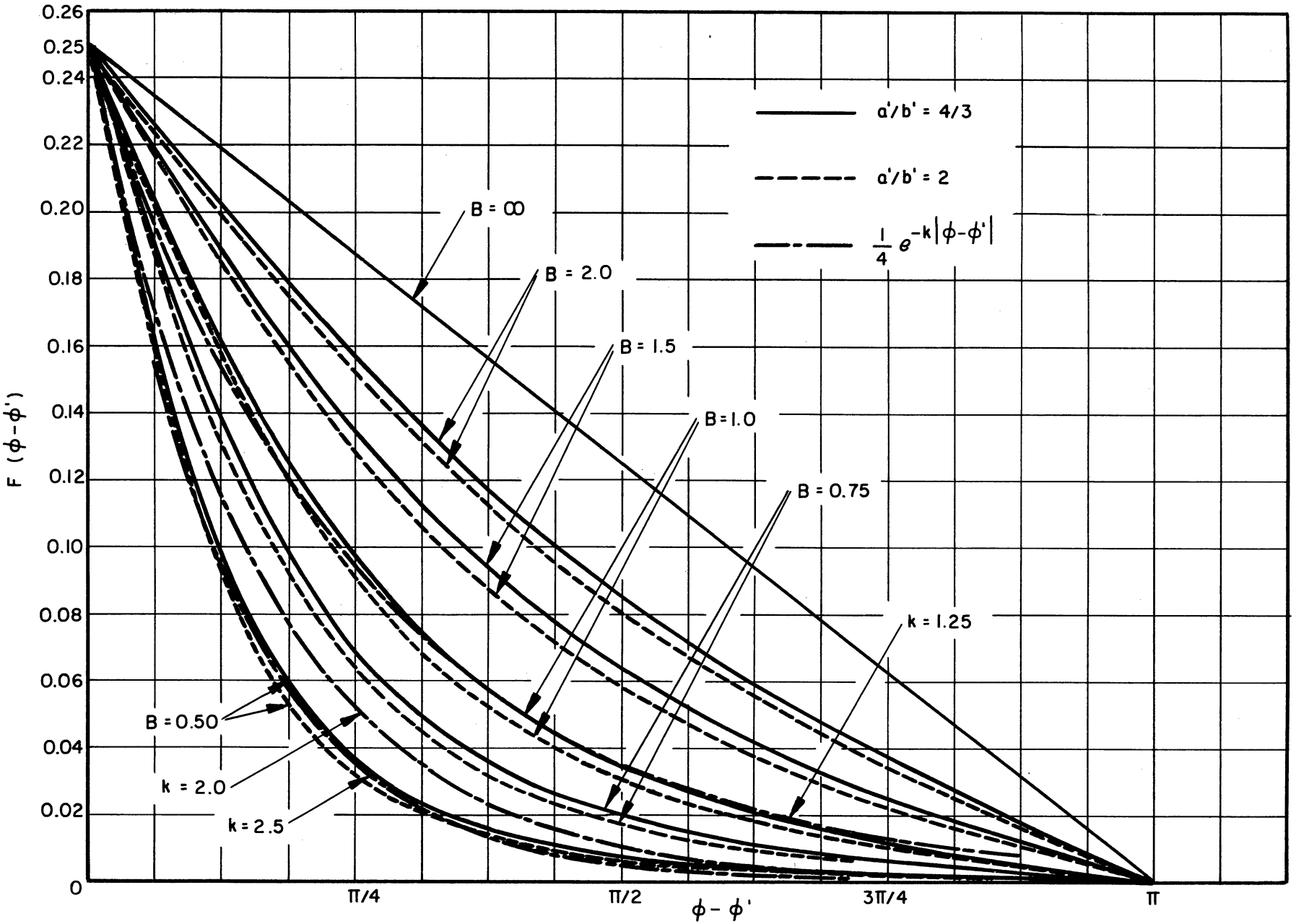

FIG. II.8 SPACE-CHARGE-FIELD WEIGHTING FUNCTION.

gave optimistic efficiencies for small values of QC. It did not appreciably affect values of QC greater than 0.125, however.

Efficiency calculations are shown in Fig. II.9 and are compared with Tien's results wherever possible. The results given are more extensive than Tien's and hence complete comparison is not possible. It is seen that the agreement is excellent when one uses the correspondence between B and k given in Eq. II.54. Efficiencies are calculated for various values of the stream diameter B assuming no radial dependence of either the circuit or space-charge fields. The effect of radial variations will be treated later. The saturation tube length is seen to depend slightly upon the stream diameter as shown in Fig. II.10. The relatively small discrepancies noted in comparing efficiencies could arise because of the departure of the k = 1.25 weighting function curve from the B = 1.0 curve for small values of $\Phi-\Phi'$. Since it is these closely spaced electrons that are most important, this difference can be reflected in the results.

The excellent agreement between these calculations reflects the equivalence between the equations as demonstrated and discussed in the previous sections.

5. Radial Electric Field Variations. All of the previous calculations were made, and the theories developed for the nonlinear amplifier with the assumption that the stream is confined by an infinite focusing field so that no radial electric motion is allowed. It was also assumed that there is no variation of the electric field due to either the circuit or the space-charge components in the radial direction. The principal reason for making these assumptions was to simplify the equations and hence shorten the computing time required for obtaining solutions. It is believed that the effects of radial field variations and radial motion are most important when the stream

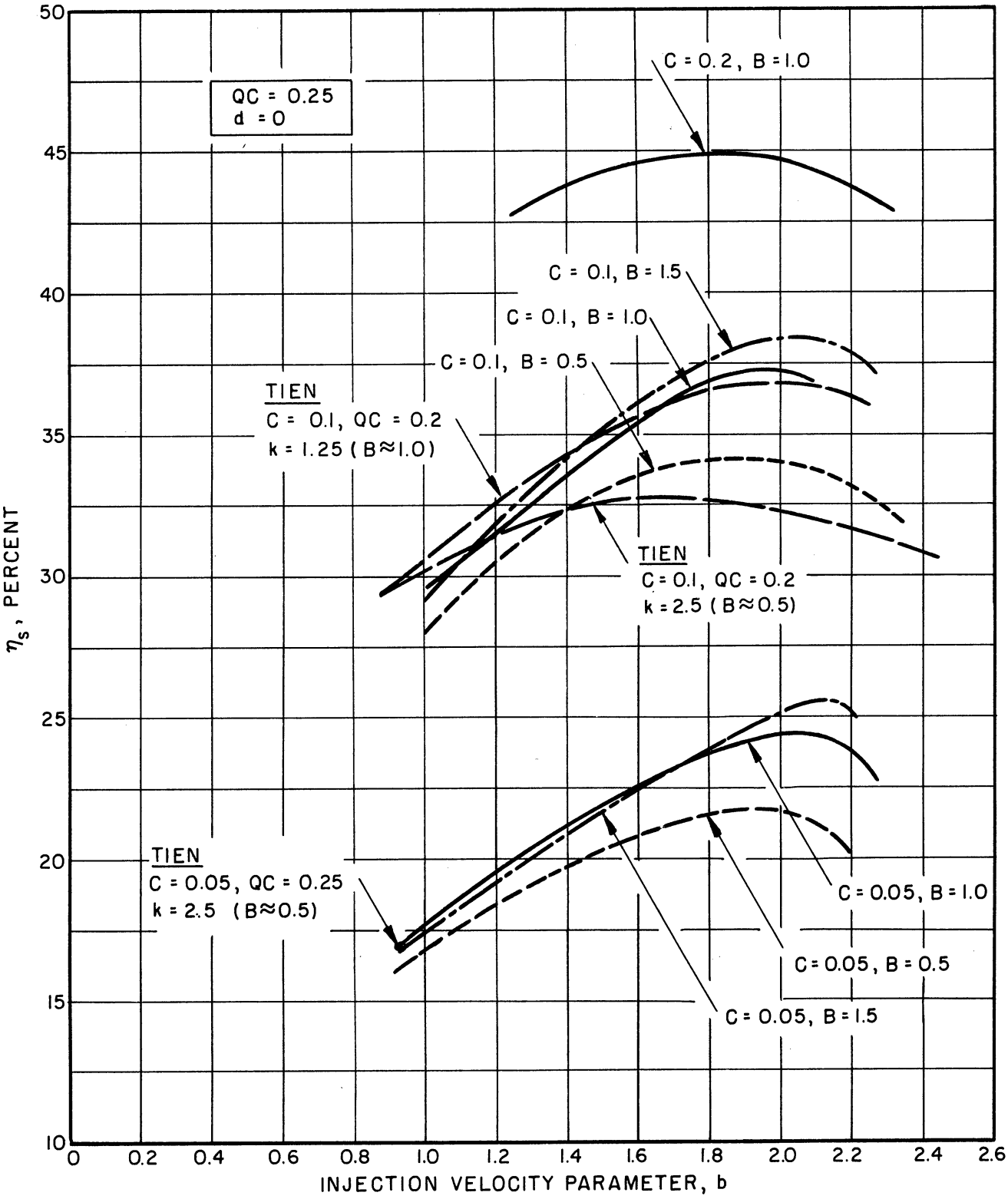

FIG. II.9 SATURATION EFFICIENCY VS. INJECTION VELOCITY PARAMETER. (QC = 0.25, d = 0)

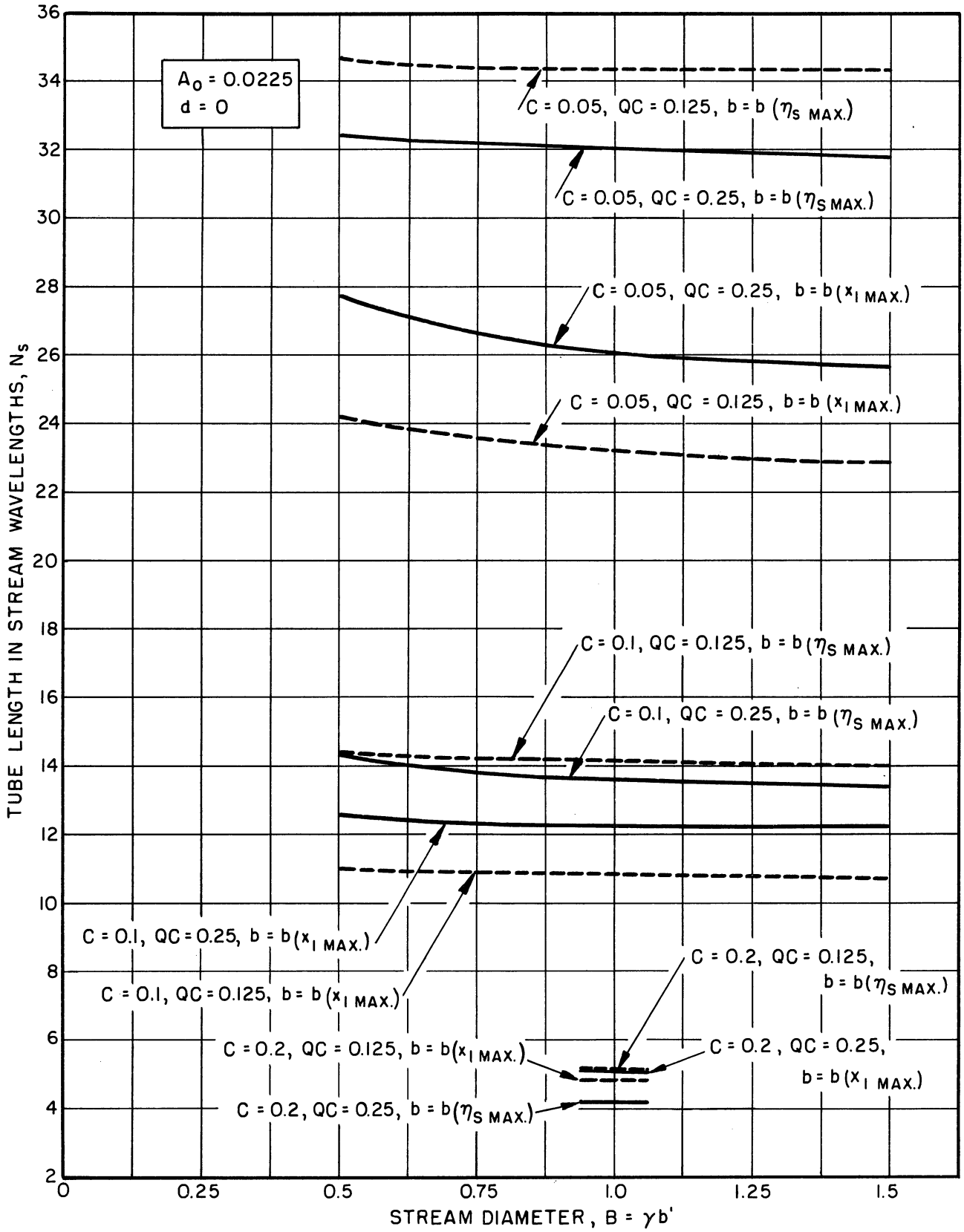

FIG. II.10 DEVICE LENGTH AT SATURATION VS. STREAM DIAMETER. (ψ = −30 db, d = 0)

diameter B is large. Some experimental information on this point has been given by Cutler[16]. It is interesting to include the effect of a radial variation of the circuit field to see its effect on the saturation efficiency.

It is felt that under certain conditions this effect is more important than rippling of the stream boundary or space-charge field dependence on radius. The working equations as developed elsewhere by the author[12] constitute four equations; two are circuit equations, one relates the dependent variables and the fourth is a combination of the force and continuity equations. In order to account for the radial circuit field variations it is assumed that the potential is given by

$$V(b',y,\Phi) = \mathrm{Re}\left[\frac{Z_o I_o}{C} A(y) f(B) e^{-j\Phi}\right] , \qquad \text{(II.55)}$$

where the variables are defined elsewhere[12] and $\gamma b' = B$. The stream radius is given by b'. The form of f(B) will depend upon whether the stream is a thin hollow stream or a solid one. The following expressions give this function for the two stream types

$$f_h(B) = \frac{I_o(\gamma b')}{I_o(\gamma a')} \quad \text{for thin hollow streams} , \qquad \text{(II.56a)}$$

$$f_s(B) = \frac{[I_o^2(\gamma b') - I_1^2(\gamma b')]^{1/2}}{I_o(\gamma a')} \quad \text{for solid streams.} \qquad \text{(II.56b)}$$

The circuit is located at radius a'. Introduction of Eq. II.55 into the circuit equation does not change the left-hand side since the

16. Cutler, C. C., "The Nature of Power Saturation in Traveling-Wave Tubes", BSTJ, vol. 35, pp. 841-876; July, 1956.

circuit is located at a', where f(B) is unity. However, the right-hand side of the circuit equation represents the effect of the space charge in the beam and hence is reduced by the coupling factor f(B). This can be handled either directly or indirectly as long as the effective beam space charge is reduced. The working equation relating dependent variables is not changed. The working equation (force equation), which includes the circuit and space-charge field components, is modified by the inclusion of f(B). The above equations become, upon introduction of the modified potential as defined in Eq. II.55

$$\ddot{A}(y) - A(y)\left[\left(\frac{1}{C} - \dot{\theta}(y)\right)^2 - \frac{(1+Cb)^2}{C^2}\right] = \frac{(1+Cb)f(B)}{\pi C}\left[\int_0^{2\pi} \frac{\cos\Phi(y,\Phi_0')d\Phi_0'}{1+2Cu(y,\Phi_0')}\right.$$

$$\left. + 2Cd\int_0^{2\pi} \frac{\sin\Phi(y,\Phi_0')d\Phi_0'}{1+2Cu(y,\Phi_0')}\right] \quad , \text{(II.57)}$$

$$A(y)\left[\ddot{\theta}(y) - \frac{2d}{C}(1+Cb)^2\right] + 2\dot{A}(y)\left(\dot{\theta}(y) - \frac{1}{C}\right)$$

$$= \frac{(1+Cb)f(B)}{\pi C}\left[\int_0^{2\pi} \frac{\sin\Phi(y,\Phi_0')d\Phi_0'}{1+2Cu(y,\Phi_0')}\right.$$

$$\left. - 2Cd\int_0^{2\pi} \frac{\cos\Phi(y,\Phi_0')d\Phi_0'}{1+2Cu(y,\Phi_0')}\right], \text{(II.58)}$$

and

$$\dot{u}(y,\Phi_o)\,[1+2Cu(y,\Phi_o)] = f(B)A(y)[1-C\dot{\theta}(y)]\sin\Phi(y,\Phi_o)$$

$$- Cf(B)\dot{A}(y)\cos\Phi(y,\Phi_o) + \frac{1}{1+Cb}\left(\frac{\omega_p}{\omega C}\right)^2 \int_0^{2\pi} \frac{F(\Phi-\Phi')d\Phi_o'}{1+2Cu(y,\Phi_o')} \quad . \qquad (II.59)$$

The dots above $A(y)$, $\theta(y)$ and $u(y,\Phi_o)$ represent differentiation with respect to y.

The conversion efficiency is given by

$$\eta = \frac{P}{I_o V_o} = 2CA^2(y)\,\frac{(1-C\dot{\theta}(y))}{1+Cb} \quad . \qquad (II.60)$$

It has been shown previously that the last factor in Eq. II.60 is approximately unity under all conditions. The above method of calculating nonlinear performance of a traveling-wave amplifier when $f(B) \neq 1$ results in a reduced r-f voltage along the structure and a reduced coupling to the stream. This results in an increased length to reach saturation. Since f(B) is a field reduction factor, it is easily shown that the effective C is reduced by $f^{2/3}(B)$ and hence the efficiency is reduced by this same factor in the regime where the efficiency is linearly related to C.

Nonlinear calculations of efficiency when f(B) is included have been carried out for a particular value of C and QC and two values of b. The resulting saturation efficiency normalized to the efficiency for unit coupling between the stream and the circuit is shown in Fig. II.11 as a function of B along with f(B) and $f^{2/3}(B)$. The efficiency reduction as a function of B can be approximately written as

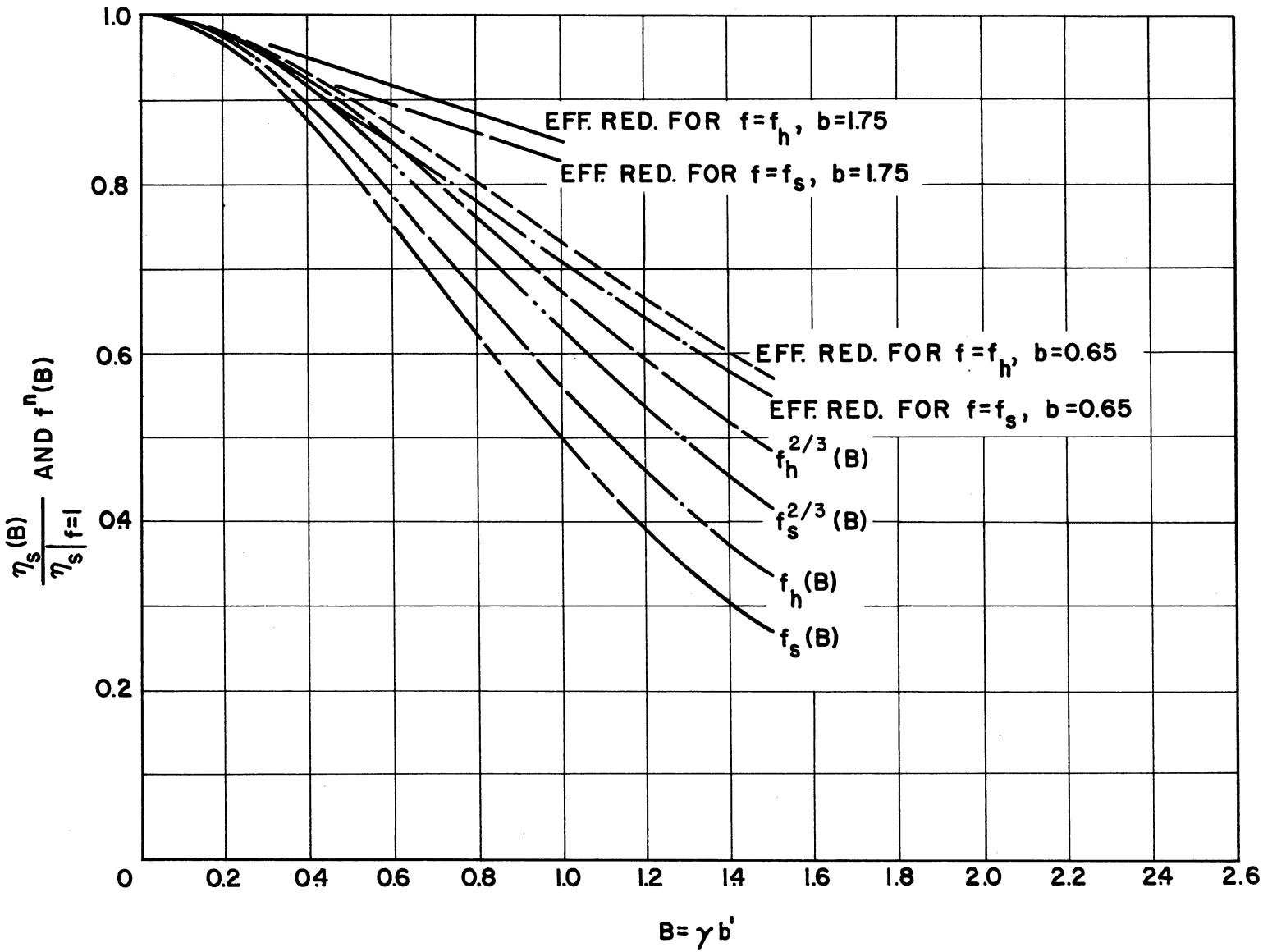

FIG.II.11 FIELD REDUCTION FACTOR AND EFFICIENCY REDUCTION VS. STREAM DIAMETER. (C=0.1, QC=0.125, d=0, a'/b'=2)

$$\frac{\eta_s(B)}{\eta_s\Big|_{f=1}} \approx f^{1/2}(B) \qquad \text{for} \quad b = b(x_1 \max) \quad , \tag{II.61a}$$

$$\frac{\eta_s(B)}{\eta_s\Big|_{f=1}} \approx f^{1/4}(B) \qquad \text{for} \quad b = b(\eta_s \max) \quad . \tag{II.61b}$$

This approximate method of evaluating field reduction effects on efficiency is in approximate agreement with Nordsieck's[11] two-beam approach for the small-C equations neglecting space-charge effects. A more accurate approach to the problem without accounting for radial motion would be to divide the stream into a number of annular rings and to solve the equations simultaneously, weighting the contributions of each stream according to its coupling to the circuit. The results shown in Fig. II.11 agree well with experimental results as given by Cutler[16].

6. Conclusions. The equivalence of the integral and differential equation methods of formulation of the nonlinear traveling-wave tube analysis has been formally demonstrated and the two different methods of treating the space charge have been shown to be essentially equivalent.

The effect of radial circuit field variations on the saturation efficiency has been approximately treated and it is seen that the efficiency reduction is given by $f^{1/2}(B)$ for $b(x_1 \max)$ and $f^{1/4}(B)$ for $b(\eta_s \max)$ when the coupling between the stream and the circuit is not unity.

D. Effect of a Beam Premodulation

1. Velocity Modulation. A small-signal theory has been developed to calculate the effect on gain of a premodulation of the electron stream in either a traveling-wave amplifier or a Crestatron. In the case of a velocity modulation of the stream by a small-amplitude voltage across a pair of short-transit-angle grids, the following relations between the velocities and currents associated with the slow and fast space-charge waves exist

$$v_{1s} = v_{1f} \quad , \tag{II.62}$$

and

$$i_{1s} = - i_{1f} \quad . \tag{II.63}$$

The expression for determining the wave amplitudes excited on the r-f circuit by such a premodulated stream is

$$\frac{V_{ci}}{V_g} = \frac{r_i}{s_i}\left\{Ae^{-j\Phi} + jC\left[\left(\frac{C\omega}{\omega_q}\right) f_i \sin \beta_q z - g_i \cos \beta_q z\right]\right\} , \tag{II.64}$$

where $A \triangleq V_c/V_g$, the fraction of modulating voltage at frequency ω applied to the r-f structure,

$4QC \triangleq \left(\frac{\omega_q}{C\omega}\right)^2$, the space-charge factor in the drift region preceding the circuit, and

$\beta_q z \triangleq$ the radian plasma drift length from the modulating structure to the input plane of the r-f structure.

The following quantities were used in Eq. II.64 to give the simple form

$$\alpha_i = 1 + jC\delta_i \quad , \tag{II.65a}$$

$$a_i = \frac{\delta_{i+1}\,\delta_{i+2}}{\delta_{i+1} - \delta_{i+2}} \quad , \tag{II.65b}$$

$$e_i = \delta_i/\alpha_i \quad , \tag{II.65c}$$

$$f_i = a_i \left[e_{i+1} - e_{i+2} \right] - 4QC\alpha_i \quad , \tag{II.65d}$$

$$g_i = a_i \left[\frac{e_{i+1}}{\delta_{i+2}} - \frac{e_{i+2}}{\delta_{i+1}} \right] \quad , \tag{II.65e}$$

$$r_i = 1 + \frac{4QC}{e_i^2} \quad , \tag{II.65f}$$

$$s_i = 1 + \frac{\delta_{i+1} e_{i+1} \left[\delta_{i+2} - \delta_i \right] + \delta_{i+2} e_{i+2} \left[\delta_i - \delta_{i+1} \right]}{\delta_i e_i \left[\delta_{i+1} - \delta_{i+2} \right]} \quad . \tag{II.65g}$$

Circuit effects are considered by replacing β_p by β_q and it is assumed that the factor ω_q/ω is the same in the drift region as in the interaction region.

2. Determination of Optimum Drift Length. Equation II.64 may be used to compute the individual wave amplitudes excited on the r-f structure as a function of the operating parameters and the drift length between the modulating grid or cavity and the entrance to the interaction region. There is an optimum value of $\beta_q L$ for excitation of any particular wave and this optimum value will be determined for several cases.

In Eq. II.64 for the circuit wave amplitudes the first term $Ae^{-j\Phi}$ represents the fraction of the stream modulating voltage applied to the r-f structure. It is assumed that neither A nor Φ are functions of $\beta_q z$. The second and third terms on the right-hand side represent

the contributions of the modulation in exciting the various waves on the r-f circuit.

The optimum (maximum) excitation of any wave will occur when the vector amplitudes of the applied signal and the modulation add in phase. The quantity V_{ci}/V_g will be maximized separately by the applied circuit voltage and the modulation. The next step is to take the derivative of the absolute value of Eq. II.64 with respect to $\beta_q z$ with $A = 0$. In the region of growing-wave gain the incremental propagation constants δ_i are complex and hence the coefficients of $\sin \beta_q z$ and $\cos \beta_q z$ are complex. Equation II.64 is rewritten in the following form

$$\frac{V_{ci}}{V_g} = (a_i + jb_i) \sin \beta_q z + (c_i + jd_i) \cos \beta_q z \quad , \qquad \text{(II.66)}$$

where a_i through d_i are functions of the δ's and the parameters. The result of taking the derivative of the square of the absolute value of Eq. II.66 and setting it equal to zero at $\beta_q L$ is

$$(\beta_q L)_{i,v} = \frac{1}{2} \arctan \frac{-2(a_i c_i + b_i d_i)}{\left(a_i^2 + b_i^2 - c_i^2 - d_i^2\right)} \quad . \qquad \text{(II.67)}$$

Since a_i, b_i, c_i and d_i are all real quantities then $\beta_q z$ will be real. Equation II.66 gives the predrift length for both maximum and minimum excited wave amplitudes and it is simplest to substitute the results of Eq. II.67 back into Eq. II.64, for particular values of A and Φ and test for a maximum. The maxima and minima are separated by a quarter space-charge wavelength. Equation II.67 gives the condition for maximizing the effect of the modulation and then an absolute maximum in the excited wave amplitude is obtained by adjusting Φ so that the applied circuit voltage adds in phase with the induced voltage due to the modulation.

Also it should be noted that Eq. II.67 may be used to determine the optimum value of $\beta_q L$ for any one of the three waves. The subscript (i,v) on the left-hand side indicates that velocity modulation is being considered for optimization of the ith wave. The most interesting cases are possible for i = 1 (the growing wave) and i = 3 (the fast wave).

The Crestatron forward-wave amplifier operates in a regime where $x_i = 0$ and hence the propagation constants are purely imaginary and the wave amplitudes purely real. Thus the waves propagate along the r-f structure with constant amplitudes and differing phase velocities. The two principal waves are 180 degrees out of phase at the input and the length is chosen so that they add in phase at the output. These two conditions are given below.

$$\frac{V_c}{V_g} = \frac{V_{c1}}{V_g} + \frac{V_{c2}}{V_g} + \frac{V_{c3}}{V_g} \quad \text{at} \quad z = 0 \quad , \tag{II.68}$$

and

$$\frac{V_c(z)}{V_g} = \left|\frac{V_{c1}}{V_g}\right| + \left|\frac{V_{c2}}{V_g}\right| + \left|\frac{V_{c3}}{V_g}\right| \quad \text{at} \quad z = L \quad . \tag{II.69}$$

Under modulation conditions the wave amplitudes are given by Eq. II.64. The gain at any point along the structure is proportional to the square of the magnitude of the r-f voltage.

$$\left|\frac{V_c(\theta)}{V_g}\right|^2 = \left| \sum_{i=1}^{3} \left(\frac{V_{ci}}{V_g}\right) e^{\delta_i \theta} \right|^2 \quad , \tag{II.70}$$

where $\theta \triangleq \beta_e C_z = 2\pi C N_s$.

In order to maximize the effect of the modulation a value of θ will be chosen to give maximum beating-wave gain.

$$\theta_{opt.} = \frac{\pi}{2(\Delta b)^{1/2}} \quad , \tag{II.71}$$

where $b_{x_1=0}$ is the positive b for which growing-wave gain ceases and $\Delta b \triangleq b - b_{x_1=0}$. The value of $\beta_q z$ is then determined to maximize the effect of modulation. Finally the phase parameter Φ is optimized so that the circuit voltages due to the applied signal and the modulation combine to give an absolute maximum. The optimum value of $\beta_q z$ will be determined with A = 0.

Combining Eqs. II.64 and II.70 gives

$$\left|\frac{V_c(\theta)}{V_g}\right|^2 = \left| \sum_{i=1}^{3} \frac{jCr_i}{s_i} \left[\left(\frac{C\omega}{\omega_q}\right) f_i \sin \beta_q z - g_i \cos \beta_q z \right] e^{\delta_i \theta} \right|^2 . \tag{II.72}$$

The coefficients of $\sin \beta_q z$ and $\cos \beta_q z$ in Eq. II.72 are in general complex and hence Eq. II.72 may also be written as

$$\left|\frac{V_c(\theta)}{V_g}\right|^2 = \left| \sum_{i=1}^{3} \left[(a_i + jb_i) \sin \beta_q z + (c_i + jd_i) \cos \beta_q z \right] \right|^2 . \tag{II.73}$$

Maximizing Eq. II.73 with respect to $\beta_q z$ yields the following relationship

$$(\beta_q z)_v = \frac{1}{2} \arctan \frac{-2(AC + BD)}{A^2 + B^2 - C^2 - D^2} \quad , \tag{II.74}$$

and

$$A \triangleq \sum_{i=1}^{3} a_i \quad ,$$

$$B \triangleq \sum_{i=1}^{3} b_i \quad ,$$

$$C \triangleq \sum_{i=1}^{3} c_i \quad ,$$

and

$$D \triangleq \sum_{i=1}^{3} d_i \quad .$$

3. Discussion of Linear Analysis Results. The equation derived above (Eq. II.64) for calculating the wave amplitudes excited under modulation may be used to obtain results for the growing-wave amplifier. In order to carry out a calculation one must select values of C, QC, d and b and then optimize the desired wave amplitude with respect to Φ and $\beta_q z$. In the case of the growing-wave amplifier it is usually desired to maximize the gain and hence wave one is optimized. For other applications such as parametric amplifier couplers it may be desirable to optimize the fast wave and this may be accomplished through the same procedure.

A linear analysis of the effects of premodulation of an electron stream can give only information on the optimum phase angles to be employed and a measure of how much improvement in the small-signal gain can be achieved. In the case of the growing-wave amplifier the gain is directly proportional to the length; hence we have to select a particular length to investigate the improvement in gain due to premodulation.

Since the Crestatron amplifier is a moderate-gain amplifier there will be more than one r-f wave present over an appreciable fraction of its length and hence all three waves must be considered in calculating the output r-f voltage. Equation II.73 gives the output voltage at any θ plane as a function of C, QC, d, b, θ and $\beta_q z$. The optimum predrift angle to be used is obtained from Eq. II.74.

A premodulation of the electron stream going into an r-f structure operated in the Crestatron regime results in an increase of the gain obtainable at the first maximum of the gain curve and tends to change the optimum length slightly. This shift in the maximum gain point is insignificant and simply represents an increase in the gain off of the center frequency. Since the effect of premodulation on the small-signal gain is directly proportional to C, it is reasonable that the improvement in gain will be greatest at high C. Since the magnitube of the gain is inversely proportional to Δb, so will be the improvement in gain due to premodulation.

A summary of the calculated results for premodulation of the traveling-wave amplifier and the Crestatron was given in Quarterly Progress Report No. 9 on this contract and will not be repeated here. A technical report has been written on this material and will be published under AF30(602)-2303.

E. General Large-Signal Traveling-Wave Amplifier Calculations

1. Introduction. During the period of this contract a number of large-signal studies, in addition to those cited earlier, have been carried out in an attempt to more fully understand and predict the characteristics of high-power amplifiers. Some of these studies have been completed while others are still in progress. The following material summarizes briefly this work.

2. General Design Procedure.[17] A general design procedure has been developed for the design of both low-power and high-power high-efficiency traveling-wave amplifiers. The design process is based on

17. Rowe, J. E., Sobol, H.,"General Design Procedure for High-Efficiency Traveling-Wave Amplifiers", Trans. PGED-IRE, vol. ED-5, No. 4, pp. 288-300; October, 1958.

the selection of optimum values, for highest efficiency, of the design parameters C, QC, B and b from the large-signal curves and design of an amplifier with the particular type of r-f structure specified by power and bandwidth requirements and operating parameters as near the optimum values as possible. In cases where the optimum design parameters cannot all be realized simultaneously, the design engineer is able to select the parameter that he wishes to adjust. A technical report and a journal article have been published on this work.

3. Power Output and Bandwidth[18]. Theoretical expressions have been developed to calculate the power output of traveling-wave amplifiers using an arbitrary r-f structure. Specific calculations were made for helix-type tubes and it was shown how to evaluate the power output capabilities of tubes using other r-f structures in terms of the calculations made for helix tubes. The principal factors accounting for higher power output of dispersive structures were presented and discussed.

The small-signal theory was used to calculate the gain and bandwidth of forward-wave helix amplifiers as a function of frequency. For high-$\gamma_0 a'$ tubes the gain in db times the frequency bandwidth is a constant as a function of helix length, whereas the gain times the bandwidth squared is a constant for low $\gamma_0 a'$ devices. This is expressed mathematically as

18. Sobol, H., Rowe, J. E., "Theoretical Power Output and Bandwidth of Traveling-Wave Amplifiers", Trans. PGED-IRE, vol. ED-7, No. 2, pp. 84-95; April, 1960.

High $\gamma_o a'$:

$$G_{db}BW = \frac{2f(\omega)M}{a_1} \tag{II.75}$$

Low $\gamma_o a'$:

$$G_{db}(BW)^2 = \frac{4M}{a_2} f(\omega) \quad . \tag{II.76}$$

4. Effect of Circuit Loss. It is well known that the presence of attenuating material along the TWA r-f structure seriously affects the saturation performance. A program has been initiated to calculate the effect of loss on the saturation efficiency using the general large-signal equations. This work is presently underway and will be continued under AF 30(602)-2303 during the next year. As part of the program a detailed comparison with experiment will be made.

5. N-Beam Analysis. The one-dimensional nonlinear TWA analysis previously developed assumed that neither the circuit field nor the space-charge field has a radial dependence when the force on the electron is calculated. It has been shown[19] that the saturation efficiency is reduced, for large stream diameters, when a radial circuit field dependence is included. This analysis is approximate, since the space-charge field was not assumed to depend on radius and also radial motion of the electrons was neglected.

Another method for handling this two-dimensional problem in an approximate manner would be to divide the stream into N annular streams, each having a different coupling to the circuit. The space-charge field will be calculated in the same way that was used in the one-dimensional

---

19. Rowe, J. E., "One Dimensional Traveling-Wave Tube Analyses and the Effect of Radial Electric Field Variations" Trans. PGED-IRE, vol. ED-7, No. 1, pp. 16-22; January, 1960.

theory except that each stream would be represented by a different space-charge field weighting function, $F(\Phi-\Phi')$. It is assumed that each stream carries the same current I_o/N and since all streams are assumed to move forward at the same velocity the space-charge density, $\rho_o = I_o/u_o$, is the same for all streams.

This problem has been programmed for the IBM-704 computer and some computations have been completed. The work will be completed under AF 30(602)-2303 and will be reported later.

III. PHASE FOCUSING IN TRAVELING-WAVE TUBES (J. G. Meeker)

A. Limitation on Conversion Efficiency in O-Type Devices

The basic principle of operation of O-type devices is the transferral of kinetic energy from an electron beam to a traveling r-f field. In principle this mechanism has an inherent advantage over other mechanisms since the spent beam might be collected at low potential, thereby guaranteeing high conversion efficiency. As a practical fact, however, two effects tend to prevent anything like complete conversion. First the electron bunches slip out of proper phase with the nearly constant-velocity traveling-wave as they give up energy and then they begin to extract rather than supply energy. Also, the individual electrons comprising the bunches accumulate a velocity spread which smears out the bunch and prevents all electrons from being collected at the same velocity. So the two effects, bunch slipping and velocity spreading, act together to limit the efficiency.

It has been the purpose of this study to investigate methods for controlling the first of these defects, i.e., bunch slipping, in a

traveling-wave amplifier. The plan has been to hold the electron bunches in favorable phase positions as long as possible to enhance the conversion efficiency. The specific approach was to introduce spatially varying parameters into the problem where constant parameters had existed before. It was recognized that the adjustment of gross tube parameters would not help much in preventing velocity spreading, a more detailed problem.

B. Methods of Phase Focusing

Certain basic methods for phase focusing the electron bunches in a traveling-wave amplifier come to mind:

1.) Prebunching the beam,

2.) Varying the circuit parameter, e.g., varying the pitch of the helix.

3.) Inserting a d-c electric gradient.

4.) A combination of these.

Each method accomplishes the same purpose. The electron bunches are moved forward relative to the circuit field at a time when they are slipping back due to loss of kinetic energy. Prebunching makes sure the bunch is in an optimum phase position from the beginning of the interaction region by carefully adjusting the injection phase of preformed bunches. Varying the pitch accomplishes the focusing by slowing down the circuit wave as the beam slows down. The d-c gradient supplies added energy to the beam to keep it in step with a constant-velocity circuit wave. To date we have concluded the large-signal prebunched beam studies, and are currently working on the variable-pitch and d-c gradient programs.

C. The Basic Large-Signal Traveling-Wave Amplifier Equations

The large-signal traveling-wave amplifier equations appear in the literature[1,2]. The approach used here follows the method used by Rowe. However, the transmission line equation has been modified to allow for spatially varying inductance and capacitance and the force equation has been augmented to include a d-c gradient term. The normalized lossless equations are

$$\frac{d^2A(y)}{dy^2} - A(y)\left[\left(\frac{1}{C_o} - \frac{d\theta(y)}{dy}\right)^2 - \left(\frac{1+C_o b(y)}{C_o}\right)^2\right] - \frac{dA(y)}{dy}\left[3\frac{d}{dy}\ln C(y)\right.$$

$$\left. + \frac{C_o}{1+C_o b(y)}\frac{db(y)}{dy}\right] = -\frac{1+C_o b(y)}{\pi C_o}\frac{C^3(y)}{C_o^3}\int_0^{2\pi}\frac{\cos\Phi(y,\Phi_o')d\Phi_o'}{1+2Cu(y,\Phi_o')}, \quad \text{(III.1)}$$

$$A(y)\left[\frac{d^2\theta(y)}{dy^2} + 3\frac{d}{dy}\ln C(y) + \frac{C_o}{1+C_o b(y)}\left(\frac{1}{C_o} - \frac{d\theta}{dy}\right)\frac{db(y)}{dy}\right]$$

$$+ 2\left(\frac{d\theta(y)}{dy} - \frac{1}{C_o}\right)\frac{dA}{dy} = -\frac{1\pm C_o b(y)}{\pi C_o}\frac{C^3(y)}{C_o^3}\int_0^{2\pi}\frac{\sin\Phi(y,\Phi_o')d\Phi_o'}{1+2Cu(y,\Phi_o')}, \quad \text{(III.2)}$$

$$\frac{d\theta(y)}{dy} + \frac{\partial\Phi(y,\Phi_o)}{\partial y} = \frac{2u(y,\Phi_o)}{1+2C_o u(y,\Phi_o)}, \quad \text{(III.3)}$$

---

1. Rowe, J. E., "A Large-Signal Analysis of the Traveling-Wave Amplifier: Theory and General Results", Trans. PGED-IRE, vol. ED-3, pp. 39-57; January, 1956.

2. Tien, P. K., "A Large-Signal Theory of Traveling-Wave Amplifiers, Including Effects of Space Charge and Finite Coupling Between Beam and Circuit", BSTJ, vol. 35, pp. 349-374; March, 1956.

$$\frac{\partial u(y,\Phi_o)}{\partial y}\left[1+2C_o u(y,\Phi_o)\right] = -A(y)\left(\frac{C}{C_o}\right)^{3/2}\left[1-C_o\frac{d\theta(y)}{dy}\right]\sin\Phi(y,\Phi_o)$$

$$+ C_o\left(\frac{C}{C_o}\right)^{3/2}\frac{dA(y)}{dy}\cos\Phi(y,\Phi_o) + C_o\frac{dA_{dc}(y)}{dy}$$

$$+ \frac{1}{1+C_o b_o}\left(\frac{\omega_p}{\omega C_o}\right)\int_0^{2\pi}\frac{F(\Phi-\Phi')d\Phi_o'}{1+2C_o u(y,\Phi_o')} \quad . \qquad \text{(III.4)}$$

Of these, Eqs. III.1 and III.2 are derivable from the transmission line equation, Eq. III.4 is the force equation, and Eq. III.3 relates certain defined dependent variables. All variables are normalized.

For purposes of this discussion it is necessary to note only that $A(y)$ and $A_{dc}(y)$ are the r-f and d-c potentials, y is the distance, and $\theta(y)$ is the phase shift between the hot traveling wave and the projected input beam if there were no interaction. $\Phi(y,\Phi_o)$ and $2C_o u(y,\Phi_o)$ are the actual phase of each electron relative to the hot wave and its varying component of velocity respectively. The term $(\omega_p/\omega C)^2$ is proportional to the space-charge density and the factor $F(\Phi-\Phi')$ is a space-charge force weighting function accounting for the profile of the force field under a particular tube geometry.

The velocity variation of the transmission line is contained in a new modified definition of the velocity parameter b relating the electron injection velocity u_o to the cold phase velocity of the structure v_o. Before where v_o was a constant, it is now allowed to vary. Thus

$$1 + C_o b(y) \triangleq \frac{u_o}{v_o(y)} \quad . \qquad \text{(III.5)}$$

The impedance of the line is allowed to vary also. Thus the Pierce gain parameter C_o becomes a function of distance and shows up in several of the terms as $C(y)$.

As with the large-signal model used by Rowe this analysis assumes no charge variation across the beam. The space-charge force term is modified to account for transverse boundaries by introducing a plasma-frequency reduction factor. Electron trajectories are allowed to cross so that a Lagrangian formulation is necessary. Thirty-two electron groups per r-f cycle are fed time-sequentially into the tube and their velocity and phase positions are tracked through the tube. The IBM-704 digital computer solves the equations numerically.

D. Prebunched Beam Studies

In a conventional traveling-wave amplifier the first part of the tube serves to set up bunching or current modulation. The bunch forms in the decelerating field of the traveling wave since normal operation involves coupling to the slow space-charge wave. The exact phase position at which the bunch builds up is a function of the tube parameters, the chief one being the velocity parameter, b. One can adjust b to get maximum small-signal gain, which means that the bunch position is optimum at low signal levels. Or one can adjust b to get maximum efficiency, which means that the bunching is optimized at high signal levels. The fact that b in the second case is always larger indicates that more overrun velocity must be initially supplied to the beam to compensate for the loss of kinetic energy at high signal level. Thus this adjustment of the velocity parameter b is really a method of phase focusing since it controls the bunching behavior.

A more direct control over the bunching would be to prebunch the beam and then inject the modulated beam into the helix. It would appear

that short, high-efficiency tubes would result if one were to inject the beam so phased that the bunches enter the tube in the retarding circuit field. The overrun velocity and the injection phase angle of the bunches could be adjusted to extract a maximum amount of beam kinetic energy.

To investigate the upper limits on gain and efficiency which one might hope to achieve by prebunching the beam we chose ideal conditions. A delta function bunch 1/20th of a wavelength long having no velocity modulation was selected. The input phase of the bunches with respect to the r-f wave was also chosen to optimize efficiency. This was done by using different injection phases and selecting the value which proved best for a wide range of parameters. A value of 30 degrees behind the maximum decelerating field gave best results in almost all cases.

Runs were made to illustrate behavior under conditions of zero, medium, and high space-charge forces, and with many different drive levels. The conclusions were as follows:

1. Tube length at saturation is invariably shorter when prebunched injection is used. This is illustrated in Fig. III.1. There are two reasons for the short tube length. First, the bunches are preformed so no active helix length is needed for current modulation to accrue. Then too, the fact that the bunch injection phase and velocity are controllable enables one to dictate the bunch trajectory. Hence the bunch can be made to spend most of its time centered about the maximum decelerating field.

2. For low-space-charge force environments, prebunching leads to remarkable enhancement of efficiency, together with high gain in a short traveling-wave tube. The behavior in this case is nearly the same as in a ballistics problem. The electron bunches are injected into the

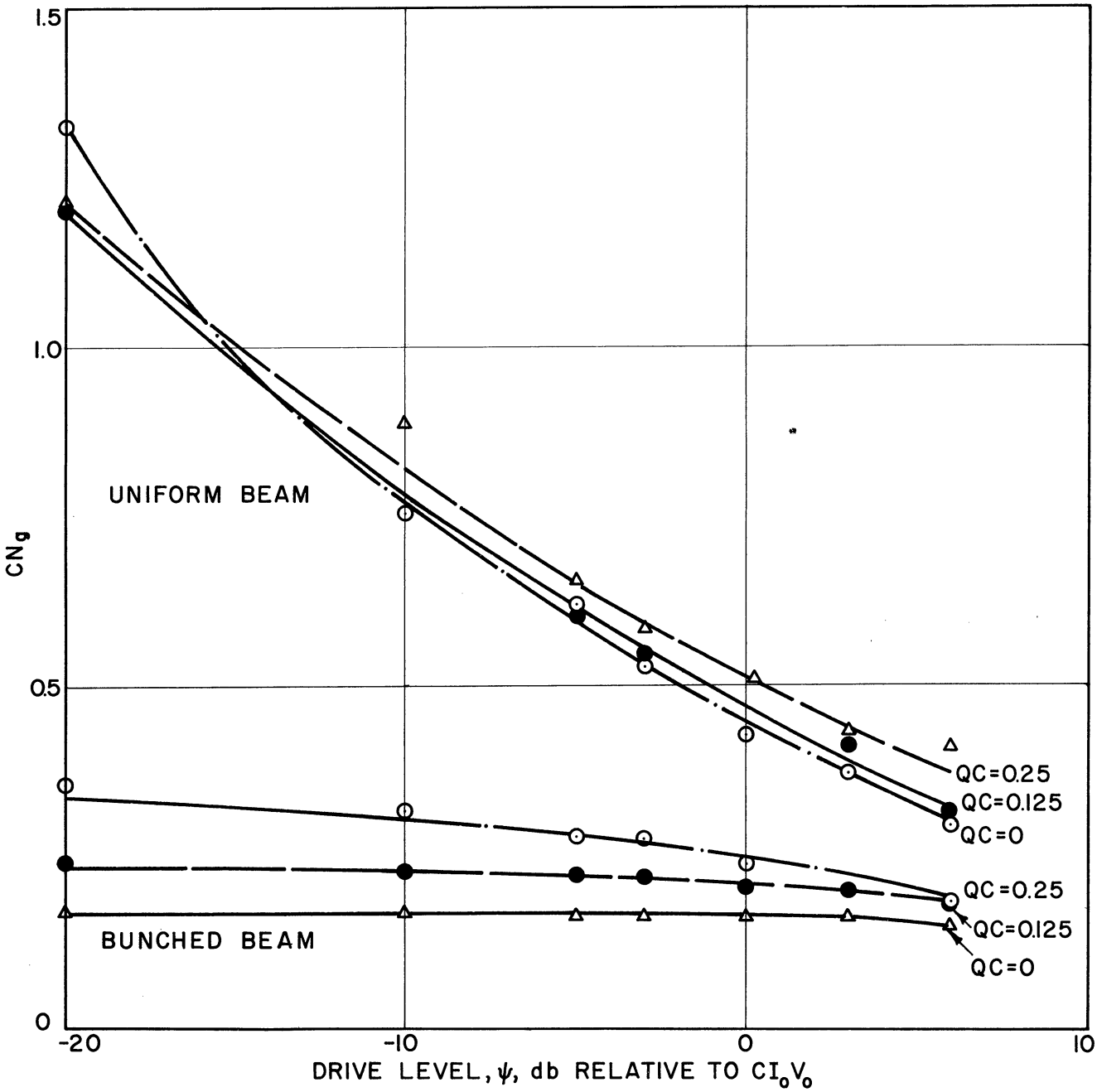

FIG. III.1 SATURATION TUBE LENGTH. (C=0.1, B=1.0, b=2.0)

retarding field of the traveling wave with just the proper overrun velocity to maintain them in a decelerating-field orbit until most of their kinetic energy is extracted. The smallest drive level which will accomplish this focusing is used in order to get high gain along with high efficiency.

Figure III.2 shows an efficiency-versus-drive-level plot and Fig. III.3 follows an electron bunch through the tube in a typical high-gain, high-efficiency run. It is interesting to analyze this case in detail. Note first that very little bunch spreading occurs. This, of course, is because space-charge forces are absent. The velocity spreading that does occur is due to the sinusoidal nature of the circuit field causing it to act differently on the various electrons in the bunch. Small as it is, this velocity spread does eventually set the upper limit on conversion efficiency at about 80 percent in this instance. The path of the bunch is easily followed from point to point along the tube. Note that the overrun injection velocity was chosen to be compatible with the signal drive level. The bunch was injected just behind the maximum decelerating field; it moved forward initially through the maximum field, losing kinetic energy all the while; it then slowed to synchronism with the wave at its most advanced phase position in the decelerating field; and finally it dropped back, slipping out of the retarding field with a small unspent kinetic energy. Since the drive level was not large, a high gain of about 30 db was realized along with the high efficiency.

Figure III.2 shows that even higher efficiencies can be theoretically obtained by using higher drive levels. Figure III.4 shows just why this is so. Once again a compatible injection velocity and drive level are chosen. In this case, however, the bunch orbit does not carry it quite so far forward in the retarding field before falling back.

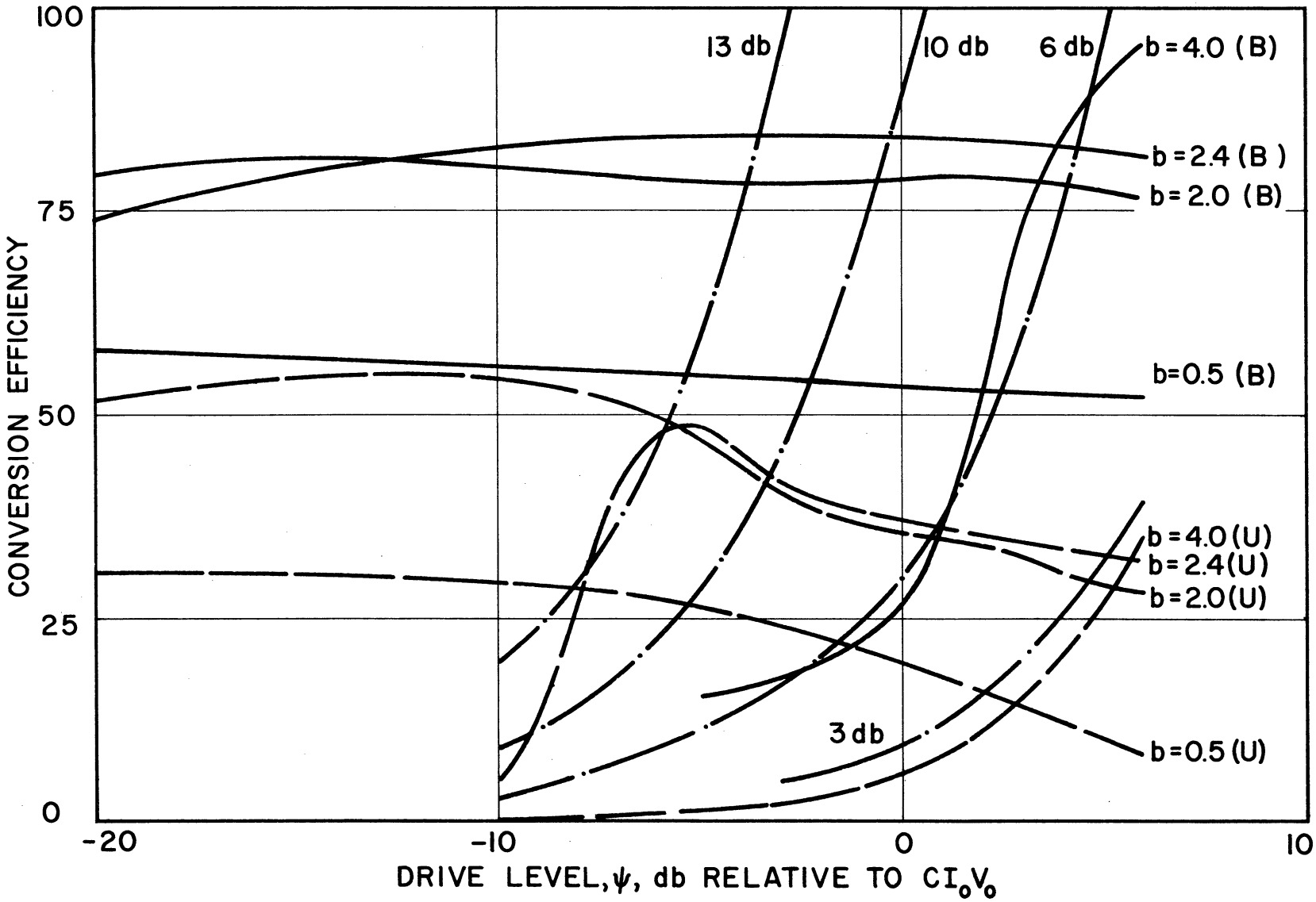

FIG. III.2 EFFICIENCY AND GAIN vs. DRIVE LEVEL. (C=0.1, B=1.0, QC=0)

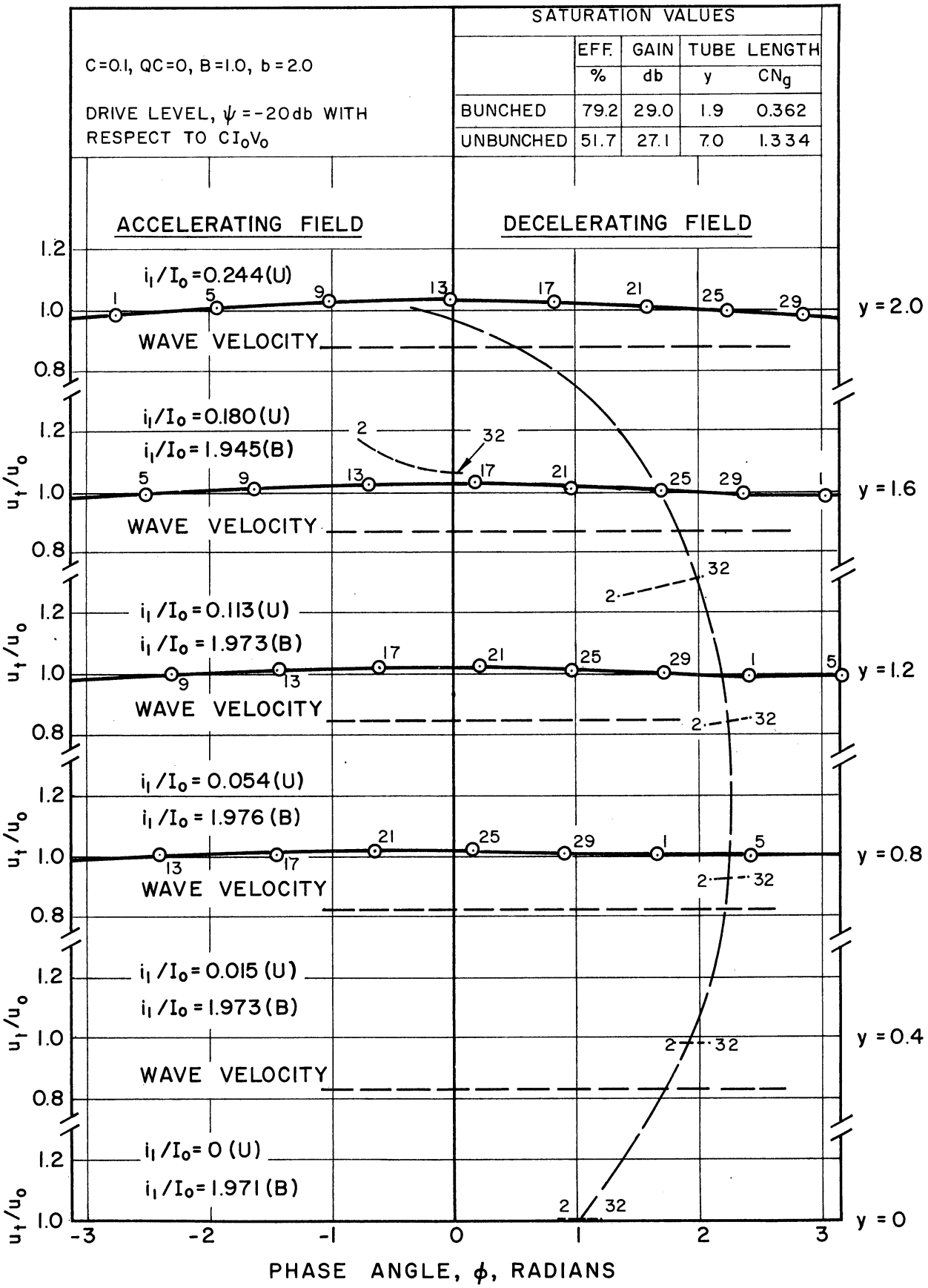

FIG. III.3 VELOCITY vs. PHASE.

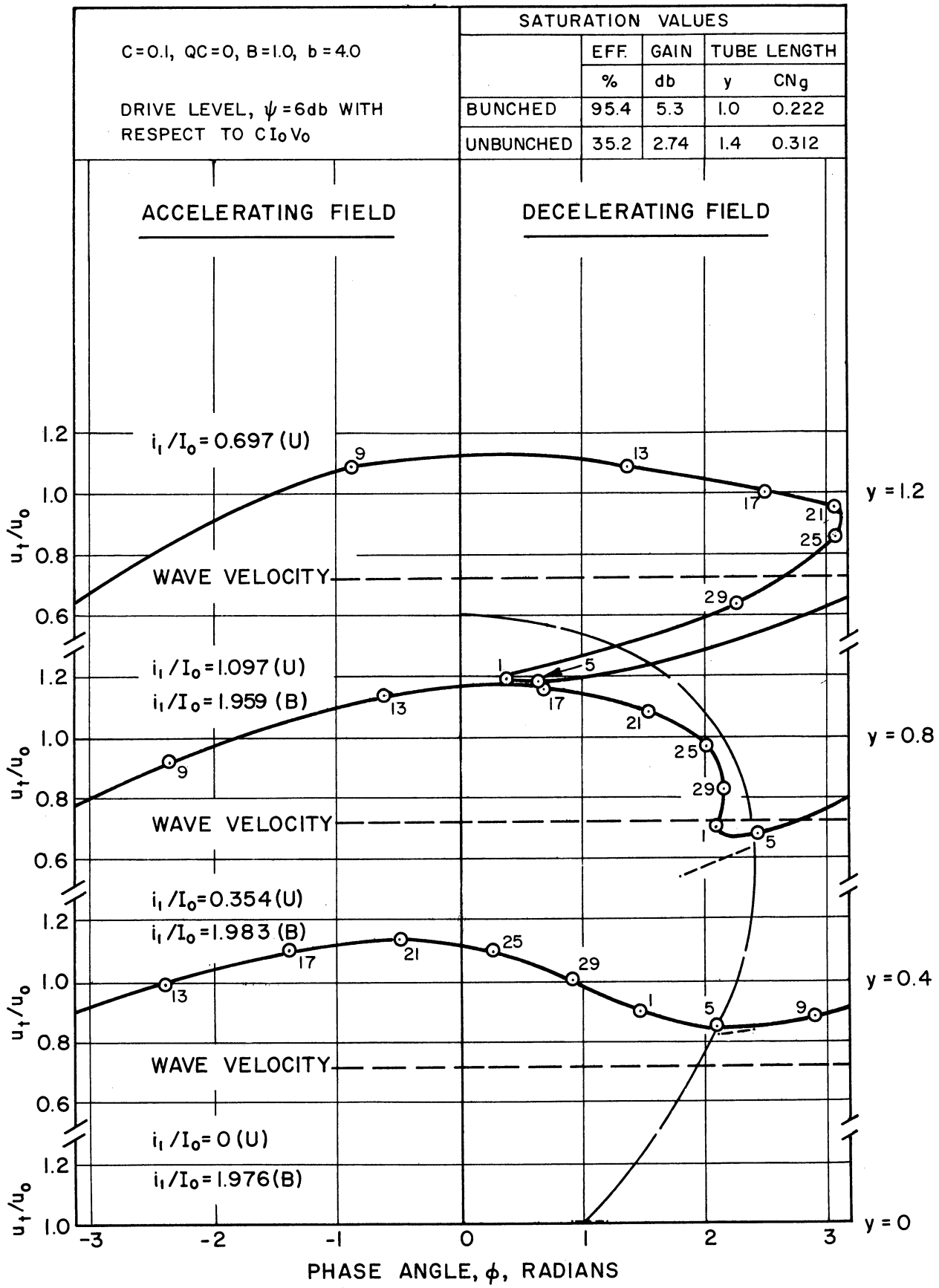

FIG. III.4 VELOCITY vs. PHASE.

Velocity spreading is less pronounced and a 96 percent conversion efficiency is obtained. However, the high drive level employed made for less gain despite the high energy extraction. Therefore the run shown in Fig. III.3 is preferred.

3. Prebunching the beam has little value in high-space-charge tubes. The reason is very clearly evident in Fig. III.5 which shows the progress of a bunch through a tube when space-charge forces are large. The bunch simply spreads out before much of its kinetic energy can be extracted. The only countermeasure is to drive the tube harder, but when this is done the gain is very low despite a reasonable efficiency. Figure III.6 shows that a very high drive level must be used to realize any advantage over a conventional uniform-beam tube.

There is some doubt about the practicability of prebunching high-perveance beams. It has been the experience of others[3] that the debunching forces may seriously impede the formation of tight bunches in practice if not in theory.

E. The Variable-Pitch Helix Program

Ever since the invention of the traveling-wave amplifier, the possibility of modifying the phase velocity along the tube to improve efficiency has intrigued tube designers. Pierce[4] and Slater[5] were among the first to mention this possibility and Cutler[6] actually did some early

---

3. Mihran, T. G., "A Theoretical Study of the Super-Bunching of Electron Streams", General Electric Company Research Laboratory Report No. RL-780, December, 1952.

4. Pierce, J. R., Traveling-Wave Tubes, D. Van Nostrand, p. 167, New York, 1950.

5. Slater, J. C., Microwave Electronics, D. Van Nostrand, p. 281, New York, 1950.

6. Cutler, C. C., "Increasing Traveling-Wave Tube Efficiency by Variation of Phase Velocity", Bell Laboratories Memorandum, MM-53-1500-28; July 31, 1953.

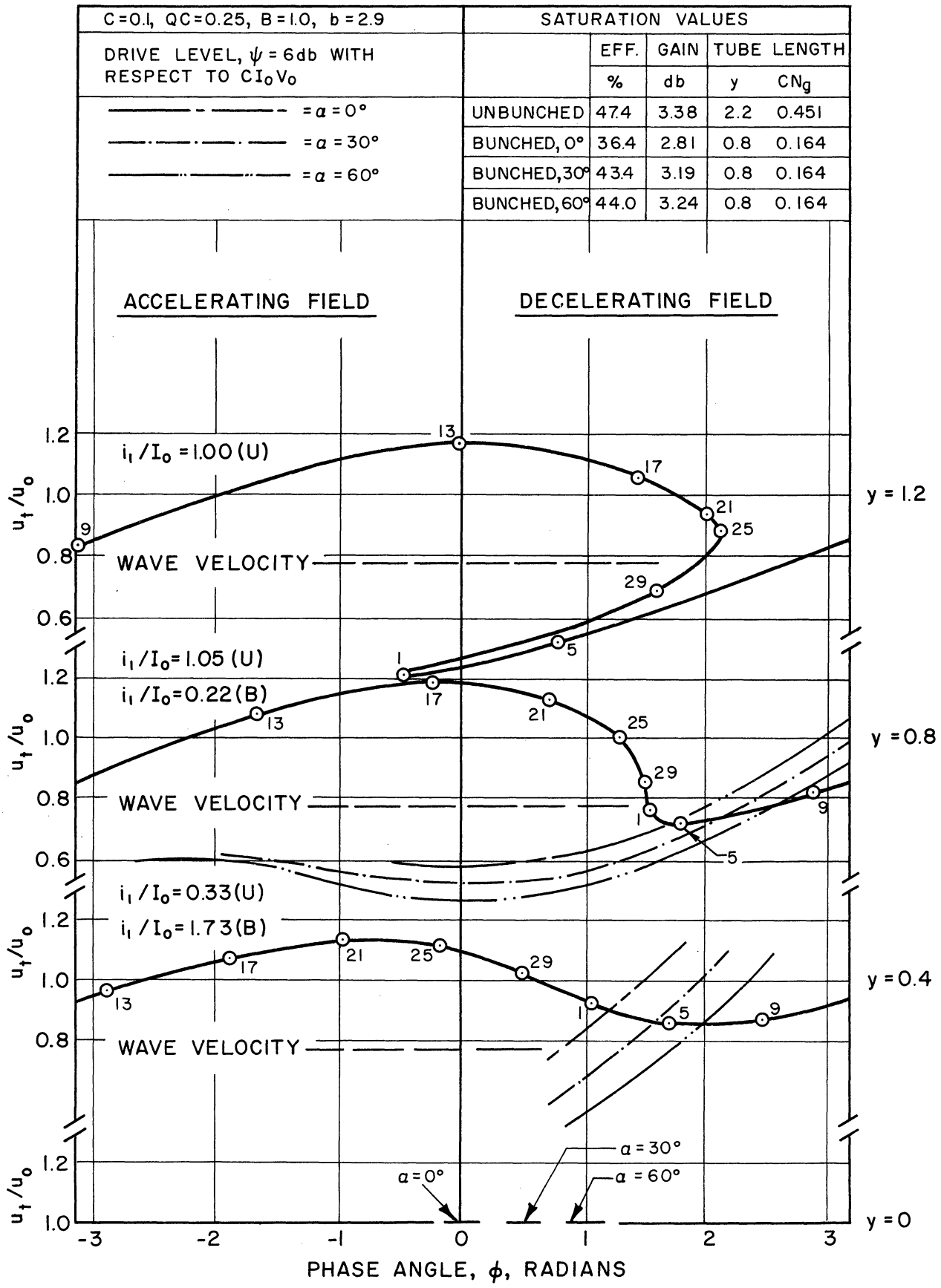

FIG. III.5 VELOCITY vs. PHASE.

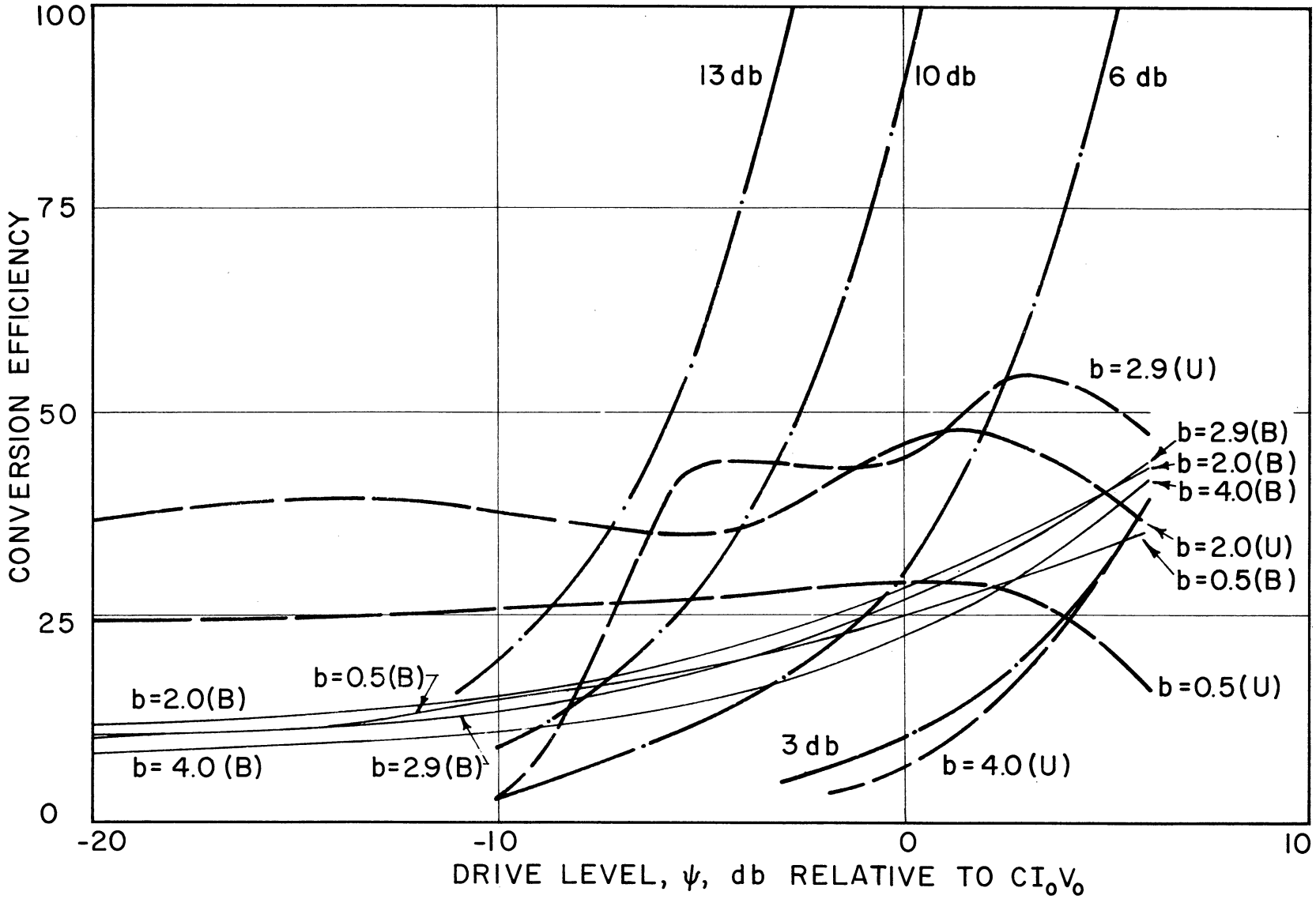

FIG. III. 6 EFFICIENCY AND GAIN vs. DRIVE LEVEL. (C=0.1, B=1.0, QC=0.25)

experimental work along these lines. He came to these conclusions. First, tapering proved necessary only very near the output end of the tube. With a calculated taper 4 db more power could be obtained at the voltage giving maximum small-signal gain, or 15 db more gain could be obtained at the voltage giving maximum power. However, he was not able to increase the absolute saturation power at that time.

Cutler had tapered the pitch to force the circuit velocity to remain synchronous with the average beam velocity. The average beam velocity in turn was calculated from the power delivered to the traveling wave. His taper formula was based on modified small-signal equations, since the large-signal equations of Rowe and Tien had not yet been reported.

It therefore seemed that the more accurate large-signal equations would make a new attempt to predict an optimum taper profitable. The equations of Section C take into account space-charge forces, velocity spread, and the change of impedance as the pitch is varied. The current variable-pitch helix program consists of the following:

1. Digital Computer Solutions. The general large-signal equations have been solved on the computer for one shift of pitch. The shift point was chosen as that position along the tube where the beam is defined as one dense bunch per wavelength. Such a beam condition lends itself most favorably to phase focusing techniques.

From the shift point several different constant pitches were used. The saturation power eventually reached was the criterion of the success of each shift. In a typical run, the best efficiency increase, from 35.4 percent to 45 percent, was achieved by a 20 percent decrease in helix phase velocity. This is shown in Fig. III.7. It should be

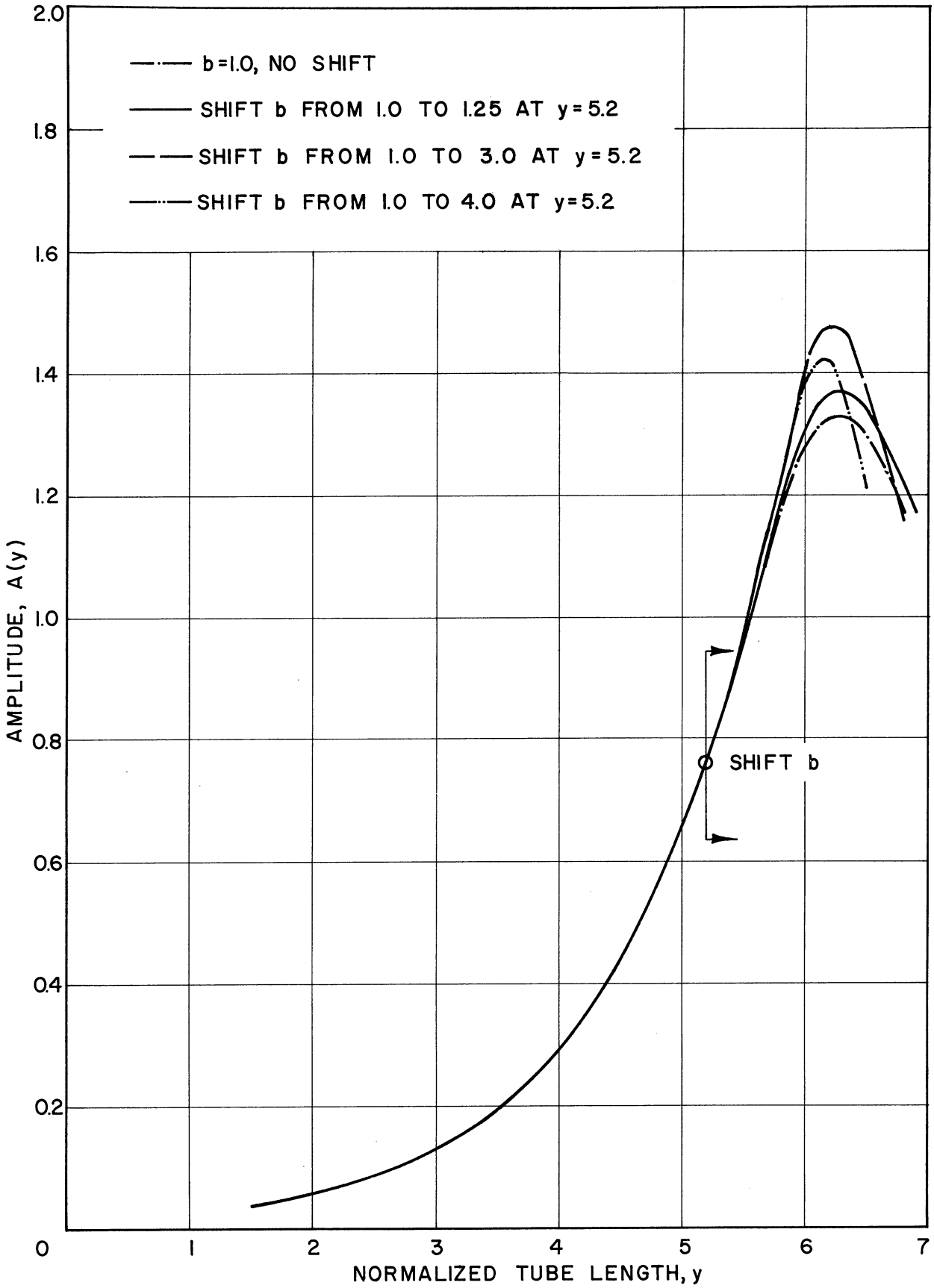

FIG. III.7 EFFECT OF ONE SHIFT OF PITCH ON SATURATION AMPLITUDE. ($C=0.1$, $QC=0$, $d=0$, $A_0=0.0225$)

repeated that this was for a single shift from the original constant pitch to a new constant pitch giving a velocity reduction of 20 percent.

Currently we are investigating the advantage gained in shifting the pitch again in the region between the first shift and saturation. The ultimate would be an infinitely variable taper, of course. There are indications though that velocity spread will make succeeding pitch shifts less effective than the first. For it is inherent in the behavior of the traveling-wave amplifier that the single tight bunch cannot be held in the face of accumulating velocity spread. Thus the first pitch shift finds the bunch shape more amenable to focusing than shifts thereafter.

2. Analog Computer Analysis. The digital computer runs are the most accurate, but they are not very flexible. They give information on particular parameter sets, but do not indicate general trends until a large number of runs have been accumulated. Therefore to augment them a reduced version of the equations was set up in analog form.

The basic simplifications were two. The electrons were assumed to be tightly bunched and space-charge forces were neglected. Thus the problem took on the appearance of a ballistics study in which the electron bunch was to be held phase locked in a force field. The pitch profile necessary to maintain phase focusing could be studied using many different drive levels and coupling coefficients. While the deleterious effects of velocity spread and space-charge debunching are not accounted for, the runs nevertheless give an appreciation for phase focusing under the most favorable conditions. Then too, the effect of impedance variation of certain simple forms can be developed.

Figure III.8 shows the pitch taper for some representative runs in which C is assumed constant through the taper region. These runs

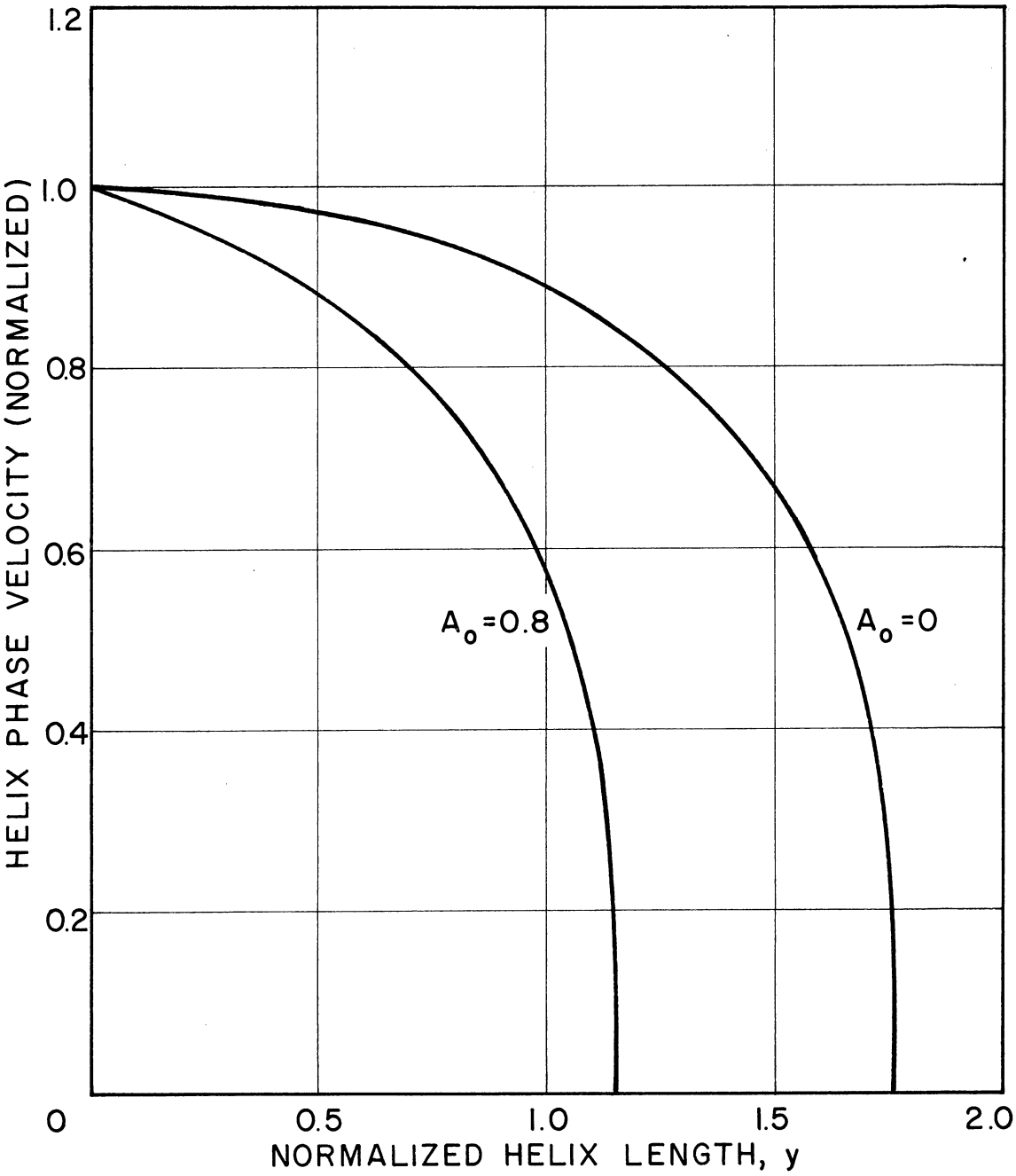

FIG. III. 8 PHASE VELOCITY vs. HELIX LENGTH. (C=0.1, ASSUMED CONSTANT THROUGHOUT; QC=0; b=0 AT INPUT; A_o= NORMALIZED INPUT)

show how rapidly the phase velocity must fall off to keep the bunches phase locked as they lose their kinetic energy. It is planned to compare these pitch tapers with those of the more general equations to evaluate the effects of velocity spread.

3. Pitch Optimization by Computer. If it should prove that multiple pitch shifts lead to undeniably more efficient operation, then a suggested refinement would be to have the digital computer itself choose an optimum pitch variation. This was spoken of in detail in previous reports, but the effort has been temporarily discontinued pending the results of the manual pitch shift study.

Success of any computer optimizing technique depends on the solution of two problems. One is the selection of a realistic criterion for choosing the pitch at each step. The other problem is furnishing the large memory storage required if it is necessary to retain many interim results pending comparison tests in the optimizing process. While these problems are not easy ones it is nonetheless felt that the method deserves more attention if infinitely variable parameter shifting looks desirable.

F. D-C Gradient Program

The d-c gradient study has gone along in parallel with the variable-pitch program. It is largely of academic interest since it is usually difficult to insert a spatially varying d-c field along a microwave traveling-wave tube. This is especially true of helix types.

It has been shown that when an accelerating gradient is applied at a point along the tube where bunching is dense, saturation gain is substantially incrased. Figure III.9 illustrates this improvement. The tube becomes somewhat larger at saturation. Efficiency does not go up correspondingly, since the d-c field adds additional power. Indeed,

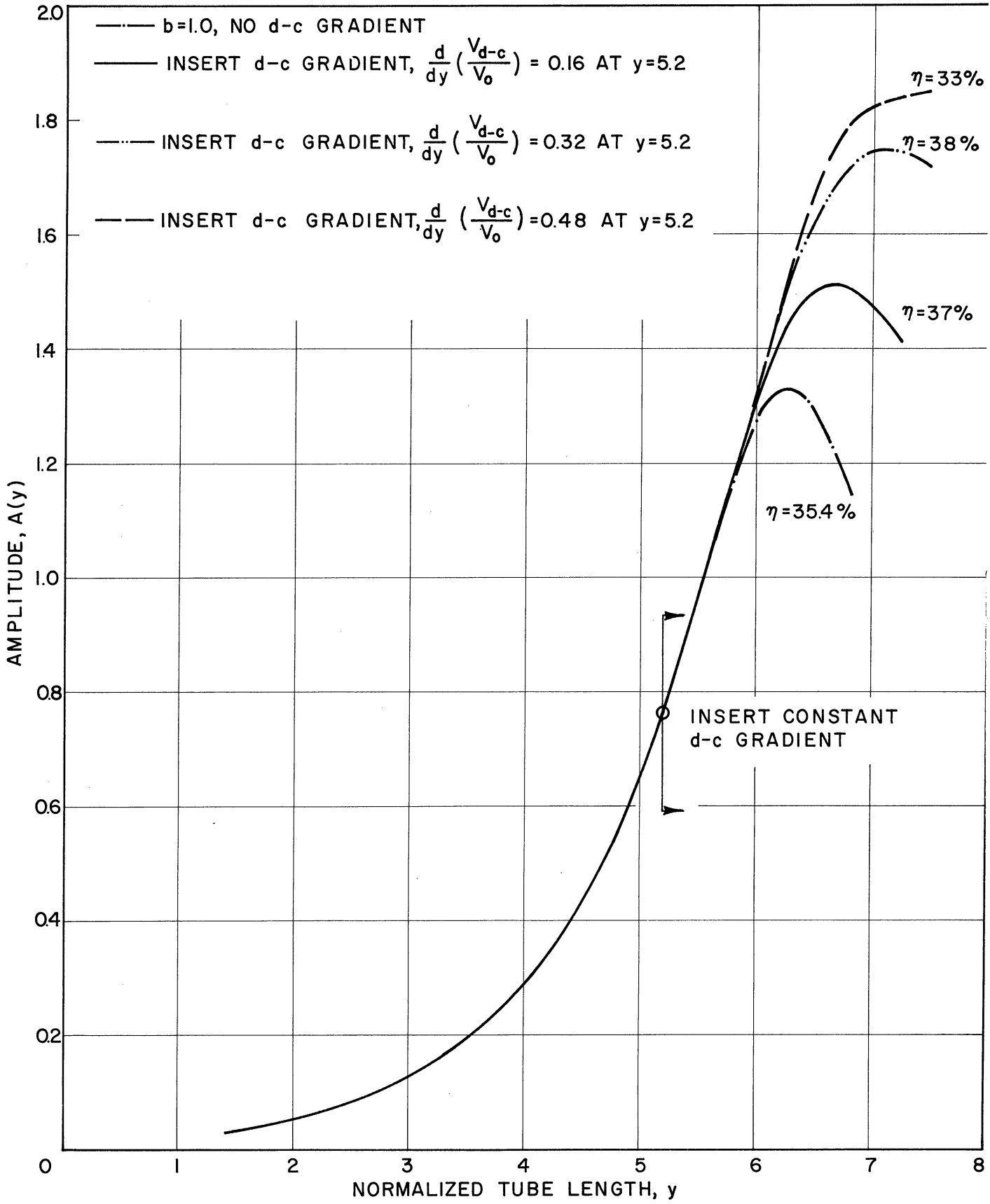

FIG. III. 9 EFFECT OF d-c GRADIENT ON SATURATION AMPLITUDE. (C=0.1, QC=0, d=0, A_o=0.0225)

there is a limit after which improved saturation gain occurs only at the cost of decreased overall efficiency. This is also indicated on Fig. III.9.

Once again it would be possible to set up an automatic program to vary the d-c gradient continuously, selecting an optimum profile based upon some legitimate criterion such as maximum efficiency. In view of the difficulties involved in applying d-c gradients to the more common r-f structures this will not be pursued at this time.

IV. X-BAND TRAVELING-WAVE AMPLIFIERS (C. P. Wen)

A. Introduction

The small-signal theory was employed in the design of a medium-gain (30 db) medium-power (1 watt cw), helix-type traveling-wave amplifier in the X-band frequency range (8.2-12.4 kmc). Three series, a total of sevel amplifiers, were constructed and tested during the period of this contract.

Originally, the helix mean diameter of 0.100 inch was selected to facilitate easy construction and the helix potential was chosen to be 2000 volts because of the availability of power supplies. The design turned out to be a 11.3-inch-long helix traveling-wave tube with $\gamma a = 3.08$ at the midband frequency (series X-2). The slow-wave structure was later shortened to 8 inches (series X-3). Amplifier X-4 was designed after the completion of r-f testing on model X-3. The increasing of the helix pitch lowered the midband γa to 2.45 while the synchronous helix voltage was raised to 3000 volts. It was hoped that the minor change in amplifier construction would improve its gain-bandwidth characteristic.

The important parameters and dimensions characteristic of the amplifiers are listed below:

TABLE IV.1

X-Band Amplifier Parameters

	Series X-2	Series X-3	Series X-4
b (beam radius), inch	0.035	0.035	0.035
a (helix radius), inch	0.050	0.050	0.050
p (pitch), TPI	36	36	28
I_o (beam current), ma	10	10	10
V_o (beam voltage), volts	1720	1720	3000
γa	3.08	3.08	2.45
ℓ (length of helix), inches	11.3	8.0	8.0

The helices were made of 0.010-inch molybdenum wire and were supported by three sapphire rods inside a precision glass vacuum envelope. The dielectric loading factor is found to be better than 92 percent at X-band. A Pierce-type immersed-flow gun is used in all series and it may be operated under space-charge-limited or temperature-limited conditions.

B. Experimental Investigation of the X-Band Amplifier

Experimental investigations were completed on only two out of the seven amplifiers built; the rest of them failed or showed poor beam transmission before r-f testing was completed.

Amplifier Series and Model Number	Cause of Malperformance
X-2-1 (11-3-inch helix)	Excessive helix interception.
X-3-1	R-F testing completed.
X-4-1	Arc-over between the helix d-c lead and cathode heat-shield.
X-4-2	Cracked vacuum envelope.
X-4-3	Gassy, 30 percent interception on the helix.
X-4-4	30-60 percent interception, filament failure.
X-4-5	R-F testing completed.

The performance of amplifiers X-3-1 and X-4-5 will be presented in the following sections.

C. Electron Gun Performance

Greater than 85 percent beam transmission was observed for amplifier X-3-1 when it was operated immersed in a uniform magnetic field of 1000 gauss. A high percentage of the electrons interception were found to be secondaries which would disappear at a slight increase of collector potential with respect to the helix. Ninety-eight percent beam transmission was obtained at one time. The forced-air cooling method was found to be incapable of handling more than 15 watts of collector dissipation. The electron beam would start to collapse due to ion bombardment at the cathode emitting surface once the collector was overheated. A collector water jacket was necessary to provide the adequate amount of cooling.

A 30-percent interception prevented amplifier X-4-5 from full-current operation. Migration of the cathode material onto the anode was suspected.

D. R-F Matching and Attenuation

Cavity-type coaxial-cavity couplers and two types of coupled-helix attenuators were employed for all the X-band amplifiers. Typical matching and attenuation curves are presented in Figs. IV.1 and IV.2 respectively.

A voltage standing wave ratio of less than 2 to 1 could be obtained across the X-band frequencies at both the input and output of the amplifier by means of the coaxial-cavity couplers. The quality of the matches did deteriorate at the band edges. An attempt was made to replace the cavity-type couplers with coupled-helix transducers. Because of the limitation imposed by the minimum thickness of the vacuum envelope and the three-dielectric-rod helix support method, the coupling between the outer and the inner helix was not tight enough to yield broad bandwidth operation.

For the same reason, coupled-helix attenuator loss drops off rapidly with increasing frequency[1]. This phenomenon happened to both the scotch-tape-kanthal-wire type and the graphite-kanthal-wire type attenuators.

E. Small-Signal and Saturation Gain

Curves of small-signal and saturation gain are presented in Figs. IV.3 and IV.4. Because of the high γa selected for the center frequency ($\gamma a = 3.08$ for amplifier X-3-1, $\gamma a = 2.45$ for amplifier X-4-5), the gain curves tended to decrease monotonically with frequency.

The theoretical nondispersive gain curve computed for amplifier X-4-5 operated at 3.8 ma collector current seemed to agree well with the

---

1. Krage, H. W., "High-Power Coupled-Helix Attenuators", Tech. Rept. No. 36, Electron Physics Laboratory, Dept. of Electrical Engineering, The University of Michigan; March, 1960.

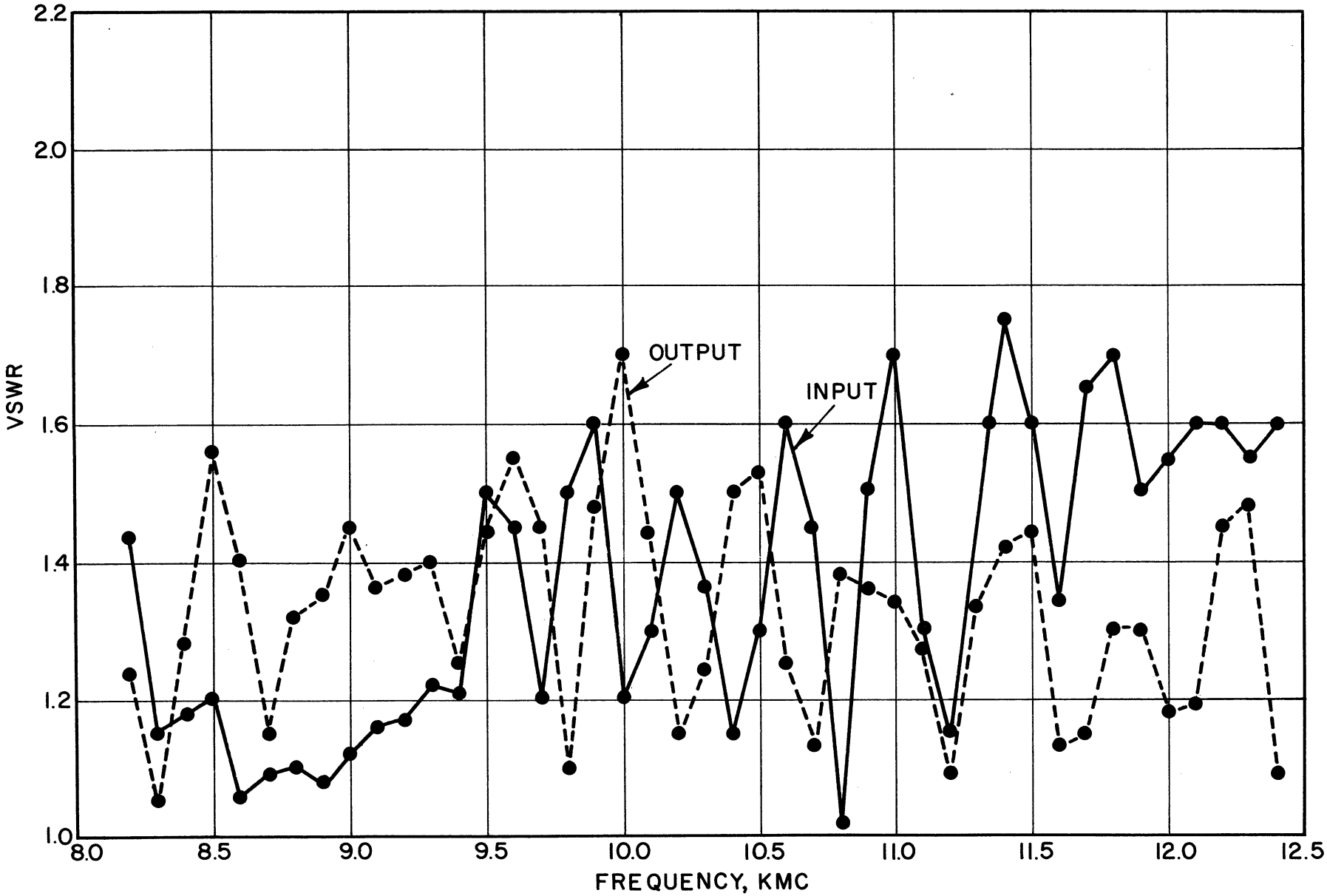

FIG. IV.1 VSWR OF INPUT AND OUTPUT COUPLERS vs. FREQUENCY FOR TWA-X-3-1.

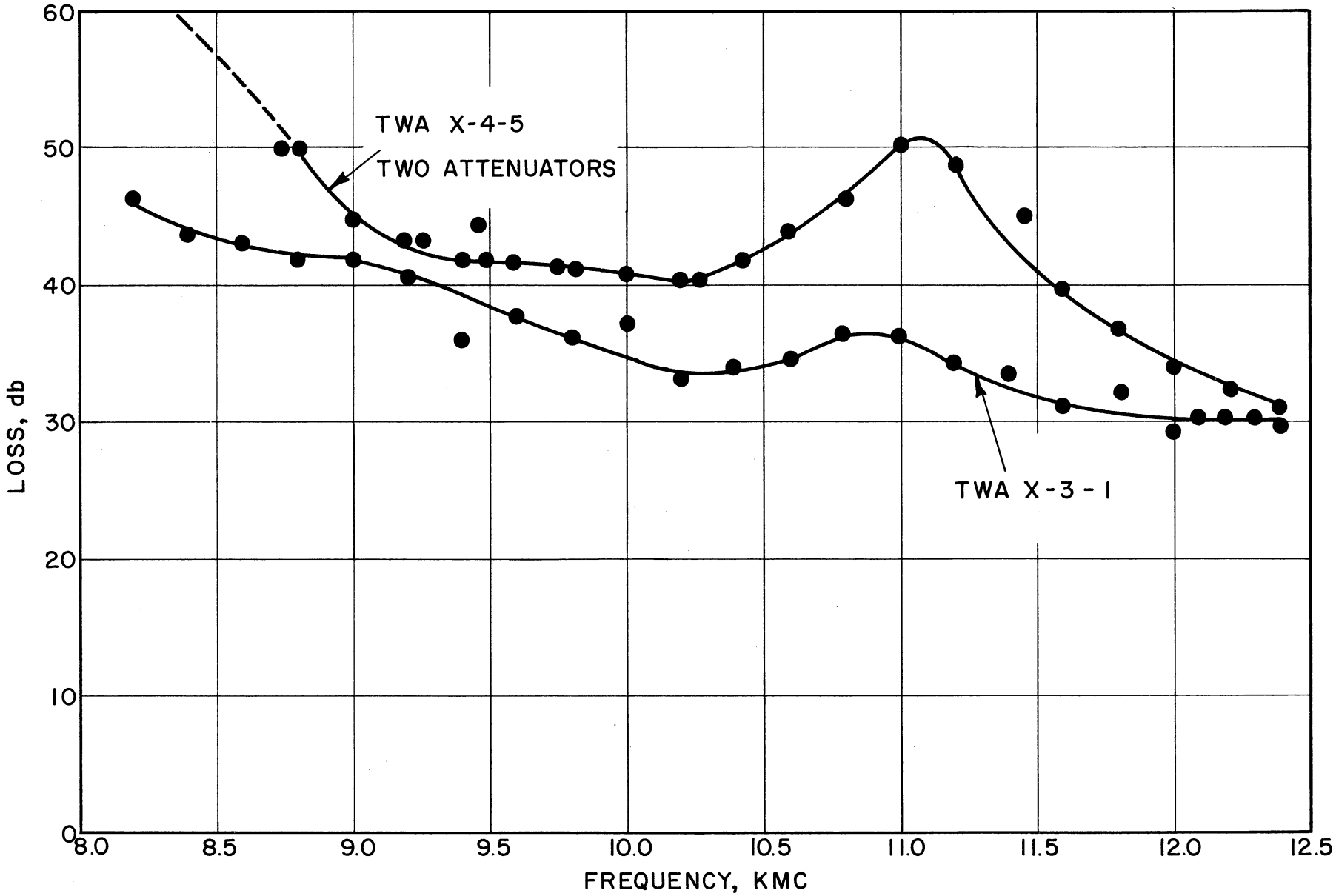

FIG. IV.2 COLD INSERTION LOSS (db) vs. FREQUENCY INCLUDING ATTENUATORS AND COUPLERS.

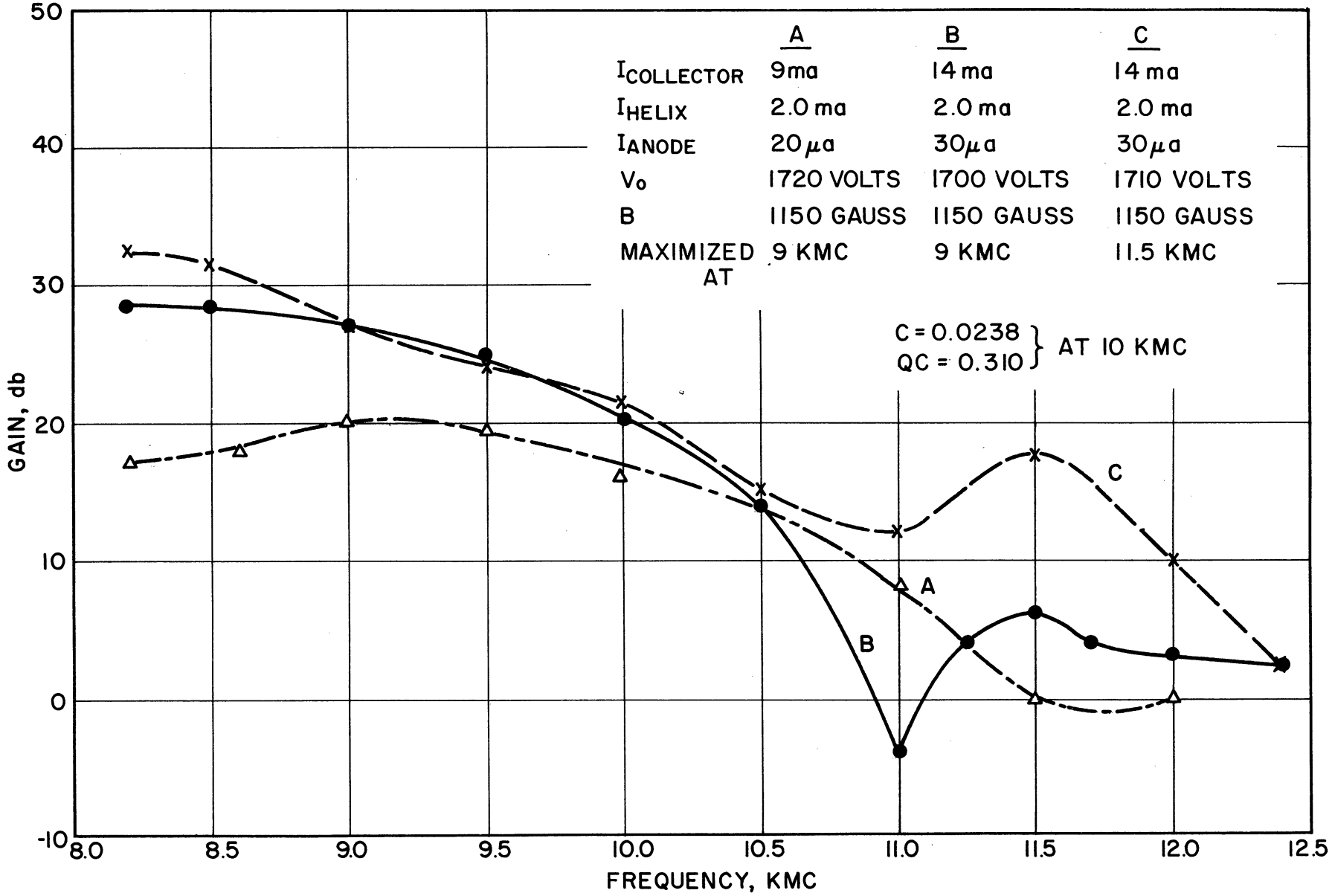

FIG. IV.3 SMALL-SIGNAL GAIN (db) vs. FREQUENCY FOR TWA-X-3-1.

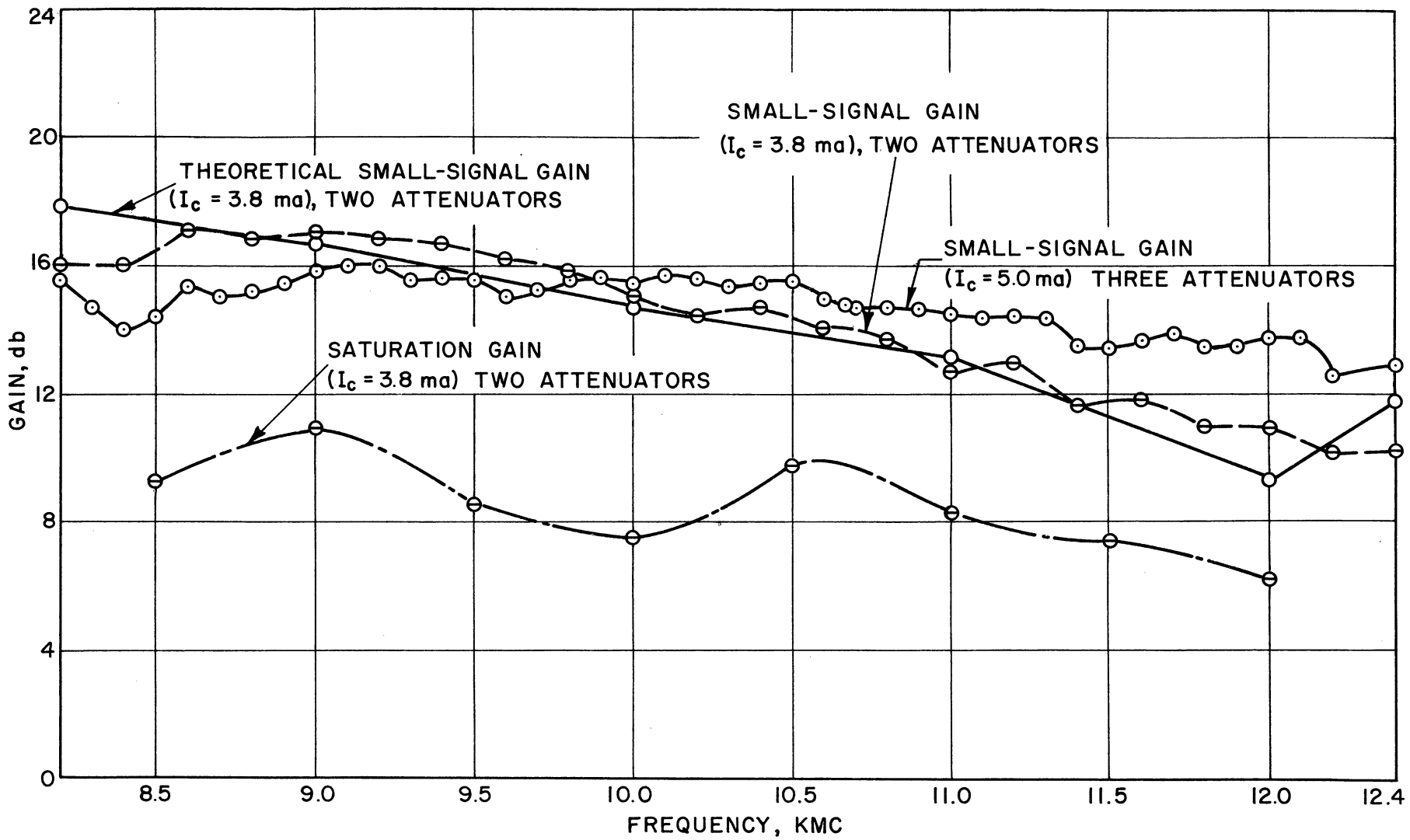

FIG. IV.4 TWA X-4-5 GAIN vs. FREQUENCY.

experimental data (assuming 5-6 db loss for the couplers and the cables). Therefore, 25-30 db gain would be expected for full-current operation.

F. Saturation Power

A saturation power of 0.85 watt was detected at 9.0 kmc for amplifier X-3-1 as shown in Fig. IV.5, and more than half a watt output was observed for amplifier X-4-5 when it was operated at $I_{co\ell} = 3.8$ ma. This is shown in Figs. IV.6 and IV.7. Both tubes seemed to have the potential of meeting the 1-watt output requirement. The maximum efficiency of either amplifier was below 3.5 percent.

G. Oscillation

Stable operation prevailed in amplifier X-3-1 up to 14 ma collector current. No oscillation was detected over the X-band frequency range.

Due to the tight coupling between the electron beam and the slow-wave structure, the backward-wave modes are strongly excited in amplifier X-4-5. The lack of sufficient isolation at high frequencies permits the establishment of backward-wave oscillations at $ka \approx 0.5$ when the amplifier gain is high enough. The beam current of the amplifier is therefore limited by the oscillation conditions.

H. Conclusion

The failure to meet the requirements in gain and bandwidth was mainly caused by the high γa value chosen for the original design. The small-signal gain, bandwidth and stability of the amplifiers could all be improved by a reduction in helix diameter ($\gamma a \approx 1.5$ for optimum conditions). Besides that, some lossy material should be placed close to the r-f circuit to provide additional attenuation and suppress high-frequency oscillations.

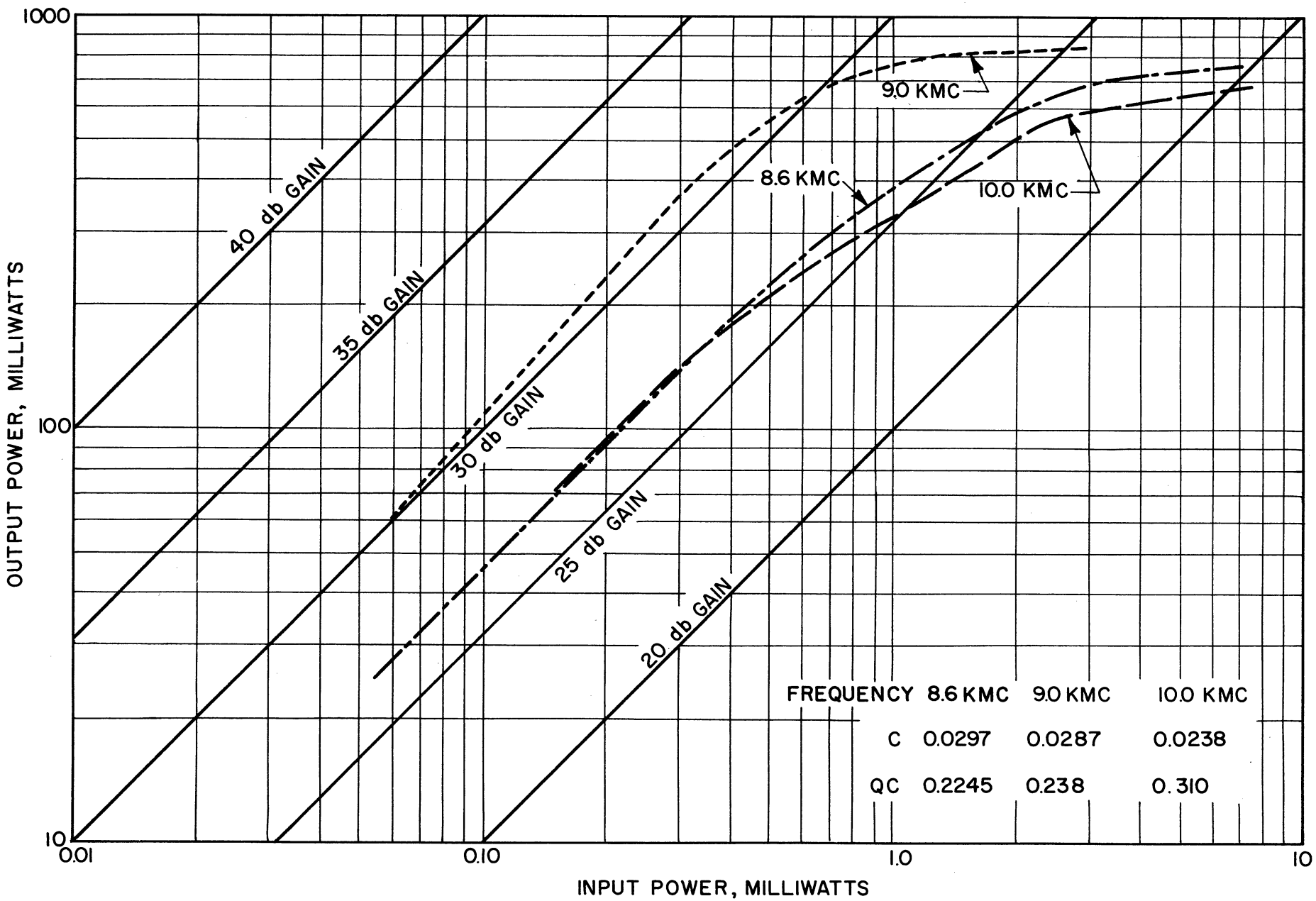

FIG. IV.5 POWER OUTPUT vs. POWER INPUT. (HELIX VOLTAGE ADJUSTED FOR MAXIMUM POWER OUTPUT AT EACH FREQUENCY) TWA X-3-1

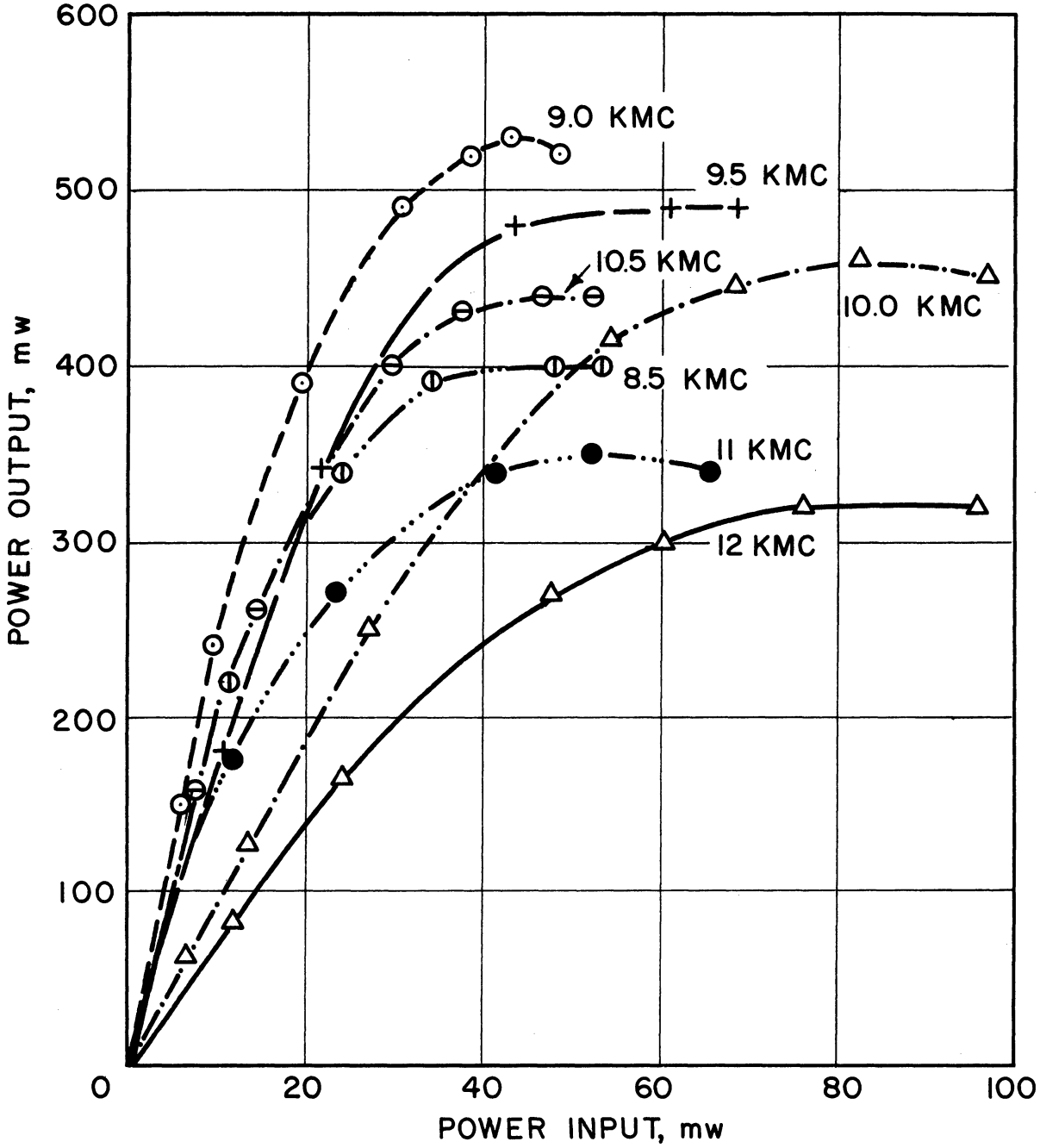

FIG. IV.6 TWA X-4-5 POWER OUTPUT vs. POWER INPUT (TWO ATTENUATORS AND I_c=3.8 ma).

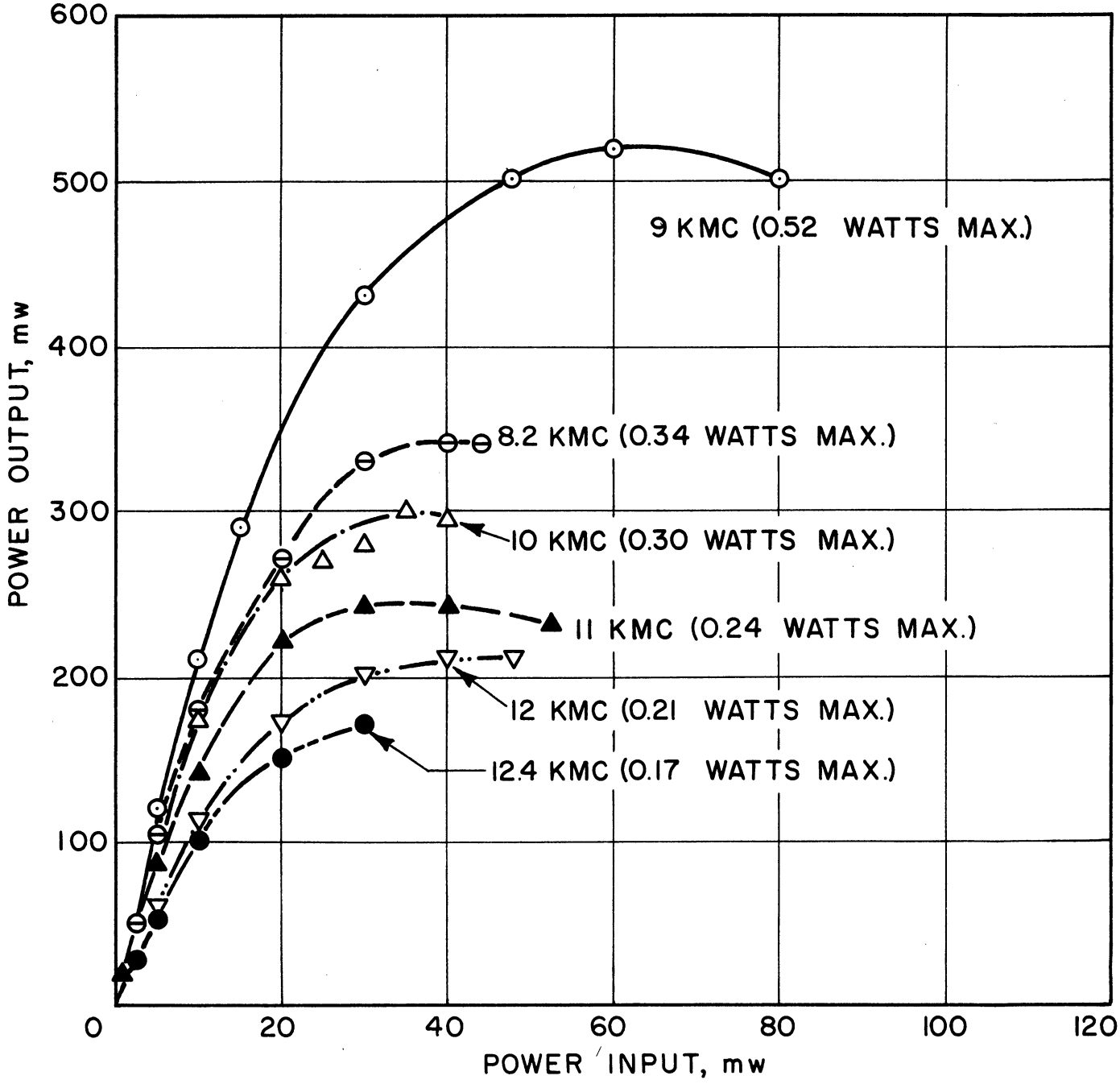

FIG. IV.7 TWA X-4-5 POWER OUTPUT vs. POWER INPUT. (THREE ATTENUATORS $I_c = 5.0$ ma)

The predicted power output of a small-signal traveling-wave amplifier is of the order of CV_oI_o, where C is the Pierce gain parameter; amplifier X-4-5 should have no trouble in delivering 1 watt with 25 db gain at full current.

V. EXPERIMENTAL STUDY OF CRESTATRONS

(G. T. Konrad)

A. Objectives of the Program

The object of this study is the correlation of the theoretical analysis of the Crestatron made by J. E. Rowe[1] with actual laboratory models of this device. To this end it was decided to construct a series of high-power cw Crestatrons in S-band frequency region. The following requirements were set.

TABLE V.1

Design Objectives

R-f power output	=	100 watts
Bandwidth	=	2.0 - 4.0 kmc
Efficiency	$\geqq$	25 percent
Focusing		magnetic
Length		in accordance with Crestatron theory
Beam Perveance	=	1.0 micropervs
R-f structure		single-filar helix

Some of the components used in this series of Crestatrons were available from a previous study of traveling-wave tubes, and were incorporated in this design.

1. Rowe, J. E., "Theory of the Crestatron: A Forward-Wave Amplifier", Proc. IRE, vol. 47, No. 4, pp. 536-545; April, 1959.

B. Electron Guns

The electron gun used for the cw Crestatron had been designed for the S-band traveling-wave amplifier investigated at this laboratory previously. The design calls for a solid-beam gun operating at a perveance of 1.0 micropervs in the voltage range of 3000 to 5000 volts. The necessary beam diameter is approximately 0.125 inch. The gun is of the shielded Pierce type and uses a tungsten impregnated cathode operating near 1150°C with a heater power of 25 to 30 watts. The gun was magnetically shielded and although the Brillouin field required was only 250 gauss the best performance was obtained with a focusing field near 1000 gauss.

During the early stages of the investigation the usual types of gun problems were encountered. Some of these were conduction along supporting members, arc-over between parts, as well as beam interception on the gun anode or helix due to misalignment or shifting of parts.

Since most of the tube parts are quite small in size and are not particularly rugged for this high an average power in S-band, it was imperative to keep the additional heating from beam interception quite low. In fact, it was found necessary to limit the portion of the beam intercepted by the helix to less than one percent and the anode interception to a few tenths of one percent. This proved to be a very stringent requirement. When the interception was tolerable the perveance was low and vice versa. It turned out that under cw conditions this gun was capable of operating at a perveance of 0.5-0.6 microperv.

Since the full advantages of the Crestatron could not be realized at this low a perveance, a pulsed gun was obtained. Under these conditions a microperveance of 1.0 and even of 1.5 could be achieved readily. The duty cycle of the Crestatron was between 0.03 and 0.04. Quite

favorable results were obtained from this investigation and will be described in the later section.

C. Slow-Wave Structure

Since the Crestatron is inherently a broadband device, it is necessary to use an r-f structure which has a broadband capability. It was felt that the only structure capable of meeting this requirement was a single-filar helix. Furthermore, since one of the main advantages of a Crestatron is its short length, it seemed desirable to construct a helix as small and short as possible in order to enhance this very advantage, commensurate with the requirement of a reasonable power-handling capability. The D.L.F. of the structure was kept as high as possible in order to ensure a short physical tube length. After investigating a number of methods for supporting the helix in the envelope, it was decided to use three 0.020 sapphire rods in intimate contact with the helix wire and the glass envelope, which was made out of Corning 7740 glass.

A summary of the critical dimensions of the r-f structure is given in Table V.2, and a cross-section through the whole helix envelope is shown in Fig. V.1.

TABLE V.2

Crestatron Dimensions

Helix wire diameter	=	0.020 inch
Mean helix radius	=	0.087 inch
T.P.I.	=	18.85
Sapphire support rods	=	0.020 inch diameter
I.D. of glass tubing	=	0.234 inch
O.D. of glass tubing	=	0.274 inch
$\frac{\text{mean helix radius}}{\text{beam radius}}$	=	$\frac{a'}{b'} = 1.4$
I.D. of helix shield	=	0.278 inch
$\frac{\text{I.D. of helix shield}}{\text{mean helix diameter}}$	=	$\frac{b}{a'} = 1.6$

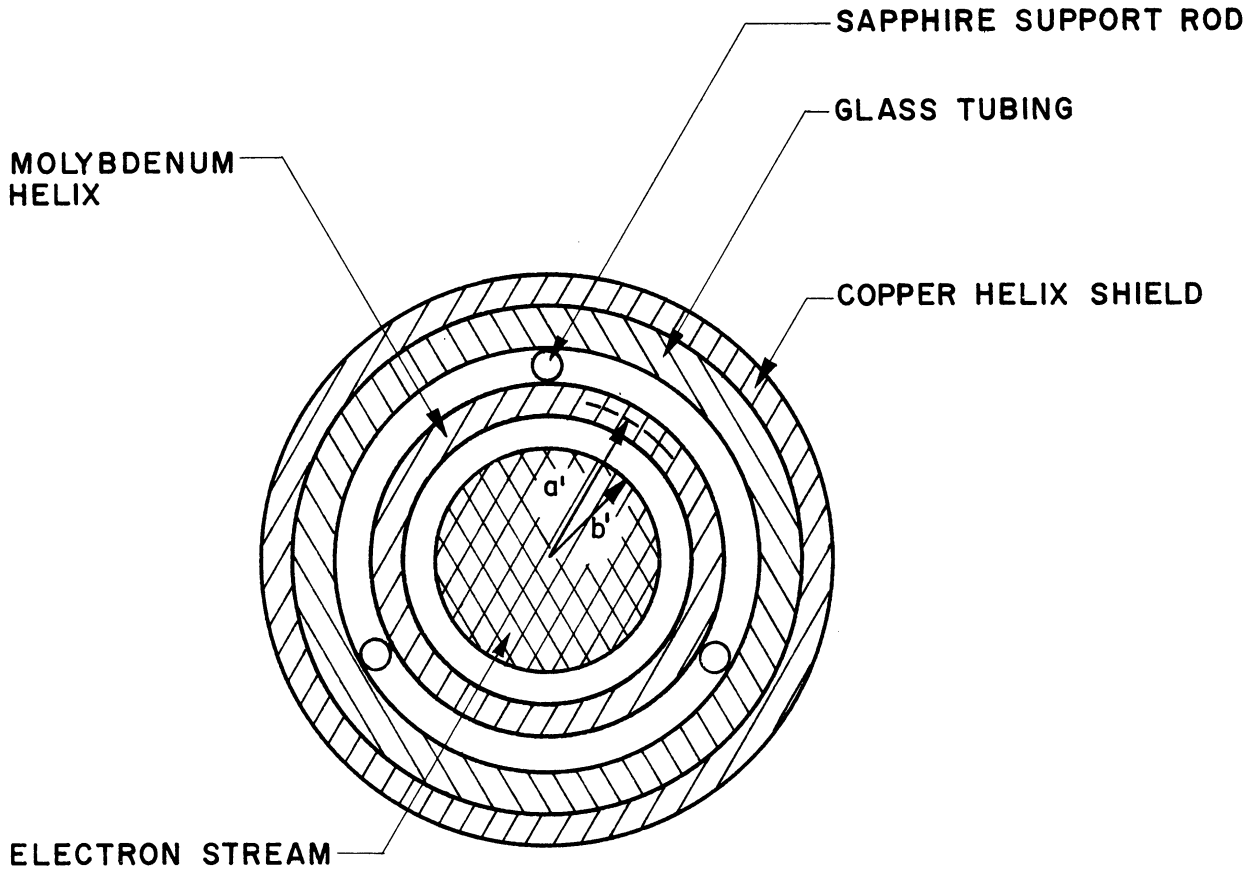

FIG. V. 1 CROSS SECTION OF CRESTATRON R-F STRUCTURE AND VACUUM ENVELOPE.

In order to increase the bandwidth of the structure, a metal shield was placed around the glass envelope at a b/a' ratio of 1.6. The presence of the metal shield decreased the dispersive nature of the helix as brought out by Fig. V.2.

Careful cold tests were conducted on the final structure in order to be able to make a meaningful comparison later between the hot test results and Rowe's Crestatron theory. The phase velocity of the structure was determined by use of a movable short and the impedance was measured by Lagerstrom's perturbation technique[2]. The results are shown in Figs. V.2 and V.3 for both shielded and unshielded cases. The D.L.F. as a function of frequency is shown in Fig. V.4. It can be seen that the loading is not very great in view of the fact that the glass envelope is quite close to the helix.

Operation of some of the early Crestatron models revealed the necessity for having a low-loss circuit. This need became particularly acute during high-drive cw measurements. Originally the helices were wound with molybdenum wire. The loss of such a structure in db per inch is shown in Fig. V.5. The r-f wave propagating on the circuit heated the wire so extensively that gas was driven out of the molybdenum wire, which raised the pressure in the tube. This reduced the cathode emission. In order to circumvent this problem, subsequent helices were constructed with tungsten wire. This did not decrease the helix loss, but did reduce the gas emission considerably. Attempts to plate the helices with copper or silver were not very effective initially. It is felt that a good

---

2. Lagerstrom, R. P., "Interaction Impedance Measurements by Perturbation of Traveling Waves", Tech. Rpt. No. 7, Stanford Electronic Laboratories, Stanford University; February, 1957.

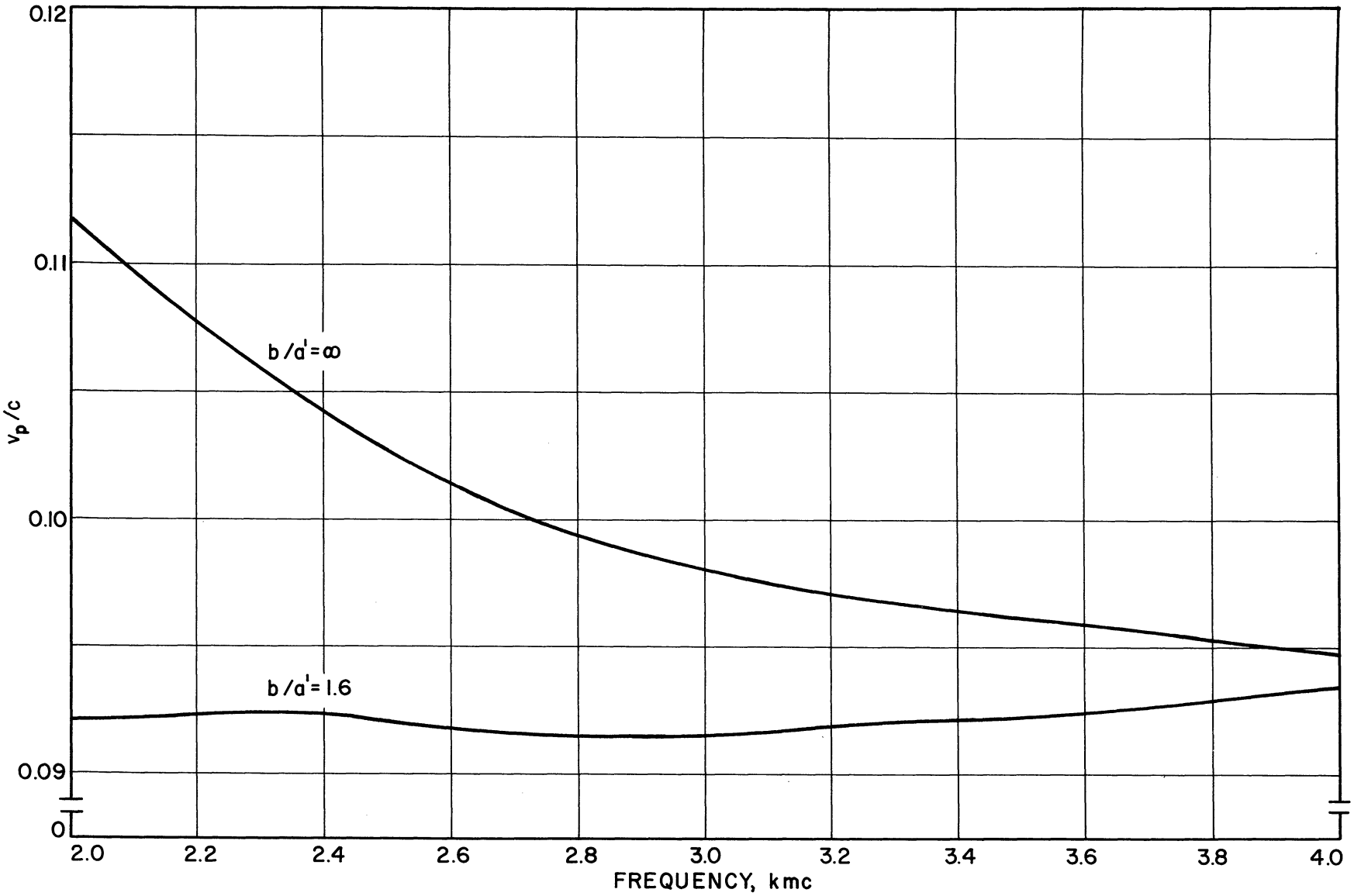

FIG. V. 2 PHASE VELOCITY AS A FUNCTION OF FREQUENCY FOR SHIELDED ($b/a' = 1.6$) AND UNSHIELDED ($b/a' = \infty$) S-BAND CRESTATRON HELICES.

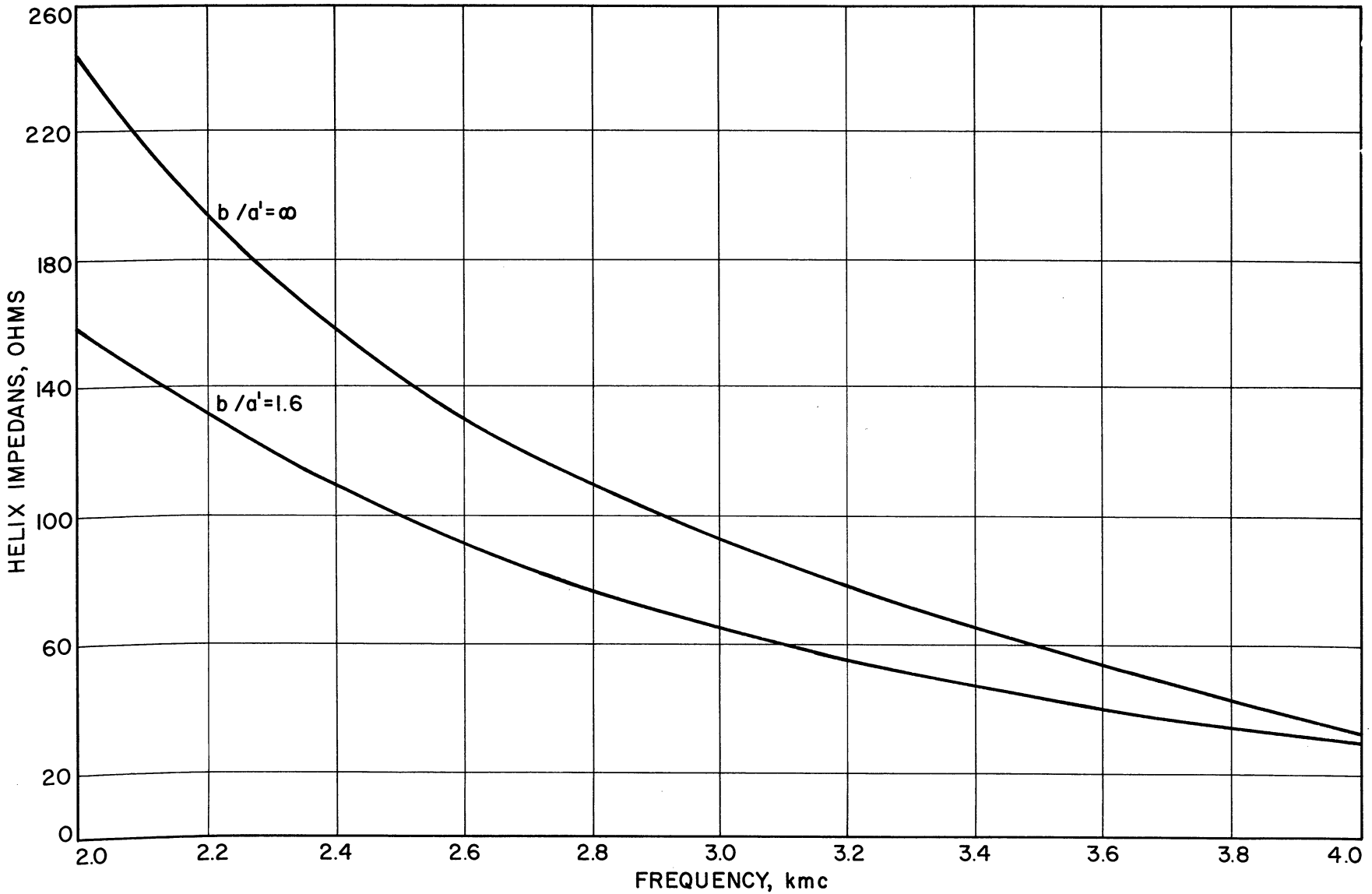

FIG. V. 3 HELIX IMPEDANCE vs. FREQUENCY FOR S-BAND CRESTATRON HELICES. SHIELDED AND UNSHIELDED CASES. ($a'/b' = 1.4$)

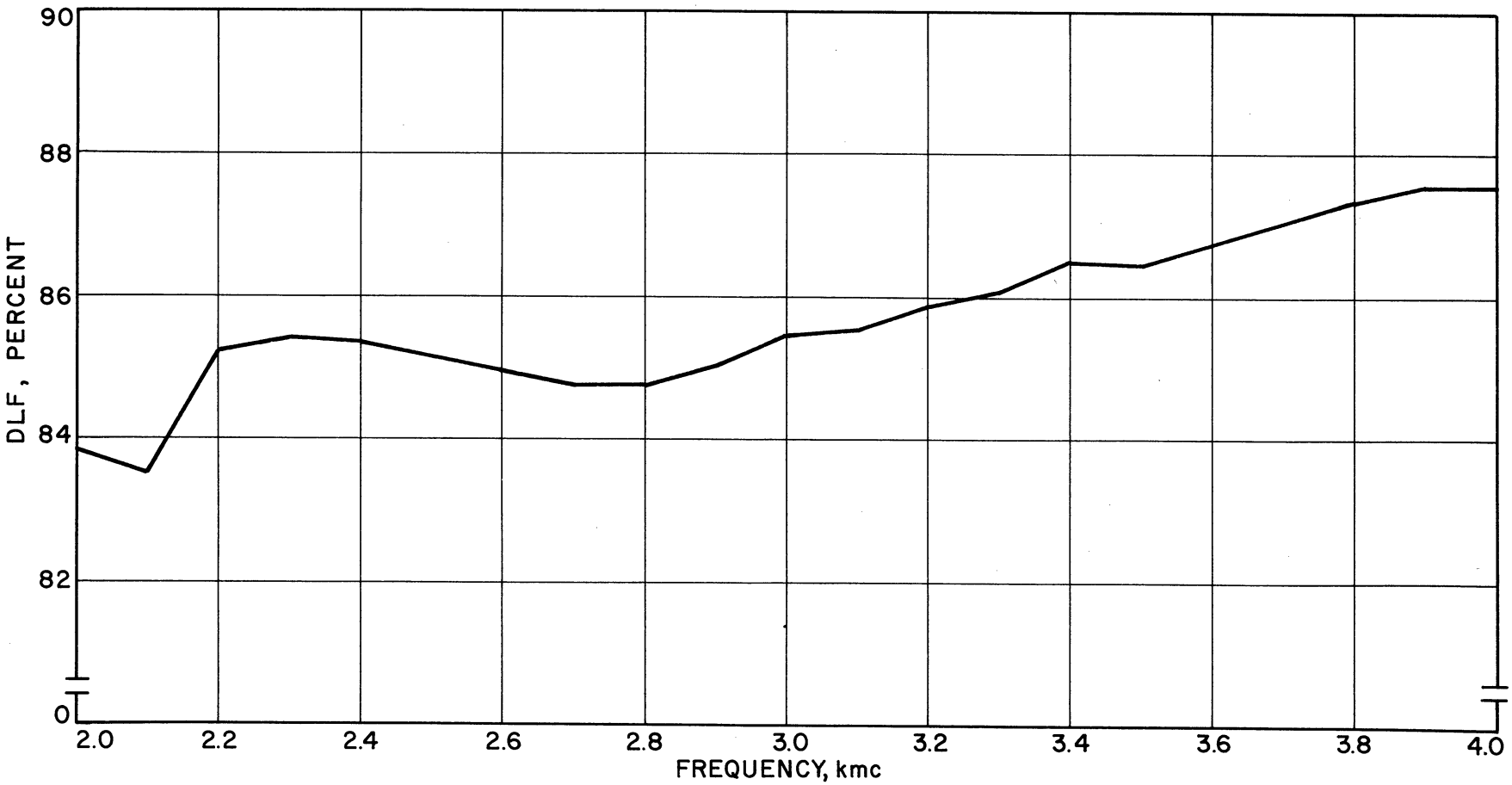

FIG. V.4 DIELECTRIC LOADING FACTOR AS A FUNCTION OF FREQUENCY FOR THE UNSHIELDED S-BAND CRESTATRON.

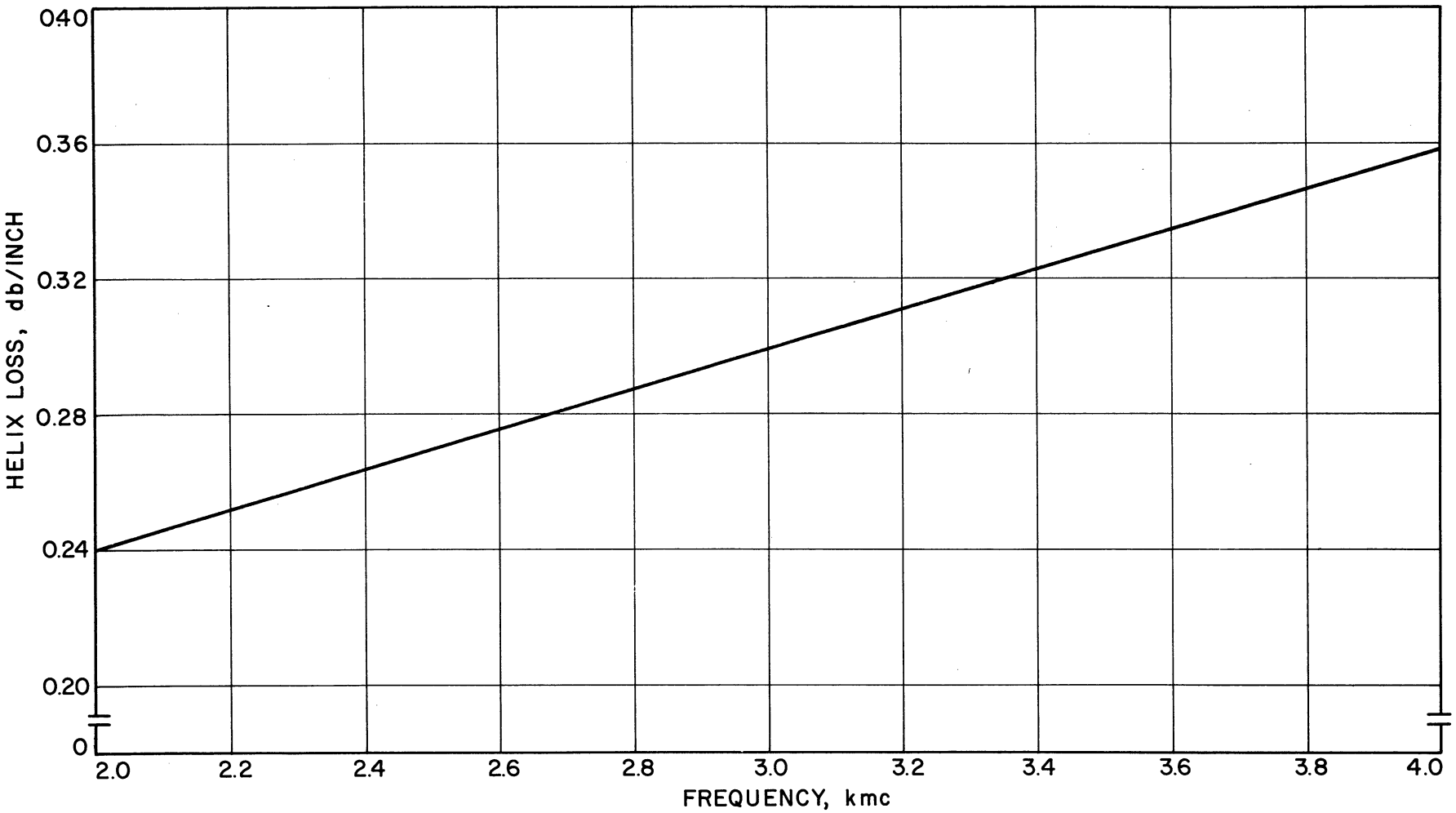

FIG. V.5 HELIX LOSS IN db PER INCH AS A FUNCTION OF FREQUENCY FOR THE S-BAND CRESTATRON.

plating method is available now, but to date no extensive investigation has been conducted.

D. Couplers and Attenuators

During the initial phase of the Crestatron tests cavity couplers were used. It was found, however, that they were inadequate due to their inherent narrow bandwidth. Furthermore, there was always the unpleasant chore of getting the couplers matched to the structure sufficiently well so that the tube would not oscillate. Consequently, it was decided to switch over to coupled-helix couplers. An enormous improvement was made, as can be seen from Fig. V.6. Subsequently, the assembly of the coupled-helix couplers was perfected to such an extent that it is now possible to construct very good couplers in a minimum length of time. The loss of a typical coupler and its directivity are shown in Fig. V.7.

Due to the short length and relatively low gain of the Crestatron, it is not necessary to use an attenuator on the r-f structure. It was found, however, that a very short attenuator placed at the back end of the coupled-helix couplers improved the VSWR of the couplers considerably. Very useful and compact attenuators have been developed at this laboratory[3]. They were found to be very useful for this application.

E. Collector Designs

The beam collectors of this series of Crestatrons were water-cooled. It must be remembered that the coupled-helix couplers used with this tube severely limit the diameter of the collector. The one-stage collector was used on all tubes and one can be seen in the photograph in Fig. V.8. Even that small and compact a collector is able to

---

3. Krage, H. W., "High-Power Coupled-Helix Attenuators", Tech. Rpt. No. 36, Electron Physics Laboratory, Dept. of Electrical Engineering, The University of Michigan; March, 1960.

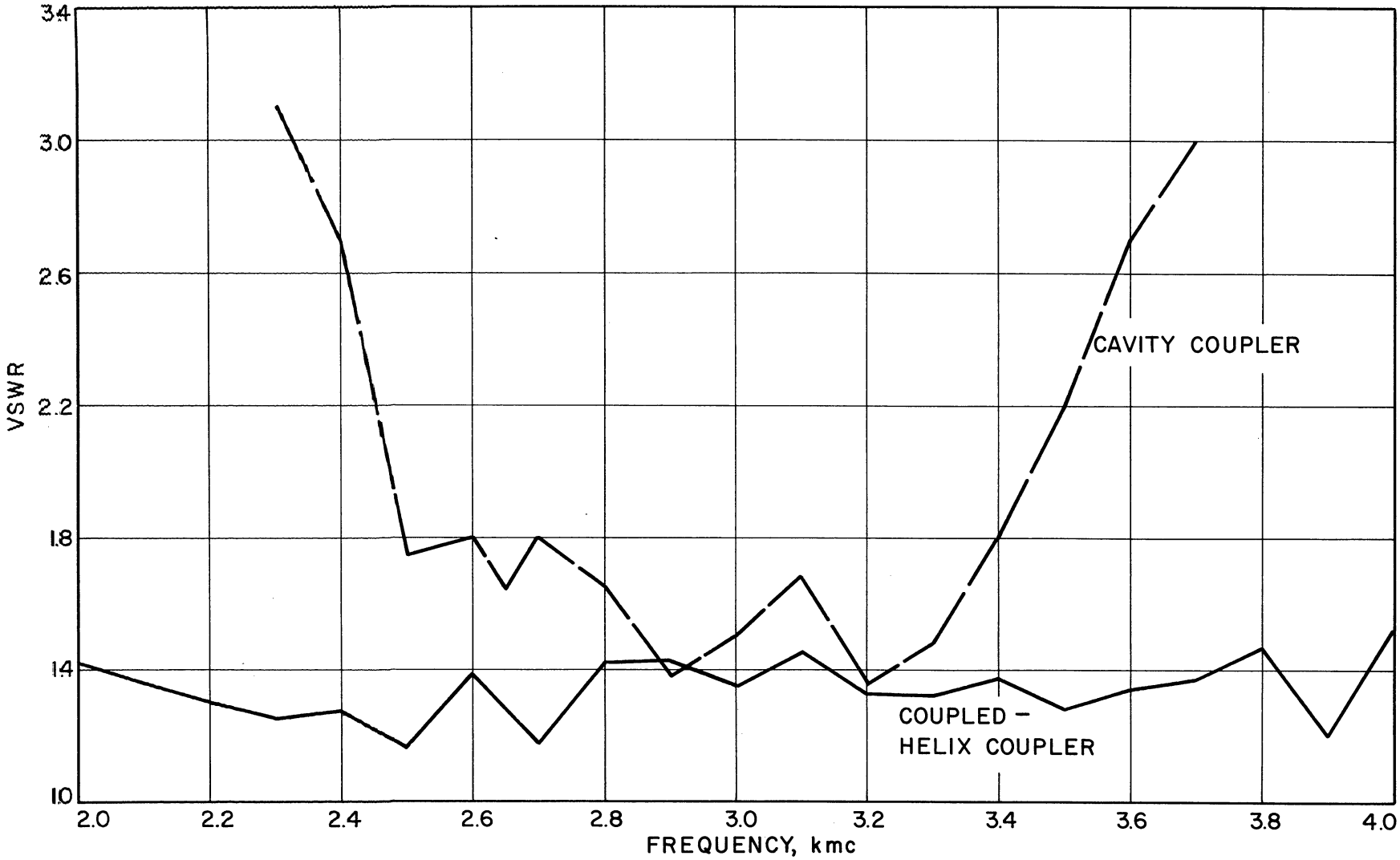

FIG. V.6 VSWR FOR TWO TYPES OF COUPLERS USED WITH THE S-BAND CRESTATRONS.

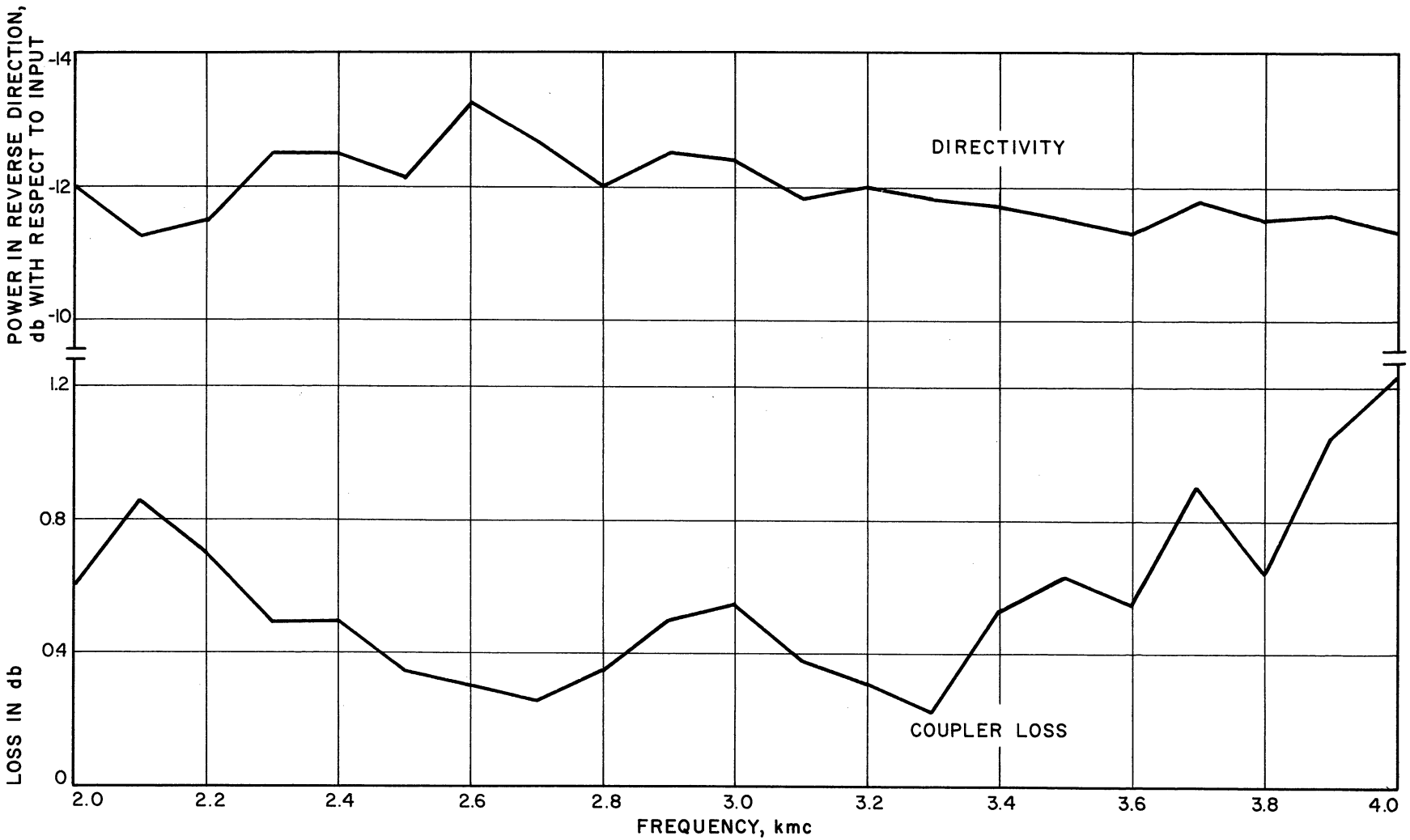

FIG. V.7 TYPICAL COUPLER LOSS AND DIRECTIVITY OF S-BAND CRESTATRON COUPLED-HELIX COUPLERS.

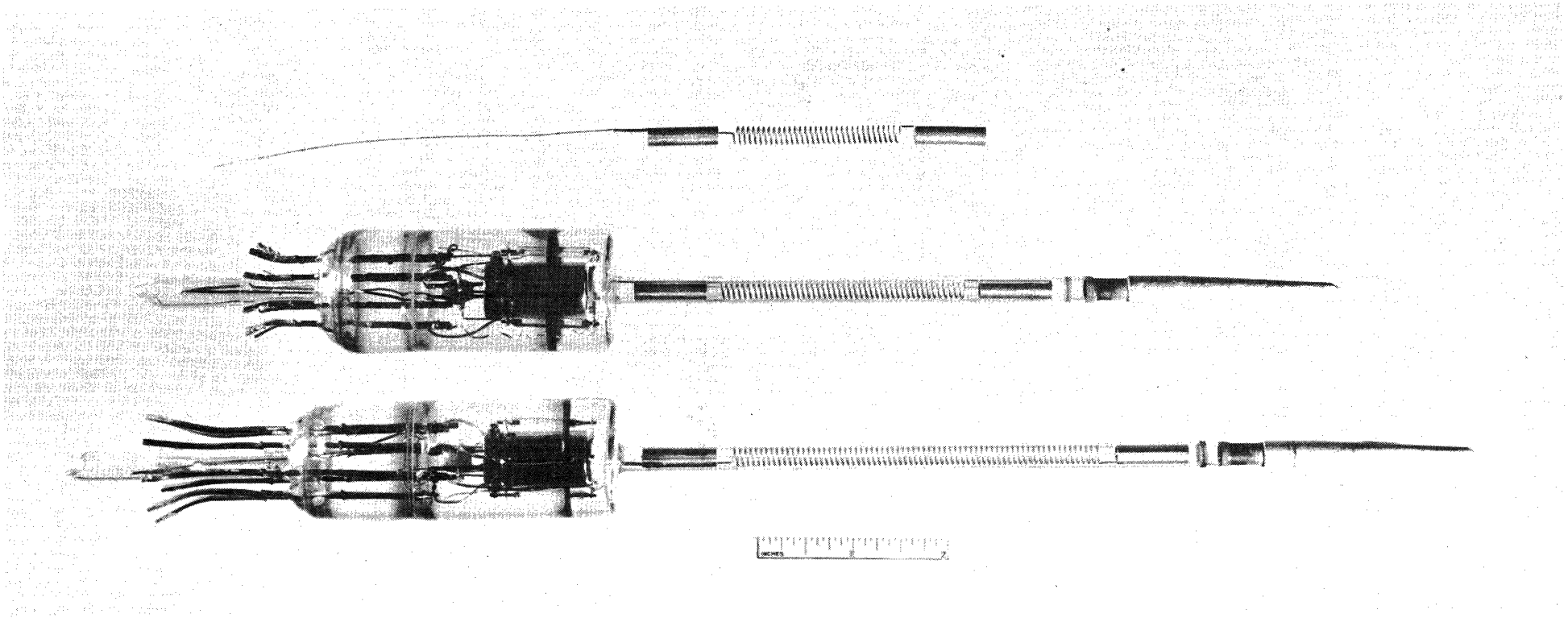

FIG. V. 8 EARLY MODELS OF THE CW S-BAND CRESTATRON.

dissipate 700-800 watts of beam power quite readily. The water flow during operation is approximately 1 liter per minute.

In spite of the severe size limitations which rule out any elaborate collector designs, a two-stage collector was constructed which would permit operation of the final beam collector considerably below beam potential. This would improve the overall efficiency of the device greatly, as pointed out by Wolkstein[4]. A tube using this type of collector was constructed and the beam transmission to the final collector was found to be quite satisfactory.

F. CW Operation of the Crestatron

During the early stages of the Crestatron investigation considerable trouble was experienced with the construction of tubes which worked in a satisfactory fashion. The main difficulty was in the assembly of the cw electron gun, which would have a high beam perveance and a low anode interception. The first cw tube from which fairly satisfactory results were obtained was the Crestatron with a 3.75-inch helix, designated the S-8-3. The perveance obtained with this tube was in the neighborhood of 0.6 microperv. Small-signal gain curves are shown in Fig. V.9. At the lower frequencies the tube is operating as a growing-wave amplifier, while for the higher frequencies operation is in the beating-wave regime. It is apparent that the transition between the two regions is gradual and smooth. The broad bandwidth of operation can be seen in Fig. V.9.

The results of saturation measurements for the S-8-3 are shown in Fig. V.10, where power output is plotted versus power input for a number of voltages, and hence values of b. These curves represent the

4. Wolkstein, H. J., "The Effect of Collector Potential on the Efficiency of Traveling-Wave Tubes", RCA Review, vol.XIX, pp. 259-282; June, 1958.

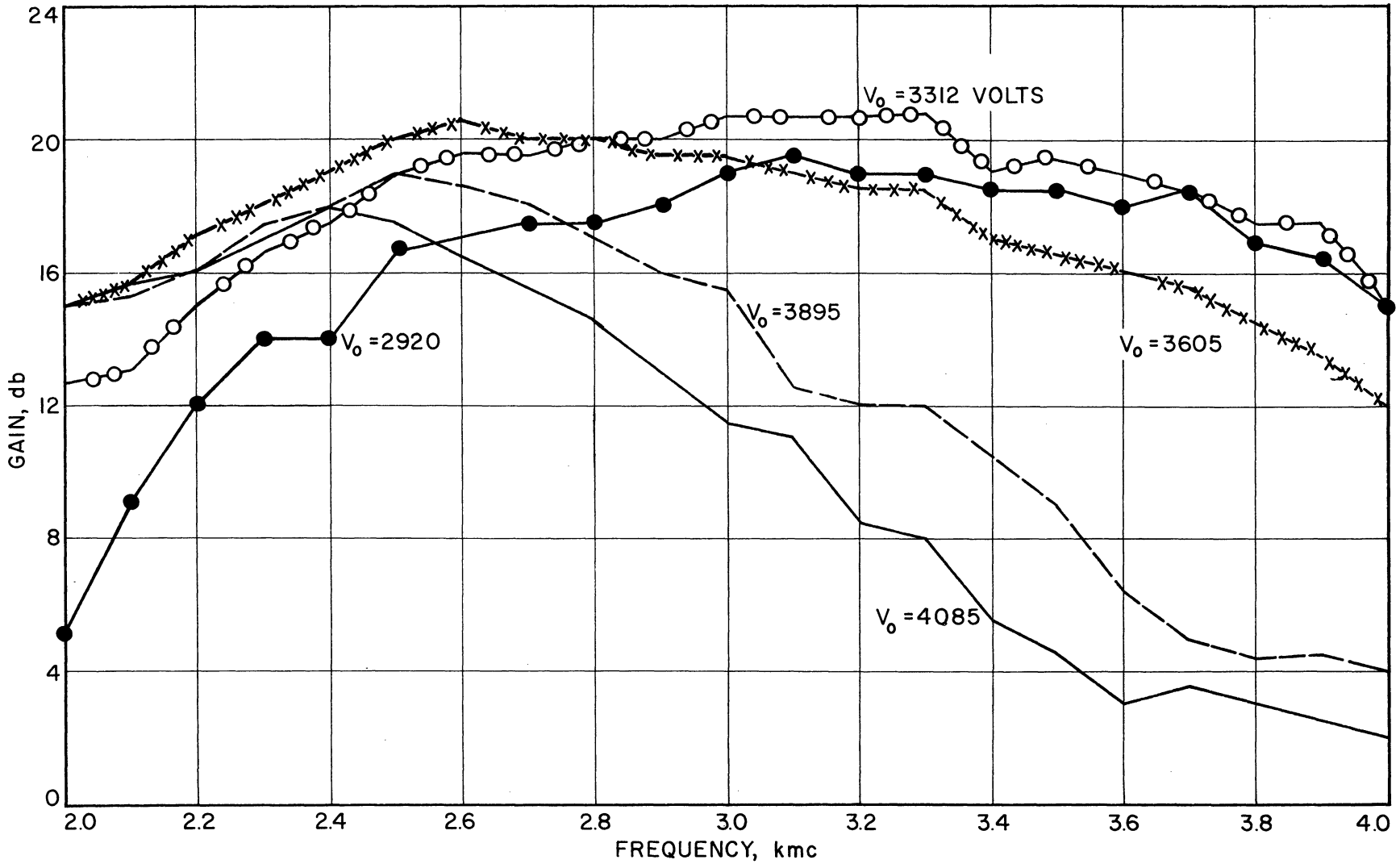

FIG. V. 9 SMALL-SIGNAL GAIN vs. FREQUENCY FOR S-8-3 CRESTATRON. DRIVE LEVEL ≅ 100 mw ; AT 3.0 KMC, C=0.095, QC=0.185, $P_\mu \cong 0.60$

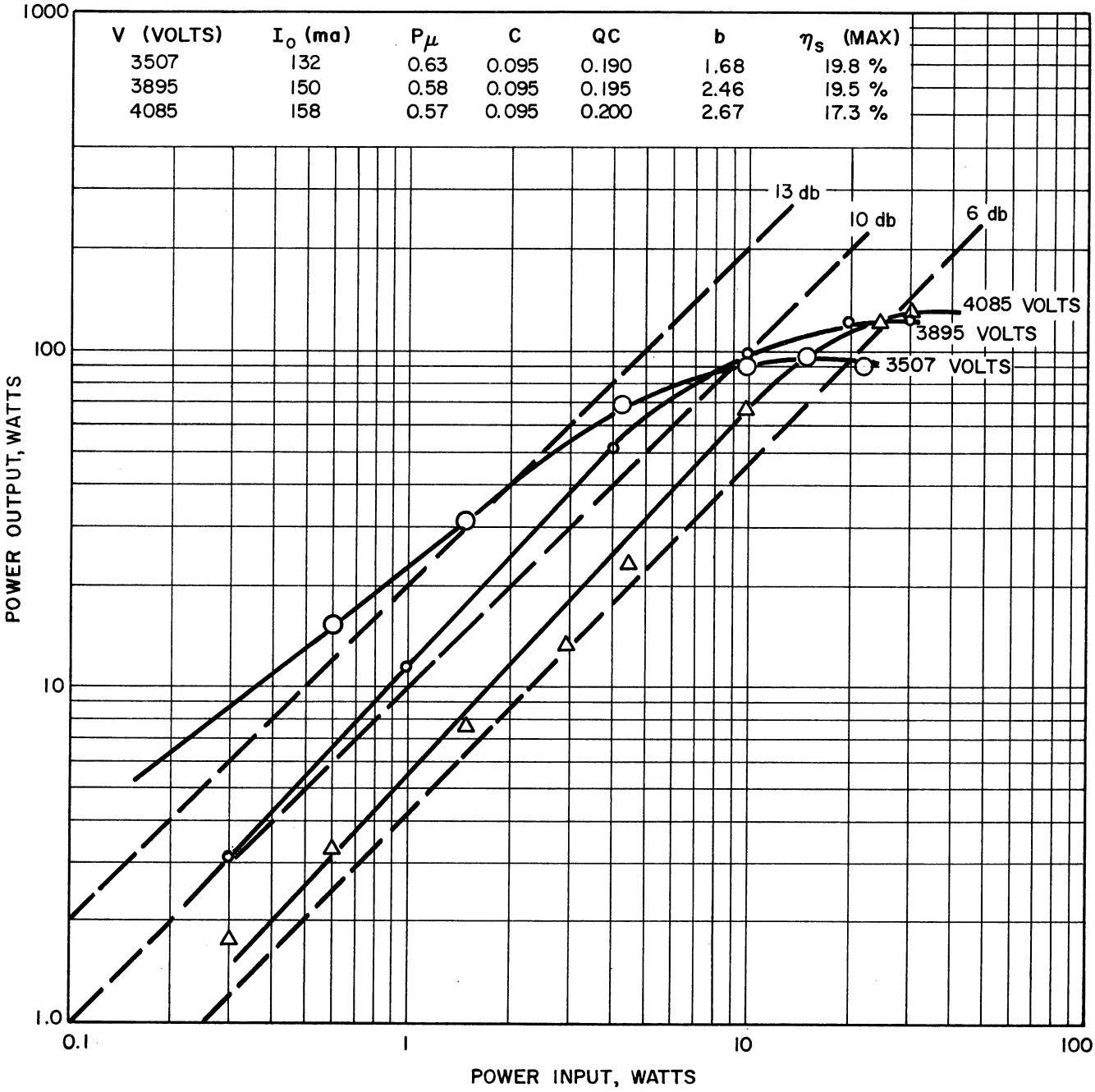

FIG. V. 10 POWER OUTPUT vs. POWER INPUT FOR THE S-8-3 CRESTATRON AT 3.0 KMC.

Crestatron operation very well and show the general nature of the saturation characteristics. Power outputs well in excess of 100 watts cw were obtained from this tube.

Theoretically it has been shown[5] that the saturation efficiency and power output increase significantly as the drive level is increased. The experimentally determined efficiency vs. drive level is shown in Fig. V.11 for various values of the injection velocity parameter. The highest efficiency of 20 percent occurred at a b of 2.5, which corresponds to a low-level gain of 15 db and a saturation gain of approximately 10 db. It should be remembered that the efficiency of the tube is computed after the input power has been subtracted from the output power, as the former is a substantial portion of the latter for a moderate-gain device like the Crestatron. Losses of the r-f couplers, which amount to 0.5-0.8 db each over the band, have also been accounted for.

In order to experimentally investigate the beating phenomenon of a Crestatron as a function of length of the tube the S-10-4 was constructed. This tube had a 7-inch helix, any desired length of which could be selected during operation by moving the coupled-helix couplers. The S-10-4 and its coupling system are shown in Fig. V.12. This tube employed a cw gun also, and the perveance achieved was just slightly less than that of the S-8-3. In Fig. V.13 the variation of gain with interaction length is shown. The curve labeled "V_0 = 4000 v" shows the characteristics of beating-wave behavior very clearly. The reason that the maxima and minima are not more sharply defined is that the coupled-helix couplers have a finite length and as a result give an average result at the critical points.

---

5. Rowe, J. E., loc. cit., (Fig. 14)

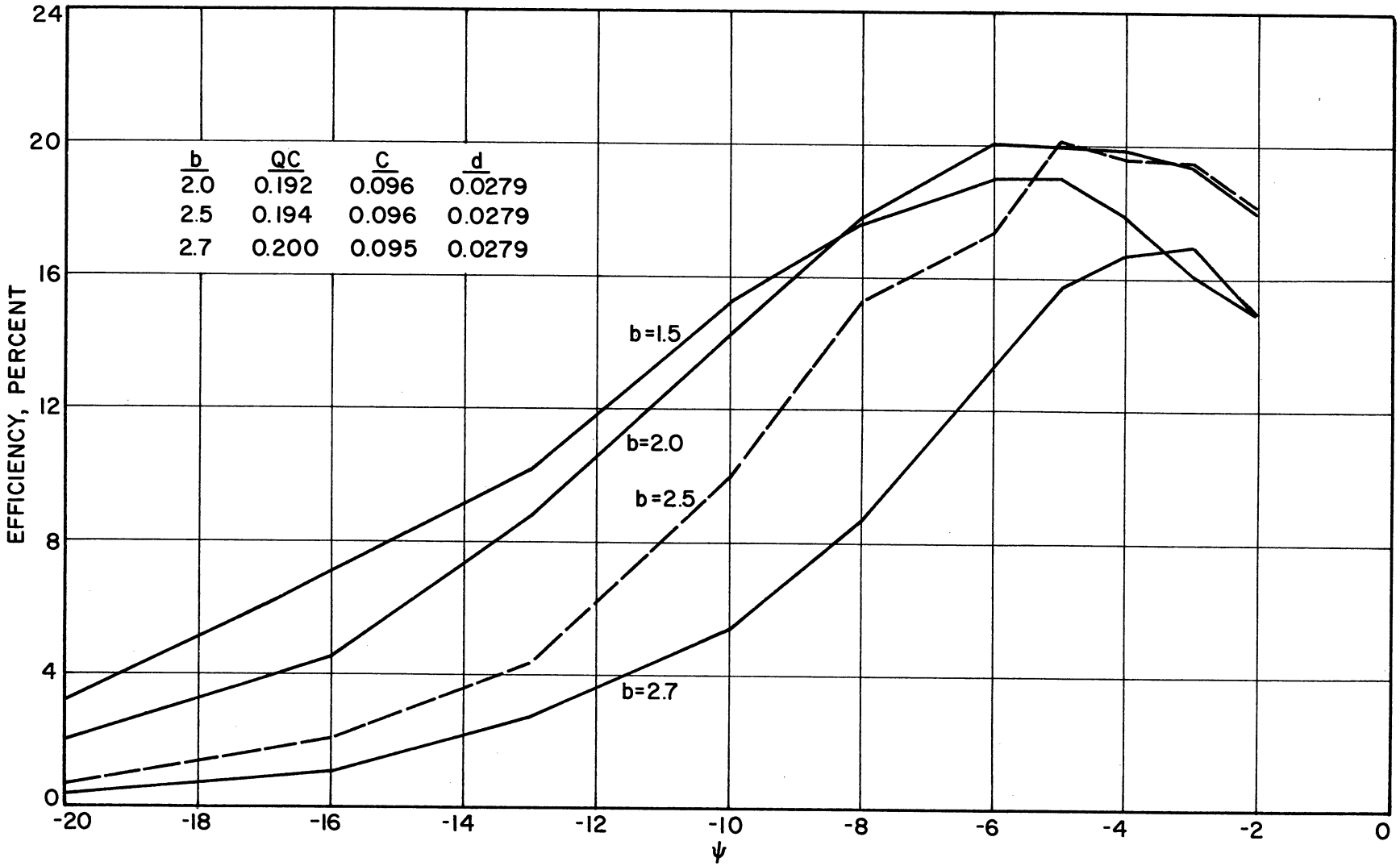

FIG. V.11 SATURATION EFFICIENCY vs. ψ (INPUT SIGNAL LEVEL IN db RELATIVE TO CI_oV_o) WITH b AS THE PARAMETER FOR THE S-8-3 CRESTATRON AT 3.0 KMC.

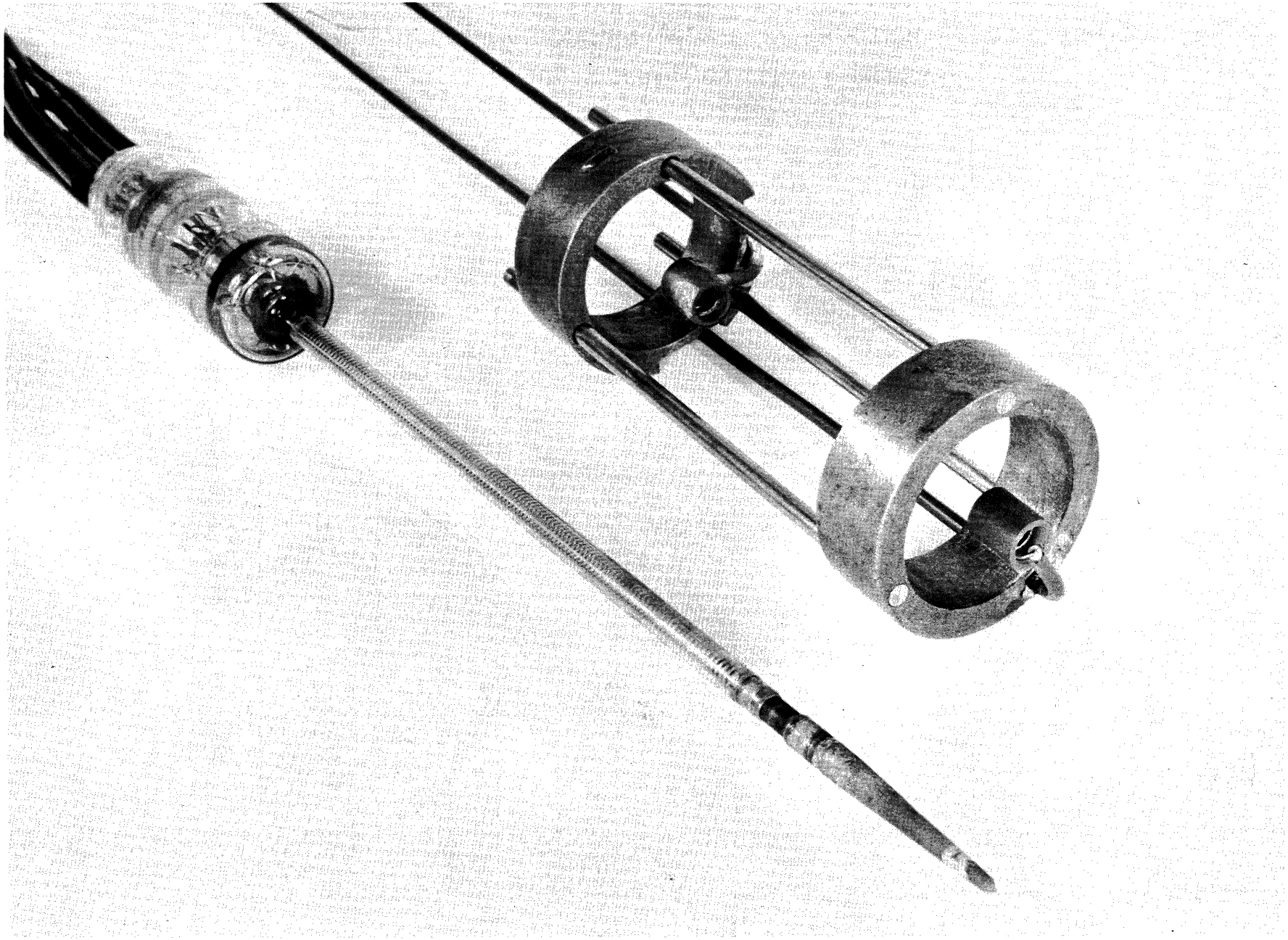

FIG. V.12 VARIABLE LENGTH S-BAND CRESTATRON AND COUPLER CARRIAGE.

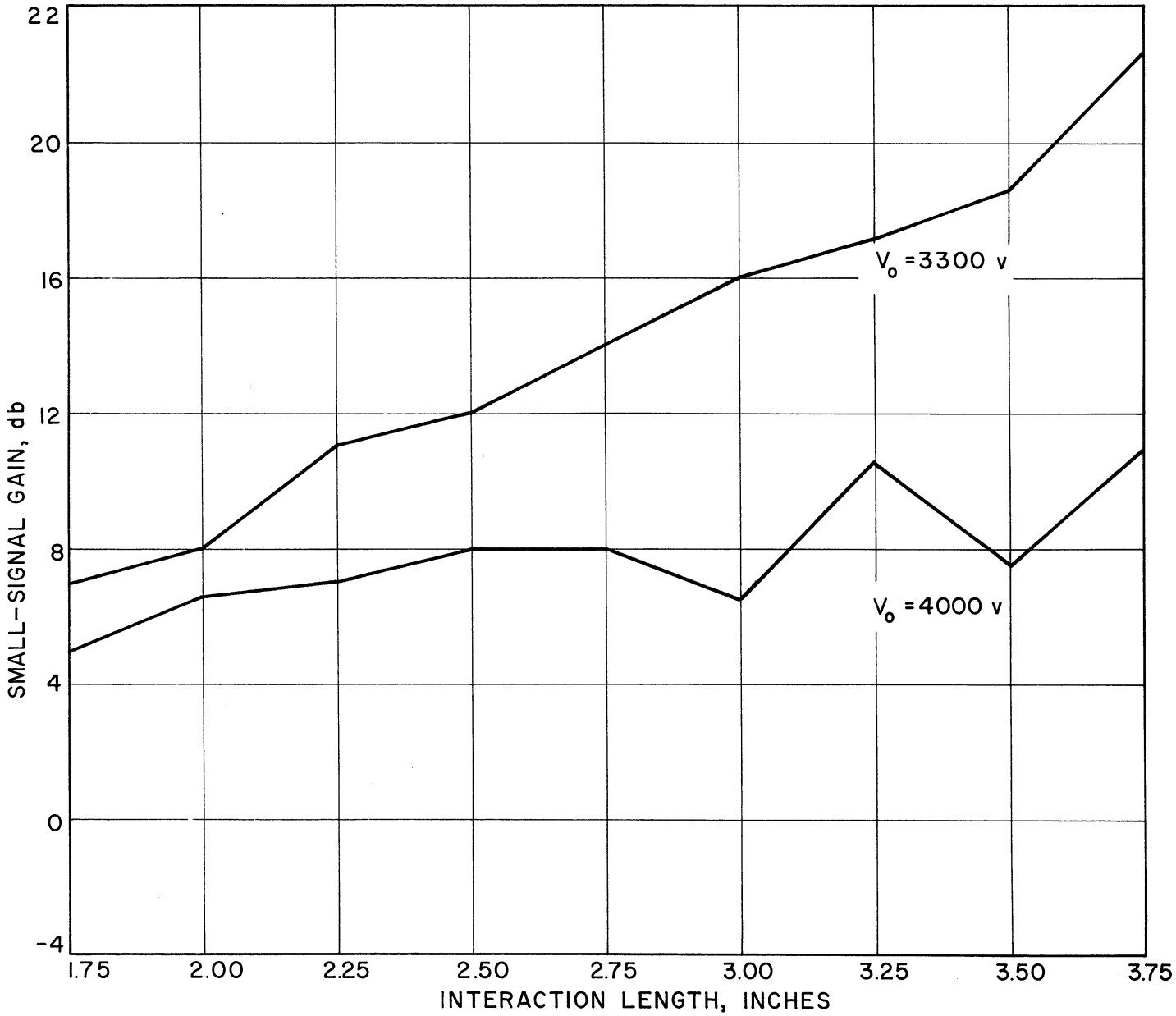

FIG.V.13 SMALL-SIGNAL GAIN vs. R-F INTERACTION LENGTH FOR S-10-4 CRESTATRON. ($b/a'=\infty$, FREQ. =3.0 kmc)

The S-10-4 was also operated with a metallic shield external to the helix. The results of small-signal measurements for a 3.0-inch interaction length are shown in Fig. V.14 for both shielded and unshielded cases. It can be seen that the gain for the shielded helix is considerably less than that for the unshielded one. Since the effect of the shield is to reduce the low-frequency impedance, the constant-gain bandwidth is generally broadened. This is not immediately obvious from Fig. V.14, because for a given voltage the values of b are different for the shielded and unshielded cases. However, the widening of the band has been clearly observed on these Crestatrons when the shield was added.

The high-power drive curves for the S-10-4 were quite similar to those for the S-8-3, except that the efficiency was slightly lower in this case due to the lowered gain parameter C. Two high-power r-f drive sources were used. One was cw and the other pulsed at a duty cycle of 0.001. The agreement between the two methods was very good. Highest power levels attained with this tube were in the neighborhood of 180 watts. A plot of maximum efficiency at saturation is shown in Fig. V.15.

In order to increase the tube efficiency considerably, the S-11-1 was constructed with a two-stage collector. Beam transmission to the last collector stage was quite satisfactory, indicating that this design is entirely feasible. A mechanical error in the construction of this tube prevented the tube from being r-f tested at operating voltages.

G. Pulsed Operation of the Crestatron

Since it did not seem feasible to obtain a sufficiently stiff beam with the cw guns without a major redesign effort, it was decided to obtain a pulsed gun capable of supplying the desired beam. The gun eventually used could be operated at a duty cycle as high as 0.01. This Crestatron was designated the S-12-1.

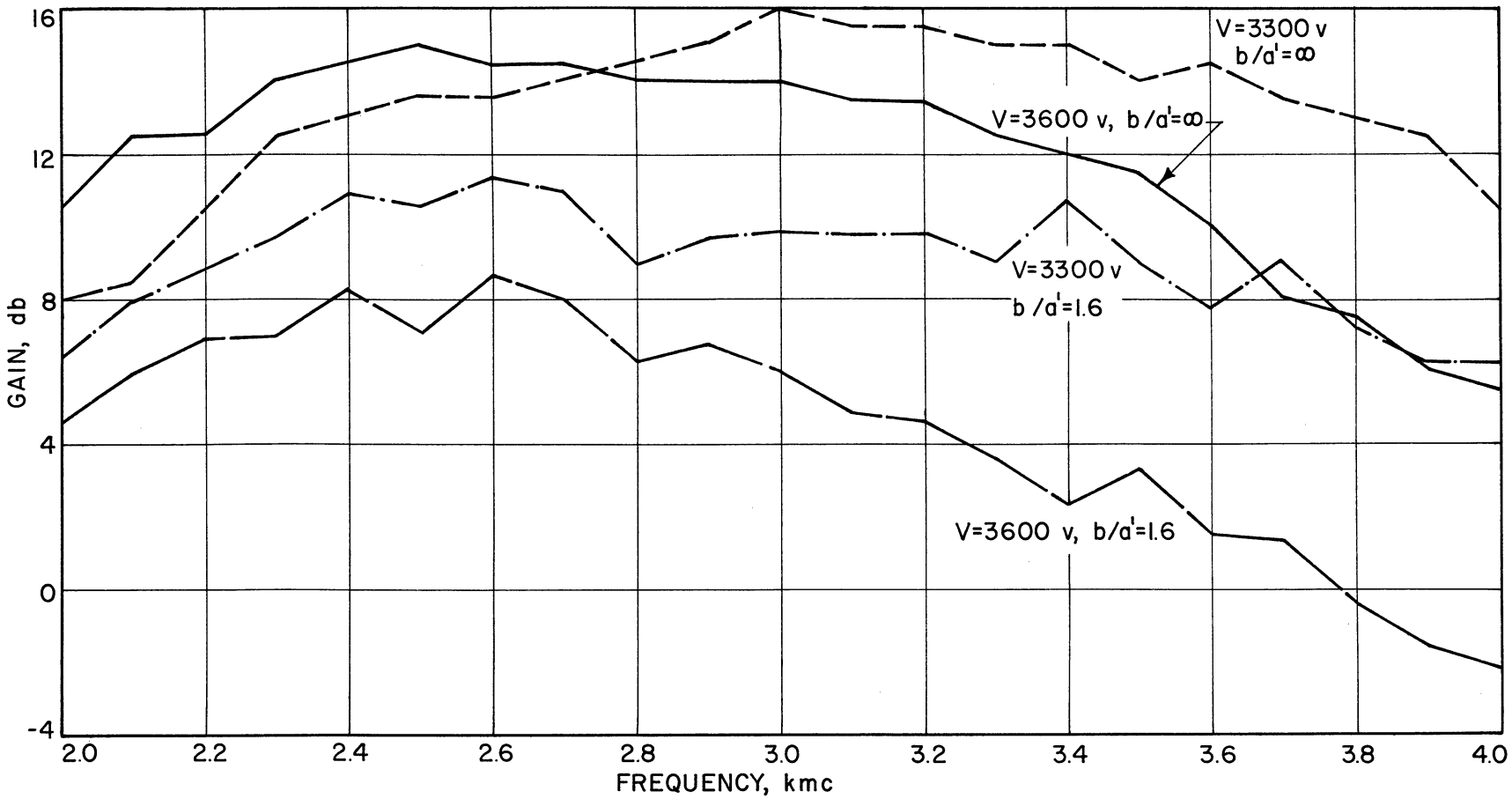

FIG. V.14 SMALL-SIGNAL GAIN vs. FREQUENCY FOR THE S-10-4 CRESTATRON WITH VOLTAGE AS A PARAMETER FOR SHIELDED AND UNSHIELDED HELICES. (LENGTH = 3.0 INCHES, DRIVE LEVEL ≅ 10 mw)

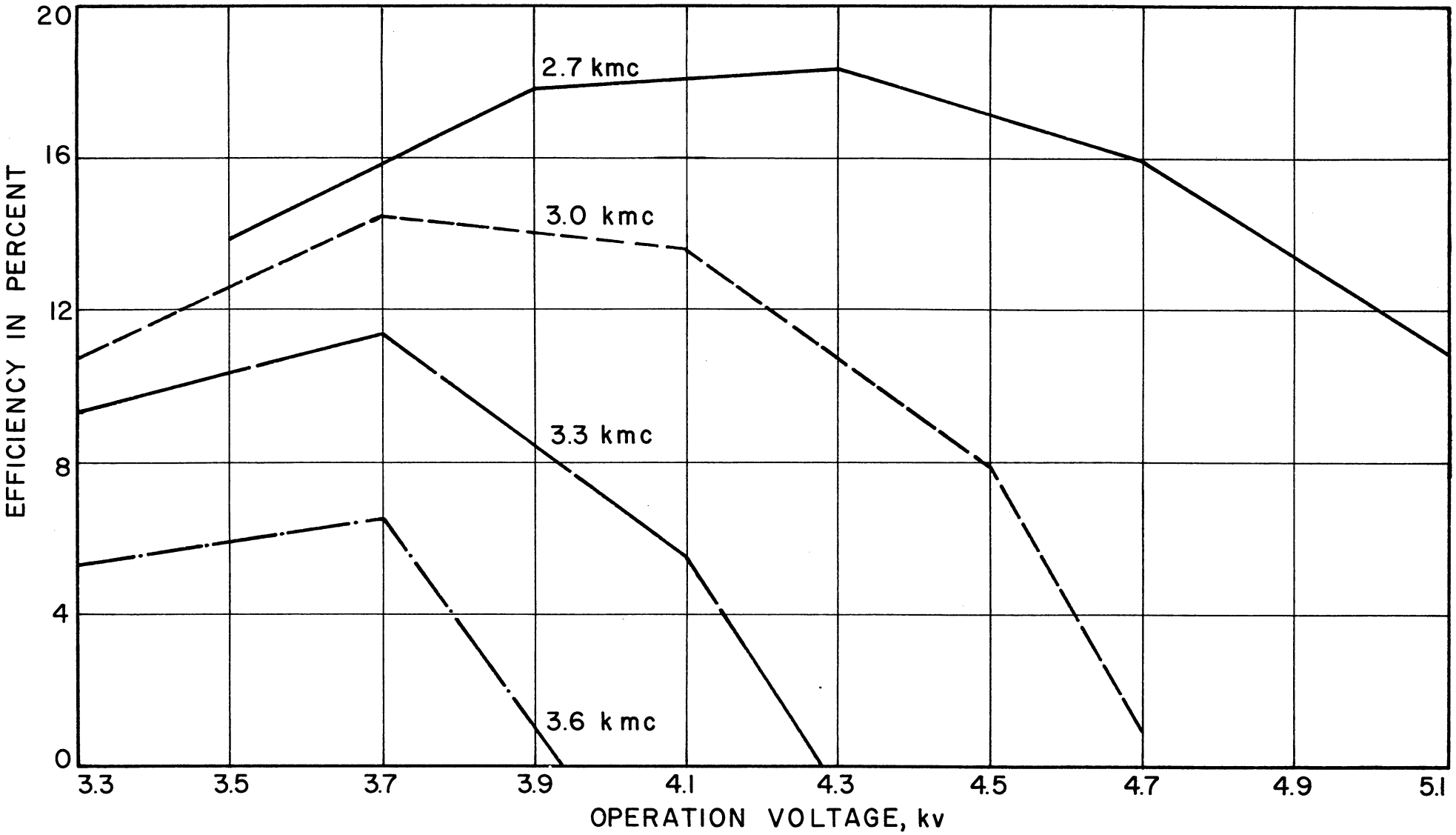

FIG. V.15 MAXIMUM SATURATION EFFICIENCY vs. OPERATING VOLTAGE FOR THE S-10-4 CRESTATRON. INTERACTION LENGTH = 3.25 INCHES

At first the S-12-1 was tested using a beam perveance of approximately 1.0 microperv which could be easily achieved by pulsing the grid to the necessary value. The small-signal results are shown in Fig. V.16. Here the smooth transition from growing- to beating-wave regimes is brought out particularly well. Saturation measurements are shown in Figs. V.17 and V.18. The highest power output values obtained under these conditions were somewhat less than 500 watts with efficiencies nearly 25 percent. It can be seen from the table accompanying each graph that the QC values were between 0.2 and 0.3. This is a fairly high value if high saturation efficiencies are desired, as the debunching forces are quite substantial.

Figures V.19 and V.20 show the saturation gain and the saturation efficiency respectively, as a function of the drive level, with the injection velocity as a parameter. Figure V.20 clearly shows that the best efficiencies are obtained in the beating-wave regime.

When the beam perveance was increased, the power output capability of the S-12-1 could be raised considerably. The improvement in efficiency was, however, only moderate. Peak output powers of well over 1 kilowatt were obtained at efficiencies of nearly 27 percent, as shown in Fig. V.21. The gain of the tube under these conditions was still near 10 db. It is believed that if the loss factor d could be reduced and the QC values held to 0.1 or a little higher, further significant improvements in the performance mentioned above could be made.

H. Conclusions

The experimental results obtained from the series of S-band Crestatrons investigated during this period fairly well substantiate the theoretical predictions. Two areas of further improvements are fairly obvious: a) reduction of helix loss coupled with good beam transmission;

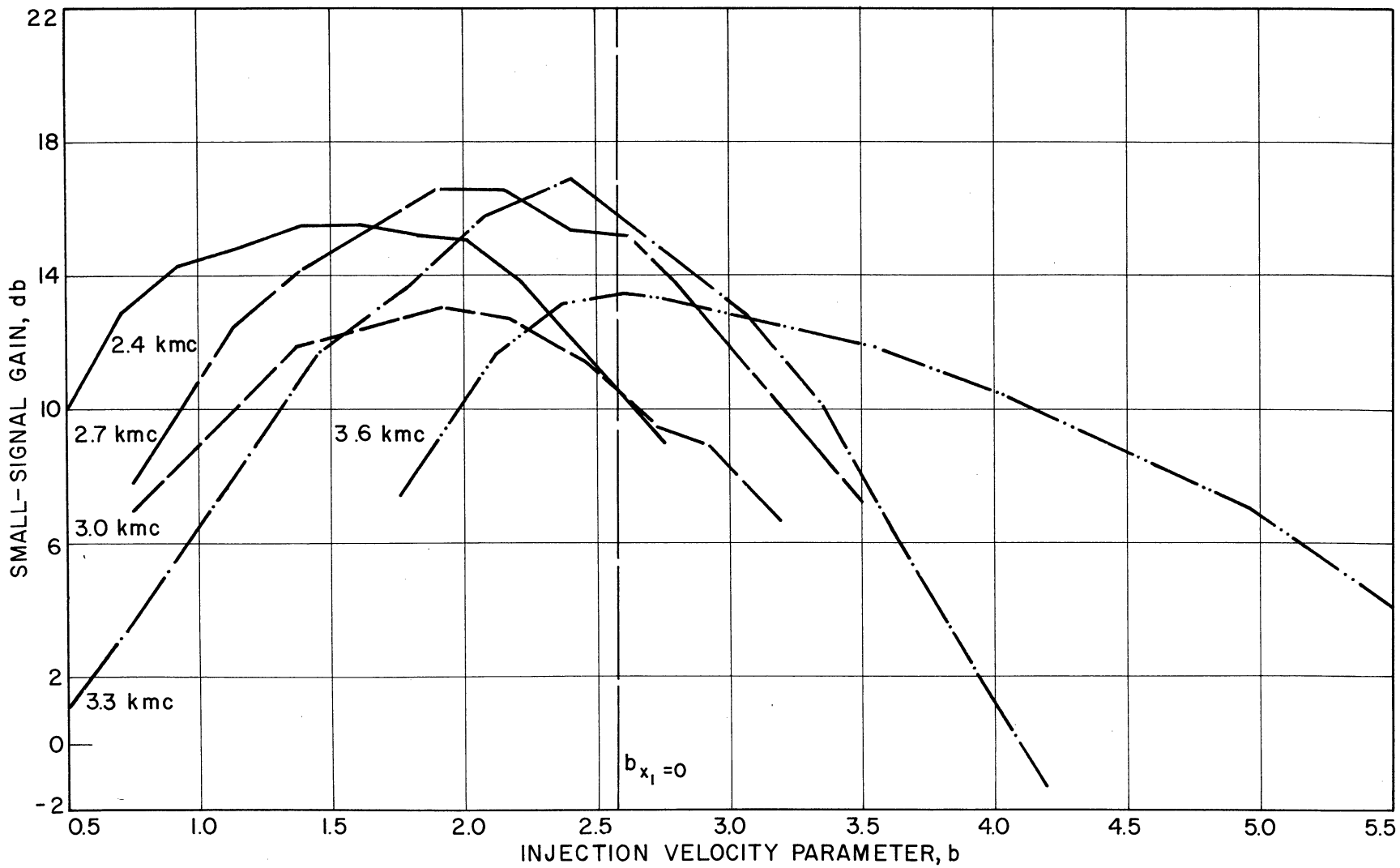

FIG. V. 16 SMALL-SIGNAL GAIN AS A FUNCTION OF b FOR THE S-12-1 PULSED CRESTATRON. INTERACTION LENGTH = 2.42 INCHES, R-F DUTY CYCLE = 0.001.

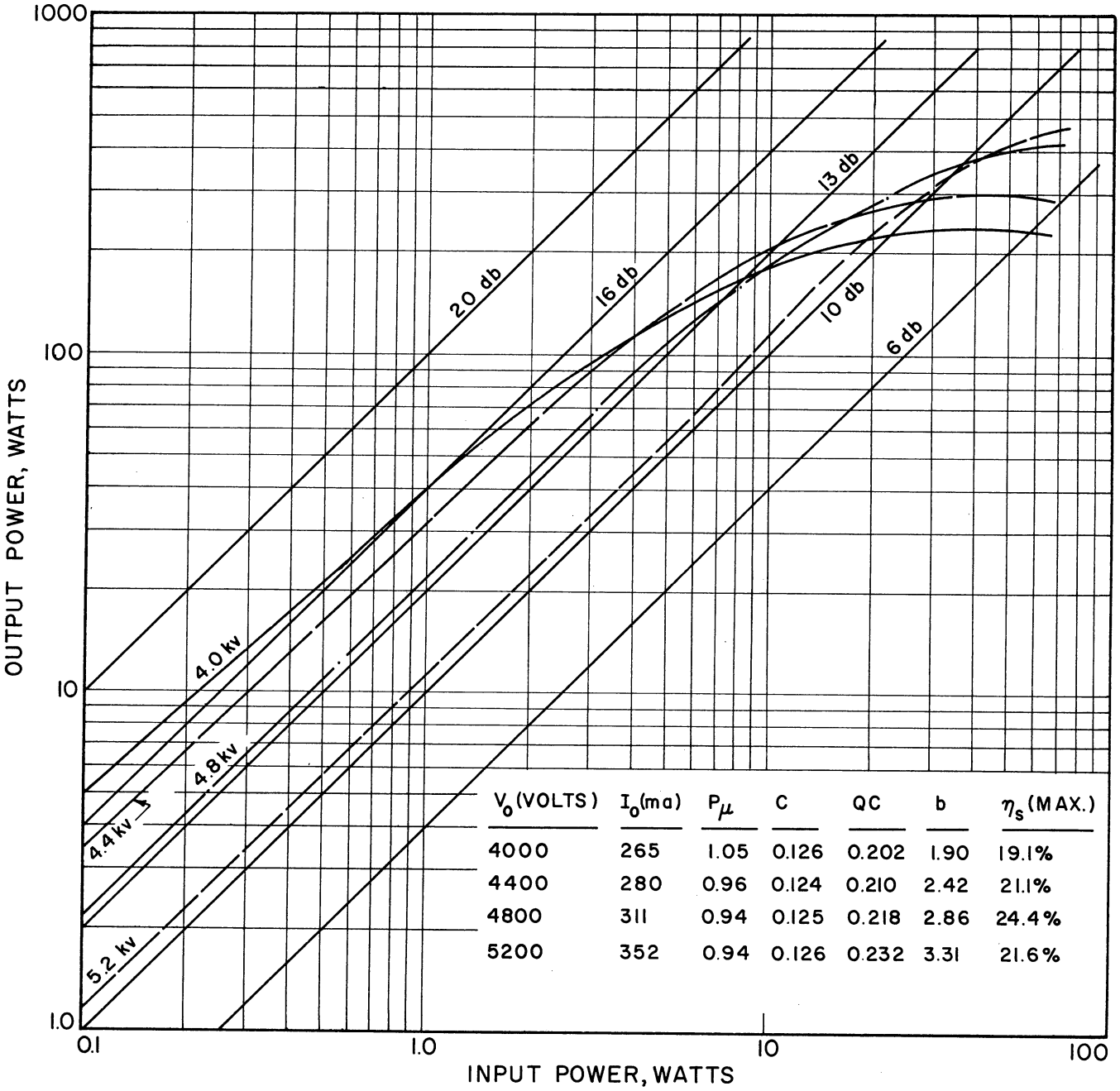

V_0 (VOLTS)	I_0 (ma)	P_μ	C	QC	b	η_s (MAX.)
4000	265	1.05	0.126	0.202	1.90	19.1%
4400	280	0.96	0.124	0.210	2.42	21.1%
4800	311	0.94	0.125	0.218	2.86	24.4%
5200	352	0.94	0.126	0.232	3.31	21.6%

FIG. V.17 SATURATION GAIN FOR THE S-12-1 PULSED CRESTATRON AT 2.7 KMC. INTERACTION LENGTH = 2.42 INCHES, R-F DUTY CYCLE = 0.001.

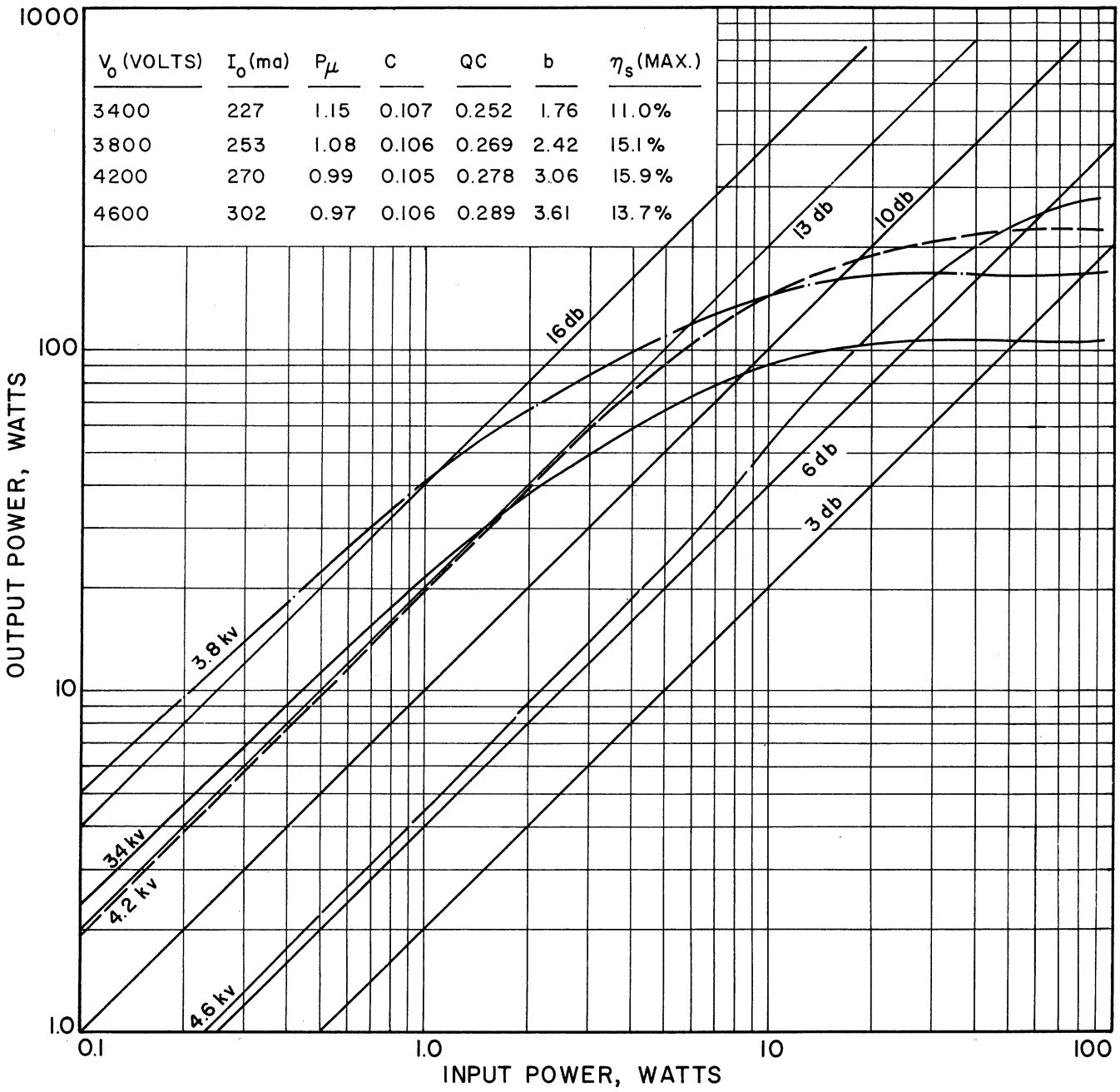

V_0 (VOLTS)	I_0 (ma)	P_μ	C	QC	b	η_s (MAX.)
3400	227	1.15	0.107	0.252	1.76	11.0%
3800	253	1.08	0.106	0.269	2.42	15.1%
4200	270	0.99	0.105	0.278	3.06	15.9%
4600	302	0.97	0.106	0.289	3.61	13.7%

FIG. V. 18 SATURATION GAIN FOR THE S-12-1 PULSED CRESTATRON AT 3.3 KMC. INTERACTION LENGTH=2.42 INCHES, R-F DUTY CYCLE =0.001.

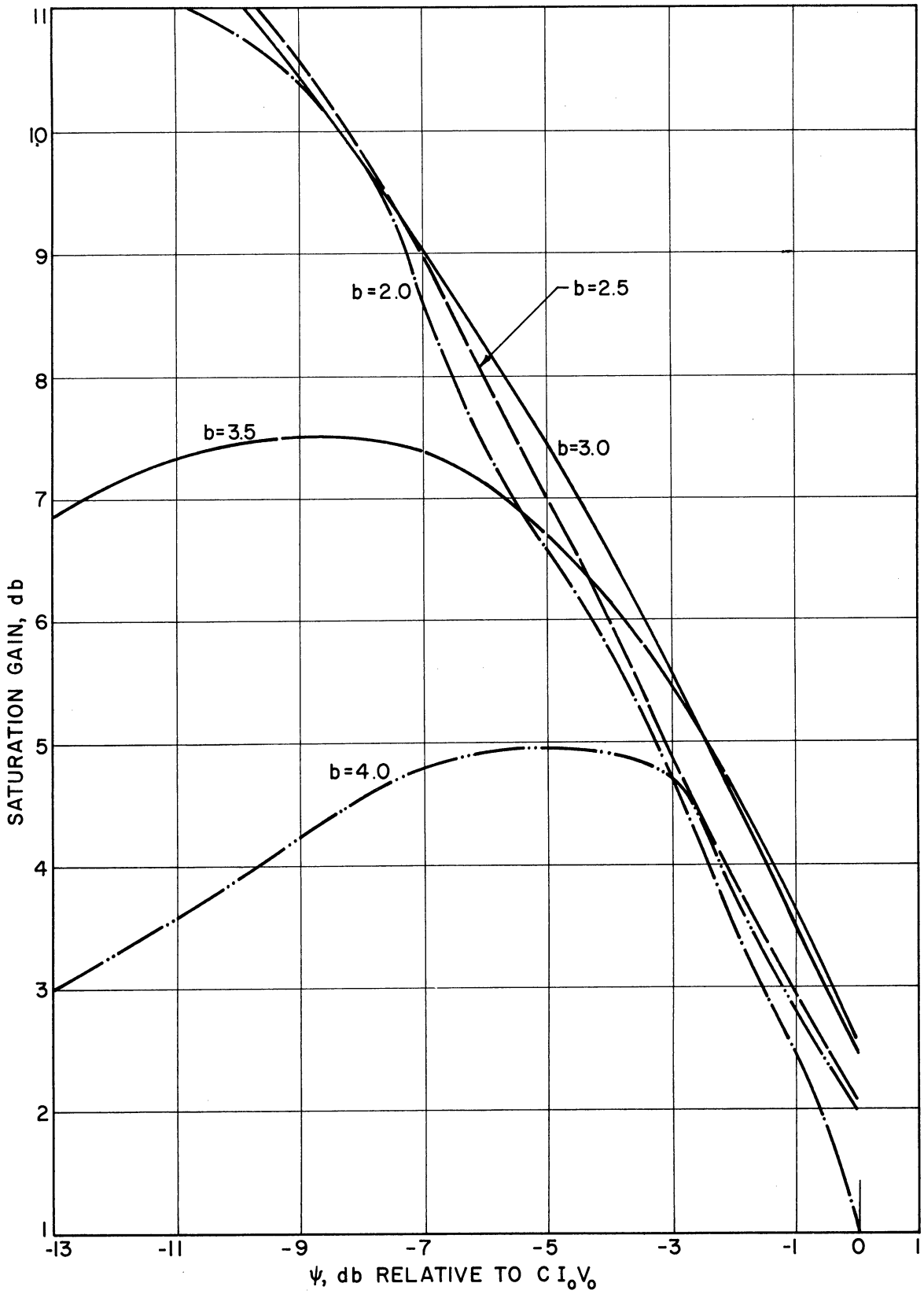

FIG.V.19 SATURATION GAIN AS A FUNCTION OF ψ (INPUT SIGNAL LEVEL IN db RELATIVE TO CI_0V_0) WITH b AS THE PARAMETER FOR THE S-12-1 PULSED CRESTATRON. INTERACTION LENGTH=2.42 INCHES. (C=0.11, QC=0.25, $b_{x_1=0}$=2.57, B=1.1, d = 0.02)

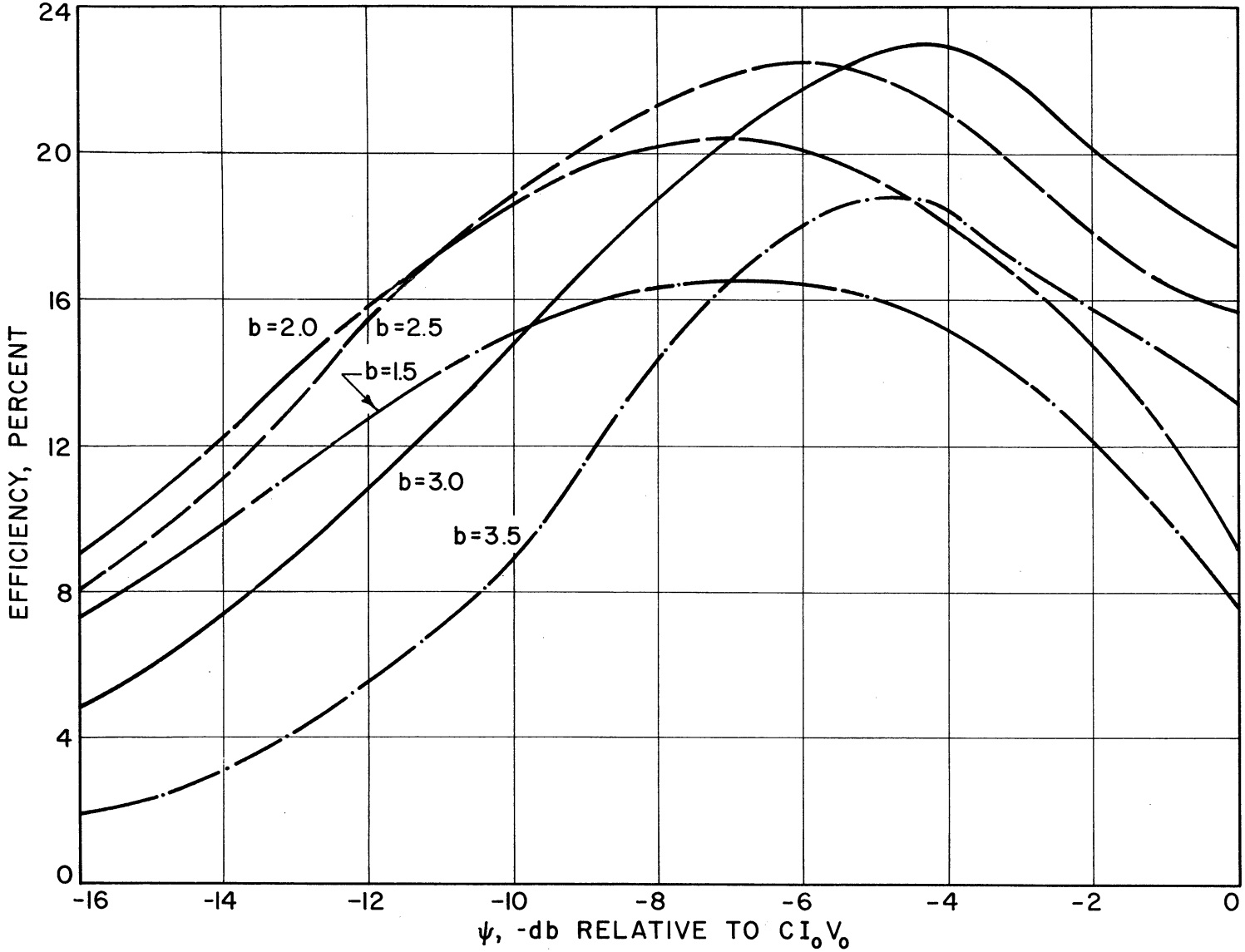

FIG. V.20 SATURATION EFFICIENCY vs. INPUT SIGNAL LEVEL RELATIVE TO CI_oV_o FOR THE S-12-1 PULSED CRESTATRON. INJECTION VELOCITY IS THE PARAMETER. LENGTH=2.42 INCHES. (C=0.12, QC=0.20, $b_{x_1}=0$, B=0.88, d=0.02)

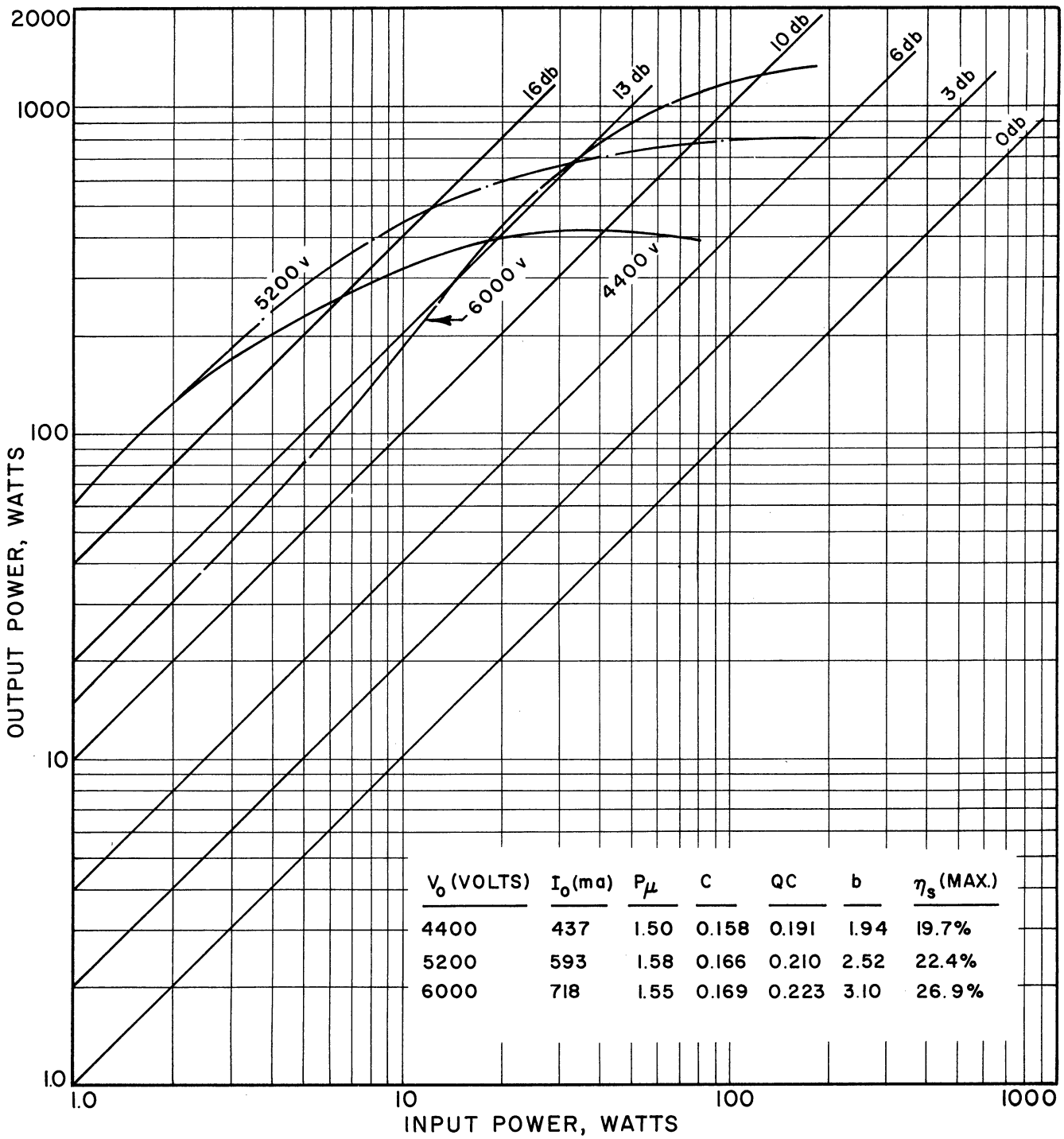

V_0 (VOLTS)	I_0 (ma)	P_μ	C	QC	b	η_s (MAX.)
4400	437	1.50	0.158	0.191	1.94	19.7%
5200	593	1.58	0.166	0.210	2.52	22.4%
6000	718	1.55	0.169	0.223	3.10	26.9%

FIG. V. 21 SATURATION GAIN FOR THE S-12-1 PULSED CRESTATRON AT 2.7 KMC. INTERACTION LENGTH = 2.42 INCHES, R-F DUTY CYCLE = 0.001.

and b) a thorough study of depressed collector operation. Other fairly fruitful approaches may be the possibility of prebunching the beam or various means of keeping a bunch, once it is formed, in synchronism with the circuit wave for a maximum length of time so that a more efficient energy interchange may take place.

VI. ANALYSIS OF MODULATED O-TYPE DEVICES (H. Sobol, J. E. Rowe)

A. Introduction

New techniques for noise reduction, higher efficiency, lighter weight and improved fabrication methods are contributing to the increased system utilization of traveling-wave tubes. The traveling-wave tube which is inherently a broadband amplifier has certain narrow-band features that make it attractive as a modulator, whereas the broadband capabilities contribute towards its usefulness as a mixer. The traveling-wave tube provides a tool for modulation and mixing near output power levels. The klystron[1] was used in similar applications several years ago.

The literature contains several analyses[2,3,4,5,6] of the modulated traveling-wave tube; however each analysis has certain drawbacks because

1. Learned, V., "The Klystron Mixer Applied to T-V Relaying", Proc. IRE, vol. 38, No. 9, pp. 1033-35; September, 1950.
2. Bray, W. J., "The Traveling-Wave Value as a Microwave Phase-Modulator and Frequency Shifter", Proc. IEE, vol. 99, (Part III), pp. 15-20; January, 1952.
3. Beam, W. R., and Blattner, D. J., "Phase Angle Distortion in Traveling-Wave Tubes", RCA Review, vol. 17, pp. 86-99; March, 1956.
4. Cumming, R. C., "The Serrodyne Frequency Translator", Proc. IRE, vol. 45, No. 2, pp. 175-185; February, 1957.
5. DeGrasse, R. W., "Frequency Mixing in Microwave-Beam Devices", Tech. Report 386-2, Stanford University, Electron Devices Laboratory, Stanford Electronics Laboratories; July, 1958.
6. Louisell, W. H., and Quate, C. F., "Parametric Amplification of Space-Charge Waves", Proc. IRE, vol. 46, No. 4, pp. 707-716; April, 1958.

of the approximations used. The purpose of this investigation was to develop a general modulation analysis in which the effects of modulation on C, QC, d, b, the initial wave amplitudes, nonlinearities, and trajectory crossings are included.

A beam modulation as discussed here is defined as a coherent disturbance or signal placed on the beam in addition to the information excited on the beam at the carrier frequency. The modulations studied below are all beam modulations. Two classes of beam modulations are considered, low-modulation-frequency and high-modulation-frequency signals. A low-modulation-frequency signal has a period very much greater than the transit time of an electron through the tube, and the frequency is much less than the carrier frequency. Transit-time effects for this class of modulations are negligible. Transit-time effects are not negligible, however, for the second class of modulations since in this instance the frequency of the modulating signal is of the same order as the carrier frequency.

In this study both the low- and high-frequency beam-modulated traveling-wave tube will be analyzed. Results are given for the low-frequency beam-modulated case, while the high-frequency analysis is used to investigate the longitudinal-beam parametric amplifier.

B. Low Modulation Frequencies - Calculations of the Modulation Device Functions

Signal falling into the low-modulation-frequency class can be excited on the beam by either of two methods. One method is to slowly vary the velocity of electrons entering the interaction region, while the second is to slowly vary the number of electrons per unit time entering the interaction region. The velocity is varied by modulating the circuit potential. The prime effect of this modulation is to

disturb the transit time of electrons, which in turn affects the phase of the r-f on the circuit. A secondary effect of this phase modulation is the amplitude modulation produced by varying the beam power. The number of electrons per unit time, or the current entering the interaction region, is modulated by varying the potential of a grid located near the cathode. The current modulation results primarily in an amplitube modulation with a small degree of accompanying phase modulation.

A quasi-static solution is used to determine the behavior of the tube with low-frequency beam modulations. It is possible under these conditions to determine the modulation characteristics by calculating the parameters at several points in the modulation cycle and then treating each point as if the tube were unmodulated. Another and more elegant way is to set up the problem in terms of the zero-modulation tube parameters and the modulating signal amplitude. In this way the phase and amplitude modulation for a set of given unmodulated conditions may be determined directly as a function of the modulation. The characteristics obtained using the second method are called modulation device functions. The amplitude of the modulating signals is introduced by postulating average beam current I_o and potential V_o, at the entrance to the interaction region, as

$$V_o = V_{o1}\left(1 + \frac{\Delta V}{V_{o1}}\right) \qquad \text{(VI.1)}$$

and

$$I_o = I_{o1}\left(1 + \frac{\Delta I}{I_{o1}}\right) \quad , \qquad \text{(VI.2)}$$

where ΔI is the amplitude of the current modulation,

ΔV is the amplitude of the potential modulation,

I_{o1} is the unmodulated average current, and

V_{o1} is the unmodulated average potential.

The modulation device functions will now be determined for two levels of carrier signal. It is possible to linearize the problem for the low-level or small-signal carrier, whereas the nonlinearities must be preserved for the large-signal carrier. In the small-signal problem, the quantities can be assumed to vary as

$$f = f_{o1} + f_1(z,\omega_1 t,\omega_2 t, \ldots \omega_n t) + f_2(z,\omega t) \quad , \qquad \text{(VI.3)}$$

where f is a general electrokinetic variable,

f_{o1} is the quiescent average value,

f_1 is the change in the average value due to modulation,

$\omega_1,\ldots\omega_n$ are the modulation frequencies,

f_2 is the perturbation due to the carrier, and

ω is the carrier frequency.

The linearized equations of motion are found in a manner analogous to Pierce's[7] derivations using the conservation of charge, Newtonian force and normal mode circuit equations in conjunction with Eqs. VI.1, VI.2 and VI.3. The linearization is introduced by assuming $f_2 \ll f_{o1}$, f_1, and the low modulating frequency is introduced by assuming

$$\frac{\partial f}{\partial t} \approx \frac{\partial f_2}{\partial t} \quad ,$$

$$\frac{\partial f}{\partial z} \approx \frac{\partial f_2}{\partial z} \quad .$$

7. Pierce, J. R., "Traveling-Wave Tubes", D. Van Nostrand, New York; 1950.

The time and distance derivatives are respectively replaced by the operators $j\omega$ and $-\Gamma$. The usual traveling-wave tube parameters are defined at zero modulation as C_o, QC_o, b_o, and d_o. A perturbation form of solution is then used in which the distance operator is given by

$$-\Gamma = -j\beta_{eo} - C_o\beta_e\delta(\Delta V, \Delta I, C_o, QC_o, b_o d_o) \quad . \qquad \text{(VI.4)}$$

β_{eo} is the beam radian wave number at zero modulation. Note that δ is the only term in Eq. VI.4 varying with modulation. The secular equation resulting in this form of perturbation solution is

$$\frac{1}{\xi_2}\left[j\,\frac{1-\xi_1}{C_o} + \xi_1\delta\right]^2 = \frac{[1+C_o(b_o-jd_o)]\,[1+C_o(2j\delta-C_o\delta^2)]}{-b_o+jd_o+j\delta+C_o\left[jb_od_o + \frac{d_o^2}{2} - \frac{b_o^2}{2} - \frac{\delta^2}{2}\right]}$$

$$- 4QC_o[1+C_o(2j\delta-C_o\delta^2)] \quad . \qquad \text{(VI.5)}$$

Two additional modulation parameters ξ_1 and ξ_2 appear in Eq. VI.5. They are defined as

$$\xi_1 = \left(1 + \frac{\Delta V}{V_{o1}}\right)^{1/2}$$

and

$$\xi_2 = \frac{1}{\xi_1}\left[1 + \frac{\Delta I}{I_{o1}}\right] \quad . \qquad \text{(VI.6)}$$

Equation VI.5 reverts to the usual secular equation for the unmodulated traveling-wave tube when no modulation is applied. The roots of Eq. VI.5 describe the propagation constants. There are, as in the unmodulated tube, four roots; however, one describes a backward traveling wave which is far from synchronism and which can be assumed not to exist when proper terminations are used. Typical plots of the

real (x_i) and imaginary (y_i) parts of the forward-wave propagation constants as a function of independent beam current and potential modulations are shown in Figs. VI.1 and VI.2.

The total r-f circuit potential can then be assumed to be the sum of three waves

$$V_c(z) = \mathrm{Re} \sum_{i=1}^{3} V_{ci} \exp\left[-j\beta_{eo} + \beta_{eo} C_o \delta_i\right] z \quad , \qquad \text{(VI.7)}$$

with V_{ci} being the initial amplitude of the ith wave. The initial wave amplitudes are found from a knowledge of the conditions at the input to the interaction region. These boundary conditions are the same as with the unmodulated traveling-wave tube since there is no additional r-f information on the beam with the low-frequency beam modulation. Assuming that an r-f potential $V(0)$ is applied and that there are no r-f perturbations at the input, the wave amplitudes are found by inverting

$$\begin{bmatrix} V(0) \\ 0 \\ 0 \end{bmatrix} = \begin{bmatrix} a_1 & a_2 & a_3 \\ b_1 & b_2 & b_3 \\ c_1 & c_2 & c_3 \end{bmatrix} \begin{bmatrix} V_{c1} \\ V_{c2} \\ V_{c3} \end{bmatrix} \quad , \qquad \text{(VI.8)}$$

where

$$a_i = 1 + \frac{4QC\xi_2}{\xi_1^2} \frac{(1+jC_o\delta_i')^2}{\delta_i'^2}$$

$$b_1 = a_i \frac{1+jC_o\delta_i'}{\delta_i'}$$

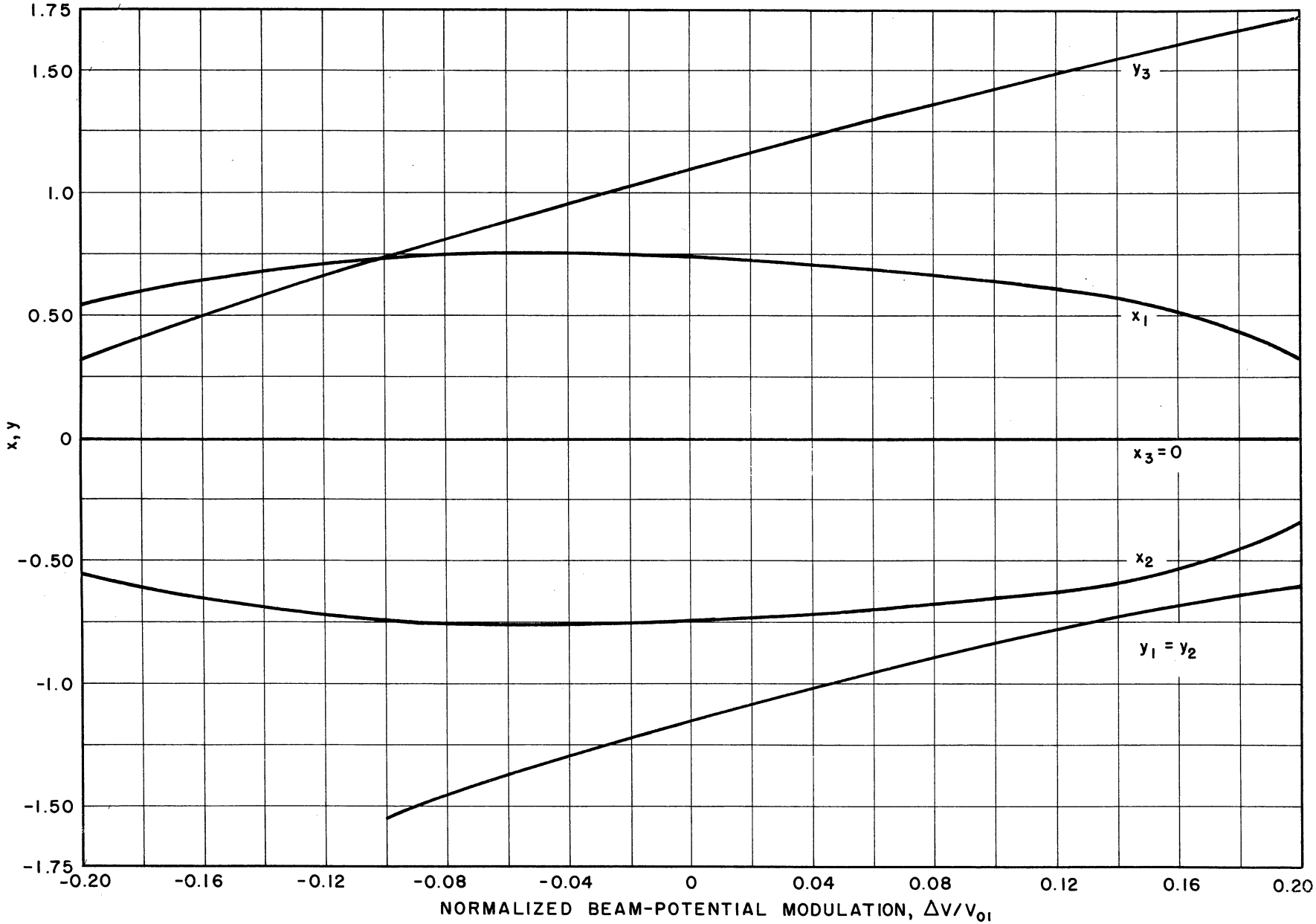

FIG. VI.1 SMALL-SIGNAL PROPAGATION CONSTANTS FOR TWA WITH MODULATED BEAM POTENTIAL. (C_0=0.10, QC_0=0.250, b_0=1.0, d_0=0, ΔI=0)

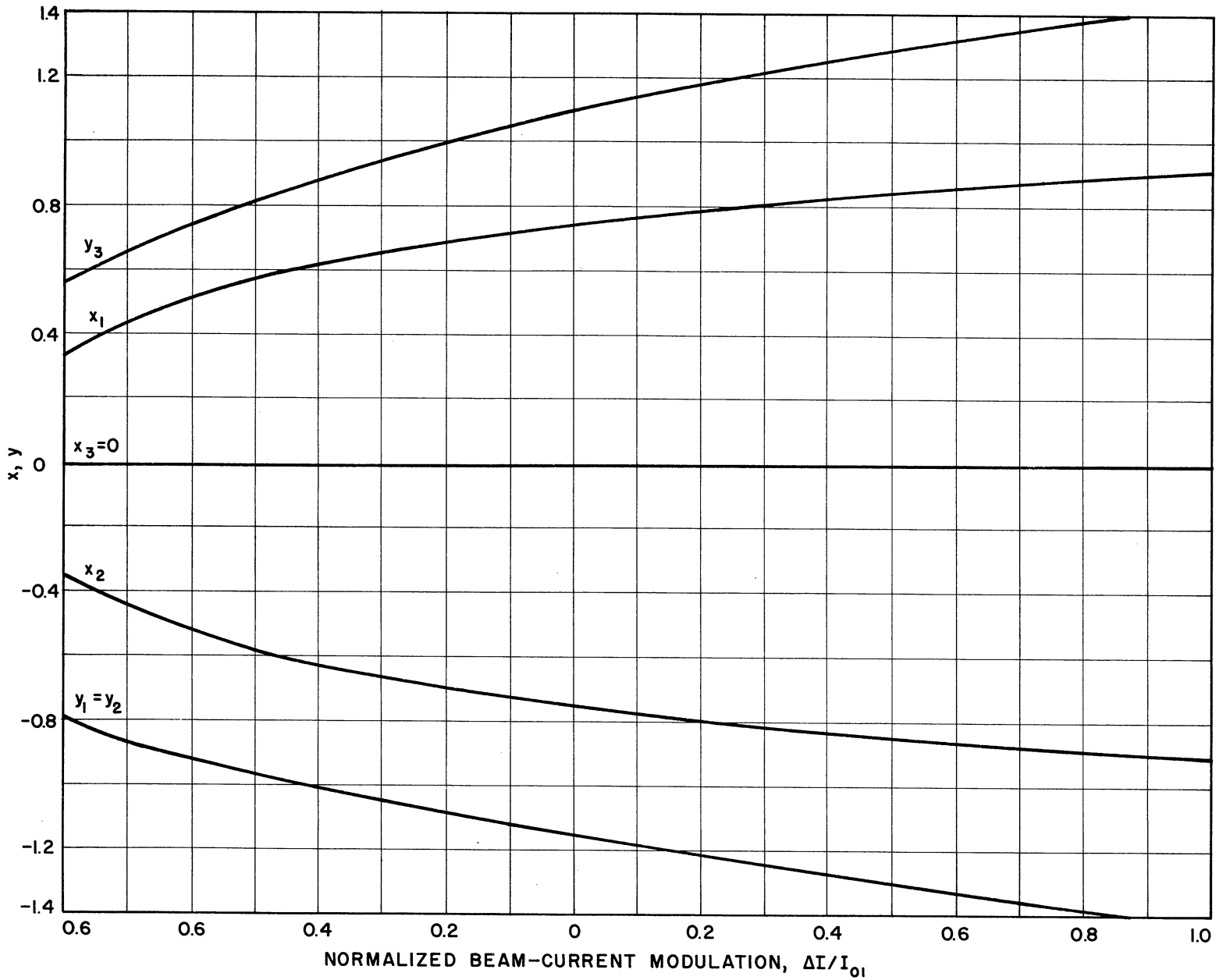

FIG. VI.2 SMALL-SIGNAL PROPAGATION CONSTANTS FOR TWA WITH MODULATED BEAM CURRENT. ($C_0=0.10$, $QC_0=0.250$, $b_0=1.0$, $\Delta V=0$)

$$c_i = a_i \frac{1+jC_o\delta_i'}{\delta_i'^2}$$

and

$$\delta_i' = j\frac{1-\xi_1}{C_o} + \delta_i\xi_1 \quad .$$

The initial wave amplitudes determined by inverting Eq. VI.8 will in general be complex numbers which can be represented by

$$V_{ci} = \hat{V}_{ci} \exp j\psi_i \quad ,$$

where $\hat{V}_{ci}$ and ψ_i are real numbers. Plots of the magnitude and phase of the amplitude of the growing wave are shown in Figs. VI.3 and VI.4 as a function of independent beam potential and current modulations. The circuit voltage can be represented in simple form as

$$V_c(z,t) = R(z) \cos [\omega t+S(z)] \quad , \qquad \text{(VI.9)}$$

where

$$R^2 = A_1^2 + A_2^2 + A_3^2 + 2A_1A_2 \cos(\zeta_1-\zeta_2)$$

$$+ 2A_2A_3 \cos(\zeta_2-\zeta_3) + 2A_3A_1 \cos(\zeta_3-\zeta_1)$$

and

$$S = \tan^{-1} \frac{A_1 \sin \zeta_1 + A_2 \sin \zeta_2 + A_3 \sin \zeta_3}{A_1 \cos \zeta_1 + A_2 \cos \zeta_2 + A_3 \cos \zeta_3} \quad ,$$

where

$$A_i = \hat{V}_{ci} \exp \beta_{eo} C_o x_i z$$

and

$$\zeta_i = \psi_i - \beta_{eo} z(1-C_o y_i) \quad .$$

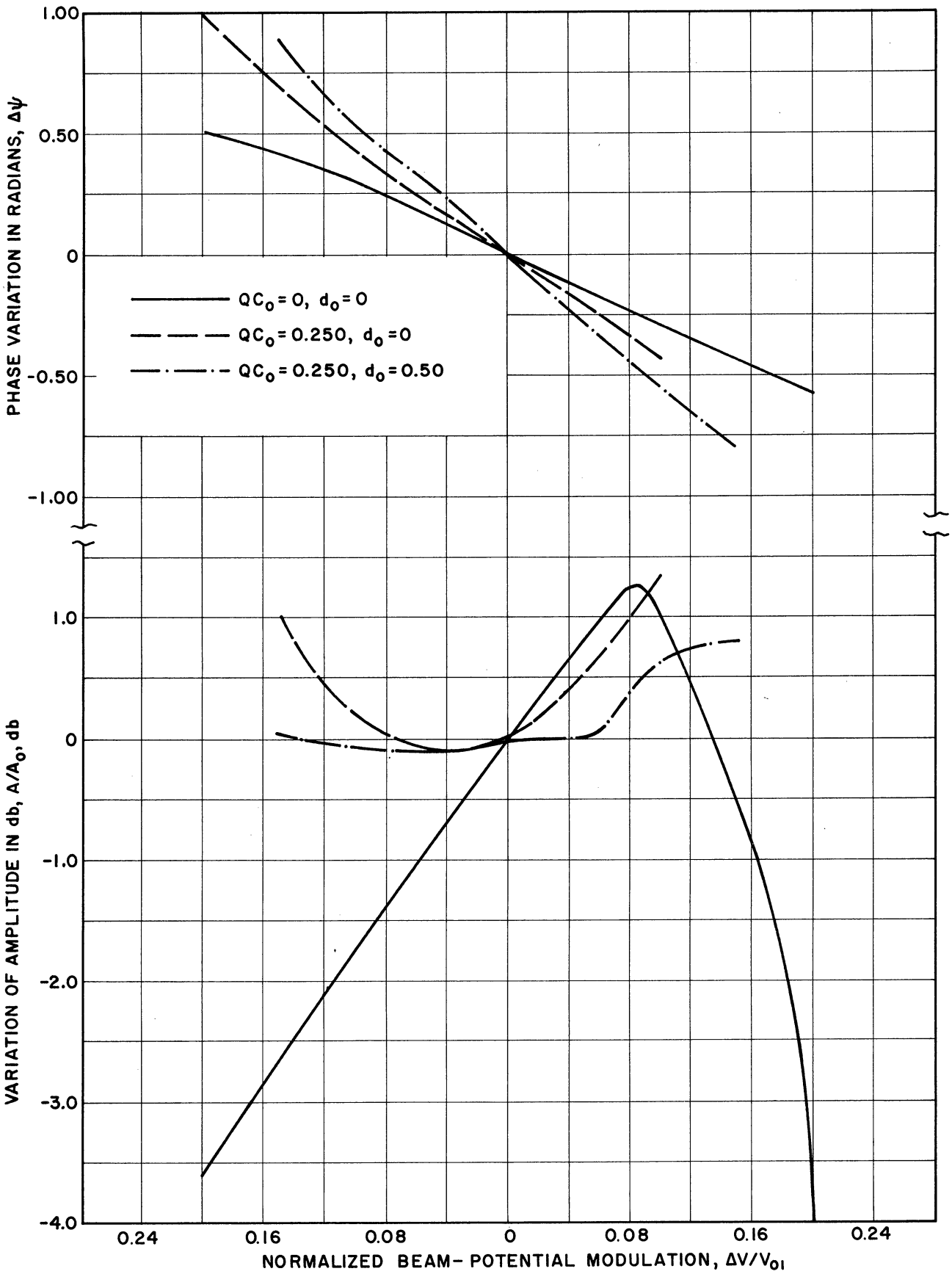

FIG. VI. 3 VARIATION OF THE PHASE AND MAGNITUDE OF "A" DURING BEAM-POTENTIAL MODULATION. (C_0=0.10, ΔI=0, b_0 ADJUSTED FOR MAXIMUM GAIN)

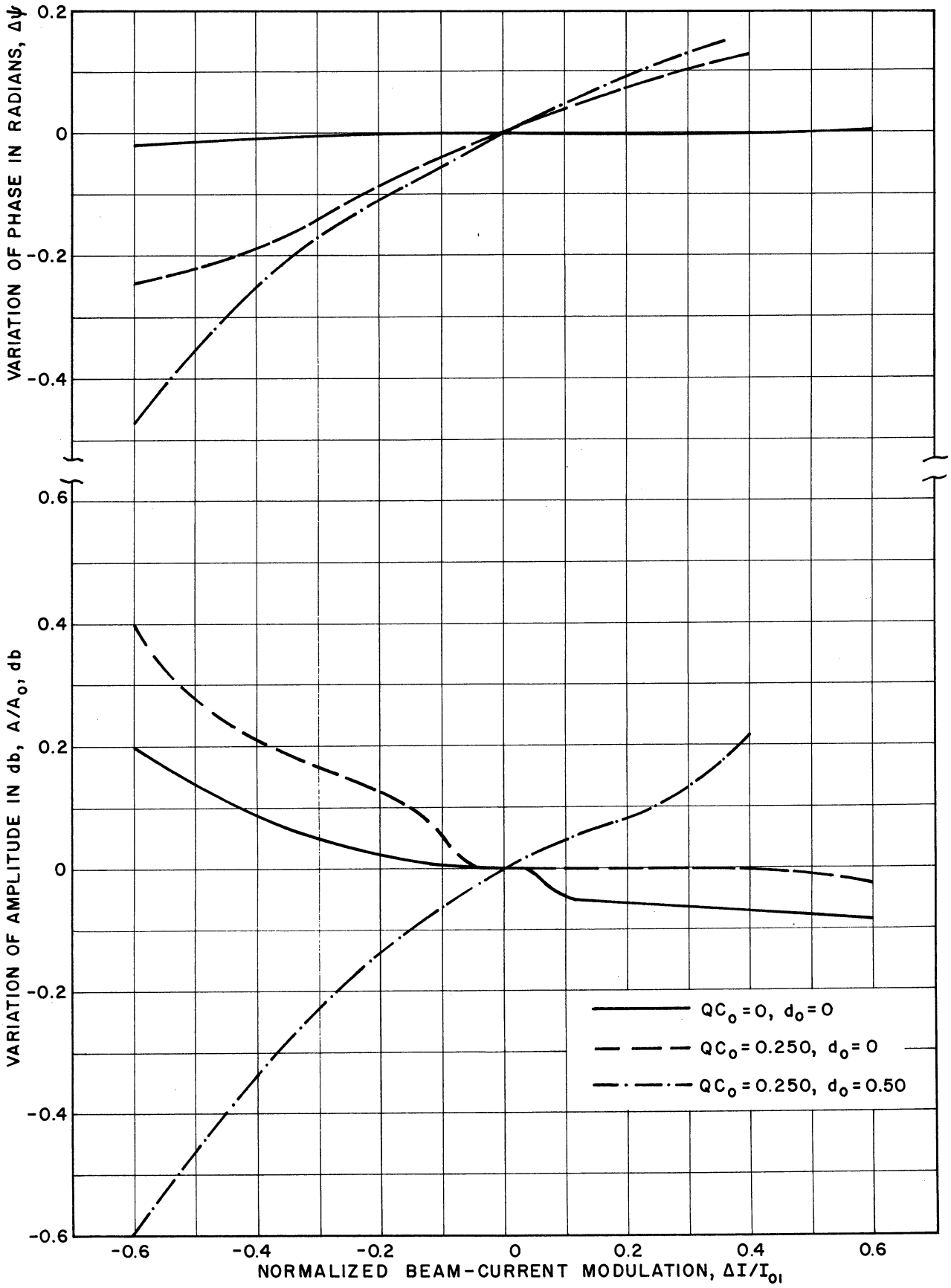

FIG. VI.4 VARIATION OF THE PHASE AND MAGNITUDE OF "A" DURING BEAM-CURRENT MODULATION. (C_0=0.10, ΔV=0, b_0 ADJUSTED FOR MAXIMUM GAIN)

For the usual traveling-wave tube it is sufficient to consider only the growing wave so that the phase and amplitude modulation, or the modulation device functions as mentioned above, are given by

$$\Delta S = 2\pi N_s C_o \{y_1(\Delta V,\Delta I) - y_1(0,0)\} + \psi_1(\Delta V,\Delta I) - \psi_1(0,0) \quad , \text{(VI.10)}$$

and

$$\Delta a_{db} = \{20 \log \frac{V_{ci}(\Delta I,\Delta V)}{V_{c1}(0,0)} + 54.6\ C_o N_s \{x_1(\Delta V,\Delta I) - x_1(0,0)\} \quad . \text{(VI.11)}$$

Typical modulation device functions as determined using Eqs. VI.10 and VI.11 are shown in Figs. VI.5 through VI.8. The modulation device functions of a short traveling-wave tube or Crestatron[8] are found by considering all three forward waves. In this case the modulation device functions are given by the general form

$$\Delta S = S(z,\Delta I,\Delta V) - S(z,0,0) \qquad \text{(VI.12)}$$

and

$$\Delta a_{db} = 20 \log \frac{R(z,\Delta V,\Delta I)}{R(z,0,0)} \quad . \qquad \text{(VI.13)}$$

The modulation device functions for a Crestatron are shown in Figs. VI.9 and VI.10. The gain of the Crestatron is proportional to $b-b_{x_1=0}$ where $b_{x_1=0}$ is the point at which the growth constant goes to zero.

The modulation device functions for the usual tube with a low-level carrier can also be found by expanding the gain and phase shift in a Taylor series about the zero-modulation operating point. The device functions therefore are given as

---

8. Rowe, J. E., "Theory of the Crestatron: A Forward-Wave Amplifier", Proc. IRE, vol. 47, pp. 536-545; April, 1959.

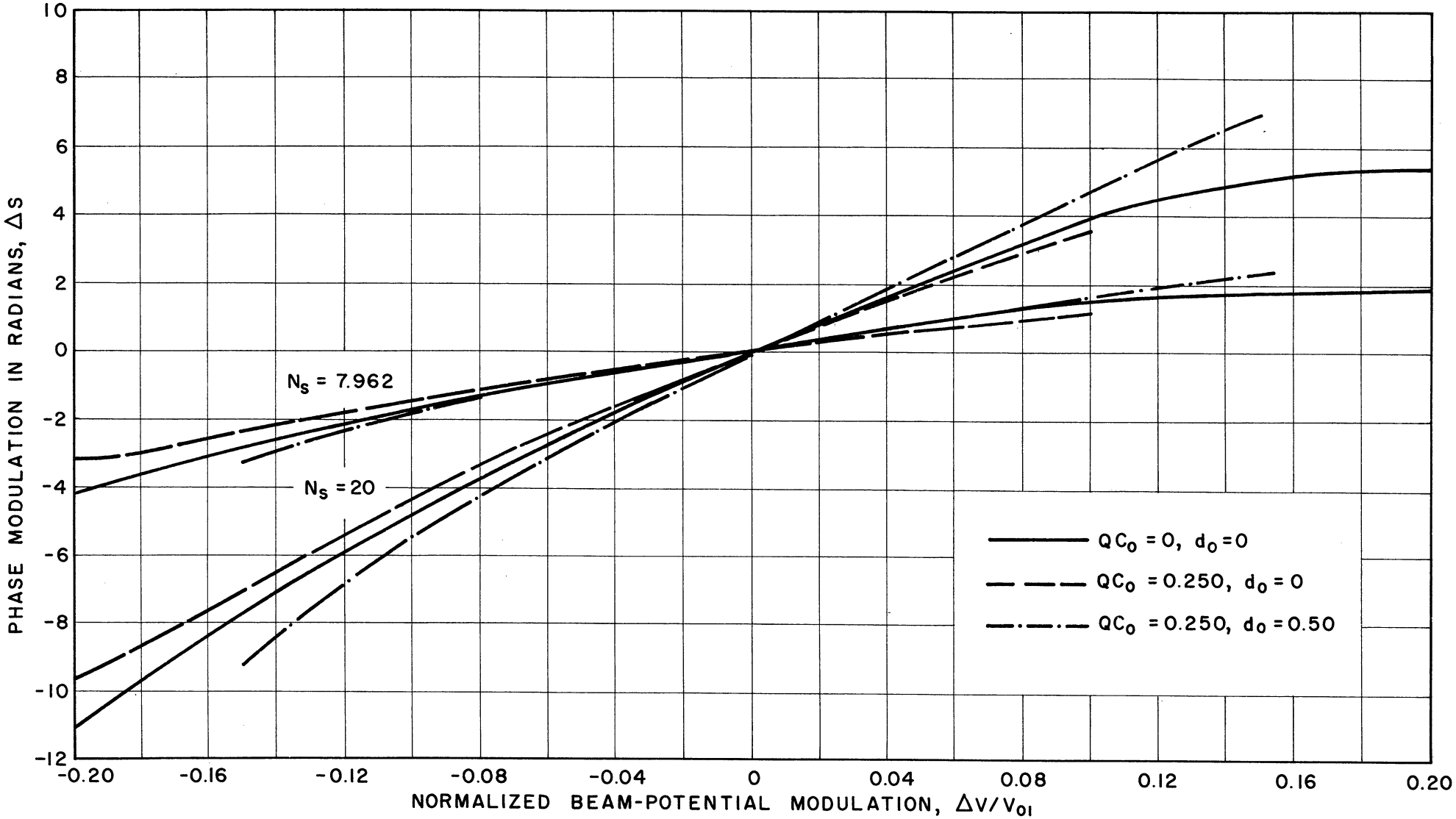

FIG. VI. 5 PHASE MODULATION DEVICE FUNCTIONS FOR BEAM-POTENTIAL MODULATION. ($C_0 = 0.10$, $\Delta I = 0$, b_0 ADJUSTED FOR MAXIMUM GAIN)

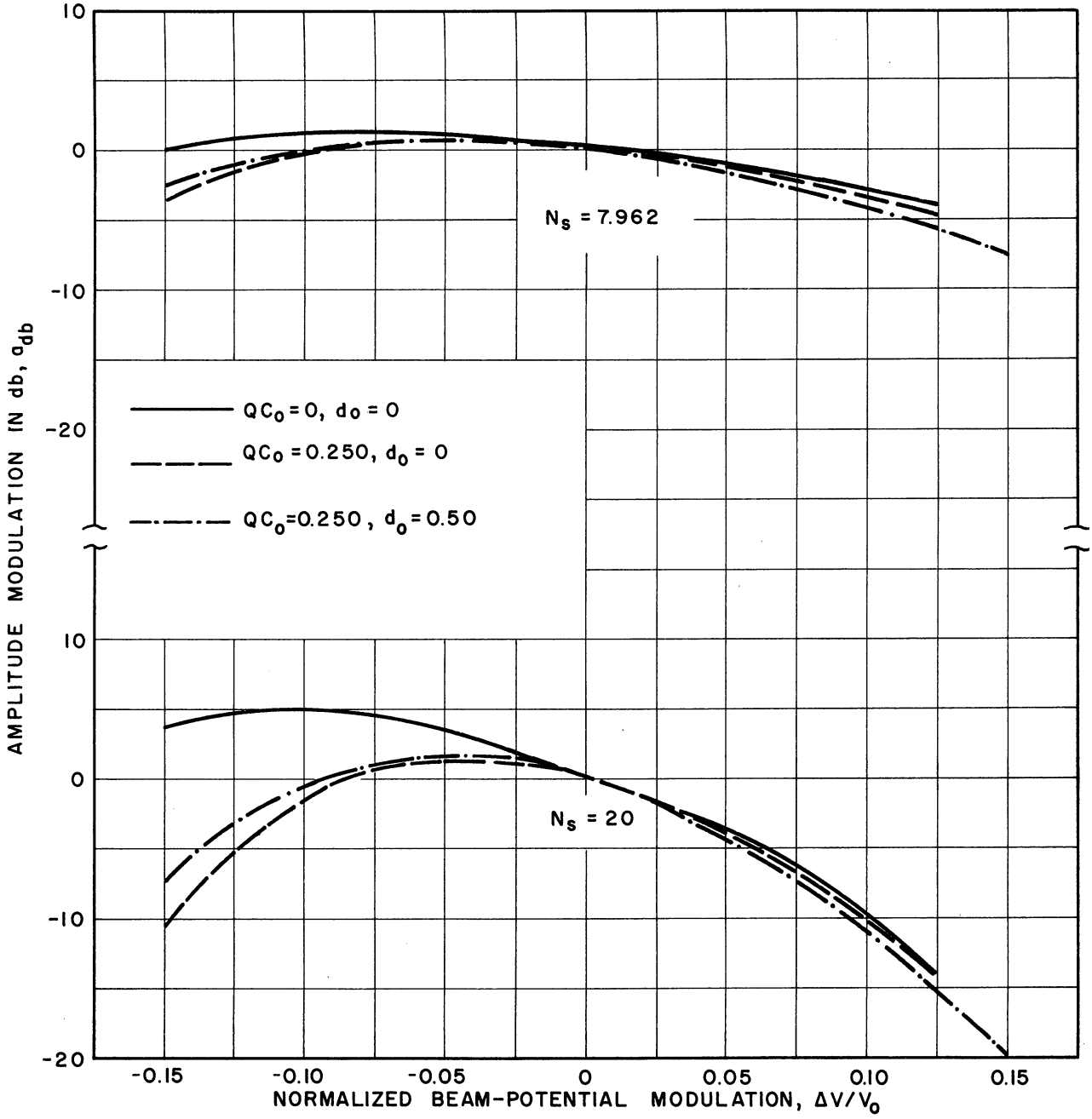

FIG. VI.6 AMPLITUDE-MODULATION DEVICE FUNCTIONS FOR BEAM-POTENTIAL MODULATION. (C_0=0.10, ΔI=0, b_0 ADJUSTED FOR MAXIMUM GAIN)

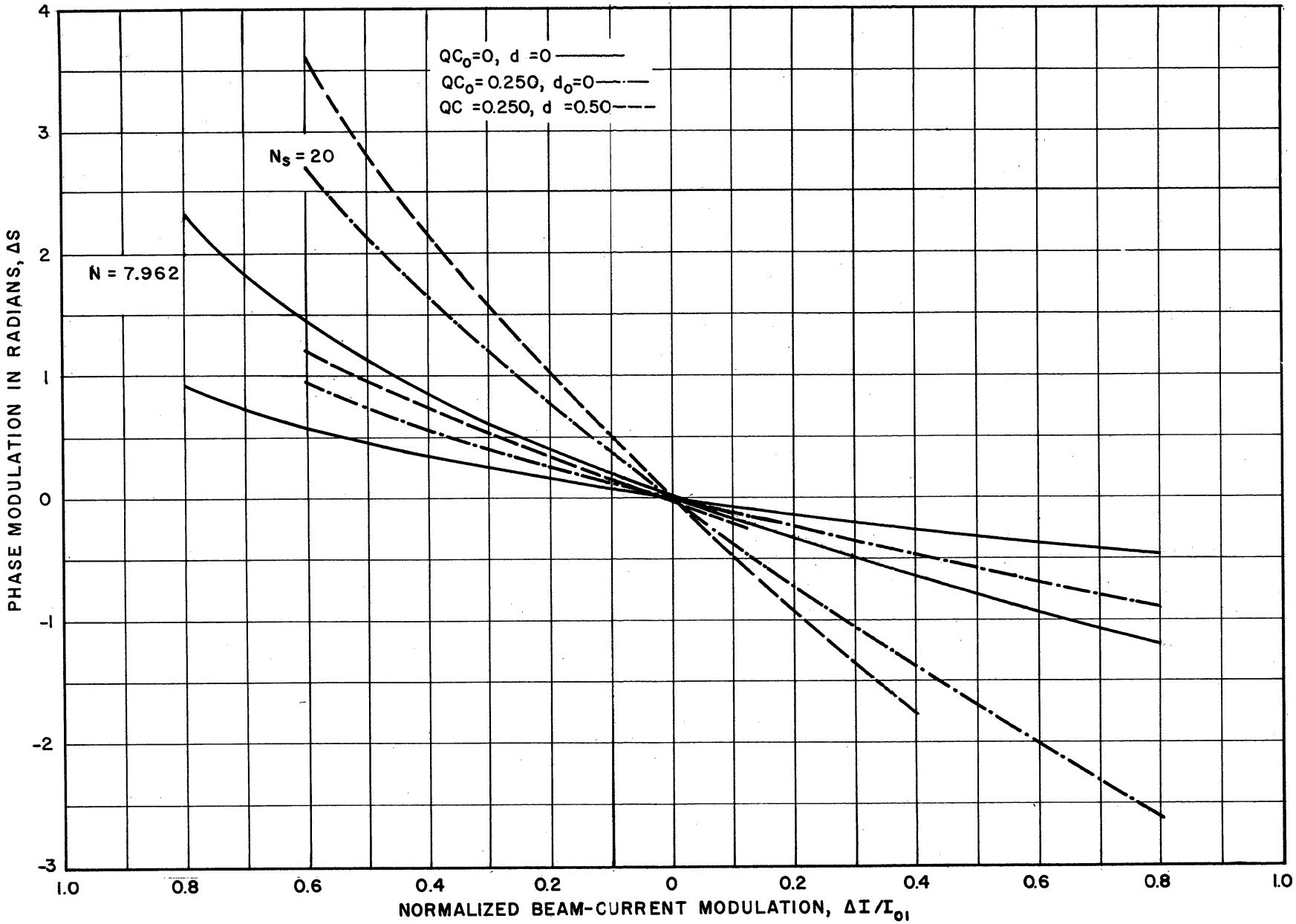

FIG. VI.7 PHASE-MODULATION DEVICE FUNCTIONS FOR BEAM-CURRENT MODULATION. (C_0=0.10, ΔV=0, b_0 ADJUSTED FOR MAXIMUM GAIN)

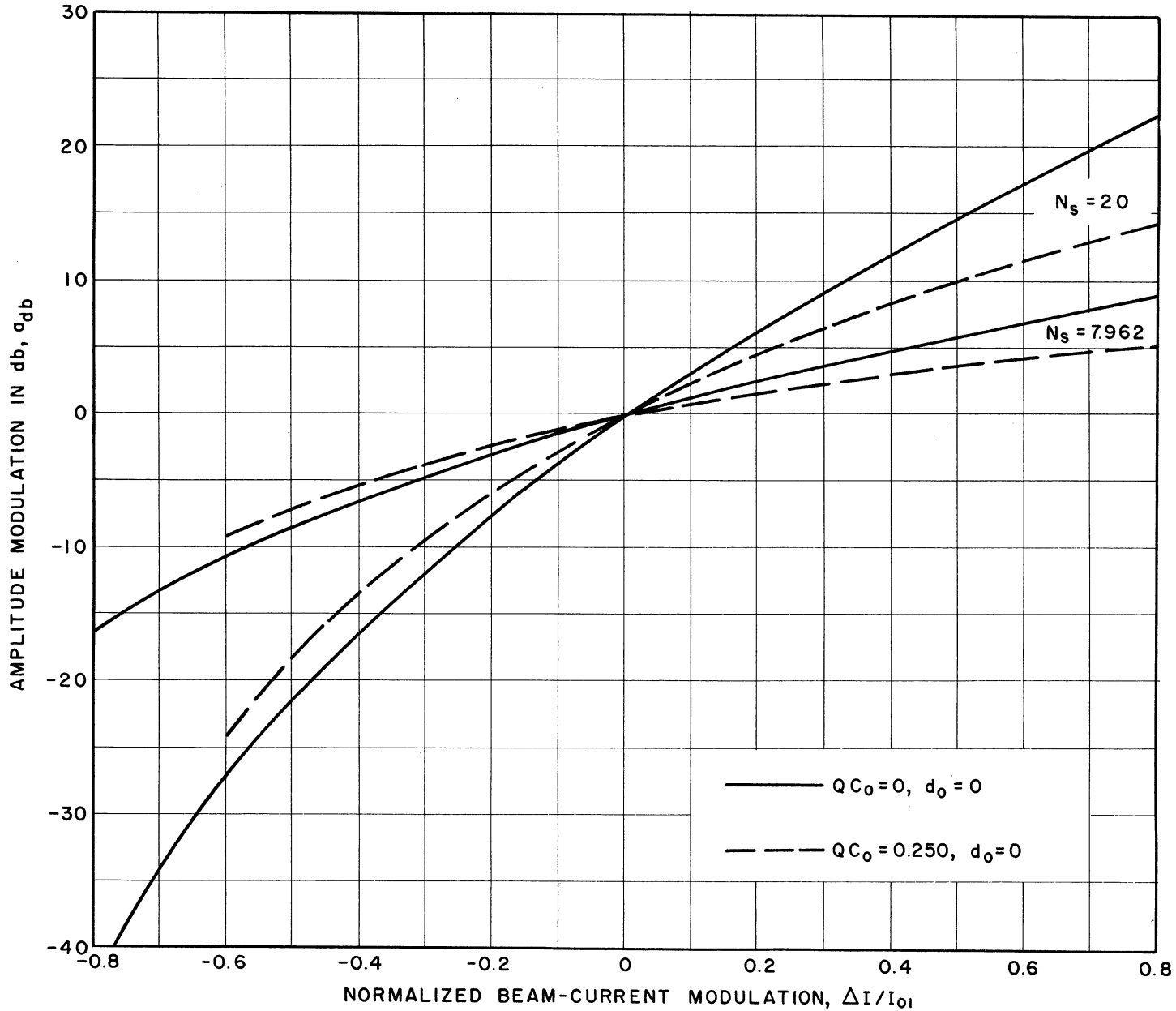

FIG. VI.8 AMPLITUDE-MODULATION DEVICE FUNCTIONS FOR BEAM-CURRENT MODULATION. ($C_0 = 0.10$, $\Delta V = 0$, b_0 ADJUSTED FOR MAXIMUM GAIN)

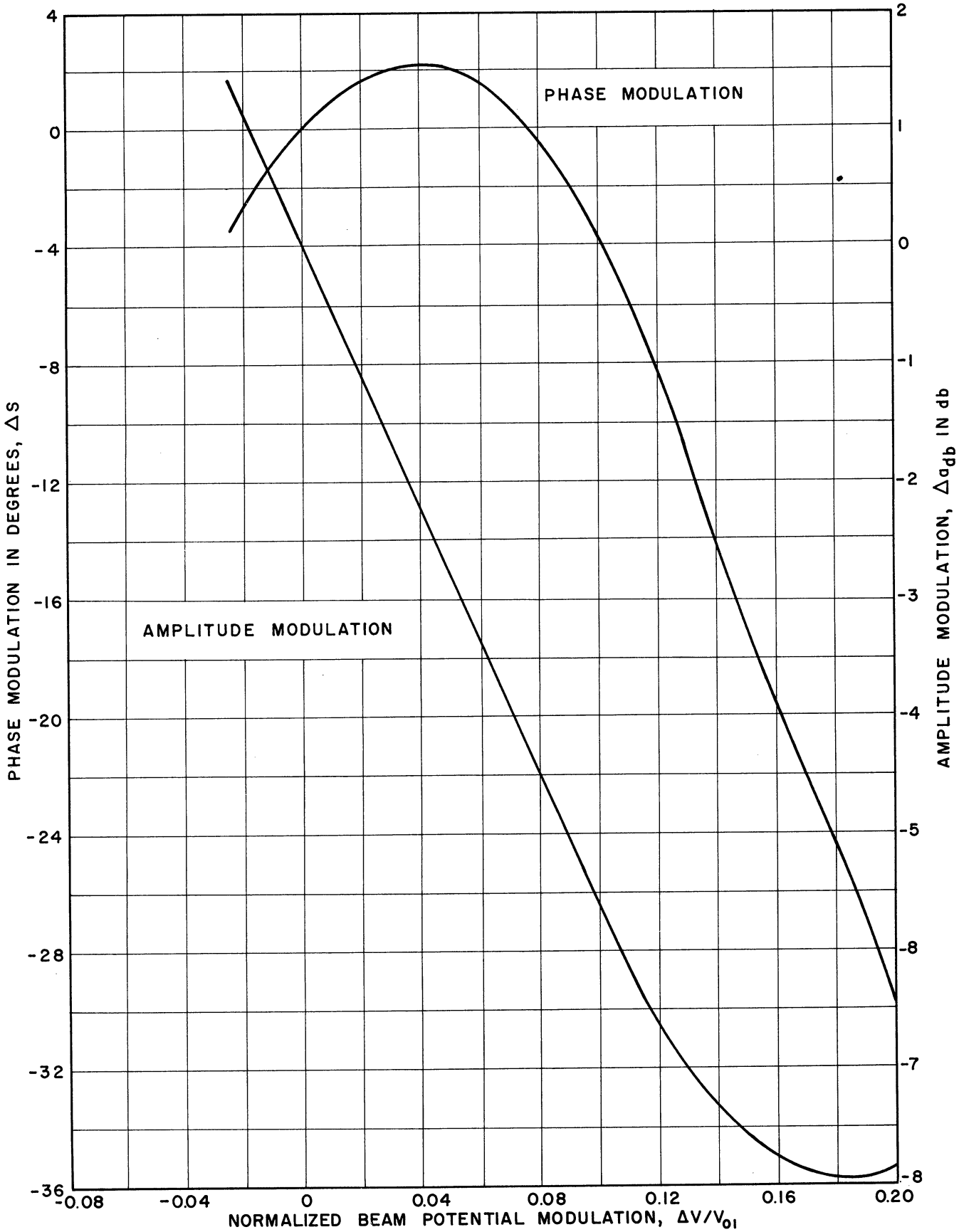

FIG. VI.9 MODULATION DEVICE FUNCTIONS FOR CRESTATRON WITH BEAM-POTENTIAL MODULATION. (C_0 =0.10, d_0=0, QC_0 =0, b_0 =2.4, $b_{0,x,=0}$ = 2.1)

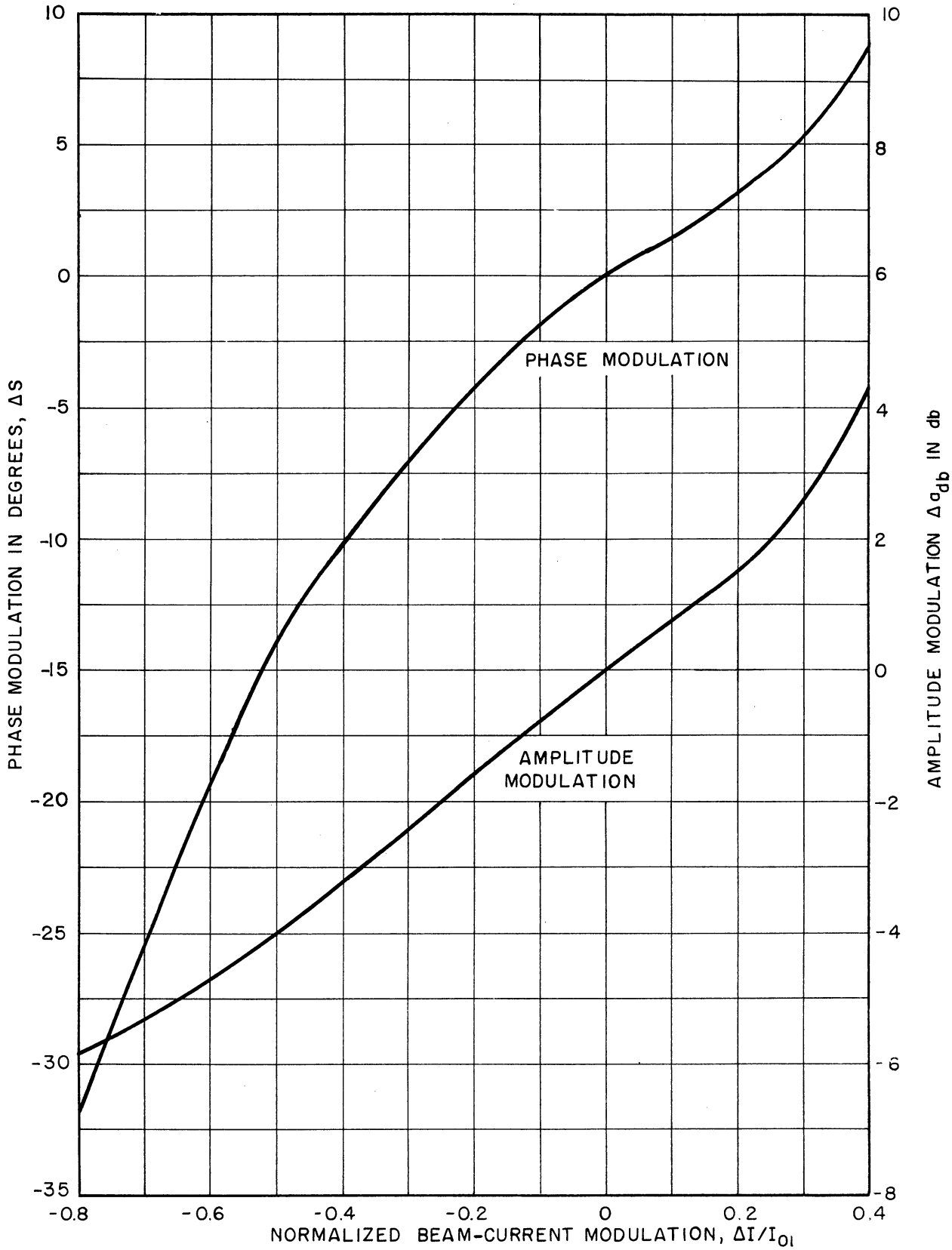

FIG. VI.10 MODULATION DEVICE FUNCTIONS FOR CRESTATRON WITH BEAM-CURRENT MODULATION. ($C_0 = 0.10$, $d_0 = 0$, $QC_0 = 0$, $b_0 = 2.4$, $b_{0,x_1=0} = 2.1$)

$$\Delta = \sum_{n=1}^{\infty} \frac{1}{n!} \left\{ \left(\frac{\partial^n f}{\partial I^n}\right)_{\Delta I=\Delta V=0} \Delta I^n + \left(\frac{\partial^n f}{\partial V^n}\right)_{\Delta I=\Delta V=0} \Delta V^n \right\}$$

$$+ \sum_{n=1}^{\infty} \frac{1}{n!} \sum_{r=1}^{\infty} C_r^n \left(\frac{\partial^n f}{\partial V^r \partial I^{n-r}}\right) \Delta V^r \Delta I^{n-r} \quad ,$$

where for phase modulation $\Delta \rightarrow \Delta S$ and $f \rightarrow \psi - \beta_e L(1-Cy_1)$, and for amplitude modulation

$$\Delta \rightarrow \Delta a \text{ and } f \rightarrow 8.864 \log_{10} \frac{V_1(\Delta V, \Delta I)}{V_1(0)} + 54.6\ CN_s\ x_1(\Delta V, \Delta I) \quad .$$

The evaluation of the coefficients of the Taylor series is indeed a laborious task. This method was tried for one case using a second-order expansion for both phase and gain. The explicit expansion for the propagation constants as determined by Sensiper[9] was used. The results are shown in Fig. VI.11 for the cases of neglecting and then including modulation effects of the initial loss parameter. A comparison is made on the figure with the previous method. As is mentioned later on, the modulation effects of the initial loss parameter are not too important for the long low-C tube. In this case a rough approximation to the phase-modulation device function as determined from the linear term of the Taylor series is

$$\Delta S = -\left[\frac{1}{3} + 0.0407\ b_o - \frac{2}{9} QC_o - C_o \left\{0.833y_{1o} + 0.278b_o - 0.0928\ b_o^2 - 1.127\ b_o d_o - \frac{5}{9} QC_o\right\}\right] \frac{\Delta V}{V_{o1}} \qquad \text{(VI.14)}$$

---

9. Sensiper, S., "Explicit Expressions for the Traveling-Wave Tube Propagation Constants", Memo No. 53-16, Hughes Research and Development Laboratories; December, 1953.

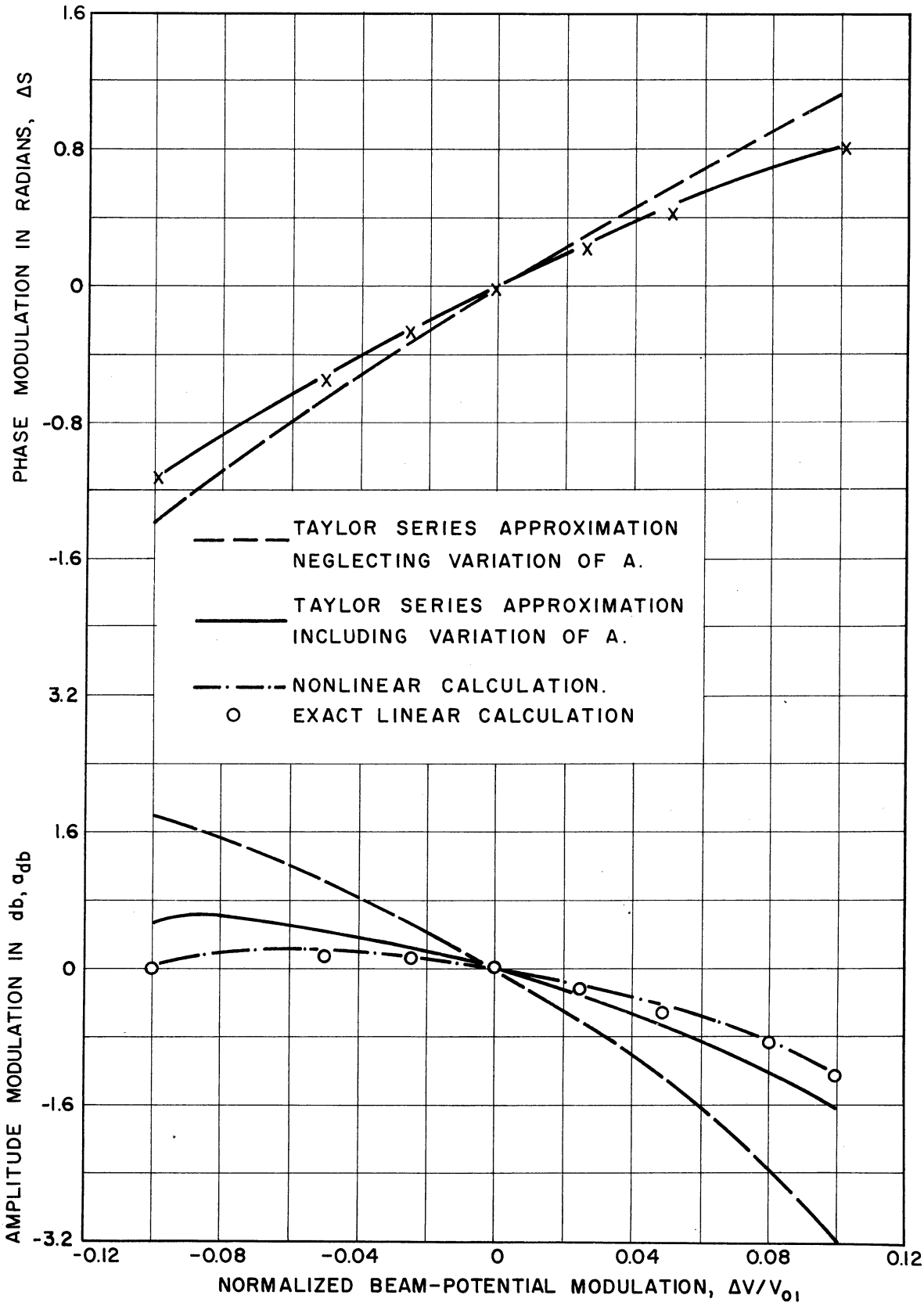

FIG. VI.11 VARIATION OF PHASE AND AMPLITUDE DURING BEAM-POTENTIAL MODULATION. (C_0=0.10, QC_0 =0, d_0 =0, b_0 =0.1525, ΔI=0, y = 3.4)

and

$$\Delta S \approx C_o \left[\frac{y_{1o}}{3} - \frac{2}{9} QC_o - 0.0369\, d_o - \frac{8}{9} C_o QC_o + 0.0369\, b_o^2 - 0.064\, b_o d_o\right] \frac{\Delta V}{I_{o1}} \quad . \text{(VI.15)}$$

Unfortunately no similarly simple expression can be given for the amplitude modulation.

As the r-f carrier level is raised, the linear analysis used above no longer is valid and one must resort to a nonlinear description to accurately describe the modulated traveing-wave tube. It is necessary not only to include nonlinearities but further to allow for multi-valued functions since there will be crossings of electron trajectories. This problem is then handled using the Lagrangian formulation rather than the Eulerian described above.

The Lagrangian analysis of the large-signal traveling-wave tube employed in this report was first presented by Nordsieck[10] and then generalized by Rowe[11]. It is now further generalized to include low-frequency beam modulations. The electrons are assumed to enter the interaction region as discrete interacting particles and the equation of motion of each particle is integrated, allowing for disturbances due to other electrons and also an external r-f field. The calculations were done assuming that thirty-two representative electrons entered the interaction region during each carrier cycle. Ideally the integration for the modulated tube should be carried out over a cycle of the modulation frequency; however employing the quasi-static conditions allows

10. Nordsieck, A. J., "Theory of the Large-Signal Behavior of Traveling Wave Amplifiers", Proc. IRE, vol. 41, No. 5, pp. 630-637; May, 1953.

11. Rowe, J. E., "A Large-Signal Analysis of the Traveling Wave Amplifier: Theory and General Results", Trans. PGED-IRE, vol. ED-3, No. 1, pp. 39-57; January, 1956.

one to integrate the path over one r-f cycle at several instantaneous points in the modulation cycle. The equations to be integrated are shown below.

$$\frac{d^2A(y)}{dy^2} - A(y)\left[\left(\frac{1}{C_o} - \frac{d\theta(y)}{dy}\right)^2 - \left(\frac{1+C_o b_o}{C_o}\right)^2\right]$$

$$= -\frac{1+C_o b_o}{\pi C_o}\,\frac{1}{M^{5/2}\left(1+\frac{\Delta I}{I_{o1}}\right)^{1/2}}\left\{\int_o^{2\pi}\frac{\cos\Phi(y,\Phi_{oi})d\Phi_o}{1+2C_o u(y,\Phi_{oi})}\right.$$

$$\left. + 2C_o d_o\int_o^{2\pi}\frac{\sin\Phi(y,\Phi_{oi})d\Phi_o}{1+2C_o u(y,\Phi_{oi})}\right\}, \qquad \text{(VI.16)}$$

$$A(y)\left[\frac{d^2\theta}{dy^2} - \frac{2d_o}{C_o}(1+C_o b_o)^2\right] + 2\,\frac{dA(y)}{dy}\left(\frac{d\theta(y)}{dy} - \frac{1}{C_o}\right)$$

$$= -\frac{1+C_o b_o}{\pi C_o}\,\frac{1}{M^{5/2}\left(1+\frac{\Delta I}{I_{o1}}\right)^{1/2}}\left\{\int_o^{2\pi}\frac{\sin\Phi(y,\Phi_{oi})d\Phi_o}{1+2C_o u(y,\Phi_{oi})}\right.$$

$$\left. - 2C_o d_o\int_o^{2\pi}\frac{\cos\Phi(y,\Phi_{oi})d\Phi_o}{1+2C_o u(y,\Phi_{oi})}\right\}, \qquad \text{(VI.17)}$$

$$\left[\frac{\partial\Phi}{\partial y}(y,\Phi_{oi})\right]_{\Phi_{oi}} + \frac{d\theta(y)}{dy} = \frac{1}{C_o}\left[1 - \frac{1}{\xi_1\left(1+2C_o u(y,\Phi_{oi})\right)}\right], \qquad \text{(VI.18)}$$

and

$$\left\{1+2C_o u(y,\Phi_{oi})\right\} \frac{\partial u}{\partial y}(y,\Phi_{oi}) = -\frac{1}{M^2} A(y) \left(1 - \frac{d\theta}{dy} C_o\right) \sin \Phi(y,\Phi_{oi})$$

$$+ \frac{C_o}{M^2} \frac{dA(y)}{dy} \cos \Phi(y,\Phi_{oi}) - \frac{1}{(1+C_o b_o)M^3 \xi_1} \left(\frac{\omega_{po}}{\omega C_o}\right)^2 \int_0^{2\pi} \frac{F(\Phi-\Phi')}{1+2C_o u(y,\Phi_{oi})} d\Phi_o' \tag{VI.19}$$

where $y = \beta_{eo} C_o z$, a normalized distance,

Φ_{oi} = initial phase of electron,

$\theta(y)$ = phase lag between circuit wave and ficticious wave traveling at unmodulated initial beam-average velocity,

$\Phi(\Phi_{oi},y)$ = the phase of the ith electron $= \omega\left(\frac{z}{u_{o1}} - t\right) - \theta(y)$,

A is defined as amplitude of circuit wave from,

V = circuit potential $= [A(y)\, C_o I_o / Z_o] \cos \Phi(y,\Phi_{oi})$,

ω_{po} = zero modulation beam plasma frequency,

$F(\Phi-\Phi')$ = space-charge weighting function,

$u(y,\Phi_{oi})$, the normalized r-f velocity of ith electron defined from, $dz/dt = u_o[1+2C_o u(\Phi_{oi},y)]$, and

$$M^3 = \frac{1+\Delta V/V_{o1}}{1+\Delta I/I_{o1}} .$$

The parameters are defined for zero modulation and the modulation device functions may be calculated from the above equations for specified unmodulated conditions and modulation amplitudes. The boundary conditions are once again the same as for the unmodulated case and may be given approximately as

$$\left(\frac{dA}{dy}\right)_o = -2d_oA(0) \tag{VI.20}$$

and

$$\left(\frac{d\theta}{dy}\right)_o = -b_o \quad . \tag{VI.21}$$

The phase-modulation device function is then calculated from

$$\Delta S = \theta(y,\Delta V,\Delta I) - \theta(y,0,0) \tag{VI.22}$$

and the amplitude-modulation device function from

$$\Delta a_{db} = A_{db}(y,\Delta I,\Delta V) - A_{db}(y,0,0) \quad . \tag{VI.23}$$

Typical plots of the device functions for the tube with a large-signal carrier are shown in Figs. VI.12 through VI.14.

Now that the method of calculating the modulation device functions has been given, their use will be discussed.

C. Low Modulation Frequencies - Using the Modulation Device Functions

Perhaps the most important use of the modulation device functions in modulation analyses is in determining output spectra of tubes for given modulation signal wave shapes. In order to calculate the output spectrum it is necessary to have an explicit form of the modulation device function as a function of the modulation signal. This can be obtained by fitting the modulation device functions with polynomials. The analytic form can also be obtained using the Taylor series for the small-signal tube. In either case it is assumed that a second-order series for the gain and phase shift will suffice. If the output signal is represented by

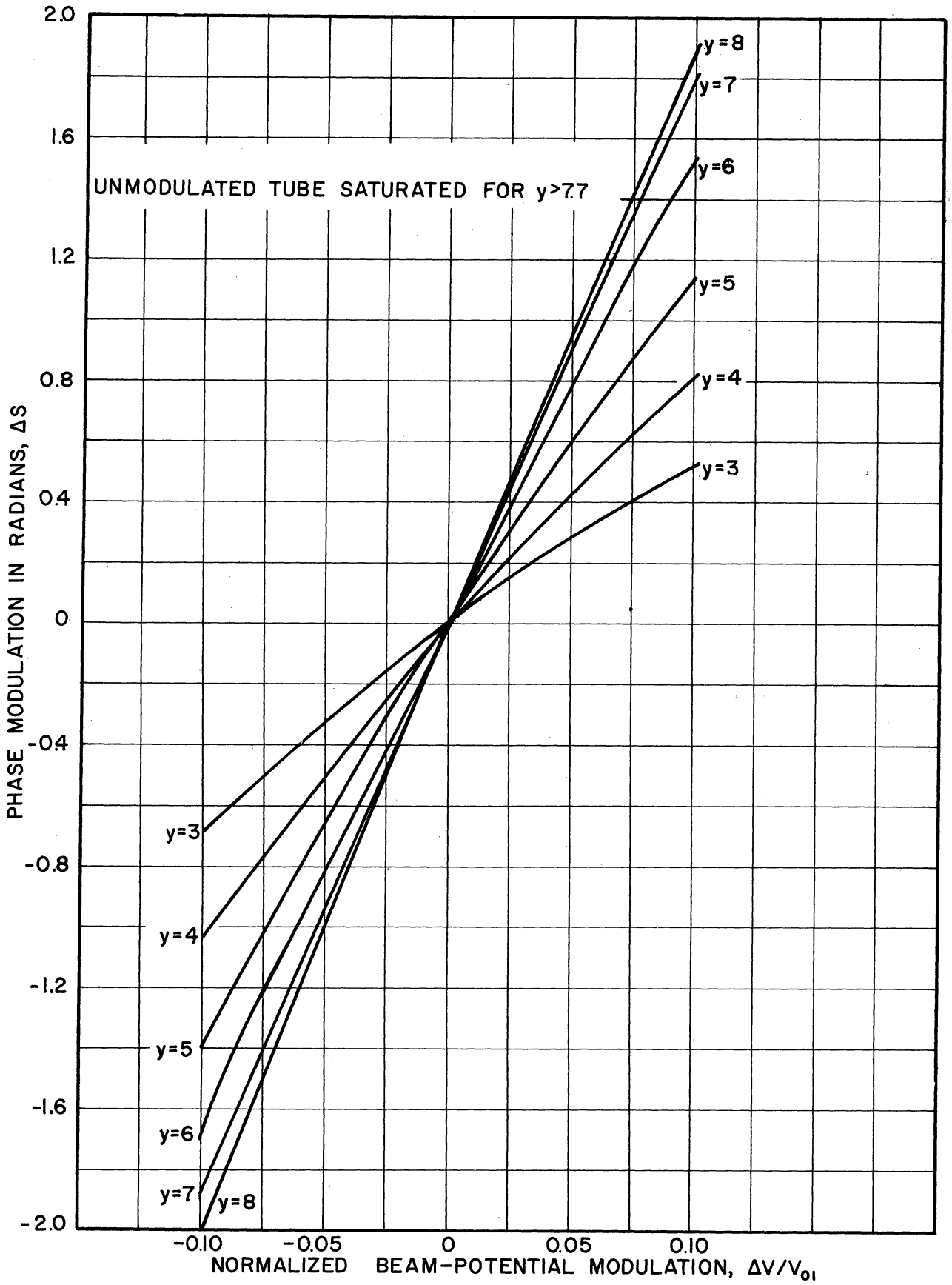

FIG VI.12 PHASE-MODULATION DEVICE FUNCTION DURING BEAM-POTENTIAL MODULATION, LARGE-SIGNAL CALCULATION. (C_0 =0.10, QC_0=0.250, d_0=0, b_0=1.0, B=1.0, a'/b'=2.0)

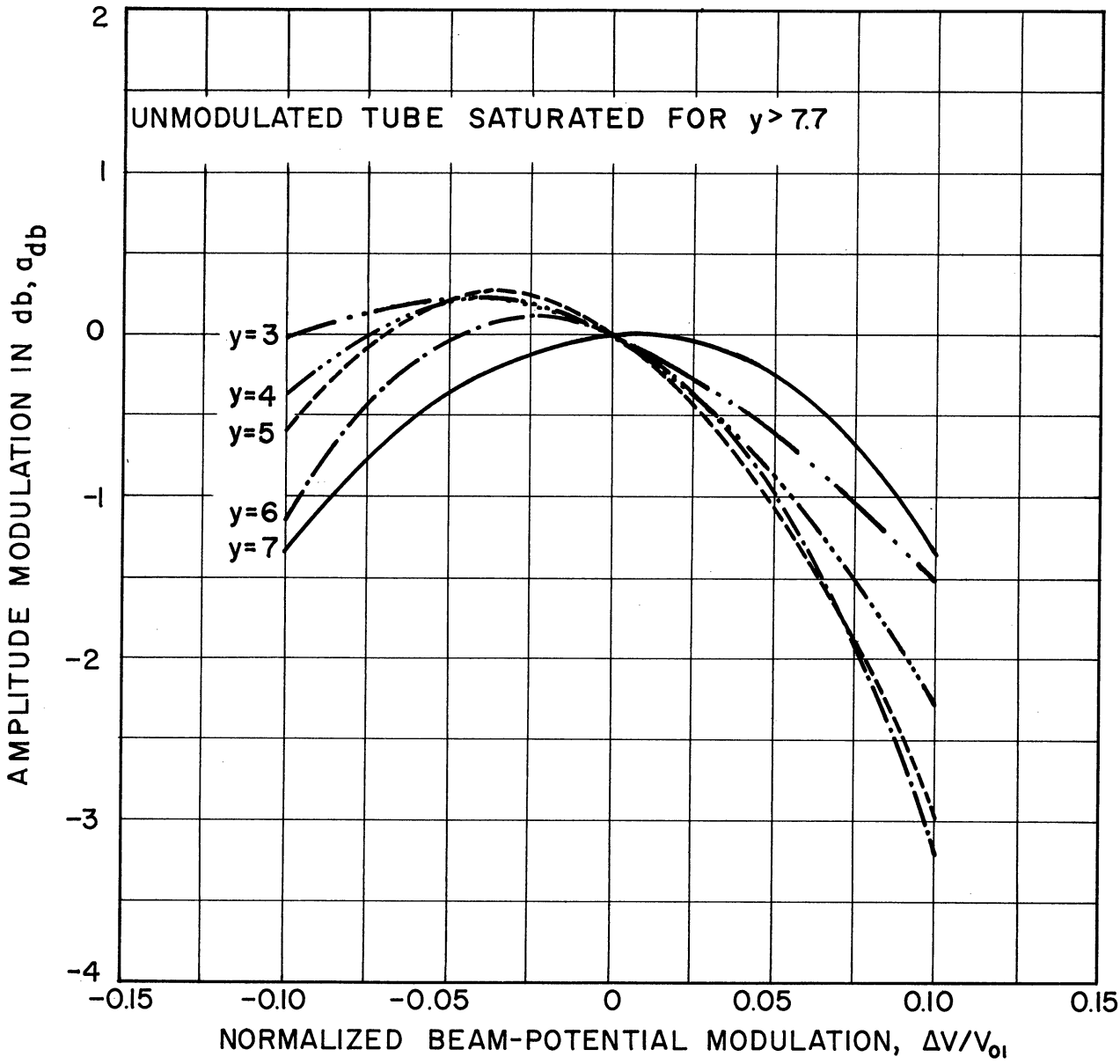

FIG. VI.13 AMPLITUDE-MODULATION DEVICE FUNCTION DURING BEAM-POTENTIAL MODULATION, LARGE-SIGNAL CALCULATION. (C_0=0.10, QC_0=0.250, d_0=0, b_0=1.0, B=1.0, a'/b'=2.0)

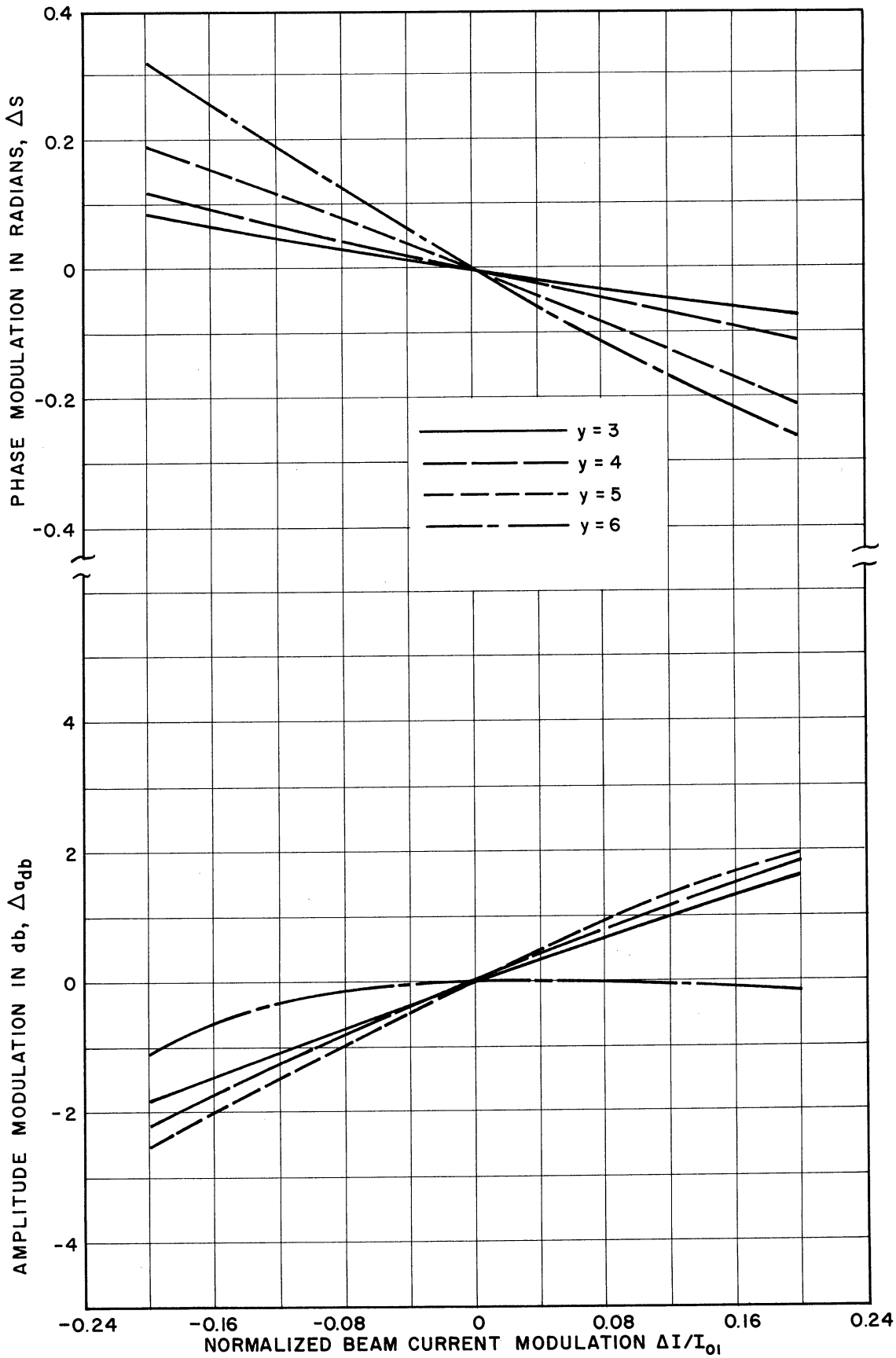

FIG. VI.14 MODULATION DEVICE FUNCTIONS DURING BEAM-CURRENT MODULATION, LARGE-SIGNAL CALCULATION. (C_0=0.10, QC_0=0, d_0=0, b_0=0.1525, ΔV=0)

$$\frac{E}{E_o} = G(\xi) \cos [\omega_c t + \Phi(\xi)] \quad , \qquad \text{(VI.24)}$$

where E = the output field with modulation,

E_o = the output field without modulation,

G = the amplitude function = $1 + h_1\xi + h_2\xi^2$,

Φ = the phase function = $\Phi_o(1 + p_1\xi + p_2\xi^2)$,

Φ_o = the phase shift without modulation, and

ξ is the modulating signal, periodic with fundamental frequency ω_a, then the output spectrum around the fundamental of the carrier signal is given by

$$A_{1m} = \frac{1}{4\pi} \int_0^{2\pi} G(\xi) \exp j[\Phi(\xi) - m\omega_a t] \, d\omega_a t$$

or

$$A_{1m} = \frac{1}{4\pi} \int_0^{2\pi} [1+h_1\xi+h_2\xi^2] \exp j[\Phi_o(1+p_1\xi+p_2\xi^2) - m\omega_a t] \, d\omega_a t \quad . \text{(VI.25)}$$

The spectral line is located at $\omega_c+m\omega_a$ with $m = 0, \pm 1, \pm 2, \pm 3 \ldots$ with amplitude $2\mathrm{Re}(A_{1m})$.

It can be seen from Figs. VI.5 and VI.12 that there is a region of beam potential modulation over which a linear phase modulation can be obtained. In certain applications such as Serrodyne[12] operation, a large linear range with minimum inherent amplitude modulation is required. It was found that the addition of loss extends the linear range. The inherent amplitude modulation can be minimized by working the tube near saturation. This will not have an adverse effect on the linearity of the phase modulation and for some cases extends the linear range. One immediate difficulty of working near saturation, however,

12. Cumming, R. C., op cit.

is that at this level of operation, any amplitude modulation on the carrier will be transformed to an additional phase modulation; therefore one can use the saturated operation only for those cases where the amplitude of the carrier does not vary appreciably. Simultaneous modulation of the beam current and potential is another method of obtaining linear phase modulation while minimizing the amplitude modulation.

In order to obtain large phase modulation indices it is probably best to use a long, low-C, voltage-modulated tube; however this tube will have considerable amplitude variation. The variation will decrease if the C is increased while the gain is kept constant. The current modulated traveling-wave tube will give linear amplitude modulation with small phase variation. The effect of the modulation of the initial loss parameter A is important in short high-C tubes or Crestatrons but is not important in the long low-C tube. Also, the effect of modulation on A is more pronounced during a voltage modulation than during a current modulation.

Experiments to check the low-frequency beam modulation analyses gave good correlation with theoretical results.

D. High Modulation Frequencies - General Analysis

The preceding sections dealt with low-frequency modulating signals where a quasi-stationary analysis could be used to describe the modulation effects. When the modulation frequency is comparable to the carrier frequency the time dependence of the modulating signal must be considered in the interaction equations; also the fact that the beam is itself a nonlinear entity will result in the generation of sidebands. These sidebands are far removed from the carrier and therefore each will

see a different impedance and propagate with a velocity other than that of the carrier. The nonlinear properties of the beam would best be described by the Lagrangian analysis used in the preceding section; however, for the case of the two-frequency problem the complexities introduced are quite formidable. Therefore it was decided to use an Eulerian analysis but to preserve the nonlinearities introduced by the ballistic equations. This of course implies that there are no crossings of electron trajectories.

The high-frequency modulation problem is equivalent to solving the problem of the interaction of a beam and circuit wave with the simultaneous application of two signals of different frequencies, ω_1 and ω_2. The boundary conditions will specify which is the carrier and which carries modulation information. The sidebands $n\omega_1 + m\omega_2$, where n,m take on all positive and negative integral values, will be produced by a mixing interaction. The electrokinetic variables may be expanded in a double Fourier series of the applied frequencies as

$$\text{Charge density, } \rho(z,t) = \sum_{n=-\infty}^{\infty} \sum_{m=-\infty}^{\infty} \rho_{nm}(z) \exp j(n\omega_1+m\omega_2)\, t \quad , \quad \text{(VI.25a)}$$

$$\text{Beam velocity, } v(z,t) = \sum_{n=-\infty}^{\infty} \sum_{m=-\infty}^{\infty} v_{nm}(z) \exp j(n\omega_1+m\omega_2)\, t \quad , \quad \text{(VI.25b)}$$

$$\text{Electric field, } E(z,t) = \sum_{n=-\infty}^{\infty} \sum_{m=-\infty}^{\infty} E_{nm}(z) \exp j(n\omega_1+m\omega_2)\, t \quad , \quad \text{(VI.25c)}$$

$$\text{Convection current, } i(z,t) = \sum_{n=-\infty}^{\infty} \sum_{m=-\infty}^{\infty} i_{nm}(z) \exp j(n\omega_1+m\omega_2)\, t \,. \quad \text{(VI.25d)}$$

As usual, the electric field is assumed to be composed of a circuit field component and of a space-charge field component and the fields are assumed to be derivable from potentials (V_c and V_{sc}). The following relations are obtained between the Fourier coefficients when Eqs. VI.23 are introduced into the forced telegrapher's Newtonian force, and conservation of charge equations.

$$i_{nm} = j \sum_{r,s=-\infty}^{\infty}{}' \frac{v_{n-r,m-s}}{r\omega_1 + s\omega_2} \frac{di_{rs}}{dz} + v_{nm}\rho_o + \sum{}'' \rho_{o_{rs}} v_{n-r,m-s} \,, \quad \text{(VI.26a)}$$

$$j(n\omega_1+m\omega_2)v_{nm} + \sum_{r,s=-\infty}^{\infty} v_{rs} \frac{dv_{n-r,m-s}}{dz} = -j\eta \frac{R_{nm}^2 i_{nm}}{\epsilon_o \sigma(n\omega_1+m\omega_2)} + \eta \frac{dV_{cnm}}{dz} \,, \quad \text{(VI.26b)}$$

$$\frac{d^2V_{cnm}}{dz^2} + \frac{(n\omega_1+m\omega_2)^2}{v_{cnm}} V_{cnm} - j \frac{Z_{onm}}{v_{cnm}} (n\omega_1+m\omega_2) \frac{di_{nm}}{dz} = 0 \,, \quad \text{(VI.26c)}$$

where the summation Σ' is over all terms where $r\omega_1+s\omega_2$ does not vanish, and the summation Σ'' is for all terms where $r\omega_1+s\omega_2 = 0$ except that for which $r,s = 0$; ρ_o is the d-c beam density, $\rho_{o_{rs}}$ is the d-c beam density corresponding to $r\omega_1+s\omega_2 = 0$; R_{nm} is the plasma frequency reduction factor at frequency $n\omega_1+m\omega_2$; σ is the beam cross sectional area; v_{cnm} is the cold circuit velocity at frequency $n\omega_1+m\omega_2$ and $Z_{o_{nm}}$ is the circuit impedance at frequency $n\omega_1+m\omega_2$. Also $f_{-n,-m} = f^*_{nm}$.

Equation VI.25 and the appropriate boundary conditions describe the mixing type of interaction. Unfortunately this set of equations

represents an infinite set of nonlinear differential equations. To facilitate the solution of these equations and also because of the very nature of mixing devices, it will be assumed that the signal at the higher frequency ω_1 has a larger amplitude than the signal at ω_2. The larger signal will be called the pump or local oscillator. The only sidebands considered in the problem will now be the upper and lower ones around the pump. The sidebands around the second and higher harmonics of the pump may certainly be significant; however they are neglected in this present study. An "r-f linearization" is made by assuming that the pump propagation is not perturbed by the interaction. The usual d-c linearizations are introduced by assuming that the r-f quantities at the pump frequency are smaller in amplitude than the corresponding average values. The solution at the pump frequency is that of the ordinary traveling-wave tube or space-charge waves if the circuit impedance is reduced to zero. The equations at the upper sideband (n=1,m=1), the lower sideband (n=1,m=-1), and the signal (n=0,m=1) are then given as

<u>(n=1,m=1)</u>

$$i_{11} = j\left\{\frac{v_{01}}{\omega_1}\frac{di_{10}}{dz} + \frac{v_{10}}{\omega_2}\frac{di_{01}}{dz} + \frac{u_0}{\omega_1+\omega_2}\frac{di_{11}}{dz}\right\} + v_{11}\rho_0 \quad , \tag{VI.27a}$$

$$j(\omega_1+\omega_2)v_{11} + \frac{d}{dz}(v_{10}v_{01}) + u_0\frac{dv_{11}}{dz} = -j\eta\frac{R_{11}^2 i_{11}}{\epsilon_0\sigma(\omega_1+\omega_2)} + \eta\frac{dV_{c11}}{dz} \quad , \tag{VI.27b}$$

and

$$\frac{d^2V_{c11}}{dz^2} + \frac{(\omega_1+\omega_2)^2}{v_{c11}^2}V_{c11} - j\frac{Z_{011}}{v_{c11}}(\omega_1+\omega_2)\frac{di_{11}}{dz} = 0 \quad . \tag{VI.27c}$$

(n=1,m=-1)

$$i_{1-1} = j\left(\frac{v_{10}}{-\omega_2}\frac{di^*_{01}}{dz} + \frac{u_o}{\omega_1-\omega_2}\frac{di_{1-1}}{dz} + \frac{v^*_{01}}{\omega_1}\frac{di_{10}}{dz}\right) + v_{1-1}\rho_o \quad , \tag{VI.28a}$$

$$j(\omega_1-\omega_2)\, v_{1-1} + \frac{d}{dz}\,(v^*_{01}v_{10}) + u_o\frac{dv_{1-1}}{dz} = -\,j\eta\,\frac{R^2_{1-1}\, i_{1-1}}{\epsilon_o\sigma(\omega_1-\omega_2)} + \eta\,\frac{dV_{c1-1}}{dz} \, , \tag{VI.28b}$$

and

$$\frac{d^2V_{c1-1}}{dz^2} + \frac{(\omega_1-\omega_2)^2}{v^2_{c1-1}}\,V_{c1-1} - j\,\frac{Z_{o_{1-1}}}{v_{c1}}\,(\omega_1-\omega_2)\,\frac{di_{1-1}}{dz} = 0 \quad . \tag{VI.28c}$$

(n=0,m=1)

$$i_{01} = j\left(\frac{v_{11}}{-\omega_1}\frac{di^*_{10}}{dz} + \frac{v^*_{1-1}}{\omega_1}\frac{di_{10}}{dz} + \frac{v_{10}}{\omega_2-\omega_1}\frac{di^*_{1-1}}{dz} + \frac{u_o}{\omega_2}\frac{di_{01}}{dz} + \frac{v^*_{10}}{\omega_1+\omega_2}\frac{di_{11}}{dz}\right) + v_{01}\rho_o \quad , \tag{VI.29a}$$

$$j\omega_2 v_{01} + \frac{d}{dz}\,(v_{11}v^*_{10}+v^*_{1-1}v_{10}) + u_o\frac{dv_{01}}{dz} = -\,j\eta\,\frac{R^2_{01}\, i_{01}}{\epsilon_o\sigma\omega_2} + \eta\,\frac{dV_{c01}}{dz} \, , \tag{VI.29b}$$

and

$$\frac{d^2V_{c01}}{dz^2} + \frac{\omega_2^2}{v^2_{c01}}\,V_{c01} - j\,\frac{Z_{o_{01}}\,\omega_2}{v_{c01}}\,\frac{di_{01}}{dz} = 0 \quad . \tag{VI.29c}$$

The simultaneous solution of Eqs. VI.26 through VI.28 subject to sufficient boundary conditions constitutes a solution. DeGrasse's[13,14] theoretical work on traveling-wave tube mixers neglected some of the coupling effects included above in addition to the assumption that the signal (n=0,m=1) propagates unperturbed.

A special solution to the above set of equations, the longitudinal-beam parametric amplifier in which there is no r-f circuit ($Z_0 = 0$) and $\omega_1 = 2\omega_2$ (degenerate frequencies), will now be given.

E. High Modulation Frequencies, Longitudinal-Beam Parametric Amplifier

The longitudinal-beam parametric amplifier has been proposed as a low-noise high-gain amplifier utilizing fast-wave amplification[15,16]. Previous work on this subject has dealt with theories based on coupling between the signal and its lower sideband and neglected coupling to the upper sidebands. Since this is a traveling-wave parametric amplifier a consideration of additional sidebands certainly becomes important. Additional justification for looking into a consideration of the effect of the upper sideband is that the high gain and low noise predicted were never attained[17] experimentally. The investigation was done using

---

13. DeGrasse, R. W., op cit.
14. DeGrasse, R. W., and Wade, G., "Microwave Mixing and Frequency Dividing", Tech. Rept. No. 386-1, Stanford University, Electron Tube Laboratory, Stanford Electronics Laboratories; November 12, 1957.
15. Louisell, W. H., and Quate, C. F., op cit.
16. Haus, H. A., "The Kinetic Power Theorem for Parametric, Longitudinal-Beam Amplifiers", Trans. PGED-IRE, vol. ED-5, No. 4, pp. 225-232; October, 1958.
17. Ashkin, A., Bridges, T. J., Louisell, W. H., Quate, C. F., "Parametric Electron-Beam Devices", paper presented at IRE WESCON meeting; August, 1958.

the above equations. A preliminary report[18] of these findings was given recently.

The solution will contain terms originally defined by Louisell and Quate[19]. Define

$$\omega_1 = 2\omega_2 = 2\omega \quad ,$$

$$-\frac{\eta\rho_o}{\sigma\epsilon_o} = \omega_p^2 \quad ; \quad \omega_q = \omega_{o1} = R_{o1}\omega_p \quad ,$$

$$\frac{R_{1o}}{R_{o1}} = \frac{R_{1o}}{R_{1-1}} = \frac{\omega q_{1o}}{\omega q_{o1}} = 2a' \quad ,$$

and

$$\frac{R_{11}}{R_{o1}} = \frac{\omega q_{11}}{\omega q_{o1}} = 3b' \quad .$$

Assume that the pump wave propagates as a single space-charge wave, which can be described as

$$i_{1o} = -I_o + \frac{m}{2} I_o \exp - 2j\beta_e \left(1 - \frac{a'\omega_q}{\omega}\right) z \qquad \text{(VI.30a)}$$

$$v_{1o} = u_o - \frac{a'\omega_q}{\omega} \frac{m}{2} u_o \exp - 2j\beta_e \left(1 - \frac{a'\omega_q}{\omega}\right) z \quad , \qquad \text{(VI.30b)}$$

where $a' > 0$ for the fast space-charge wave,

$a' < 0$ for the slow space-charge wave, and

m = depth of current modulation (a vector).

Also define

$$v_1 = u_1(z) \exp - j\beta_e \left(1 - \frac{a'\omega_q}{\omega}\right) z \qquad \text{(VI.31a)}$$

---

18. Sobol, H., "Extension of Longitudinal-Beam Parametric-Amplifier Theory", Letter to the Editor, Proc. IRE, (to be published)

19. Louisell, W. H., and Quate, C. F., op cit.

$$v_{11} = u_{11}(z) \exp - 3j\beta_e \left(1 - \frac{a'\omega_q}{\omega}\right) z \qquad \text{(VI.31b)}$$

and assume $\frac{a'\omega_q}{\omega} \ll 1$.

When Eqs. VI.29 and VI.30 along with the above definitions are substituted into Eqs. VI.26 through VI.28, two second-order linear differential equations are found after considerable mathematical manipulation.

$$\frac{d^2u_1}{dz^2} + 2j\beta_q a' \frac{du_1}{dz} - \beta_q^2 \left[a'^2 \left(1 + \frac{|m|^2}{4}\right) - 1 + \left(\frac{a'}{b'}\right)^2 \frac{|m|^2}{4}\right] u_1$$

$$- \beta_q^2 \frac{m}{2} (1+2a'^2)\, u_1^* + j\beta_q a' \frac{m^*}{2} \left[1 + \frac{1}{3b'^2}\right] \frac{du_{11}}{dz}$$

$$- \beta_q^2 \frac{m^*}{2} \left[1 + a'^2 \left(1 + \frac{1}{b'^2}\right)\right] u_{11} - a'^2 \beta_q^2 \frac{m^2}{4} u_{11}^* = 0. \qquad \text{(VI.32)}$$

and

$$\frac{d^2u_{11}}{dz^2} + 6j\beta_q a' \frac{du_{11}}{dz} - 9\beta_q^2 \left[a'^2 \left(1+b'^2\right) \frac{|m|^2}{4} - b'^2\right] u_{11}$$

$$+ j\beta_q a' \frac{3m}{2} \left[1+3b'^2\right] \frac{du_1}{dz} - 9\beta_q^2 \frac{m}{2} \left[a'^2 (1+b'^2) + b'^2\right] u_1$$

$$- 9a'^2 b'^2 \beta_q^2 \frac{m^2}{4} u_1^* = 0 \quad . \qquad \text{(VI.33)}$$

These equations can be solved by assuming a real and imaginary part for u_1 and u_{11} and defining the linear operator

$$\frac{d}{dz} = \beta_q \mu \quad .$$

Substitution of the operator form and separation of the equations into real and imaginary parts gives four linear homogeneous equations of the form

$$\begin{bmatrix} \Phi_{11}(\mu) & \Phi_{12}(\mu) & \Phi_{13}(\mu) & \Phi_{14}(\mu) \\ \Phi_{21}(\mu) & \Phi_{22}(\mu) & \Phi_{23}(\mu) & \Phi_{24}(\mu) \\ \Phi_{31}(\mu) & \Phi_{32}(\mu) & \Phi_{33}(\mu) & \Phi_{34}(\mu) \\ \Phi_{41}(\mu) & \Phi_{42}(\mu) & \Phi_{43}(\mu) & \Phi_{44}(\mu) \end{bmatrix} \begin{bmatrix} u_{1R} \\ u_{1i} \\ u_{11R} \\ u_{11i} \end{bmatrix} = 0 \quad . \tag{VI.34}$$

The condition for a solution to exist is that the determinant of the coefficients must vanish. When the determinant is expanded and set equal to zero an eighth-order polynomial, the characteristic equation, results. The characteristic equation has terms in a'^2 and b'^2 so that the same roots are found for the fast- or slow-wave excitation. The characteristic equation is also independent of pump phase. This description of the amplifier gives eight waves. The simple solution for a very thin beam ($a'=b'=1$) is given approximately as

$$\mu_{1,2} \approx \pm 2j \quad ,$$

$$\mu_{3,4} \approx \pm 6j \quad ,$$

$$\mu_{5,6} \approx \left(\frac{3}{8} \pm j\,\frac{5}{4}\right) |m| \quad ,$$

$$\mu_{7,8} \approx \left(-\frac{3}{8} \pm j\,\frac{5}{4}\right) |m| \quad . \tag{VI.35}$$

The roots for the thin beam are plotted in Figs. VI.15, while those for a beam of finite size are plotted in Fig. VI.16. Since there are eight roots, there will be eight wave amplitudes to determine for each of the real and imaginary components of the velocities u_1 and u_{11}. Eight of the constants will be arbitrary, being specified by the real and imaginary components of the velocities and the distance derivative of velocities at the input. This means that the remaining twenty-four constants are not arbitrary. Relations between the coefficients can be obtained from Eq. VI.33 and the roots as

$$\begin{bmatrix} -\Phi_{11}(\mu_i)\epsilon_i \\ -\Phi_{21}(\mu_i)\epsilon_i \\ -\Phi_{31}(\mu_i)\epsilon_i \end{bmatrix} = \begin{bmatrix} \Phi_{12}(\mu_i) & \Phi_{13}(\mu_i) & \Phi_{14}(\mu_i) \\ \Phi_{22}(\mu_i) & \Phi_{23}(\mu_i) & \Phi_{24}(\mu_i) \\ \Phi_{32}(\mu_i) & \Phi_{33}(\mu_i) & \Phi_{34}(\mu_i) \end{bmatrix} \begin{bmatrix} \eta_i \\ \tau_i \\ \pi_i \end{bmatrix}, \quad \text{(VI.36)}$$

where ϵ_i = coefficient of u_{1R},

η_i = coefficient of u_{1i},

τ_i = coefficient of u_{11R}, and

π_i = coefficient of u_{11i}.

When the index i is allowed to run from 1 to 8, the amplitudes η, τ, and π can be obtained in terms of the amplitude of ϵ; therefore the necessary relations have been determined. The boundary conditions are that the signal wave enters as an ordinary signal space-charge wave but the upper sideband is initially unexcited. The wave amplitudes were calculated for the thin beam case with fast wave excitation and with the roots given in Eq. VI.34. The depth of modulation factor m was specified as $m = |m| \exp j\theta$. For $\theta = 90$ degrees, only the growing waves (roots 5 and 6) are excited and the velocities are given as

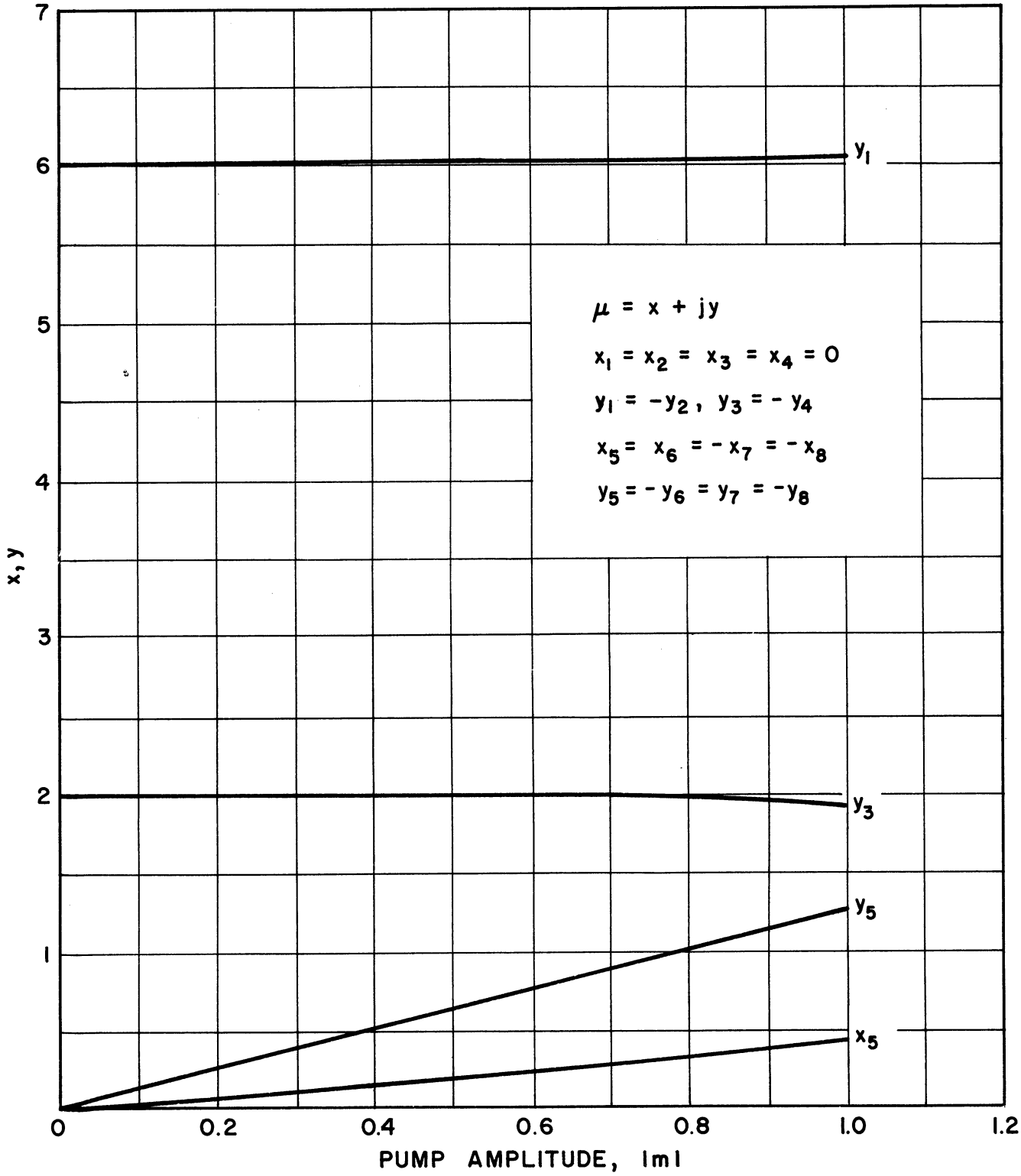

FIG. VI. 15 LONGITUDINAL-BEAM PARAMETRIC-AMPLIFIER PROPAGATION CONSTANTS AS FUNCTIONS OF THE PUMP AMPLITUDE ($a' = b' = 1.0$).

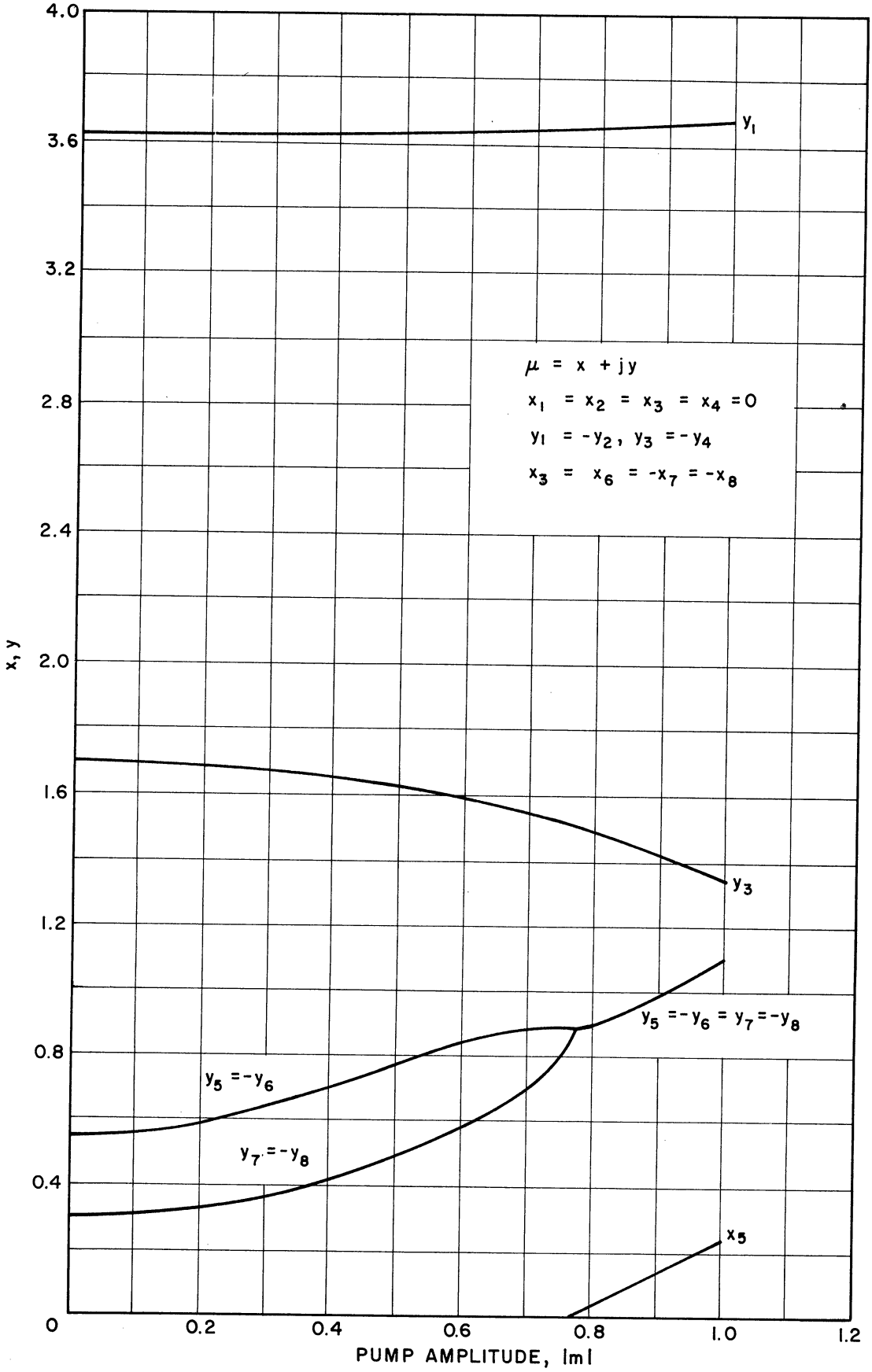

FIG. VI. 16 LONGITUDINAL-BEAM PARAMETRIC-AMPLIFIER PROPAGATION CONSTANTS AS FUNCTIONS OF THE PUMP AMPLITUDE. ($a' = 0.697$, $b' = 0.513$)

$$v_1 \approx 1.051 \cos\left[\frac{5}{4}|m|\beta_q z - 17.84°\right] \exp \frac{3}{8}|m|\beta_q z \exp - j\beta_e\left(1 - \frac{\omega_q}{\omega}\right)z$$

$$v_{11} \approx 1.822 \sin\left(\frac{5}{4}|m|\beta_q z\right) \exp \frac{3}{8}|m|\beta_q z \exp - 3j\beta_e\left(1 - \frac{\omega_q}{\omega}\right)z. \quad \text{(VI.37)}$$

When a phase of -90 degrees is used, only the declining waves (roots 7 and 8) are excited. In this case the velocities are given as

$$v_1 \approx 1.051 \cos\left[\frac{5}{4}|m|\beta_q z + 17.84°\right] \exp - \frac{3}{8}|m|\beta_q z \exp - j\beta_e\left(1 - \frac{\omega_q}{\omega}\right)z$$

$$v_{11} \approx 1.822 \sin \frac{5}{4}|m|\beta_q z \exp - \frac{3}{8}|m|\beta_q z \exp - 3j\beta_e\left(1 - \frac{\omega_q}{\omega}\right)z. \quad \text{(VI.38)}$$

The dependence on the phase closely resembles the conditions in order parametric amplifiers operating at degenerate frequencies.

The rate of growth indicated in Eq. VI.36 is one-half of the value obtained by Louisell and Quate[20] in their work where only the lower sideband was considered. Also it is seen that the upper sideband is very heavily excited; therefore noise at this frequency would be an important consideration. These results of lower gain and heavy upper sideband excitation explain in part the discrepancy between the experimental results and results from the previous theory. The inclusion of additional sidebands, especially those around the second pump harmonic, would lead to more accurate answers than those obtained here.

---

20. Ibid.

The theoretical results presented here are in accord with a prediction in the recent paper of Roe and Boyd[21], where it is shown that with a dispersionless case there will be no exponential gain but as dispersion is added to the system gain will result. The longitudinal-beam parametric amplifier has dispersion introduced by the plasma frequency reduction factor.

F. Conclusion

The modulated-beam-traveling-wave tube has been studied for modulating signals with frequencies very much less than the carrier and also for modulation signals with frequencies comparable to the carrier. The following has been shown for the low-frequency signals: 1.) The range of linear phase modulation during beam-potential modulation can be extended by the addition of loss. 2.) It is possible to minimize the inherent amplitude modulation during beam-voltage modulation without destroying the phase linearity by using large carrier signals. 3.) Large phase-modulation indices can be obtained with long low-C tubes. 4.) It is important in the linear analysis to include modulation effects of the initial wave amplitudes for short tubes or Crestatrons. Also, the modulation effects on the initial loss parameter are more pronounced during voltage modulation than during current modulation.

The longitudinal-beam parametric amplifier has been investigated using the high-modulating-frequency analysis. The effect of the upper sideband around the pump fundamental has been considered. It has been shown that: 1.) The signal at the upper sideband is very strongly excited, indicating the presence of noise at this frequency, and 2.) The

---

21. Roe, G. M. and Boyd, M. R., "Parametric Energy Conversion in Distributed Systems", Proc. IRE, vol. 47, No. 7, pp. 1213-1218; July, 1959.

gain will be very much less than the gain obtained considering only the lower sideband.

VII. DISK AND HELICALLY LOADED COAXIAL AND WAVEGUIDE TWA STRUCTURES (R. W. Larson)

A. Introduction

The disk and helically loaded coax and waveguide structures shown in Figs. VII.1,e through ℓ, have been proposed and used as high-power traveling-wave tube structures. It is obvious that because of size, they are capable of greater power-handling capacity than the smaller, more delicate helices shown in (a) through (e) of Fig. VII.1. However, other characteristics are equally important. This report is intended to illustrate several methods of analysis which may be used in evaluationg the ω-β diagram and the interaction impedance.

Apparently the first to consider this problem for the helicoid was Field[1] in 1949, but his results were inconclusive and in fact do not agree well with later results. Rowe[2] and Kleen and Ruppel[3] later mentioned this structure but apparently the first design and experimental analysis of the helicoid was given by Valtersson[4] at the Congres Tubes Hyperfrequencies, Paris, 1956. Others have worked on the problem,

---

1. Field, L. M., "Some Slow-Wave Structures for Traveling-Wave Tubes", Proc. IRE, vol. 37, No. 1, pp. 34-40; January, 1949.
2. Rowe, J. E., "A Wide Band Structure for High-Power Traveling-Wave Tubes", Trans. PGED, vol. ED-1, No. 1, pp. 55-56; December, 1953.
3. Kleen, W. and Ruppel, W., "Delay Lines as Circuit Elements of Electron Tubes", Archiv. der. Electr., vol. 40, No. 5, pp. 280-304; 1952.
4. Valtersson, B., "Phase Velocity in Helical Waveguides", L'Onde Electrique; October, 1957.

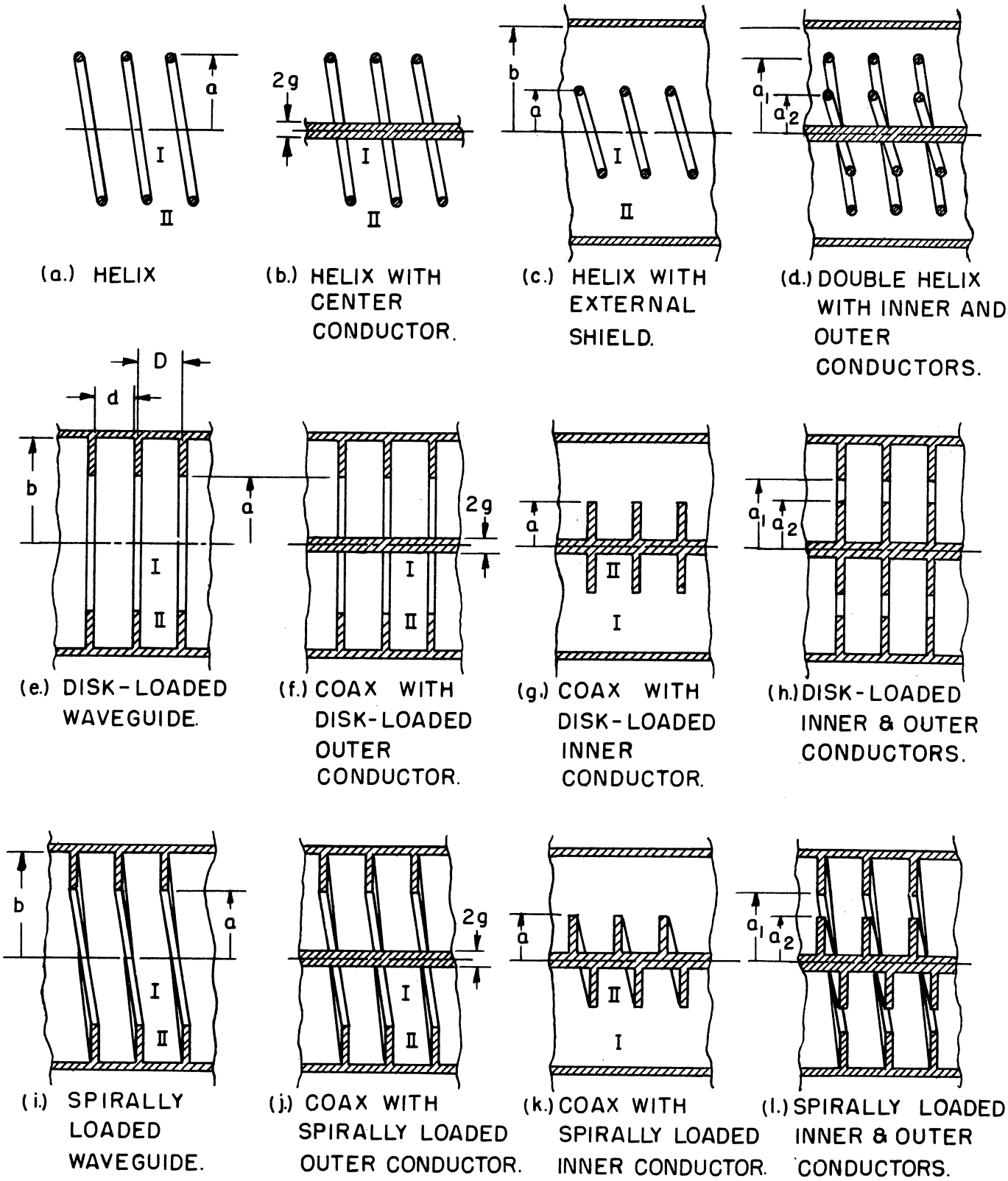

FIG. VII.1 SOME POSSIBLE SLOW-WAVE STRUCTURES WITH HELICAL OR CYLINDRICAL GEOMETRY.

especially a group at Stanford[5] whose work will be mentioned later, but the outstanding reference to date is by Hennoch[6].

The main attempt in the following analysis will be to understand the helically loaded coax, of Fig. VII.1j, but it is apparent that the similarity to disk structures will mean a certain emphasis must be placed on these structures also. The differences will be discussed more fully in Section G. To this end then, we will study several valid approaches to this problem in a rather arbitrary order of increasing complexity:

B. Filter Theory

C. Perturbations

D. Developed Structures, Altered Geometry

E. First Limiting Case; Enclosed Helicoid

1. Wrapped Rectangular Guide

2. "Exact" Helicoid Solutions

F. Second Limiting Case, Disk-Structure

G. "Exact" Open Helicoid

H. Modifications, Conclusions

The following symbols have been chosen to describe the dimensions, physical quantities and parameters. The nomenclature in this area is not yet standardized and therefore other common symbols are included in parenthesis at the end of each definition, to facilitate reading and future choice.

---

5. Consolidated Quarterly Progress Report No. 9, Electron Devices Laboratory, Stanford Electronics Laboratory; January 1 to March 31, 1959.

6. Hennoch, B. T., "Investigations of the Disk-Loaded and Helical Waveguide", Trans. Royal Inst. of Tech., No. 129, Stockholm, Sweden; 1958.

SYMBOLS

a	inner radius of slow wave structures (b)
b	outer radius of slow wave structures (a)
B	magnetic field strength
c	velocity of light
C	Pierce gain parameter
d	breadth of disk or groove space (δ)
D	disk or helicoid periodicity or pitch (s,p)
E	electric field strength
g	rod or innermost radius (c)
G_{mn}, H_{mn}	special combinations of regular and modified Bessel functions
$I_\nu(x), K_\nu(x)$	modified Bessel functions of order ν and argument x, 1st and 2nd kind
$J_\nu(x) = Y_\nu(x), N_\nu(x)$	regular Bessel functions of order ν and argument x, 1st and 2nd kinds respectively and related to the modified Bessel functions by Eq. VII.21
n	integral values of the order of the Bessel function and the order of the Fourier harmonic
P	power transfer
v	velocity (u)
V_o	beam voltage
W	width of rectangular guide, or in wrapped guide, $W = b-a$
α	normalized slot area admittance
β	axial propagation constant, $\omega/v(\beta_o, \gamma_o)$
β_n	axial propagation constant of the nth space harmonic, $\beta_n = \beta_o + 2\pi n/D(\gamma_n)$

γ_n	radial propagation constant of the nth space harmonic defined by Eq. VII.12 $\gamma_n^2 = k^2-\kappa^2$ for the enclosed helicoid and by Eq. VII.20 $\gamma_n^2 = \beta_n^2-k^2$ for the disk cases (Γ_n)
k	free-space propagation constant, $\omega/c(\beta_o,\kappa_o)$
κ	alternative constant for giving field dependence in the z-direction (β)
Φ	normalized beam area admittance
ν	fractional order of Bessel function and fractional angular propagation constant

B. Filter Theory Approach

To obtain an appreciation for the frequency characteristics of the disk-loaded structures, we can consider the equivalent filters for these structures. To the extent that the helicoids look like the disk structures, this filter analogy will also apply to them.

To obtain a form for the filter, we must consider the series and parallel values of impedance as seen at the edges of the disks. Looking out into the cavities of the structure of Fig. VII.1f as a representative case, we know from more elementary work[7] that there is a capacitance seen between disks or vanes and there is also a short inductive section of transmission line. When looking toward the center in the center rod case we see essentially a capacitance. When no center rod is present we again see a parallel L-C combination. These circuits are summarized in Fig. VII.2. This analysis shows us that to achieve a low-pass type of structure we must have a center rod. An increase in C_2 in this low-pass case, with its accompanying decrease in phase velocity, can be

7. Ramo, S. and Whinnery, J., Fields and Waves in Modern Radio, John Wiley and Sons, Inc., New York; 1949.

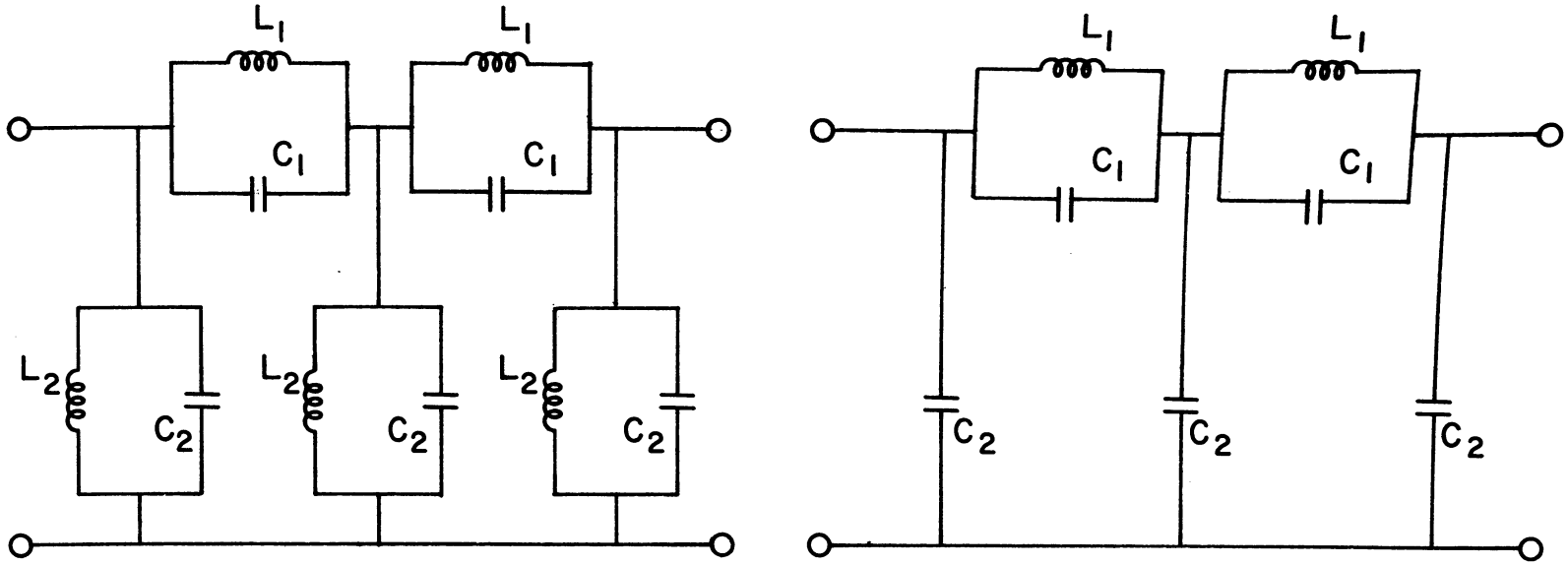

a. WITHOUT CENTER CONDUCTOR
BAND-PASS CASE

b. WITH CENTER CONDUCTOR
LOW-PASS CASE

FIG. VII.2 EQUIVALENT FILTERS FOR DISK-LOADED WAVEGUIDE WITH ANGULARLY SYMMETRIC FIELD.

accomplished by increasing the rod size. Correspondingly an increase in the relative groove depth will mean an increase in L_1 with a corresponding decrease in the resonant frequency $\omega_0 = 1/\sqrt{LC}$. Much more can be said of the analogies with filter theory but nother exact can be obtained without exact L-C values and their frequency characteristics.

C. Perturbation Technique

For small groove depth, somewhat more accurate results may be obtained by utilizing the known results for ordinary circular waveguide and coax. This is the usual technique in perturbation analyses of all sorts. In this case we know, for instance, that for TM and TE modes in cylindrical and coaxial guides respectively[7]

$$\text{TM: cylindrical;} \quad I_n(\gamma_n b) = 0 \qquad \text{(VII.1)}$$

$$\text{coaxial ;} \quad I_n(\gamma_n g)\, K_n(\gamma_n b) - K_n(\gamma_n g)\, I_n(\gamma_n b) = 0 \quad \text{,(VII.2)}$$

$$\text{TE: cylindrical;} \quad I_n'(\gamma_n b) = 0 \qquad \text{(VII.3)}$$

$$\text{coaxial ;} \quad I_n'(\gamma_n g)\, K_n'(\gamma_n b) - K_n'(\gamma_n g)\, I_n'(\gamma_n b) = 0 \quad . \text{(VII.4)}$$

It has been shown[8] that for $n > 0$ the TE modes are unstable in the presence of a helical perturbation, while the TM modes are stable. Hennoch[6] has given the matching equations for the admittances in the case of small perturbations. It is obvious that there will be a certain simplification in the arithmetical calculations. However, it is not possible to extend the results beyond the region where they are mathematically valid.

---

8. Karbowiak, A. E., "Microwave Propagation in Anisotropic Waveguides", Proc. IEE, Mon. 147 R; August, 1955.

D. Developed Structures, Altered Geometry

A logical approach to the understanding of the helicoid is to "develop" or unwrap the helicoid. This artificial slow-wave structure may then be analyzed just as we propose to analyze the disk and helicoid structures in Sections F and G. The advantage is in now being able to work with trigonometric and hyperbolic functions. Their advantage over cylindrical Bessel functions is only in familiarity and availability of relationships and tabulated values. Valtersson's[4] approach to the analysis of the helicoid was this last one. This curve is shown in Fig. VII.3, curve C, for comparison with several other results. This phase velocity was obtained for the case: $b/a = 4$, $a/g = 1.25$, $D/a = 0.5$, $d/D = 0.4$. It is to be expected that this analogy would not stand up too well when the radius of curvature is small compared to the wavelength. Moreover, the results given by Valtersson more nearly coincide with the disk results, rather than the helicoid results to be given later. This is a fundamental limitation in this method of analysis as in all analyses involving "development".

E. First Limiting Case - Enclosed Helicoid

1. "Wrapped" Rectangular Guide. It may be enlightening to consider wrapping a rectangular waveguide carrying the TE_{10} mode. It is apparent that there can now be no analogy with disk-loaded guides since the inner cavity boundary is now replaced by a metal wall and we must be content with analyzing a completely different circuit. Disman[9] has shown by this technique that the maximum useful bandwidth is only 5 percent. This is the frequency difference between the low-frequency

9. Disman, M. I., "A Preliminary Investigation of a High-Power Hollow-Beam TWT Amplifier," Technical Report No. 458-1, Electron Devices Laboratory, Stanford University; November 4, 1958.

cutoff at λL and the so-called "π" cutoff at λ_1, where the angular propagation constant $\nu = 1/2$ or $\beta D = \pi$. From Ramo and Whinnery[7] we know that the phase shift in the helical direction (using rectangular waveguide results) is

$$\beta_g = \frac{2\pi}{\lambda}\sqrt{1 - \left(\frac{\lambda}{2W}\right)^2} , \qquad \text{(VII.5)}$$

where $W = b - a$.

We can convert this to a phase shift β in the longitudinal direction by multiplying by the ratio of circumferential to longitudinal path length.

$$\frac{\sqrt{\left[2\pi\left(\frac{W}{2} + a\right)\right]^2 + D^2}}{D} ,$$

if we take the average length of the path as that at the center of the grid. To find the π cutoff at λ_1 we let $\beta D = \pi$. If the low-frequency cutoff can be considered to occur for $\lambda_L = 2W = 2(b-a)$, then

$$\left(\frac{\lambda_L}{\lambda_1}\right)^2 = \frac{W^2}{\left[2\pi\left(\frac{W}{2} + a\right)\right]^2 + D^2} + 1 . \qquad \text{(VII.6a)}$$

Since (λ_L/λ_1) is maximized for a and D both equal to zero,

$$\frac{\lambda_L}{\lambda_1} = \sqrt{1 + \left(\frac{1}{\pi}\right)^2} , \qquad \text{(VII.6b)}$$

so that the maximum available bandwidth is indeed approximately 5 percent.

2. Exact Helicoid Solutions. Waldron[10,11] approached the helicoid only as a mathematical problem and so was not interested in the enclosed helicoid as a slow-wave circuit. However, his analysis is of interest since it is expected that the open helicoids must possess certain similarities to the enclosed helicoid. Waldron has proven by means of a perturbation analysis that the helicoid may have the inherently difficult helical character removed by straightening the guide out to an "infinite wrapped rectangular guide". The helical side walls now become disks, but we need not restrain ourselves to the condition $F(\theta) = F(\theta + 2\pi)$. Mathematically this means that the angular propagation constant need no longer be an integer (or zero). Using cylindrical coordinates r, θ, z then, he chooses a general field

$$\underline{E} = \left\{\underline{\bar{r}}\, E_r + \underline{\bar{\theta}} E_\theta + \underline{\bar{z}} E_z\right\}\left\{e^{j\kappa z} + Pe^{-j\kappa z}\right\} e^{-j\nu\theta} e^{j\omega t} \quad , \qquad \text{(VII.7)}$$

$$\underline{H} = \left\{\underline{\bar{r}}\, H_r + \underline{\bar{\theta}} H_\theta + \underline{\bar{z}} H_z\right\}\left\{e^{j\kappa z} + Qe^{-j\kappa z}\right\} e^{-j\nu\theta} e^{j\omega t} \quad . \qquad \text{(VII.8)}$$

By substituting the above into Maxwell's equations and eliminating the radial and tangential field components one obtains the wave equations

$$(\nabla_o^2 + \gamma^2)\, E_z = 0 \quad , \qquad \text{(VII.9)}$$

$$(\nabla_o^2 + \gamma^2)\, H_z = 0 \quad , \qquad \text{(VII.10)}$$

where

$$\nabla_o = \nabla - \underline{\bar{z}}\, \frac{\partial}{\partial z} \quad , \qquad \text{(VII.11)}$$

---

10. Waldron, R. A., "Theory of the Helical Waveguide of Rectangular Cross-Section", Journ. Brit. IRE, vol. 17, No. 10, pp. 577-592; October, 1957.

11. Waldron, R. A., "A Helical Coordinate System and Its Application in Electromagnetic Theory", Quarterly Journ. of Mech. and Appl. Math., vol. 11, Pt. 4, pp. 438-461; November, 1958.

and

$$\gamma^2 = \omega^2\epsilon_o\mu_o - \kappa^2 \quad . \tag{VII.12}$$

We next may consider two sets of normal modes, the E and H modes, respectively characterized by $H_z = 0$ and $E_z = 0$. These are not related to the usual waveguide modes where propagation is in the z-direction, since now we have propagation in the θ direction and κ takes on only integral values.

The solutions of the wave equation are

<u>E Modes</u>:

$$E_z = \left\{Fe^{j\kappa z} + Ge^{-j\kappa z}\right\}\left\{J_\nu(\gamma r) + RN_\nu(\gamma r)\right\} e^{-j\nu\theta}e^{j\omega t} \quad ,$$

$$H_z = 0 \quad . \tag{VII.13a}$$

<u>H Modes</u>:

$$E_z = 0 \quad ,$$

$$H_z = \left\{F'e^{j\kappa z} + G'e^{-j\kappa z}\right\}\left\{J_\nu(\gamma r) + R'N_\nu(\gamma r)\right\} e^{-j\nu\theta}e^{j\omega t} \quad , \tag{VII.13b}$$

where F, F', G, G', R and R' are arbitrary integration constants to be evaluated from the boundary conditions. The other components for both modes are

$$H_r = \frac{1}{\gamma^2}\left[\frac{\partial}{\partial z}\left(\frac{\partial H_z}{\partial r}\right) + \frac{j\omega\epsilon_o}{r}\frac{\partial E_z}{\partial \theta}\right] ,$$

$$H_\theta = \frac{1}{\gamma^2}\left[\frac{1}{r}\frac{\partial}{\partial z}\left(\frac{\partial H_z}{\partial \theta}\right) - j\omega\epsilon_o\frac{\partial E_z}{\partial r}\right] ,$$

$$E_r = \frac{1}{\gamma^2}\left[-\frac{j\omega\mu_o}{r}\frac{\partial H_z}{\partial \theta} + \frac{\partial}{\partial z}\left(\frac{\partial E_z}{\partial r}\right)\right] ,$$

$$E_\theta = \frac{1}{\gamma^2}\left[j\omega\mu_o\frac{\partial H_z}{\partial r} + \frac{1}{r}\frac{\partial}{\partial z}\left(\frac{\partial E_z}{\partial \theta}\right)\right] . \qquad \text{(VII.14)}$$

Considering the E mode first, we note that at $z = 0$ and $z = d$, the electric field must be entirely normal to the disks, so $E_r = E_\theta = 0$. Hence, $F = G$ and $\kappa = m\pi/d$, where m is an integer. For the same reason $E_\theta = E_z = 0$ at $r = a$ and $r = b$ so that

$$J_\nu(\gamma a) + RN_\nu(\gamma a) = 0 ,$$

$$J_\nu(\gamma b) + RN_\nu(\gamma b) = 0 . \qquad \text{(VII.15)}$$

The only solution which gives the same value of R is

$$H_{\nu,\nu}(a,b) = J_\nu(\gamma a)\, N_\nu(\gamma b) - J_\nu(\gamma b)\, N_\nu(\gamma a) = 0 . \qquad \text{(VII.16)}$$

The remaining field components may now be obtained and they are

$$E_r = -\frac{m\pi}{\gamma b} H_{\nu'\nu}(r,b) \sin\frac{m\pi z}{d} e^{-j\nu\theta} e^{j\omega t} ,$$

$$E_\theta = +\frac{jm\pi\nu}{\gamma^2 rd} H_{\nu\nu}(r,b) \sin\frac{m\pi z}{d} e^{-j\nu\theta} e^{j\omega t} ,$$

$$E_z = H_{\nu\nu}(r,b) \cos\frac{m\pi z}{d} e^{-j\nu\theta} e^{j\omega t} ,$$

$$H_r = \frac{\omega\epsilon_o \nu}{\gamma^2 r} H_{\nu\nu}(r,b) \sin\frac{m\pi z}{d} e^{-j\nu\theta} e^{j\omega t} ,$$

$$H_\theta = \frac{j\omega\epsilon_o}{\gamma} H_{\nu'\nu}(r,b) \cos\frac{m\pi z}{d} e^{-j\nu\theta} e^{j\omega t} ,$$

$$H_z = 0 . \qquad \text{(VII.17)}$$

The "ω-β" curve is now replaced by an "ω-ν" curve which is determined from Eq. VII.16; tabulated data are given in Waldron's article[11] as well as in Jahnke and Emde[12]. When ν has been determined as a function of frequency, we may then translate this into longitudinal velocity information by means of the relationship

$$v = \frac{\omega D}{2\pi\nu} \quad \text{or} \quad \frac{v}{c} = \frac{kD}{2\pi\nu} , \qquad \text{(VII.18a)}$$

which may be considered as arising from multiplying the velocity in the helical direction by the tangent of the pitch angle

$$v = \left(\frac{\omega r}{\nu}\right)\left(\frac{D}{2\pi r}\right) . \qquad \text{(VII.18b)}$$

---

12. Jahnke, E., and Emde, F., Tables of Functions, Dover Publications, New York; 1945.

One such curve is shown in Fig. VII.3d, where the following data have been chosen.

$$b/a = \text{outer to inner radii ratio} = 5.0$$

$$D/a = \text{pitch to inner radius ratio} = 0.5$$

and the lowest-order ($\kappa = 0$) E mode has been assumed, since κ comes into the calculation of γ from k(or ω). This curve shows the highly dispersive character noted in the preceding section and in fact is perhaps even more severe than stated there. Clarke[13] states that the phase velocity for b/a = 5 falls from ∞ at cutoff to Dc/b-a at the π mode in a 3 percent frequency band.

We expect to see the general helicoid nature of this structure as well as the disk results of the next section in the final open-helicoid results.

F. Second Limiting Case - Disk Structure

This section might logically be considered to be an end in itself, since the disk-loaded coax structures have been known for some time, and some noteworthy high-power traveling-wave tubes have been tested. Besides Field's early work[1], a group at the Federal Telecommunications Laboratories, Inc.[14] worked on the disk-loaded coax structure. In the following we will not only be interested in the disk structures as an idealized simplification of the helicoid, valid in certain frequency ranges as yet to be determined, but we will also be interested in the disk structures for their own value as high-power slow-wave structures.

---

13. Clarke, G. M., "Helical Waveguides - Closed, Open and Coaxial", Journ. Brit. IRE, vol. 18, No. 6, pp. 359-361; June, 1958.

14. Dewey, G. C., Parzen, P., and Marchese, T. J., "Periodic-Waveguide Traveling-Wave Amplifier for Medium Powers", Proc. IRE, vol. 39, No. 2; February, 1951.

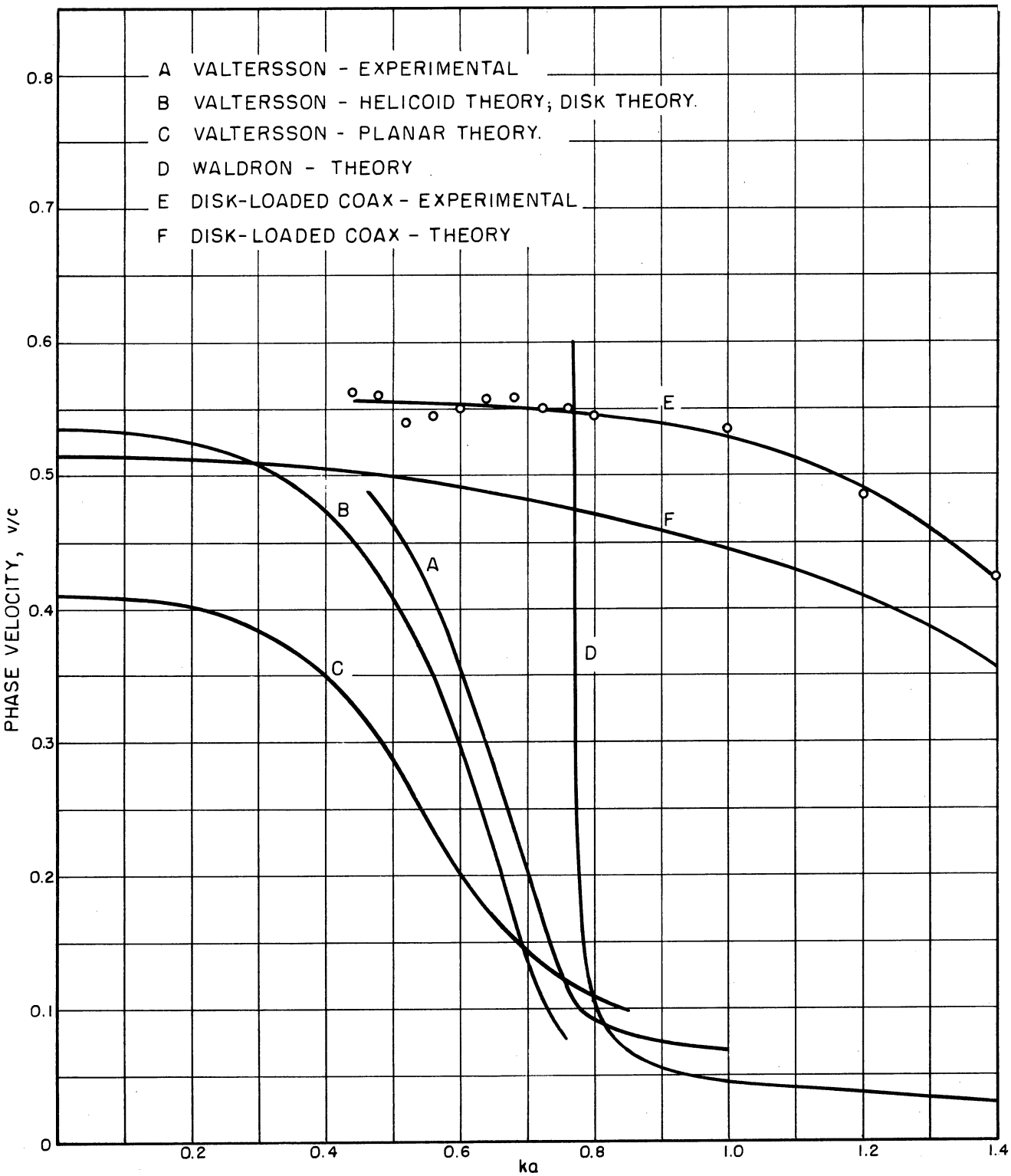

FIG. VII.3 PHASE VELOCITY VS. ka FOR VARIOUS R-F STRUCTURES.

Many of the ideas of the previous section may now be used in this disk analysis. In the helicoid analysis we assumed an angular propagation constant ν which could take on all values even though our analysis was in cylindrical coordinates. In addition we assumed a longitudinal propagation constant $\kappa = m\pi/d$ which was determined for integral m. We now find that both of these choices may be simplified since for $F(\theta) = F(\theta + 2\pi)$ we must have $\nu = N$ an integer. In addition $\kappa = m = 0$ is a good choice for the field variation across the disk gap, especially for small gap width d. If $N = 0$, we then have from Eqs. VII.17 only two components

$$E_z = H_{oo}(r,b)\, e^{j\omega t} \quad ,$$

$$H_\theta = -\frac{j\omega\epsilon_o}{k} H'_{oo}(r,b)\, e^{j\omega t} \quad , \qquad \text{(VII.19)}$$

where $H'_{oo}(r,b) = -H_{1o}(r,b) = -\left\{J_1(kr)\, N_o(kb) - N_1(kr)\, J_o(kb)\right\}$, and

$$\gamma = k \text{ since } \kappa = 0.$$

In the event that there is an angle-dependent field on the outside, Eqs. VII.17 show that H_r is also present and the functions $H_{oo}(r,b)$, $H'_{oo}(r,b)$ go over to $H_{N,N}(r,b)$, $H'_{N,N}(r,b)$.

The inner fields (in the open space) are traveling waves rather than standing waves and this fact is reflected in the radial propagation constant defined by Eq. VII.12. Rather than taking our propagation constant as $\gamma = \sqrt{\omega^2\mu\epsilon - \kappa^2}$ let us take the more usual choice of propagation as

$$e^{-j\beta_n z} = e^{-j\left(\beta_o + \frac{2\pi n}{D}\right) z}$$

so

$$\gamma_n = \sqrt{k^2 - \beta_b^2} \quad .$$

Note that for slow waves and $n > 0$, $\beta_n^2 > k^2$, so γ_n is imaginary.

This choice allows us to find the field components from Eq. VII.15 just as in the previous case when we chose propagation in the z-direction as $(Fe^{+j\kappa z}+Ge^{-j\kappa z})$ and found that $F = G$ so that we obtained a cosinusoidal behavior. Our wave equation is essentially the same; however, since our old definition of Eq. VII.12 gives imaginary γ_n we will change our definition of γ to read

$$\gamma_n^2 = \beta_n^2 - \omega^2\mu\epsilon = \beta_n^2 - k^2 \quad . \qquad \text{(VII.20)}$$

This now coincides with the choice of most other authors, including Pierce[15], and Sensiper[16] and offers the advantage of working with real γ_n. This difference in sign changes the wave equation and we find that the new solution contains modified Bessel functions $I_n(\gamma_n r)$, and $K_n(\gamma_n r)$ which are related simply to $J_n(\gamma_n r)$ and $H_n^{(1)}(\gamma_n r)$ by

$$I_\nu(z) = \exp\left(-j\,\frac{\nu\pi}{2}\right) J_\nu(jz) \quad ,$$

$$K_\nu(z) = j\,\frac{\pi}{2}\exp\left(j\,\frac{\nu\pi}{2}\right) H_\nu^{(1)}(jz) \quad . \qquad \text{(VII.21)}$$

---

15. Pierce, J. R., Traveling-Wave Tubes, Van Nostrand Company, New York; 1950.

16. Sensiper, S., "Electromagnetic-Wave Propagation on Helical Conductors", Tech. Rpt. No. 194, Research Laboratory of Electronics, Massachusetts Institute of Technology; 1951.

This change in definition of Eq. VII.12 is necessary in order to avoid the transformation of Eq. VII.21 at a later time, and especially because of the availability of tabulated values for I_ν's and K_ν's whereas none seem available for $N_\nu(jz)$.

Thus the solution of the wave equation is now

$$E_z = \left\{AI_N(\gamma_n r) + BK_N(\gamma_n r)\right\} e^{-j\beta_n z} e^{jN\theta} e^{j\omega t} \quad , \qquad \text{(VII.22)}$$

and for $H_z = 0$, we may find the remainder of the components from Eqs. VII.15. The introduction of the disk periodicity gives an infinite number of space harmonics traveling at different phase velocities but with the same group velocity. The field components in the most general case are obtainable from the Maxwell equations and are given by Hennoch, in forms such as

$$E_z = e^{jN\theta} \cdot e^{-j\omega t} \sum_{n=-\infty}^{n=+\infty} A_n \left[K_N(\gamma_n g) I_N(\gamma_n r) - I_N(\gamma_n g) K_N(\gamma_n r)\right] e^{j\beta_n z} \quad . \qquad \text{(VII.23)}$$

All $K_N(\gamma_n r)$ or $K_N(\gamma_n g)$ terms will drop out if there is no center rod, since the fields must be finite on the axis, and $K_N(0) = \infty$. Also, if the center space fields are circularly symmetric ($N = 0$) then for the TM waves, E_θ and H_r are zero.

Focusing our attention hereforth on only the TM waves since TE waves are often not excited, we find that one way to evaluate the coefficients A_n is to let

$$E_z \Big|_{r=a}^{\text{groove}} = E_z \Big|_{r=a}^{\text{center}} \quad , \qquad \text{(VII.24a)}$$

and

$$\int_{gap} B_\theta \Big|_{r=a}^{groove} dz = \int_{gap} B_\theta \Big|_{r=a}^{center} dz \quad . \tag{VII.24b}$$

Because of the disk width, we find that the average effect of the groove fields at the radius r = b, is that given by Eq. VII.22 multiplied by the factor

$$\frac{d}{D} \sum_{n=-\infty}^{n=+\infty} \frac{\sin\left[\left(\beta_o + \frac{2\pi n}{D}\right)\frac{d}{2}\right]}{\left[\left(\beta_o + \frac{2\pi n}{D}\right)\frac{d}{2}\right]} , \tag{VII.25}$$

which is a standard factor for matching fields at such a boundary. For N = 0, and n = 0 only, then

$$\frac{1}{ka}\frac{H'_{oo}(b,a)}{H_{oo}(b,a)} = -\frac{d}{D}\frac{1}{\gamma_o a}\frac{G'_{oo}(g,a)}{G_{oo}(g,a)}\left\{\frac{\sin\left(\gamma_o \frac{d}{2}\right)}{\left(\gamma_o \frac{d}{2}\right)}\right\}^2 . \tag{VII.26}$$

Alternatively, a simpler approach is to match admittances at the gap boundary. This was employed in an earlier project quarterly[17] and the resultant admittances are shown in Figs. VII.4 and VII.5 where

17. Larson, R. W., et al., "Theoretical and Experimental Investigation of Large-Signal Traveling-Wave Tubes", Quarterly Progress Report No. 5, Project No. 2562, Contract No. AF30(602)-1596, Electron Tube Laboratory, The University of Michigan; November, 1957.

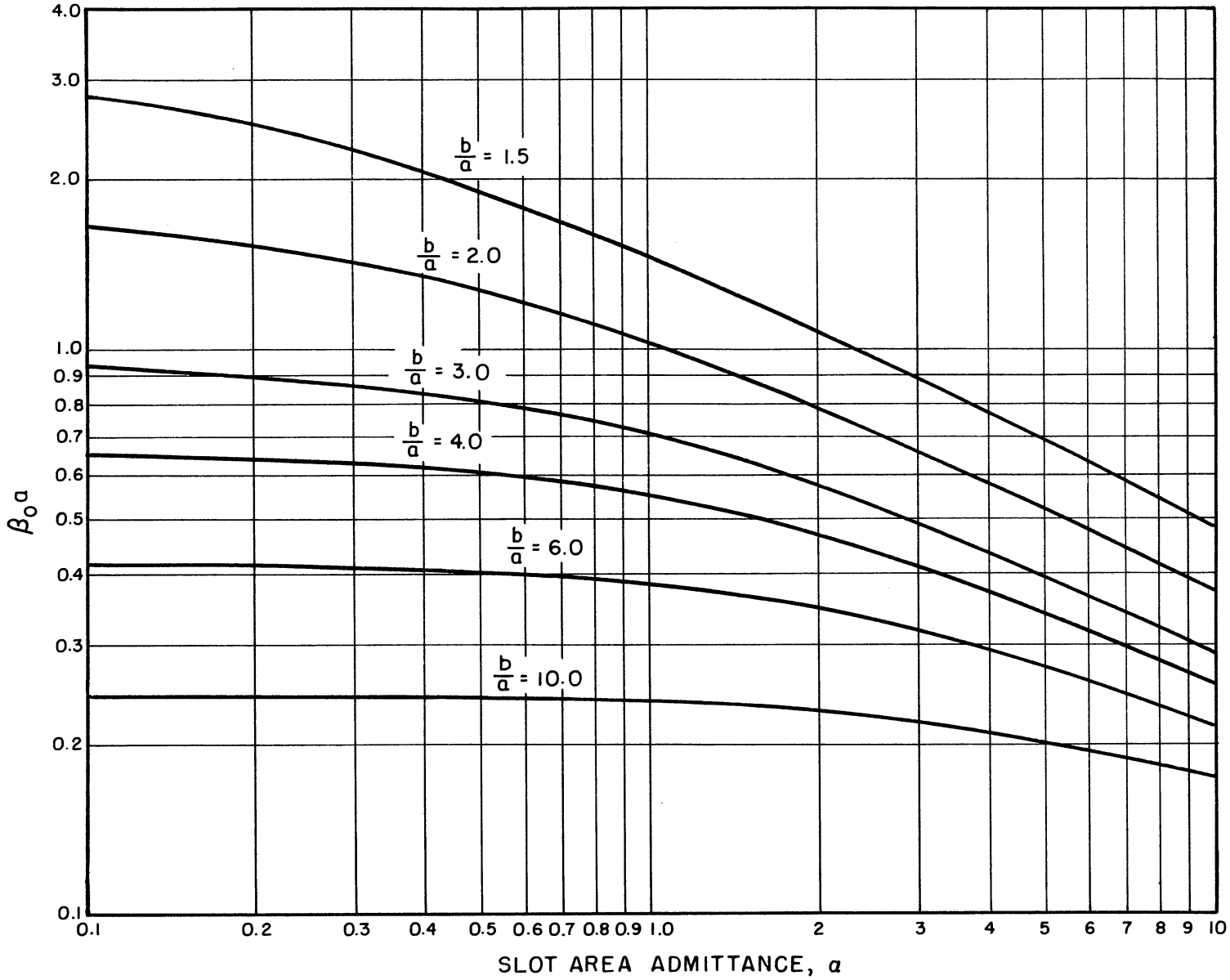

FIG. VII.4 NORMALIZED SLOT AREA ADMITTANCE PARAMETER, α, VS. $\beta_0 a$ WITH RATIO OF DISK HOLE RADIUS TO SHIELD RADIUS AS PARAMETER.

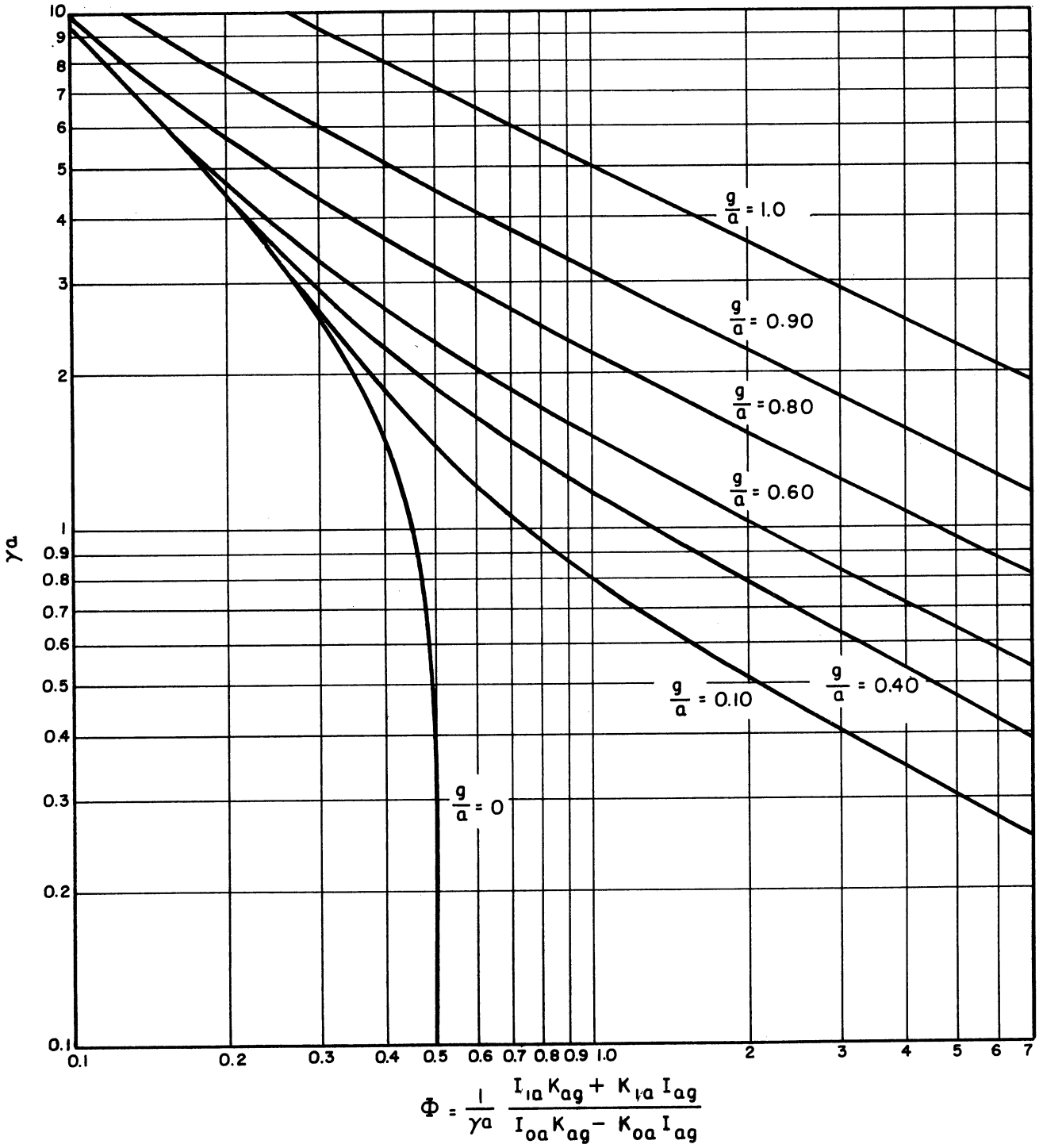

FIG. VII.5 BEAM AREA ADMITTANCE VS. γa WITH RATIO OF ROD RADIUS TO DISK HOLE RADIUS AS PARAMETER.

$$\alpha = \frac{1}{ka} \frac{J_{1a}N_{ob} - N_{1a}J_{ob}}{J_{oa}N_{oa} - N_{oa}J_{ob}} = \frac{1}{ka} \frac{-H'_{oo}(a,b)}{H_{oo}(a,b)} ,$$

$$\Phi = \frac{1}{\gamma a} \frac{I_{1a}K_{og} + K_{1a}I_{og}}{I_{oa}K_{og} - K_{oa}I_{og}} = \frac{1}{\gamma a} \frac{G'_{oo}(a,g)}{G_{oo}(a,g)} . \qquad \text{(VII.27)}$$

A matching of these equations, in this graphical form, thus allows us to find β as a function of k. This allows the approximate phase velocity to be determined from Eq. VII.20 and the definition of β

$$\frac{v}{c} = \frac{k}{\beta} = \left[1 + \left(\frac{\gamma a}{ka}\right)^2\right]^{-1/2} . \qquad \text{(VII.28)}$$

This is an approximate result, since only the zero-order solution has been obtained and a more precise picture can be obtained only by utilizing at least several components. The complete matching equation will be given shortly, but first let us examine the matching of Eqs. VII.27 for very small arguments, using

$$I_o(x) = 1 \quad ; \quad K_o(x) = -\ln\left(\frac{\gamma^* x}{2}\right) \quad ; \quad \ln\gamma^* = 0.5772$$

$$I_1(x) = \frac{x}{2} \quad ; \quad K_1(x) = \frac{x}{2}\ln\left(\frac{\gamma^* x}{2}\right) . \qquad \text{(VII.29)}$$

Thus

$$\frac{D}{d}\alpha = \frac{D}{d} \frac{1}{(ka)^2 \ln\frac{b}{a}} = \frac{1}{(\gamma a)^2 \ln\frac{a}{g}} = \Phi , \qquad \text{(VII.30)}$$

so

$$\frac{v}{c} = \left[1 + \frac{d}{D} \frac{\ln\frac{b}{a}}{\ln\frac{a}{g}}\right]^{-1/2} . \qquad \text{(VII.31)}$$

This approximate formula (plotted in Fig. VII.6), which is entirely valid for small arguments, thus shows us clearly the way we should proceed in order to achieve low phase velocities for the constant-velocity region shown in Fig. VII.3, and indicated also by the parallel straight-line regions of Figs. VII.4 and VII.5. We obviously want d/D and b/a large and a/g nearly 1. Unfortunately, as a few trials will show, to obtain the low velocities used in traveling-wave tubes of moderate power, the geometry requires a very small beam width (a-g).

The most complete matching formula has been given by Hennoch and is

$$\frac{1}{ka}\,\frac{J_N(kb)\,N_N'(ka) - N_N(kb)\,J_N'(ka)}{J_N(kb)\,N_N(ka) - N_N(kb)\,J_N(ka)}$$

$$= \frac{d}{D}\sum_{n=-\infty}^{+\infty}\frac{1}{\gamma_n a}\left\{\frac{K_N(\gamma_n g)\,I_N'(\gamma_n a) - I_N(\gamma_n g)\,K_N'(\gamma_n a)}{K_N(\gamma_n g)\,I_N'(\gamma_n a) - I_N(\gamma_n g)\,K_N(\gamma_n a)}\right.$$

$$\left. - \frac{\beta_n^2\left(\frac{N}{a}\right)^2}{k^2\gamma_n^2}\,\frac{K_N'(\gamma_n g)\,I_N(\gamma_n a) - I_N'(\gamma_n g)\,K_N'(\gamma_n a)}{K_N'(\gamma_n g)\,I_N'(\gamma_n a) - I_N'(\gamma_n g)\,K_N'(\gamma_n a)}\right\}\left\{\frac{\sin\beta_n\frac{d}{2}}{\beta_n\frac{d}{2}}\right\}^2 . \qquad \text{(VII.32)}$$

Hennoch has plotted ω-β curves for several values of b/a, d/D, D/a and g/a for both N = 0 and N = 1, using n = 0, -1, and -2.

Leaving the area of velocity characteristics, we turn next to calculating the power flow and impedance when the field components can be given explicitly. Pierce[15] showed that the gain of a traveling-wave tube was proportional to an amplification factor C which he chose to define as

$$C = \left(\frac{I_o}{8V_o}\right)^{2/3}\left(\frac{E_z^2}{\beta^2 P}\right) . \qquad \text{(VII.33)}$$

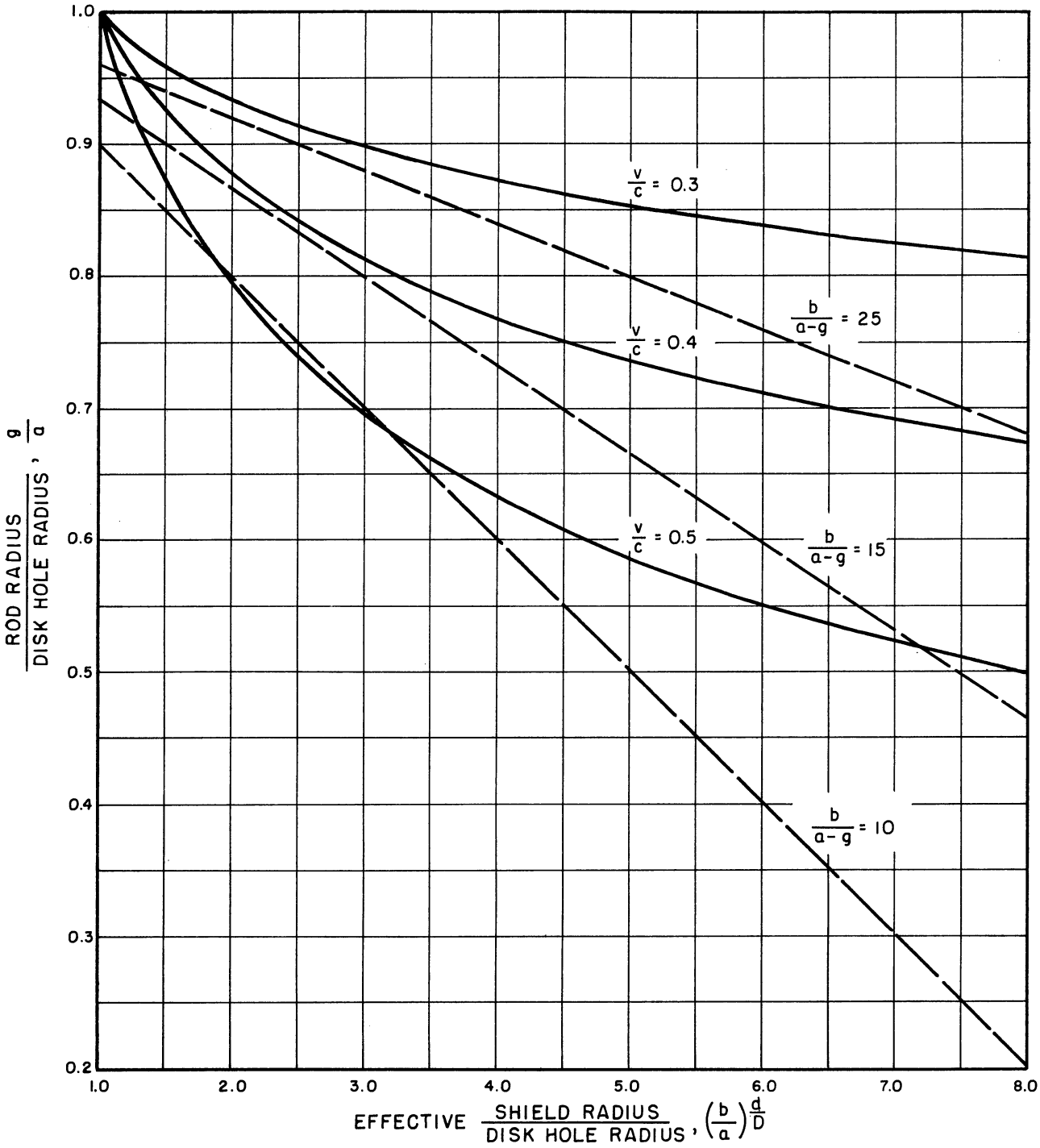

FIG. VII.6 $\frac{\text{ROD RADIUS}}{\text{DISK HOLE RADIUS}}$ VS. $\frac{\text{SHIELD RADIUS}}{\text{DISK HOLE RADIUS}}$ WITH $\frac{v}{c}$ AND $\frac{\text{SHIELD RADIUS}}{\text{BEAM AREA GAP}}$ AS PARAMETERS.

The first factor depends on the electron beam, while the second is a function of the particular slow-wave circuit under investigation and is known as the coupling impedance. P is defined in the usual way

$$P = \frac{1}{2} \mathrm{Re} \int_s [E_r H_\theta^* - E_\theta H_r^*] \, ds \quad . \tag{VII.34}$$

Integration of the combinations of Bessel functions arising from the proper insertion of the field components into this expression may be obtained from the following form obtained from Erdelyi[18]

$$\int z \, \omega_\nu(az) \, w_\nu(az) \, dz = \frac{1}{4} z^2 \, [2\omega_\nu(az) \, w_\nu(az) - \omega_{\nu+1}(az) \, w_{\nu-1}(az) - \omega_{\nu-1}(az) \, w_{\nu+1}(az)] \quad , \tag{VII.35}$$

where ω and w may be any Bessel functions of the first, second or third types of order ν.

The quantity $E^2/\beta^2 P$ is generally expressed as

$$\left[\frac{E^2}{\beta^2 P}\right]^{1/3} = \left(\frac{\beta}{k}\right)^{1/3} \left(\frac{\gamma}{\beta}\right)^{4/3} F \quad . \tag{VII.36}$$

F is given in an earlier project quarterly[17]. From the small-argument expansions of Eq. VII.29, F reduces to

$$F \approx 240^{1/3} \left(\frac{1}{2} \ln \frac{a}{g}\right)^{1/3} \quad . \tag{VII.37}$$

The complete expression for F is plotted in Fig. VII.7.

Hennoch has given similar equations for some of the more complete solutions, and his calculated curves agree well with Fig. VII.7 for the low-frequency region. However, when the upper cutoff frequency

18. Erdélyi, A., Bateman Manuscript Project, McGraw-Hill, New York, 1954.

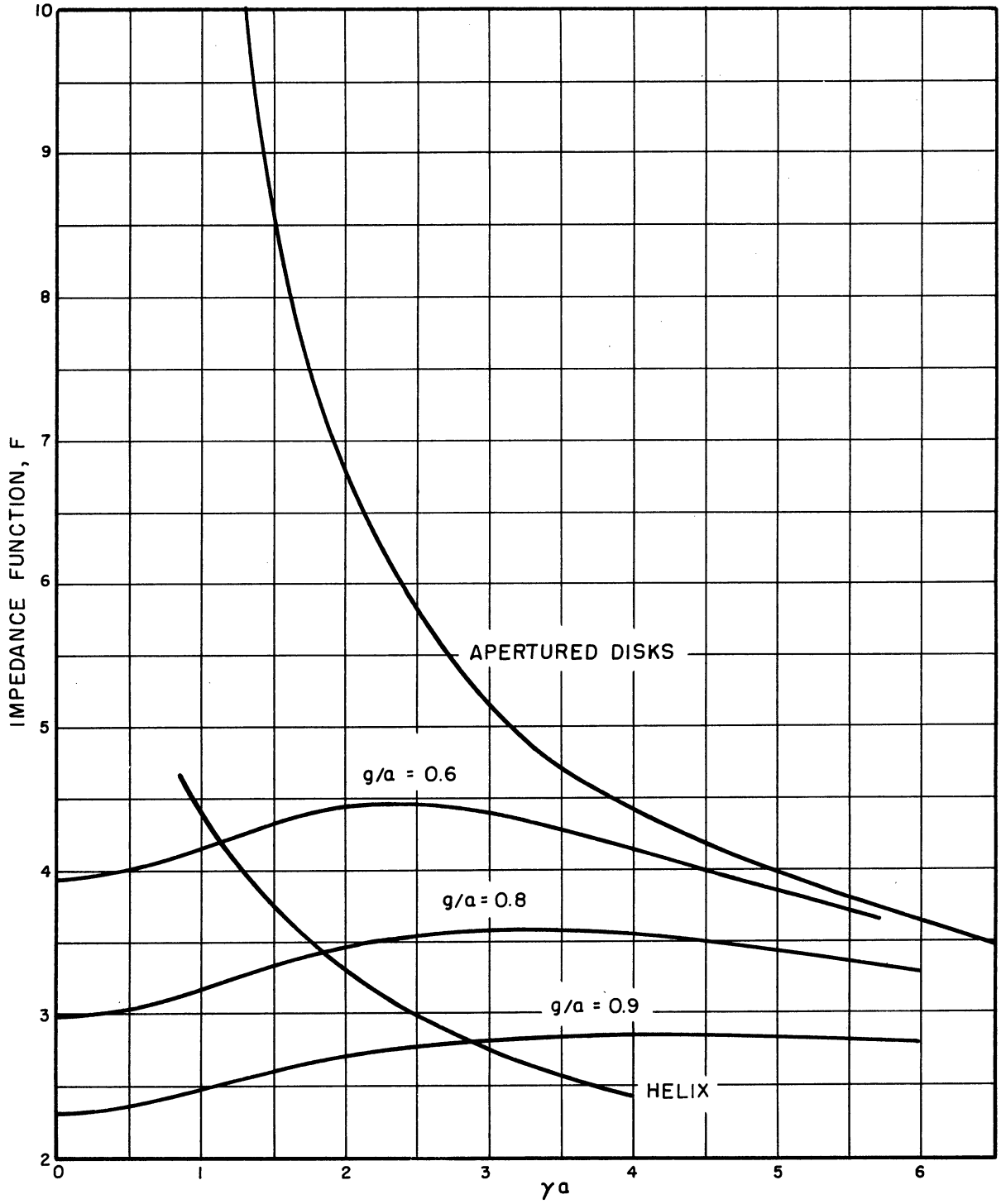

FIG. VII. 7 IMPEDANCE FUNCTION, F, VS. γa WITH ROD RADIUS/ DISK HOLE RADIUS AS THE PARAMETER.

is reached, there is total reflection of the energy and the forward and backward wave energies become equal. This of course demands the inclusion of the effect of this harmonic in the calculations and causes the coupling factor to become infinite at that point.

Before proceeding to the helicoid it should be noted that the coupling factor F, although it is very high for the apertured disk structure, is not useful because of the extremely narrow bandwidth of this structure. The relatively uniform region of F for low values of ka in the disk-loaded coax cases is therefore encouraging, although it does indicate nonuniform overall gain since there are fewer wavelengths in the structure at low frequencies. This is perhaps the greatest reason for the success of the helix as a slow-wave circuit: the coupling factor F, which is roughly the gain per wavelength, falls off with frequency in such a way as to compensate for the increasing number of beam wavelengths.

G. "Exact" Helicoid

As a result of having discussed several similar structures, the analysis of the structures shown in Figs. VII.1i-ℓ becomes much simpler. In fact, the expressions for the various fields in Regions I and II have been given already. Thus in the helically spiraling regions, we may apply the formulae developed in Section E.1 for the enclosed helicoid, Eqs. VII.13, VII.14 and VII.15. In the free-space regions, the fields given in the last section apply, namely those of Eqs. VII.22, VII.23 and VII.24.

The matching of these different fields at the transition boundary for the case of Fig. VII.1j is given by

$$\frac{1}{ka}\,\frac{H_{\nu\nu'}(b,a)}{H_{\nu\nu}(b,a)} = -\frac{d}{D}\sum_{n=-\infty}^{+\infty}\frac{1}{\gamma_n a}\left[\frac{G_{nn'}(g,a)}{G_{nn}(g,a)}\right.$$

$$\left.-\frac{\left(\frac{n\beta_n}{a}-\gamma_n^2\,\mathrm{tg}\,\psi\right)^2}{k^2\gamma_n^2}\,\frac{G_{n'n}(g,a)}{G_{nn}(g,a)}\right]\left\{\frac{\sin\left(\frac{\beta_n d}{2}\right)}{\frac{\beta_{n'}d}{2}}\right\}. \quad \text{(VII.38)}$$

The evaluation of this equation is a more difficult matter than in the disk case; but only in practice, not in theory. The reason for this is the sparsity of tabulated values of fractional-order Bessel functions. Formulae exist for calculating them from tabulated data for the integral orders and from such tabulated orders as $\nu = 1/2,\ 1/3,\ 1/4$. However, the application of these formulae to a problem of this sort is prohibitive.

Fortunately, the Bessel functions with fractional order behave similarly to those with integral order--the transition is a smooth one. Thus in the region of low ka and low ν, the propagation may be expected to be very similar to that seen in the disk case, always assuming similar types of modes. As the frequency is increased, we might then expect that the resultant ω-β curve would approach that for the open helicoid, rather than the cutoff of the disk guides. This may be though of as being caused by having now allowed the power which was being dissipated in a standing wave in the disk-region to be channeled into a traveling wave in the helicoid region. Hence the field components can be described by forms similar to those of Eq. VII.17, of Section E.2. However, because we now expect a maximum rather than zero field at the inner radius $r = a$, the limiting curve is given by

$$J_\nu(kb)\, J'_{-\nu}(ka) - J_{-\nu}(kb)\, J'_\nu(ka) = 0 \quad . \qquad \text{(VII.39)}$$

Hennoch gives the k-ν plot for this case, having used three harmonics in the free-space region. The asymptotic open helical wave-guide curve is of the same form as that for the closed. The conclusion is that in the low-frequency range, the helically loaded guide offers no advantage over the simpler disk structure. In higher-frequency ranges and at higher harmonics, it is possible that someone may see some feature of the k-ν curve which indicates an acceptable region of operation and which is certainly not seen in the disk case.

Power transfer and interaction impedance calculations must now be somewhat more complicated than in the disk cases, since power transfer may be in both regions. The partial power transfer in the free-space region may be calculated just as in the preceding section. That in the groove region is given by

$$P_{groove} = \frac{d}{2}\ \mathrm{Re} \int_a^b (E_z \times H_r^*)\, dr \quad . \qquad \text{(VII.40)}$$

Using both of these forms, Hennoch has also plotted the coupling factor for the helicoid. As was to be expected by the preceding arguments, the behavior for small arguments is nearly the same as for the disk structures. In order to achieve large coupling factors at large ka, a small groove depth is indicated. For small ka, the coupling factor is independent of groove depth, but has the same dependence on the free-space geometry as indicated in Eq. VII.37 for the disk structures. The differences in the impedance can be seen only for larger ka, and this may be thought of as being caused by the increased power flow in the groove for this frequency range.

H. Modifications, Conclusions

As for the helix, a bifilar helicoid structure operating in an "even" mode may be employed to extend the frequency range. The reason for this is that now

$$\beta_n = \frac{2\pi}{D}(\nu + 2n) \quad , \qquad \text{(VII.41)}$$

so that the first zero appears at $\nu = 2$, rather than at 1, for $n = -1$. The difficulty is of course in the suppression of the odd mode, which may prove as troublesome here as it does in bifilar helices. In fact, an unstrapped bifilar helix makes an excellent structure for a backward-wave oscillator.

Another modification is the "quasi-helical" guide proposed by Valtersson[4] and discussed by Hennoch[6]. This is a disk structure in which each disk has a radial metal ridge and slot extending between radial disk boundaries. The disks would be so arranged as to simulate the helicoid structure by means of the ridges and slots. The effect is to cause increased coupling between disks over that of the central hole coupling case. The experimental results from this structure did indeed seem to indicate circumferential propagation in the disk region, which correlated well with the limiting curve defined by Eq. VII.39.

A final form which does not fit into the above analyses is given in several recent quarterly reports from Stanford[5]. Their helicoid is similar to those under discussion, but without a center conductor, and with ridges extending longitudinally from the inner radius towards each other to form a narrow gap between ridges. The T-shaped vanes thus support a wave which is said to propagate longitudinally with a velocity given by

$$\frac{v}{c} = \sin\left(\tan^{-1}\frac{D}{2\pi r}\right) \quad . \tag{VII.42}$$

Since it has been found that the TM modes, which have been assumed to exist, never show this behavior, another form of wave propagation is sought to explain this form of velocity. This form is that seen in the helix the slowing down is achieved only by virtue of the length of circumferential path followed. Needless to say, this is a highly desirable characteristic since it is not independent of frequency and may be easily designed with good tolerance for any given velocity, while not even requiring a center rod. If this is truly the manner of propagation, then the mode must be a helix-type mode, with little energy near the axis and little in the helicoid groove region. Most certainly, a good deal of energy in the groove region would not allow angular propagation to be determined by the radius of the inner cylindrical wall alone.

In conclusion, this analysis of the helicoid has shown several methods of attack on simple slow-wave structure geometries. The exact field theory approach to several different cylindrical (including helical) problems has been given in sufficient completeness to serve as design criterion for cylindrical structures. As to relative merits of the various structures analyzed, the following points might be stressed.

The enclosed helicoid of Section E is far too dispersive to serve as a satisfactory traveling-wave tube structure. The helically loaded guides having fields similar to those of the disk-loaded guides have been shown to have similar properties in the low-frequency range. The properties are somewhat different for higher frequencies, as shown in Section G. Finally, other types of helical wave may exist, supported by various types of helical structures. Their analysis is not given, but

if the energy transfer is essentially that of helically wrapped strip lines, then analysis on the basis of developed structures should be quite satisfactory. Another area of future investigation might be attempting to find suitable methods for further slowing the helical wave down in the groove region in order to achieve a lower phase velocity than is currently available.

VIII. UHF CRESTATRON

(J. W. Ward)

A. Introduction

The purpose of this investigation was to design and build a high-powered uhf Crestatron having a power output of 5-10 kw (pulsed) in the 300-900-mc frequency range. Specifically, 10 db gain and a saturation efficiency of at least 25 percent were target goals for this tube. In order to achieve this high efficiency a high-perveance hollow-beam gun was used. This report describes the final electrical and mechanical design and initial experimental results on the three tubes which have been built. These tubes are identical except for minor differences in supporting the electron gun electrodes. Complete evaluation of this tube, including saturation measurements, awaits the arrival of a suitable driver.

B. Principles of Crestatron Operation

The Crestatron recently invented by Rowe[1] is a forward-wave amplifier which, like the backward-wave oscillator, operates on a

1. Rowe, J. E., "Theory of the Crestatron: A Forward-Wave Amplifier", Tech. Rpt. No. 27, Electron Tube Laboratory, The University of Michigan; September, 1958.

beating-wave principle. However, there is an important difference between the operation of these two devices. Since the Crestatron uses a forward traveling wave the density modulation in the stream and the circuit field producing this modulation travel in the same direction, resulting in an inherently more efficient type of operation. Typical efficiencies are 25-30 percent compared to 3-5 percent for BWO's and BWA's. The two beating waves in the Crestatron are the slow space-charge wave and the circuit wave; the fast wave is not excited. At the input these two waves are 180 degrees out of phase and naturally must add up to the applied signal. Since these two waves have different propagation constants, there is a point farther down the tube where they add in phase, typically at a length where CN = 0.30 to 0.50. The gain is primarily a function of Δb, where

$$\Delta b \triangleq b - b_{x_1=0}$$

and

$$b = \frac{1}{C}\left(\frac{u_o}{v_p} - 1\right) \qquad \text{(VIII.1)}$$

As Δb approaches zero the two waves have nearly the same propagation constant, so a compromise must be made between length and gain since the maximum gain increases as Δb approaches zero, while the length to achieve this high gain increases. Typical values of Δb for 10 db gain at CN = 0.50 are around 0.20. As in the traveling-wave amplifier it is desirable to have high C and low QC for high-efficiency operation.

C. General Design Considerations

A brief summary of the approach taken in designing helix-type Crestatrons follows. No claim is made that this is the best or fastest method, but it is much faster than some other approaches tried. The main problem is to keep the relative injection velocity b constant over the frequency range of operation. The quantity Δb, which determines the maximum Crestatron gain, is then nearly constant because $b_{x_1=0}$ is a slowly varying function of C and QC. To keep b constant requires both low dispersion and low impedance variation across the frequency band. For wide bandwidths these two requirements necessitate having a helix with a fairly close surrounding metal shield, usually with a shield-to-helix radii ratio between 1.4 and 2.0.

The first step in the design procedure is to choose a beam power from the desired r-f power output and the expected efficiency. For most Crestatrons with hollow beams, 25 percent is a conservative efficiency to use in this step. Next, choose a low-frequency value of ka which, together with the frequency range, should determine an inside circuit diameter consistent with current density limitations. From the beam voltage and the fact that $1+Cb \approx 1.5$ for most Crestatrons with hollow beams, the low-frequency γa can be calculated using

$$\frac{u_o}{v_p} = 1+Cb = \frac{\sqrt{V_o}}{506}\,\frac{\gamma a}{ka} \quad . \qquad \text{(VIII.2)}$$

If this value of γa is in the range 0.5 to 1.0, the approximate v_p/c required can be calculated and a shield-to-helix radii ratio selected in the range of 1.4-2.0. Now make a guess at the probable DLF, preferably from a tube already constructed in this frequency range which uses similar geometry and materials in supporting the r-f circuit. A trial helix design can be made by using

$$\frac{v_p}{c} \cong \frac{1}{(\cot \psi)_{sheath}} = \frac{DLF}{(\cot \psi)_{actual}} \quad , \qquad \text{(VIII.3)}$$

or

$$p \cong \frac{2\pi a}{DLF}\left(\frac{ka}{\gamma a}\right) \quad . \qquad \text{(VIII.4)}$$

Now v_p/c and 1+Cb vs. frequency can be calculated for this helix design. From a chosen beam geometry C can be calculated and hence b is determined; b should be around 2.5 to 3.0, depending on the value of QC found from

$$QC \triangleq \frac{1}{4C^2}\left(\frac{\frac{\omega_q}{\omega}}{1 + \frac{\omega_q}{\omega}}\right)^2 \quad , \qquad \text{(VIII.5)}$$

where

$$\frac{\omega_q}{\omega} = \left(\frac{\omega_q}{\omega_p}\right)\left(\frac{\omega_p}{\omega}\right) = R\,\frac{\omega_p}{\omega}$$

and

$$\omega_p = 1.83\text{x}10^8\left(\frac{J_o}{V_o}\right)^{1/2} \quad .$$

The plasma frequency reduction factor R can be found from Branch and Mihran[2], who have presented graphs of R vs. γa for different beam geometries.

As mentioned previously, Crestatron gain and efficiency depend primarily upon having the proper injection velocity which results in Δb being slightly positive. Figure VIII.1 shows b as a function of C

---

2. Branch, G., Mihran T., "Plasma Frequency Reduction Factors in Electron Beams", Trans. PGED-IRE, vol. ED-2, No. 2, pp. 3-11; April, 1955.

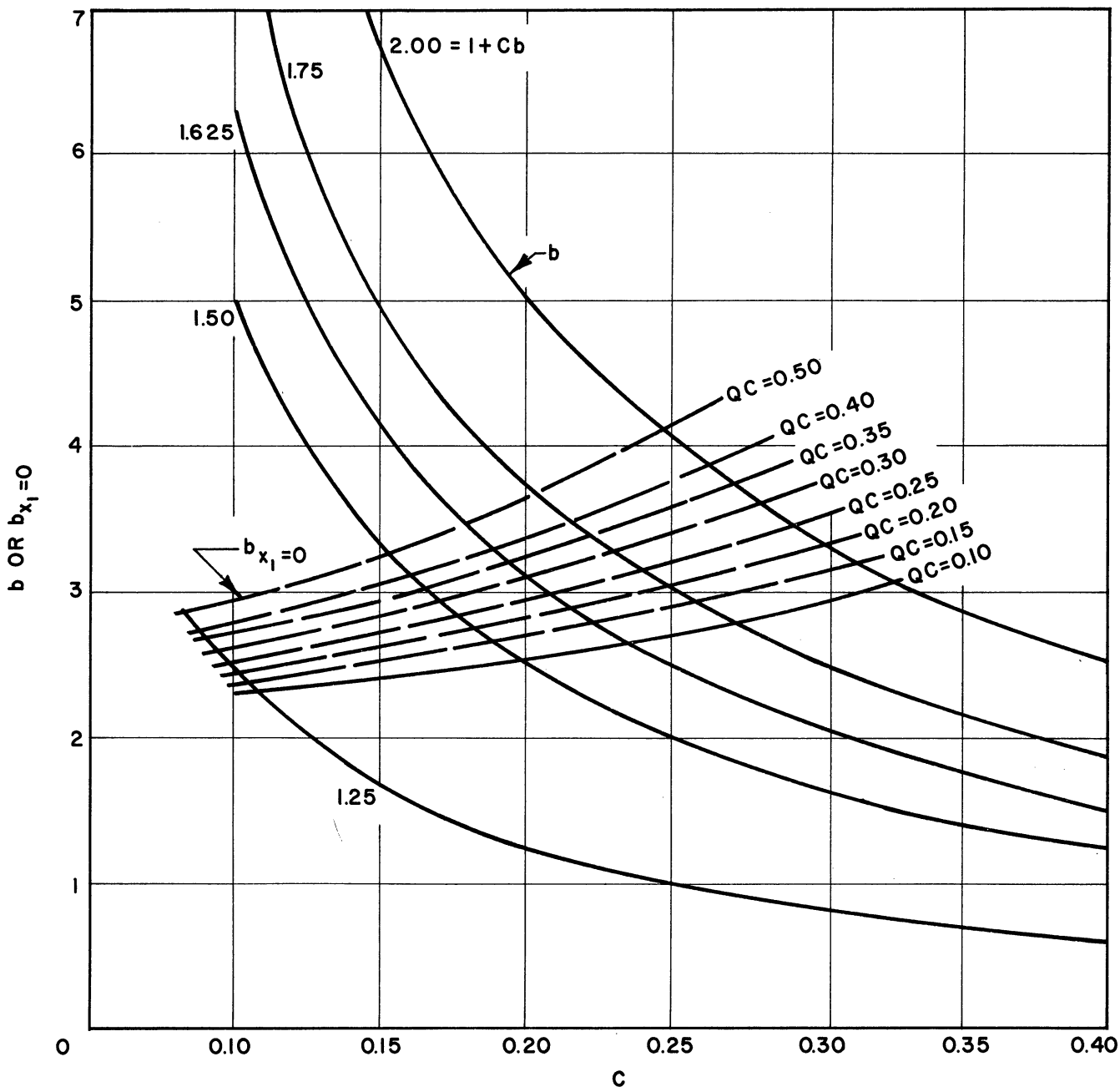

FIG. VIII.1 $b_{x_1=0}$ vs. C WITH QC AS A PARAMETER AND b vs. C WITH 1 + Cb AS A PARAMETER.

for different values of u_o/v_p and also $b_{x_1=0}$ as a function of C with QC as the parameter. This graph greatly facilitates finding Δb for a given u_o/v_p, C and QC. If Δb is not in the range of 0.1 to 0.30, either the voltage or helix pitch should be adjusted to bring Δb into the aforementioned range. Once Δb, C and QC as a function of frequency are known, maximum Crestatron gain can be found using Reference 1. A length can be calculated by making CN $\approx$ 0.35 at the low-frequency end. Efficiency and gain vs. frequency can then be calculated for different drive levels.

D. Helix Design and Cold Test Measurements

The circuit used in this tube is a single-filar molybdenum helix supported in a precision-bore Nonex envelope by three sapphire rods notched at each helix turn. This support insures good alignment of each turn in addition to providing mechanical rigidity of the structure. Some difficulty was experienced with early helices which were wound on a stainless steel mandrel. When the helix was fired the difference in expansion between the molybdenum and stainless steel caused a permanent spring-out, making it difficult to load the helix into the glass tubing without breaking the sapphire rods which were required to hold the helix in compression because of the spring-out. This problem was eliminated when a molybdenum mandrel was used.

The electrical design of the helix follows the method outlined in Section C. Table VIII.1 summarizes the final design of the helix.

TABLE VIII.1

UHF Helix Parameters

Pitch:	0.250 inch
cot ψ:	9.45
Mean diameter:	0.752 inch
Wire diameter:	0.100 inch
Material:	molybdenum
Helix supports:	0.080 inch notched sapphire rods
ka at 300 mc:	0.06

The measured phase velocity and DLF for this helix design are shown in Fig. VIII.2 for an unshielded helix and for a shield-to-helix radii ratio of 1.5. It is seen that the shield greatly reduces the dispersion from the unshielded case. Of course the penalty is essentially an increase in tube length because C is lowered approximately 25 percent at 300 mc and approximately 10 percent at 900 mc. Notice that there is a gradual increase in phase velocity from 300 to 900 mc. This negative dispersion behavior[3] results from the dielectric surroundings producing an effective shunt capacity per unit length which decreases with increasing frequency. At low frequencies the electric field extends farther into the dielectric and effectively increases the energy storage and reduces the helix impedance.

An interesting fact useful in comparing the shielded and unshielded sheath helix is shown in Fig. VIII.3, where the ratio of the phase-to-group velocities (v_p/v_g) is plotted versus γa. It is seen

3. Jones, E. M. T., "A Negative Dispersion Helix Structure", Electron Research Laboratory, Tech. Rpt. No. 27, p. 3, Stanford University; August 7, 1950.

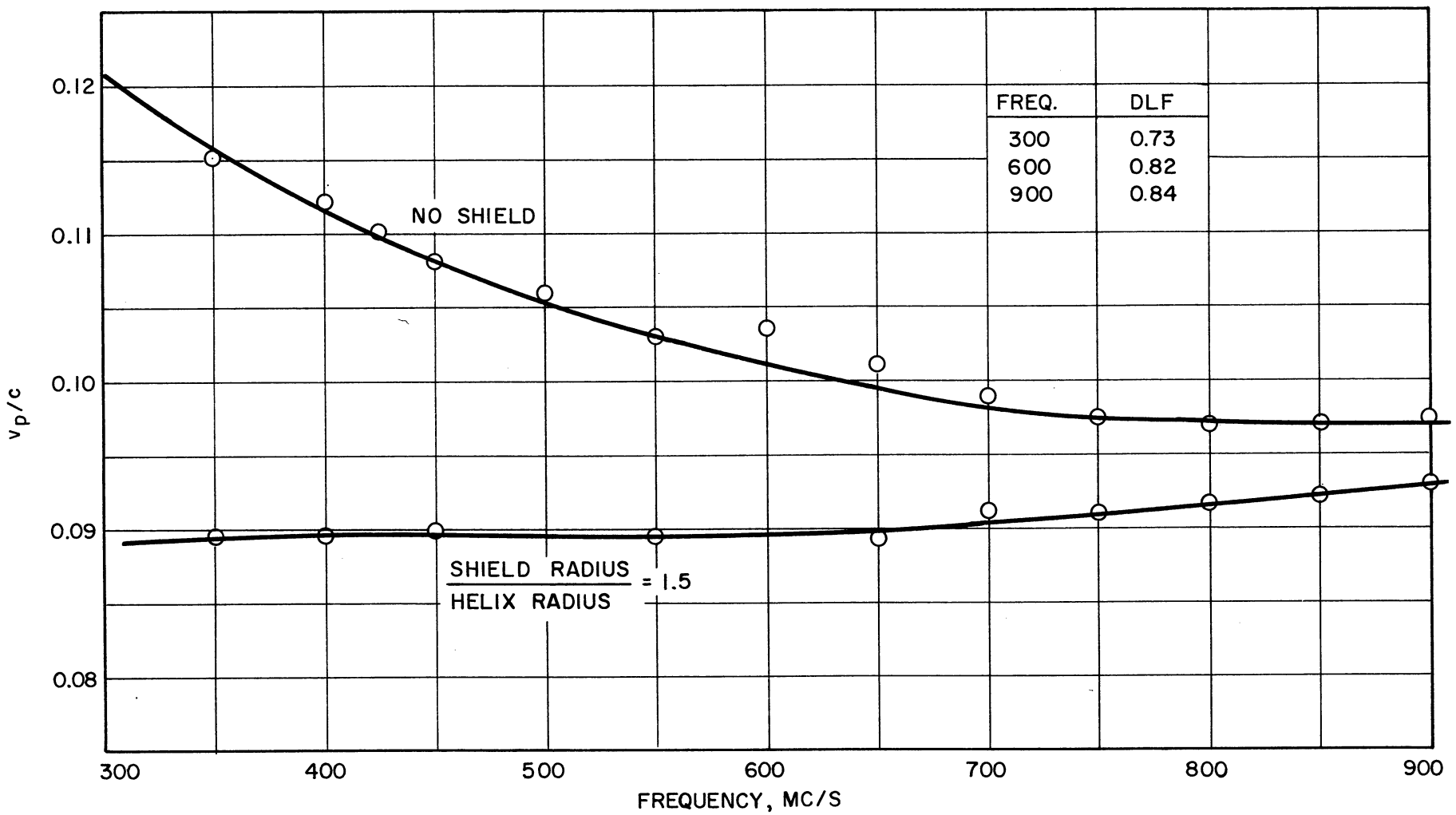

FIG. VIII.2 MEASURED PHASE VELOCITY vs. FREQUENCY.

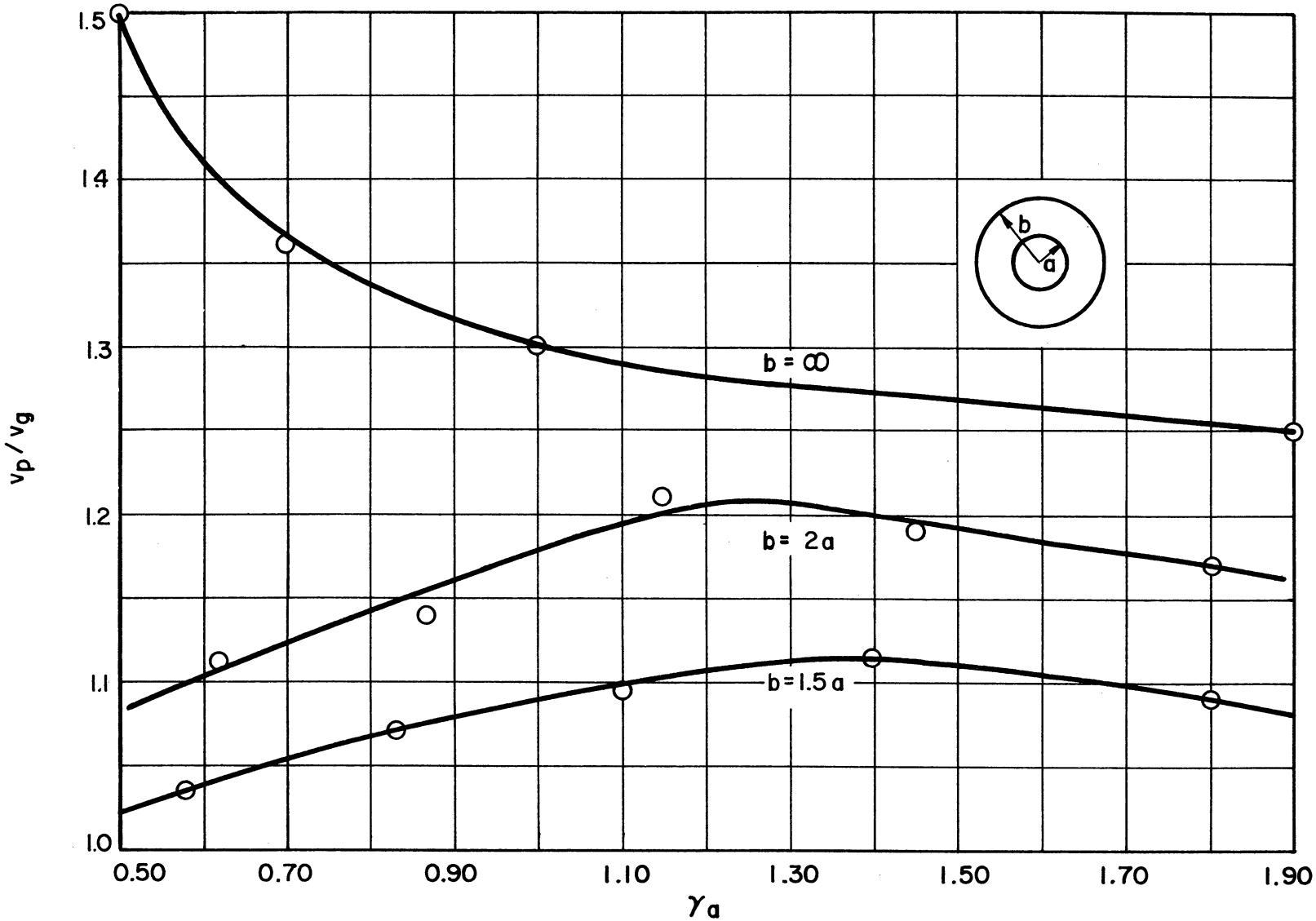

FIG. VIII.3 CALCULATED RATIO OF PHASE TO GROUP VELOCITY FOR SHEATH HELIX WITH EXTERNAL SHIELD.

that for an unshielded helix a γa lower than approximately 0.80 results in a rapid increase in dispersion because of the rapid rise in v_p/v_g at this point. Notice that the reverse is true for the shielded helix. Of course this property could not be used for high-power tubes at higher frequencies than perhaps S-band because the hole size and beam-power considerations would not allow the low γa permitted by dispersion considerations. However, for most uhf tubes, current density limitations are not present and for many cases the increased bandwidth resulting from negligible dispersion will compensate for the reduction in C and the increase in length, especially for low-gain tubes such as Crestatrons.

It is recalled that the phase velocity v_p and the group velocity v_g are given by

$$v_p = \frac{ka}{\gamma a} = \frac{\omega}{\beta} \quad , \qquad \text{(VIII.6)}$$

and

$$v_g = \frac{\partial\omega}{\partial\beta} \quad . \qquad \text{(VIII.7)}$$

Ayers[4] has arrived at the frequency bandwidth corresponding to a change in $b(\Delta b)$, which is as follows

$$\frac{\Delta\omega}{\omega} = \frac{v_p}{u_o} \frac{C\Delta b}{\left(\frac{v_p}{v_g} - 1\right)} \qquad \text{(for constant C)} \quad . \qquad \text{(VIII.8)}$$

For the Crestatron[5] the exact change in gain due to a change in b is a complicated function of C, QC, b and CN. However, a good guess

4. Ayers, W. R., "High Power Applications of the Connected Ring Structure in Traveling Tubes", Microwave Laboratory, Rpt. No. 554, p. 126, Stanford University; December, 1958.

5. Rowe, J. E., op. cit., Reference 1.

at the maximum bandwidth can be made using the above formula. For most Crestatron designs the gain has dropped about 3 db for $\Delta b \cong 0.60$. Usually $u_o/v_p \cong 1.5$ for high-C tubes. From Fig. VIII.3 $v_p/v_g \approx 1.10$ for a shield-to-helix radii ratio of 1.5. Thus, for C = 0.25

$$\frac{\Delta\omega}{\omega} \cong \frac{1}{1.5} \frac{(0.25)(0.60)}{[1.10-1.0]} \approx 1 \quad \text{or a 3:1 bandwidth} \quad . \qquad \text{(VIII.9)}$$

E. Helix-Impedance Measurement

Experimental measurements using a method described by Lagerstrom[6] where a dielectric rod perturbs mainly the TE fields of the helix were used to measure the helix impedance. A 0.100-inch-diameter sapphire rod was inserted on the axis and the resulting change in phase was noted by observing the shift in the position of the minimum on a slotted line in one arm of the phase bridge. The change in the position of a minimum Δx when using a dielectric rod of radius b with dielectric constant ϵ' is related to the impedance on the axis K(r=0) as follows

$$K(r=0) = \frac{480\left(\frac{\Delta x}{D}\right)}{(\gamma b)(\epsilon'-1)p_e} \quad \text{(ohms)} \quad ,$$

where p_e is a shape factor to account for the finite size of the perturbing rod. This impedance was transformed to the mean beam radius $r=r_o$ using

$$K(r=r_o) = K(r=0)\, I_o^2(\gamma r_o) \quad . \qquad \text{(VIII.10)}$$

The above assumes the beam is thin enough so that the field does not vary across it. This is nearly true for the hollow beam used in this

6. Lagerstrom, R. P., "Interaction-Impedance Measurements by Perturbation of Traveling Waves", Stanford Electronics Laboratory, Tech. Rpt. No. 7; February 11, 1957.

tube, which has a thickness of 0.030 inch compared to a mean diameter of 0.507 inch. It was found nonreproducible, confusing results were obtained at frequencies where the match VSWR was worse than approximately 1.15. Because of this no experimental impedance measurements are presented for the shielded helix for which the VSWR averaged around 1.50. Figure VIII.4 shows both the experimentally measured points and the sheath helix impedance calculated using the measured DLF. Good agreement between the theoretical and measured values was obtained.

F. Hollow-Beam Gun

A schematic drawing of the hollow-beam guns used in tubes No. 1, 2 and 3 is shown in Fig. VIII.5. The center anode electrode in these tubes was held by a spoke spot-welded to the inside of the outer anode below the cathode assembly. Because of assembly difficulties with this method, tube No. 3 will have the center electrode held by three 0.005-inch-thick molybdenum tabs going directly to the outer anode. Figure VIII.6 shows a picture of the latter gun, which is identical to the previous guns except for the different support method for the center anode.

This gun is a conventional immersed, rectilinear-flow Pierce gun which was designed to operate with the focus electrodes at cathode potential. The cathode-anode distance was chosen to give a microperveance per square of 0.13 and a total microperveance of 5.9. The cathode is a Phillips type B with a mean radius of 0.507 inch and emitter thickness of 0.025 inch. The electrodes are molybdenum cylinders held by supports attached to a Vicor disk which can be seen in Fig. VIII.6.

The diode characteristics of the gun are shown in Fig. VIII.7. A current of 3 amperes corresponds to a current density of $\approx$ 10 amps/cm^2.

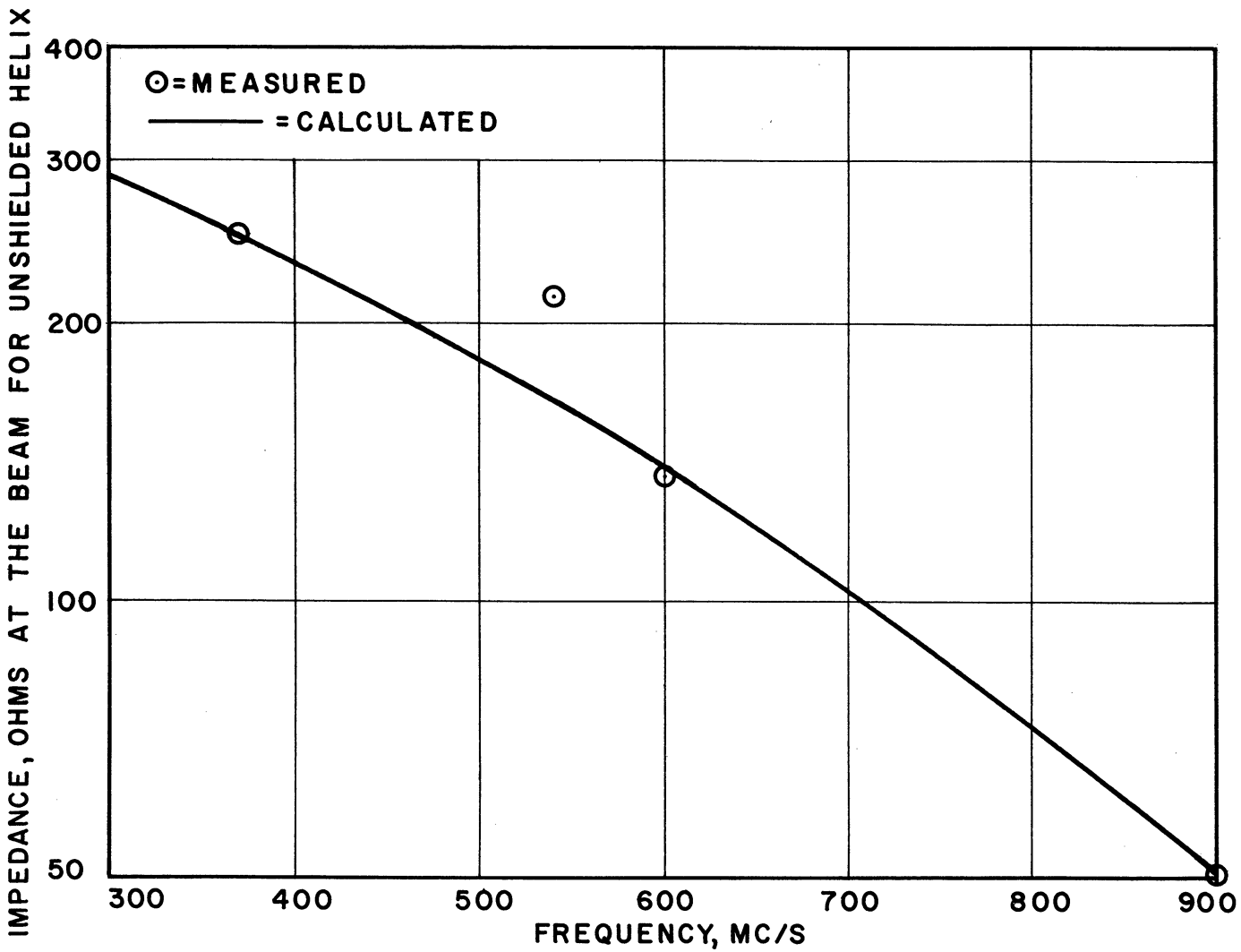

FIG. VIII.4 MEASURED AND CALCULATED IMPEDANCE, $E_z^2/2\beta^2P$, FOR UNSHIELDED HELIX.

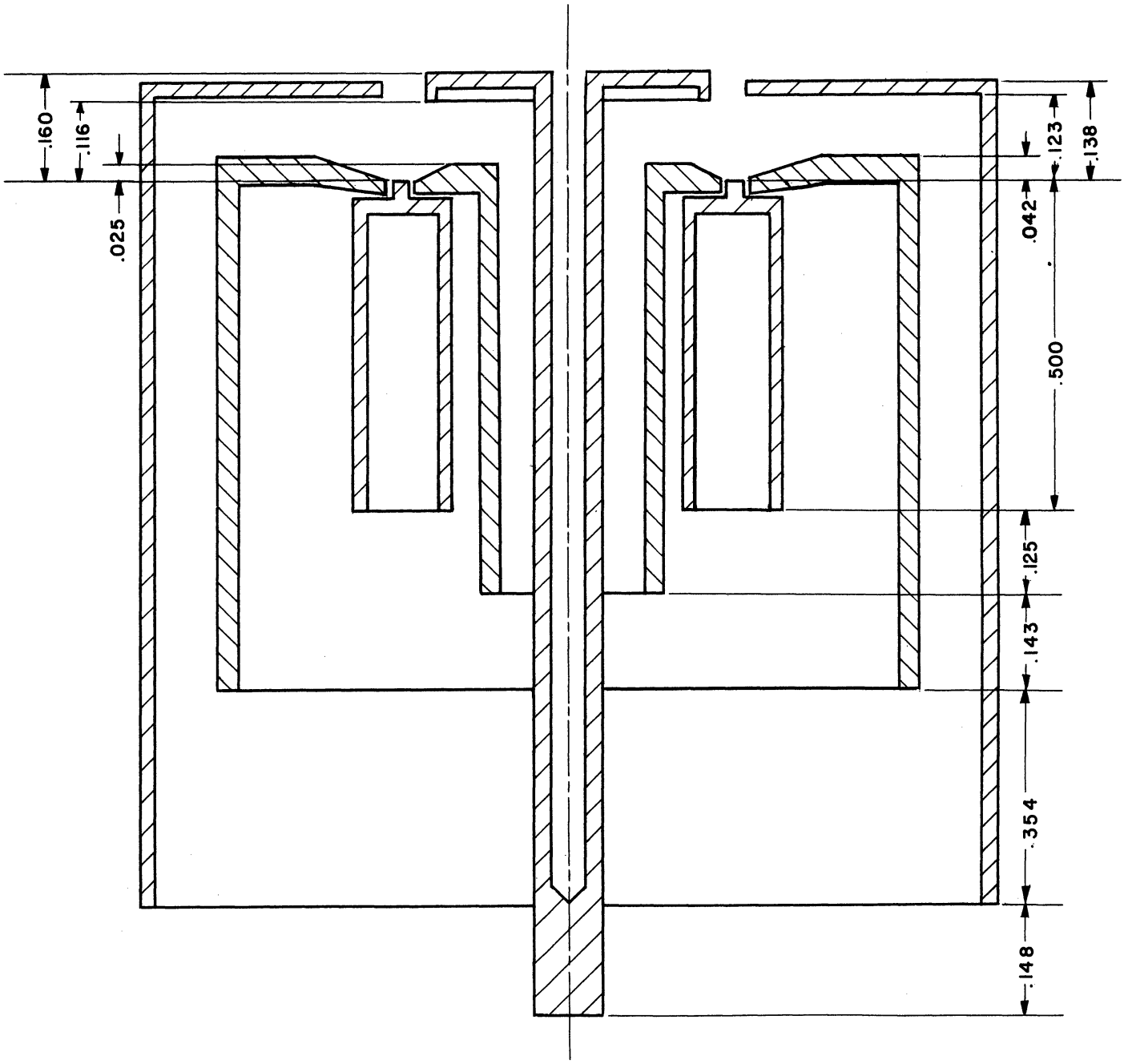

FIG. VIII.5 SCHEMATIC DRAWING OF A HOLLOW-BEAM ELECTRON GUN.

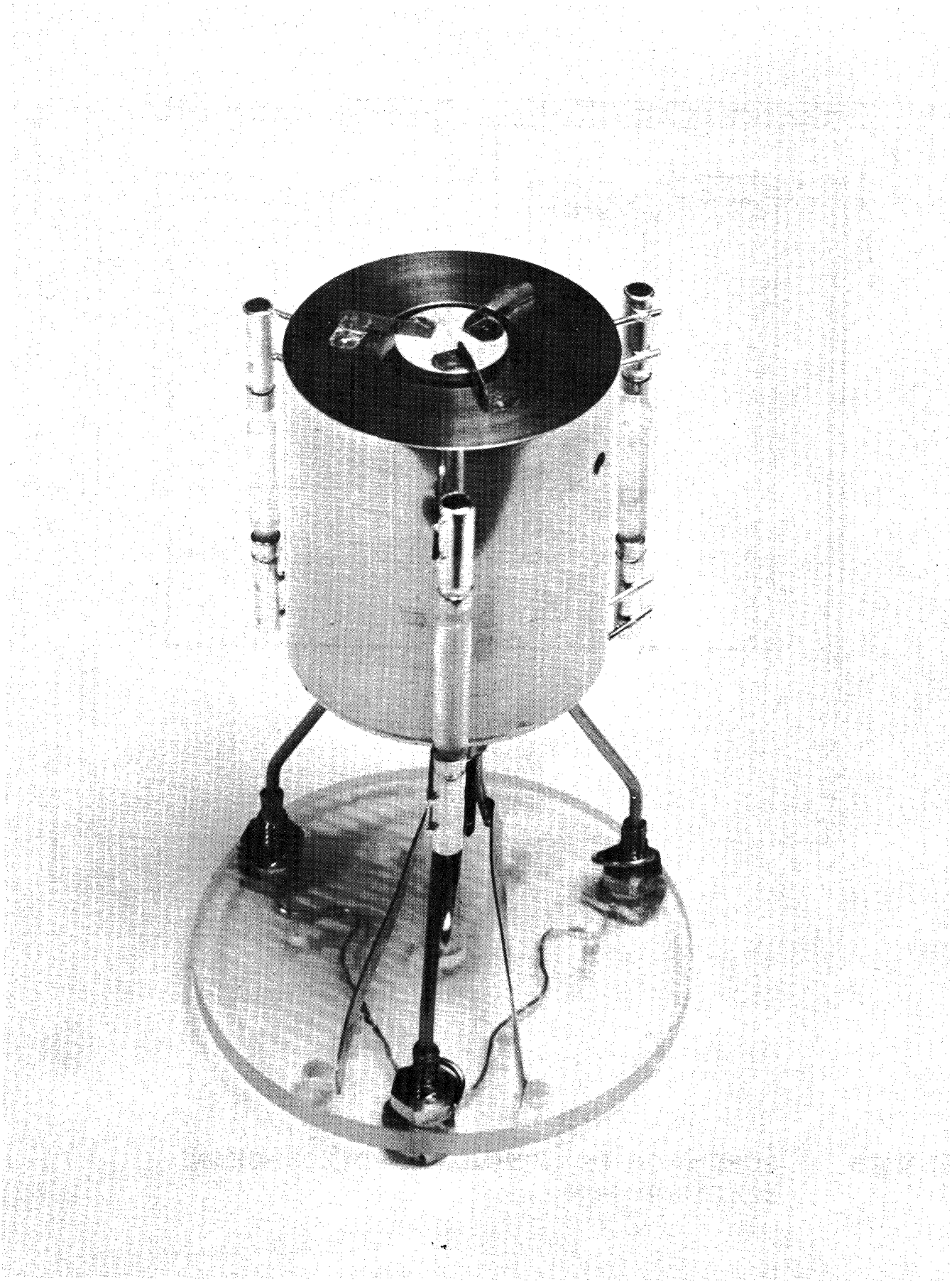

FIG. VIII.6 UHF HOLLOW-BEAM GUN.

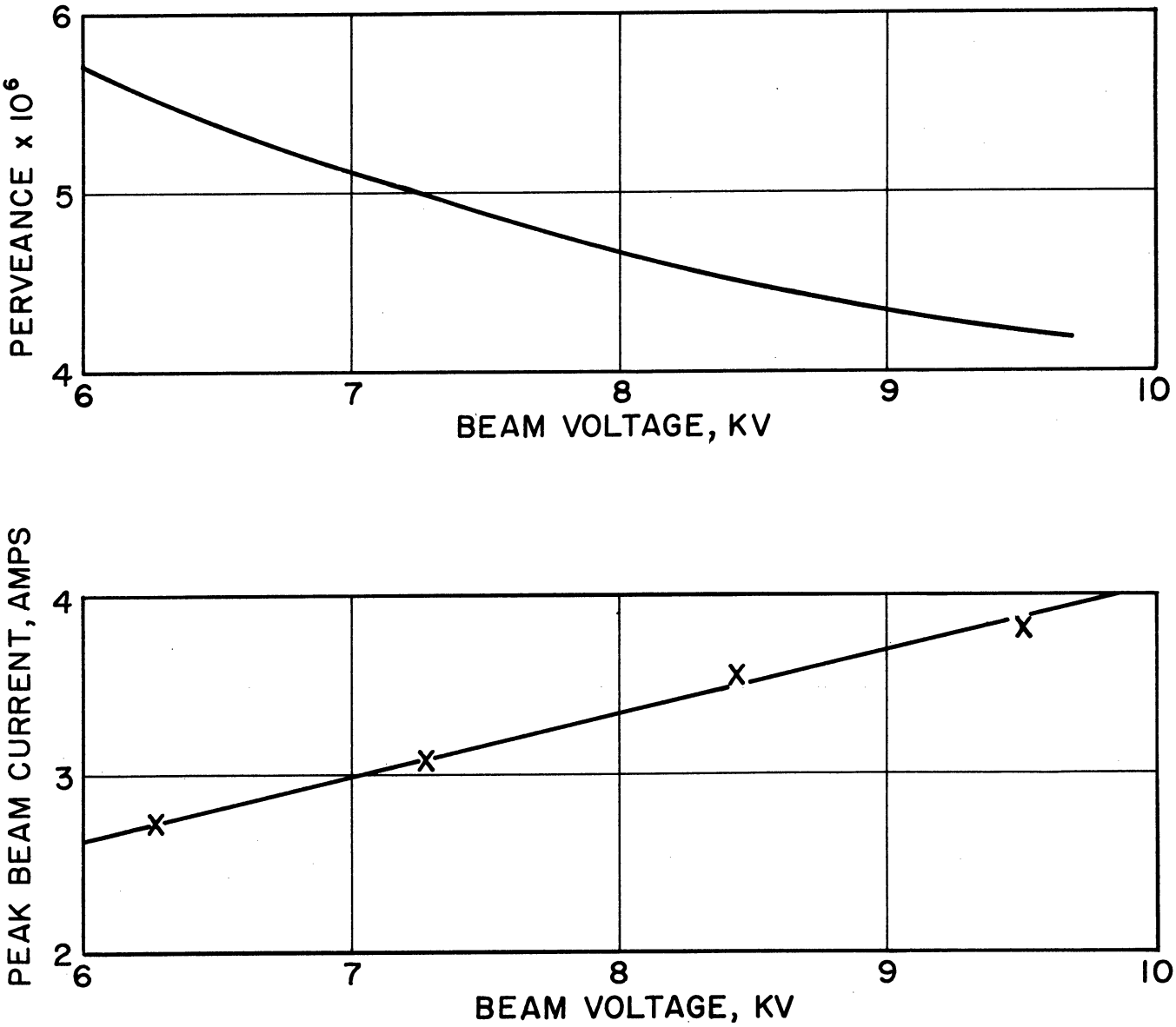

FIG. VIII.7 PERVEANCE AND BEAM CURRENT vs. BEAM VOLTAGE FOR UHF CRESTATRON HOLLOW-BEAM GUN.

The perveance drops from 6.5 micropervs to 4 micropervs as the voltage is raised from 6 to 10 kv. No evidence of voltage breakdown has been noted at voltages up to 11 kv.

G. Tube Design

The electrical parameters resulting from the design procedure outlined in Section C using the helix and beam described previously are shown in Table VIII.2 below.

TABLE VIII.2

Summary of Electrical Design Parameters

V_o = 6 kv μp_o = 5.9 a = 0.376 inch

I_o = 3.1 amps μp = 0.11 r_o = 0.254 inch

u_o/c = 0.153 J_o = 10 amps/cm^2 $2\pi r_o\Delta$ = 0.308 cm^2

Freq. (mcs)	300	400	500	600	700	800	900
ka	0.06	0.08	0.10	0.12	0.14	0.16	0.18
DLF	0.726	0.756	0.788	0.82	0.82	0.82	0.84
v_p/c	0.089	0.895	0.090	0.090	0.0905	0.0915	0.0930
γa	0.675	0.895	1.11	1.335	1.55	1.75	1.94
kr_o	0.0405	0.0540	0.0674	0.0809	0.0944	0.108	0.121
γr_o	0.455	0.603	0.749	0.900	1.05	1.18	1.31
$F=F_1F_2$	0.43	0.44	0.49	0.53	0.52	0.51	0.51
K(ohms)	260	182	147	112	81.1	60.8	46.5
$\gamma\Delta$	0.054	0.0716	0.089	0.107	0.124	0.140	0.155
R	0.115	0.14	0.16	0.18	0.195	0.21	0.225
ω_q/ω	0.430	0.392	0.358	0.337	0.320	0.294	0.285
C	0.239	0.228	0.218	0.214	0.191	0.183	0.179
QC	0.39	0.38	0.36	0.34	0.40	0.39	0.38
b	3.01	3.12	3.21	3.27	3.61	3.66	3.63
$b_{x_1=o}$	3.70	3.58	3.40	3.35	3.30	3.28	3.27
Δb	-0.69	-0.46	-0.19	-0.08	0.31	0.38	0.36

N(L=8 inches)	1.33	1.77	2.22	2.66	3.08	3.54	4.00
CN	0.318	0.404	0.484	0.570	0.588	0.647	0.716
Max. Gain (db)	8.2	10.8	11.2	11.8	6.5	5.5	5.0

It should be pointed out that a slight change in voltage can be used to raise and optimize the gain vs. frequency curve, as will be shown in a later section.

H. R-F Transitions

Early in the development of this project it was planned to use pin matches in which the coaxial center conductor was connected to the helix through pins passing through the glass envelope. Experiments using this method were rather disappointing. Even with a closely spaced shield surrounding the helix it appeared the helix impedance at the low-frequency end was too high to match into a 50-ohm coaxial line. For a shield-to-helix radii ratio of 1.5 the calculated helix impedance defined on a power, current basis[7] varies from approximately 200 ohms at 300 mc to 125 ohms at 900 mc. By stretching out the last two turns a fairly good match (VSWR $\leq$ 2) could be obtained from 500 to 900 mc.

Because of the marginal performance obtained with this method of coupling it was decided to try a coupled-helix transition. A series of tests was made on coupled helices with different TPI's and outer shield diameters. All units had an I.D. = 1.10 inch, which is slightly larger than the glass envelope used. They were supported by a closely fitting glass tube which slid into the brass shield (see Fig. VIII.8). The transition from coax to the coupling helix was made through an

7. Mathers, G., Kino. G., "Some Properties of a Sheath Helix with a Center Conductor or External Shield", Tech. Rpt. No. 65, Electronics Research Laboratory, Stanford University; June 17, 1953.

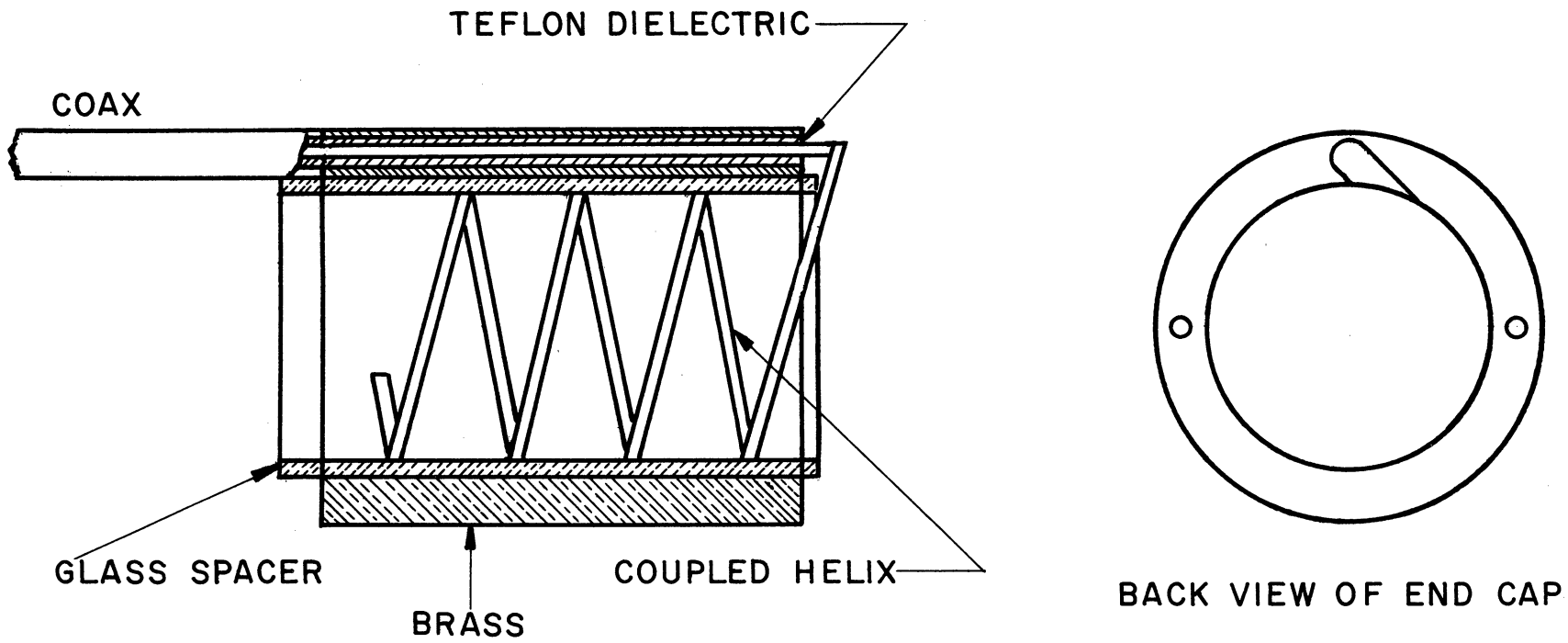

FIG. VIII. 8 UHF COUPLER.

off-center slot cut in the end cap which permitted the center conductor of the coax to be tangential to the helix at the junction where they were soldered together.

Best results were obtained with a coupler having the dimensions listed below

TABLE .VIII.3

UHF Coupler Dimensions

T.P.I.:	2.25
Inside diameter:	1.135 inch
Wire diameter:	0.080 inch
Shield diameter:	1.50 inches
Shield length:	2-3/8 inches
Turns:	3-1/2

Figure VIII.9 shows the VSWR vs. frequency for one coupler with the main helix terminated in a matched load. It is seen that this coupler has better than a 2:1 VSWR across the frequency band.

I. Experimental Results

The test setup for applying the peak voltage to this tube is shown in Fig. VIII.10. Most tests were run using a pulse length of 4 microseconds at a repetition rate of 250 pps. The beam current transmission and interception were monitored using the average current meters shown in the above figure. The peak cathode voltage was measured with a Gertsch peak reading voltmeter connected across a 100:1 vacuum capacitor divider, while the peak collector current was monitored by measuring the voltage pulse across a precision one-ohm current-viewing resister with a calibrated scope.

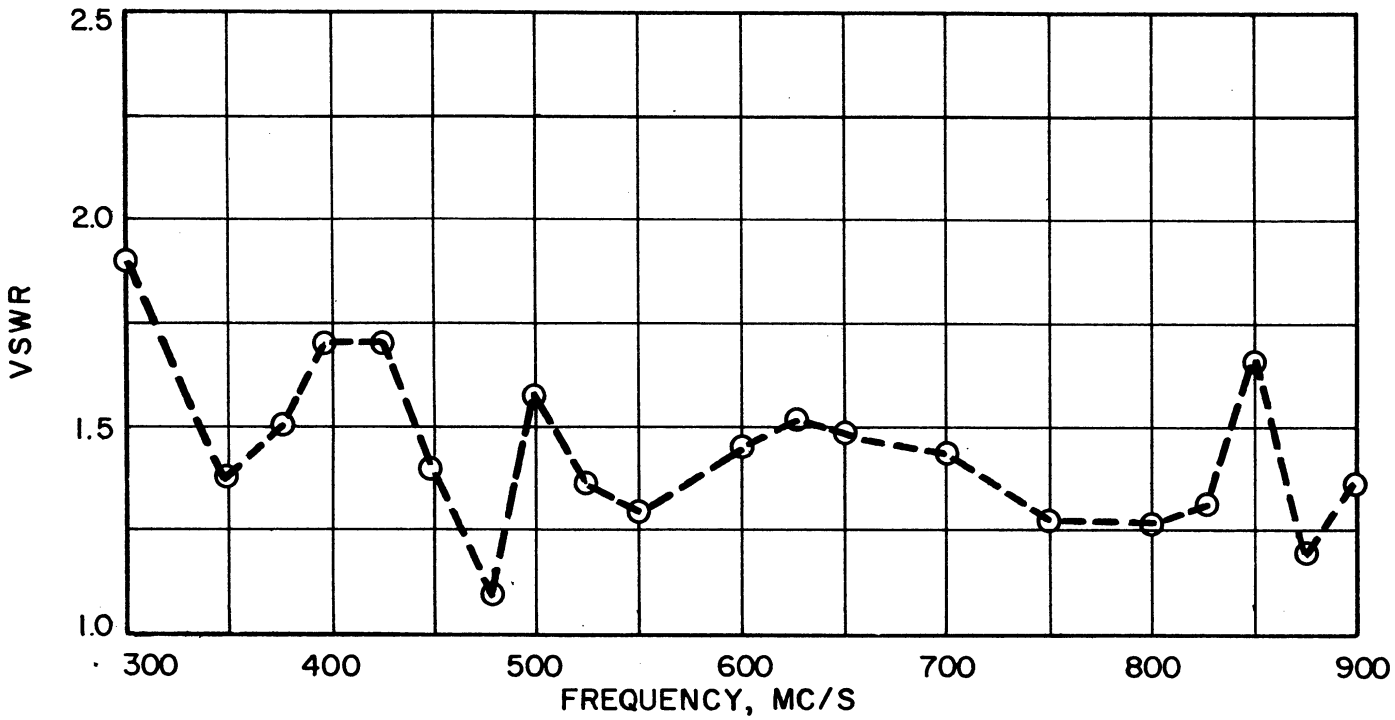

FIG. VIII.9 MEASURED VSWR WITH HELIX TERMINATED IN MATCHED LOAD.

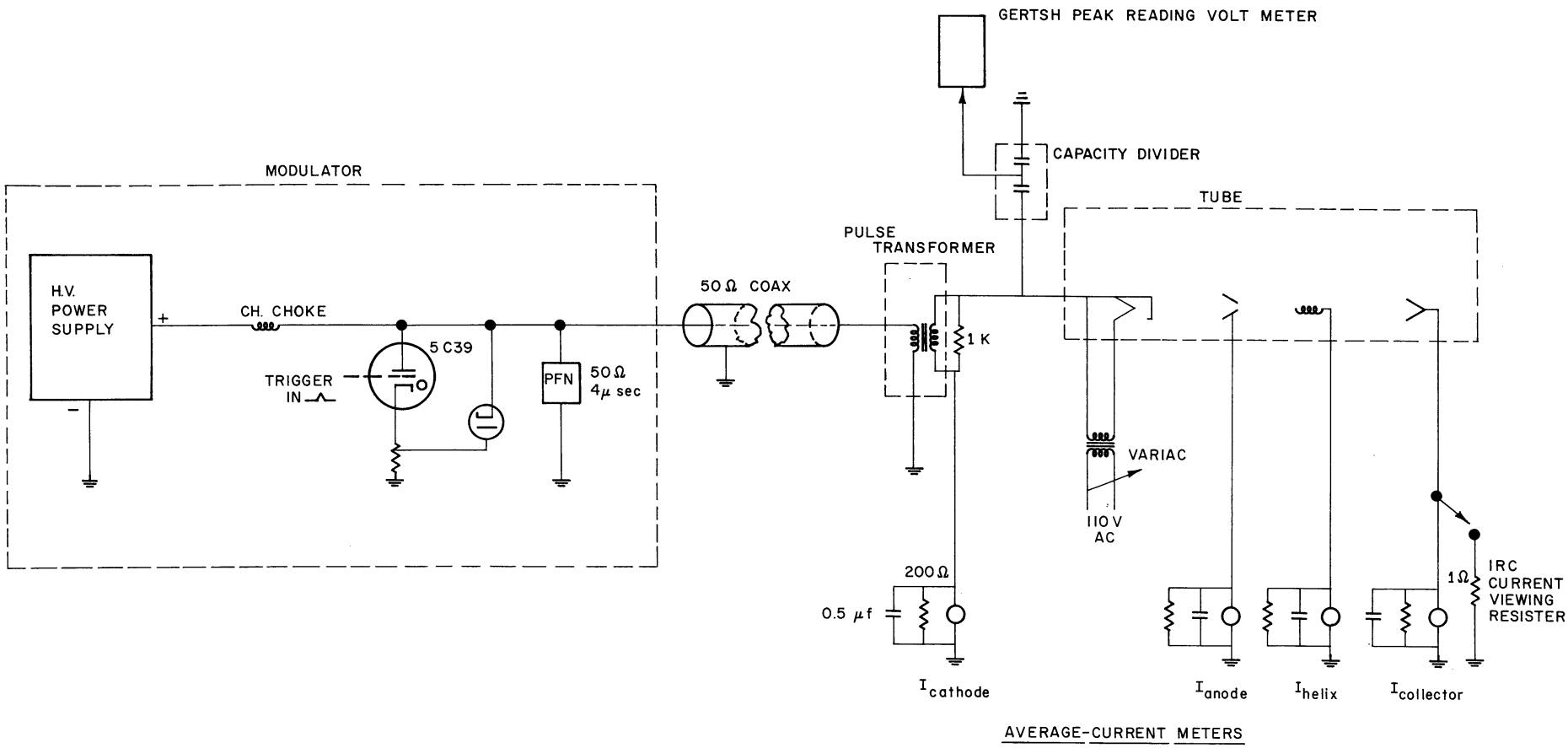

FIG. VIII. 10 EXPERIMENTAL TEST SETUP.

There have been three tubes built so far, though essentially only d-c tests have been made on the latest tube. A picture of tube No. 2 is shown in Fig. VIII.11 and the same tube placed in its coupler assembly is shown in Fig. VIII.12.

Tube No. 1 had poor transmission (≈ 50 percent) and was unstable. Strong forward-wave oscillations were observed near the band edges at 330 mc and 920 mc. A peak oscillation power of approximately 5 kw was observed at these frequencies. Subsequently the transmission became even worse. When this tube was opened up it was found that the three spotwelds holding the cathode assembly in place had failed, resulting in a badly tilted cathode.

Tube No. 2 had much better transmission (90 percent) and fairly extensive small-signal data were taken before this tube failed because of a crack developing in the envelope near the gun.

Some results are shown in Fig. VIII.13, where small-signal gain versus frequency is shown for two different voltages. This curve is for the unshielded helix. It is seen that the gain is greater than 8 db over nearly an octave bandwidth. Gain vs. voltage at a fixed frequency of 650 mc is shown in Fig. VIII.14 for both the shielded and unshielded helices. A maximum gain of 13 db was obtained at a beam voltage of 8.5 KV for the unshielded case, while 12 db was obtained for the shielded helix at a beam voltage of 6.5 KV. The square root of the ratio of these two synchronous voltages is approximately equal to the ratio of the two cold phase velocities, as might be expected.

Figure VIII.15 shows the linearity up to a power output of 1200 watts at a gain of 13 db. Further output is limited by the present AIL power oscillator, which has a maximum output of 60 watts after being

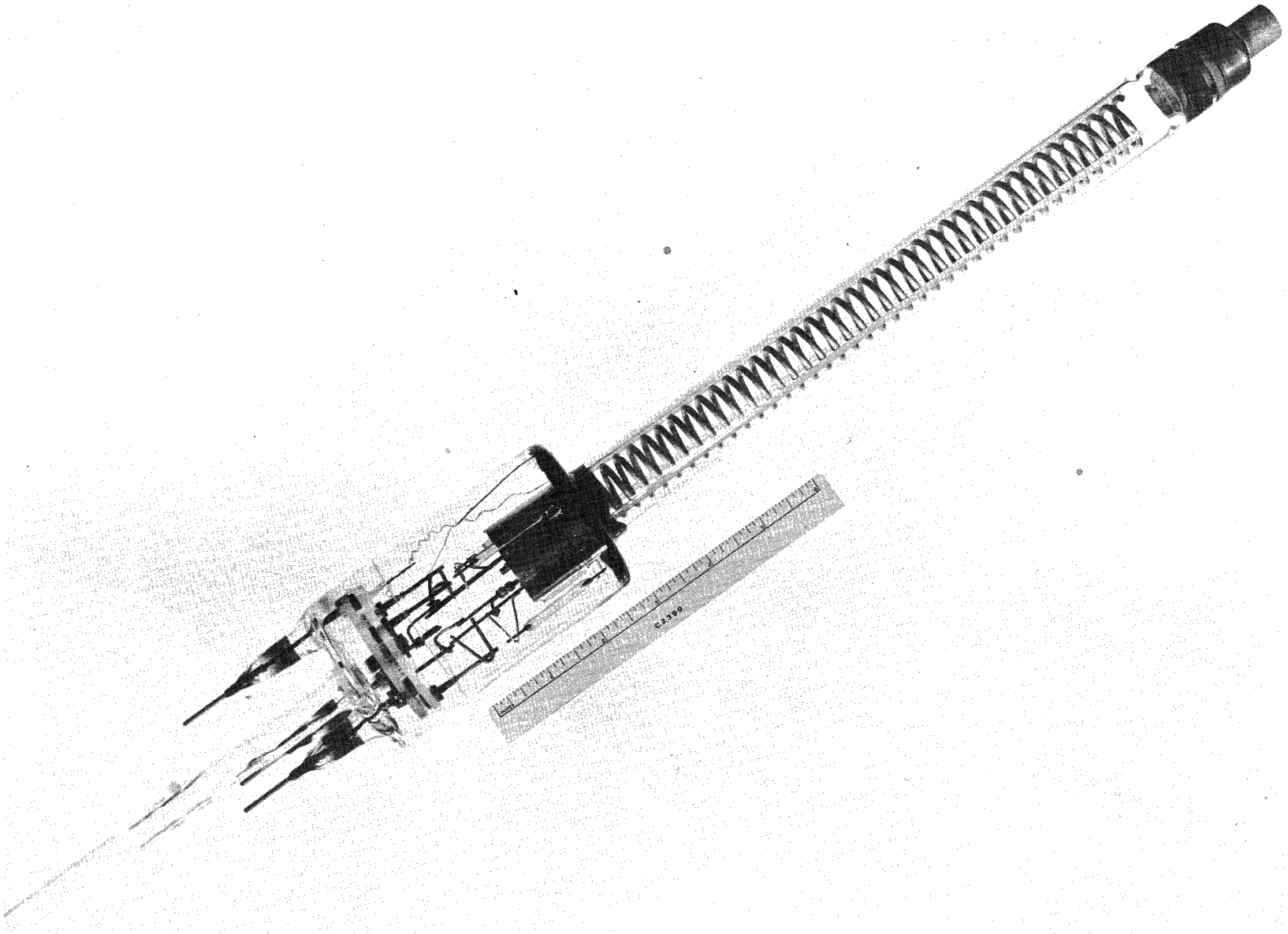

FIG. VIII.11 5-10 KW UHF CRESTATRON.

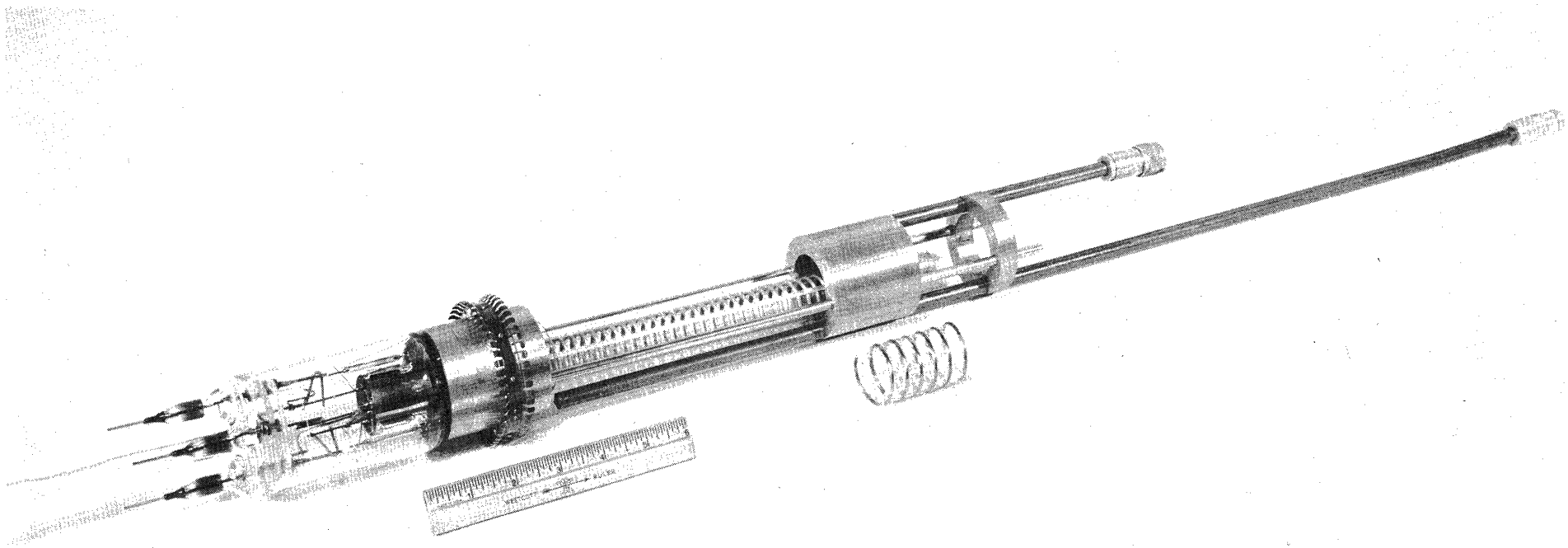

FIG. VIII. 12 UHF CRESTATRON AND COUPLED-HELIX COUPLERS.

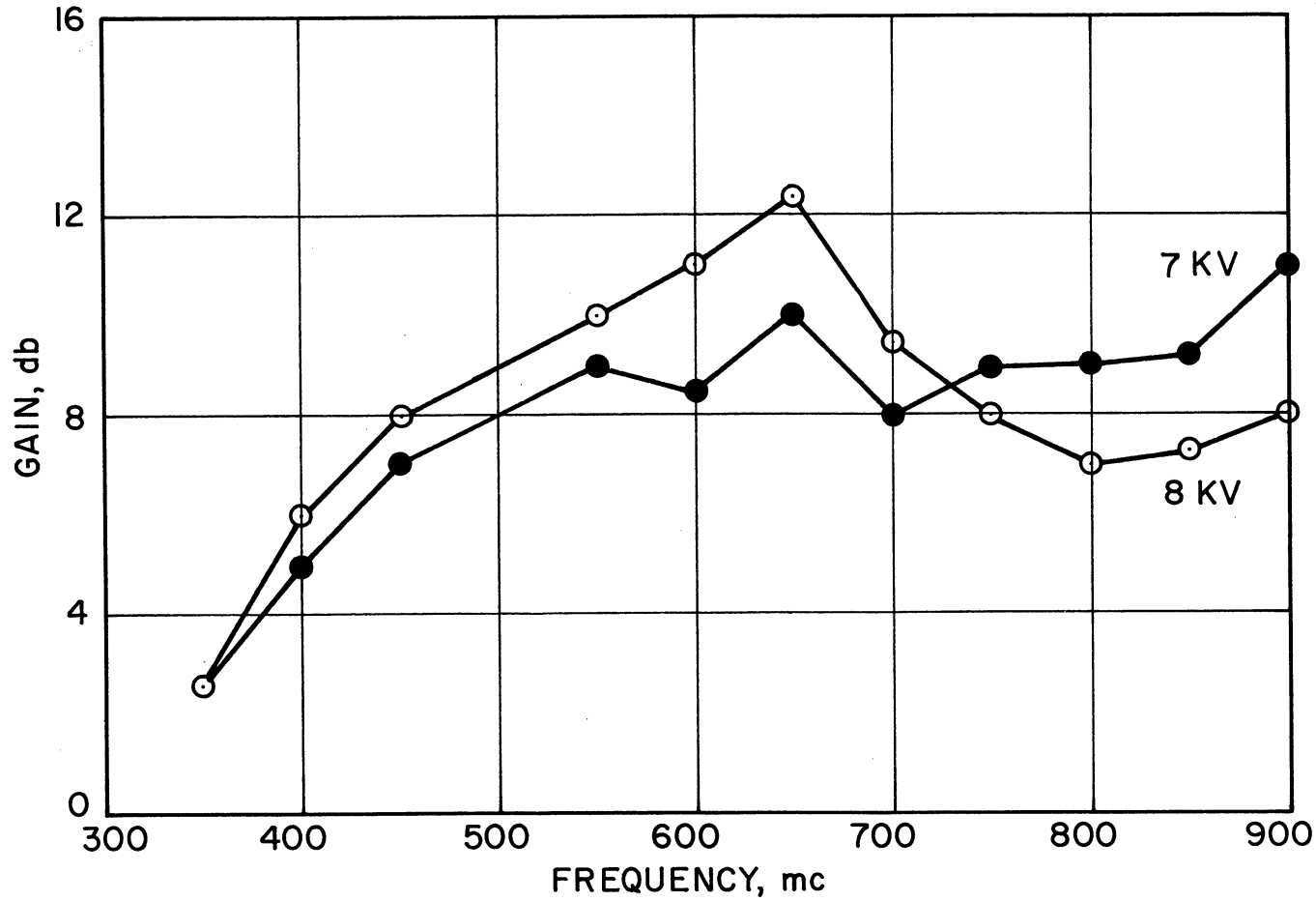

FIG. VIII.13 SMALL-SIGNAL GAIN vs. FREQUENCY FOR UHF CRESTATRON WITH VOLTAGE AS PARAMETER. LENGTH=7.5 INCHES. (DRIVE LEVEL ≅ 60 WATTS, 4μ sec. PULSE AT 250 pps.)

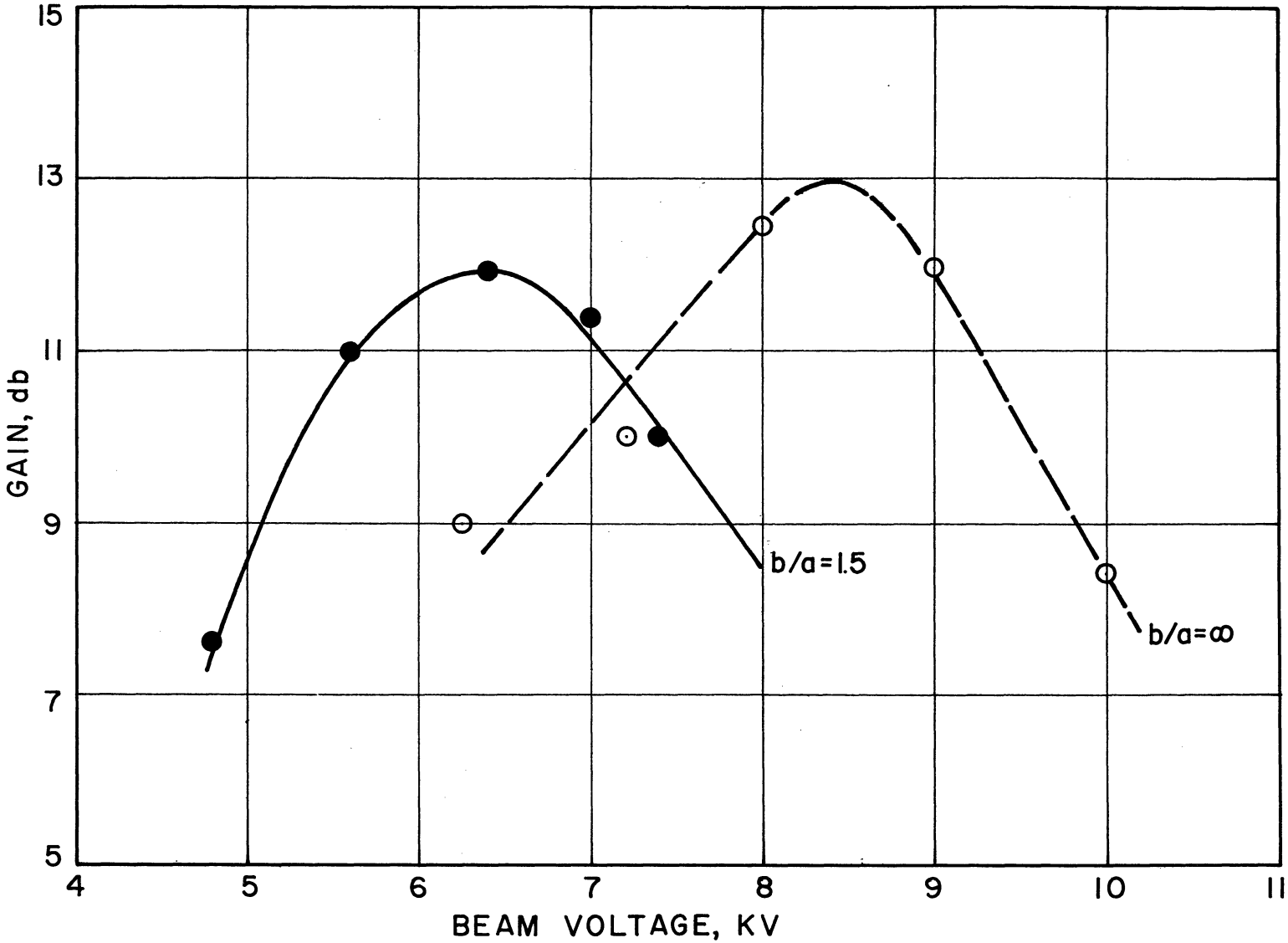

FIG. VIII.14 SMALL-SIGNAL GAIN vs. BEAM VOLTAGE FOR UHF CRESTATRON FOR SHIELDED AND UNSHIELDED HELICES. (FREQUENCY=650 mc, PULSE LENGTH=4 μ sec., pps.=250)

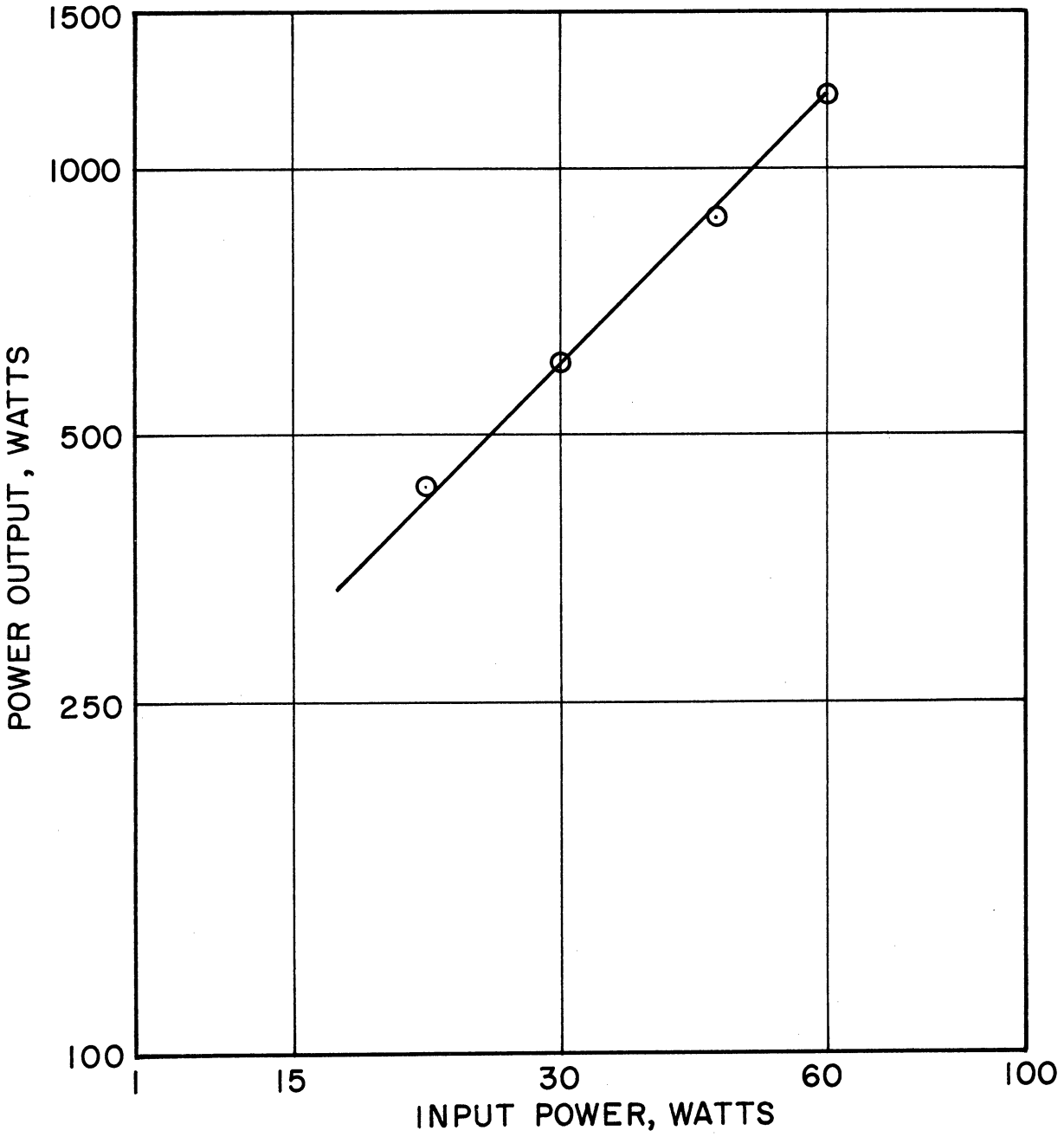

FIG. VIII .15 POWER OUTPUT vs. DRIVE LEVEL FOR UHF CRESTATRON. (FREQUENCY=650 mc, V_0=8.5 KV, I_0=3.5 amps., 4μ sec. PULSES, 250pps.)

modified by increasing the plate voltage applied to the 2C39 output tube by 500 volts.

During testing immediately previous to the failure of tube No. 2 a number of erratic characteristics were observed. Among these was a gradual increase of average cathode current followed by a gradual decrease. Equilibrium was then established when the average cathode current was slightly below the average collector current. This negative anode current could result from secondary emission. Another, more probable explanation is that the anode was either thermionically emitting or simply collecting positive ions during the positive spike when the cathode is positive with respect to the anode. The negative voltage pulse applied to the cathode from the pulse transformer has a positive overshoot at the trailing edge.

Initial d-c tests on tube No. 3 show a transmission of 75 percent; all the intercepted current goes to the helix. This tube is being continuously pumped using a small 1-liter appendage pump. None of the erratic behavior described above has been observed testing this tube. Large-signal saturation measurements on this tube will begin soon, since a 1-kw Federal tube has recently arrived.

IX. GENERAL CONCLUSIONS

The particular topics of study discussed in this report represent the major phases of the research program over the contract period. In addition to these, various other particular studies have been carried out. All of these investigations were directed toward obtaining a greater understanding of the detailed operation of O-type electron stream devices. Also considerable effort has been devoted to the

consideration of means of basically improving the performance of these devices or finding new types of interaction which will be particularly suited for some applications. Further study of many of these topics along with several others will be carried forward during the next year under a new contract, AF 30(602)-2303.

In particular it is planned to study the use of the Poisson Cell in the design of both solid- and hollow-beam electron guns for O-type devices. This Cell is a solid volume conducting medium which facilitates obtaining the solution to potential problems, including arbitrary distributions of sources such as space charge.

The general class of beating-wave devices will be further investigated, particularly along the line of utilizing this type of interaction to obtain power tubes with relatively low noise figures.

The work reported in this report on phase focusing in traveling-wave tubes will also be continued during the next year.

DISTRIBUTION LIST

No. Copies	Agency
2	Commander, Rome Air Development Center, ATTN: RCLRR-3, Griffiss Air Force Base, New York
1	Commander, Rome Air Development Center, ATTN: RCSST-4, Griffiss Air Force Base, New York
2	Commander, Rome Air Development Center, ATTN: RCSSL-1, Griffiss Air Force Base, New York
All add. copies	Armed Services Technical Information Agency, Documents Service Center, Arlington Hall Station, Arlington 12, Virginia
1	Commander, Air Force Cambridge Research Center, ATTN: CRQSL-1, Laurence G. Hanscom Field, Bedford, Massachusetts
1	Director, Air University Library, ATTN: AUL-7736, Maxwell Air Force Base, Alabama
2	Commander, Wright Air Development Center, ATTN: WCOSI-3, Wright-Patterson Air Force Base, Ohio
2	Commander, Wright Air Development Center, ATTN: WCOSR, Wright-Patterson Air Force Base, Ohio
1	Mr. Hans Jenny, RCA Electron Tube Division, 415 South 5th Street, Harrison, New Jersey
1	Air Force Field Representative, Naval Research Laboratory, ATTN: Code 1010, Washington 25, D. C.
1	Chief, Naval Research Laboratory, ATTN: Code 2021, Washington 25, D. C.
1	Chief, Bureau of Ships, ATTN: Code 312, Washington 25, D. C.
1	Commanding Officer, Signal Corps Engineering Laboratories, ATTN: Technical Reports Library, Fort Monmouth, New Jersey
1	Chief, Research & Development Office of the Chief Signal Officer, Washington 25, D. C.
1	Commander, Air Research and Development Command, ATTN: RDSFIF, Andrews Air Force Base, Washington 25, D. C.
1	Commander, Air Research and Development Command, ATTN: RDTC, Andrews Air Force Base, Washington 25, D. C.
1	Applied Radiation Company, Walnut Creek, California, ATTN: Mr. Neil J. Norris

DISTRIBUTION LIST
(Continued)

No. Copies	Agency
1	Director, Signal Corps Engineering Laboratories, ATTN: Thermionics Branch, Evans Signal Laboratory, Belmar, New Jersey
1	Secretariat, Advisory Group on Electron Tubes, 346 Broadway, New York 13, New York
1	Chief, European Office, Air Research and Development Command, 60 Rue Canterstein, Brussels, Belgium
1	Prof. L. M. Field, California Institute of Technology, Department of Electrical Engineering, Pasadena, California
1	The Electronics Research Laboratory, 427 Cory Hall, The University of California, Berkeley 4, California, ATTN: Mrs. Simmons
1	Prof. W. G. Worcester, University of Colorado, Department of Electrical Engineering, Boulder, Colorado
1	Mr. C. Dalman, Cornell University, Department of Electrical Engineering, Ithaca, New York
1	Mr. E. D. McArthur, General Electric Company, Electron Tube Division of Research Laboratory, The Knolls, Schenectady, New York
1	Mr. S. Webber, General Electric Microwave Laboratory, 601 California Avenue, Palo Alto, California
1	Mr. L. A. Roberts, Watkins-Johnson Company, Palo Alto, California
1	Mr. T. Milek, Hughes Aircraft Company, Electron Tube Laboratory, Culver City, California
1	Dr. W. M. Webster, Director, Electronic Research Laboratory, RCA Laboratories, Princeton, New Jersey
1	Dr. Bernard Arfin, Eitel-McCullough, Inc., San Bruno, California
1	Columbia Radiation Laboratory, Columbia University, 538 West 120th Street, New York 27, New York
1	University of Illinois, Department of Electrical Engineering, Electron Tube Section, Urbana, Illinois
1	University of Florida, Department of Electrical Engineering, Gainesville, Florida

DISTRIBUTION LIST
(Continued)

No. Copies	Agency
1	Dr. D. D. King, John Hopkins University, Radiation Laboratory, Baltimore 2, Maryland
1	Varian Associates, 611 Hansen Way, Palo Alto, California, ATTN: Technical Library
1	Dr. M. Chodorow, Stanford University, Microwave Laboratory, Stanford, California
1	Dr. D. A. Watkins, Stanford University, Stanford Electronics Laboratory, Stanford, California
1	Mr. Skoworon, Raytheon Manufacturing Company, Spencer Laboratory Burlington, Massachusetts
1	Mr. T. Marchese, Federal Telecommunication Laboratories, Inc., 500 Washington Avenue, Nutley, New Jersey
1	Mr. Donald Priest, Eitel-McCullough, Inc., San Bruno, California
1	Dr. Norman Moore, Litton Industries, 960 Industrial Road, San Carlos, California
1	Massachusetts Institute of Technology, Research Laboratory of Electronics, Cambridge 39, Massachusetts, ATTN: Documents Library
1	Sperry Gyroscope Company, Great Neck, New York, ATTN: Engineering Library
1	Dr. D. Goodman, Sylvania Microwave Tube Laboratory, 500 Evelyn Avenue, Mountain View, California
1	Dr. M. Ettenberg, Polytechnic Institute of Brooklyn, Microwave Research Institute, Brooklyn 1, New York
1	Harvard University, Cruft Laboratory, Cambridge, Massachusetts, ATTN: Technical Library
1	Dr. R. G. E. Hutter, Sylvania Electric Products, Inc., Mountain View, California
1	Mr. A. E. Harrison, University of Washington, Department of Electrical Engineering, Seattle 5, Washington
1	Mr. Robert Butman, Massachusetts Institute of Technology, Lincoln Laboratory, Lexington, Massachusetts

DISTRIBUTION LIST
(Concluded)

No. Copies	Agency
1	Mr. A. G. Peifer, Bendix Aviation Corporation, Research Laboratories, Northwestern Highway and 10-1/2 Mile Road, Detroit 35, Michigan
1	Mr. James B. Maher, Librarian, R and D Technical Library, Hughes Aircraft Company, Culver City, California
1	Dr. Robert T. Young, Chief, Electron Tube Branch, Diamond Ordnance Fuze Laboratories, Washington 25, D. C.
1	Bendix Aviation Corporation, Systems Planning Division, Ann Arbor, Michigan. ATTN: Technical Library
1	Mr. Gerald Klein, Manager, Microwave Tubes Section, Applied Research Department, Westinghouse Electric Corp., Box 746, Baltimore 3, Maryland
1	Department of Electrical Engineering, University of Minnesota, Minneapolis, Minnesota, ATTN: Dr. W. G. Shepherd
1	Director, Evans Signal Laboratory, Belmar, New Jersey, ATTN: Dr. Gerald E. Pokorney, Microwave Tube Branch, Electron Devices Division
1	Sperry Corporation, Electronic Tube Division, Gainesville, Florida, ATTN: Mr. P. Bergman
1	Mr. Shelden S. King, Engineering Librarian, Westinghouse Electric Corporation, P. O. Box 284. Elmira, New York
1	RCA Laboratories, Princeton, New Jersey, ATTN: Dr. Bernard Hershenov
1	Microwave Electronics Corporation, 4061 Transport Street, Palo Alto, California, ATTN: Dr. S. F. Kaisel
1	Librarian, Microwave Library, Stanford University, Stanford, California
1	Wright Air Development Division, Air Research and Development Command, Wright-Patterson Air Force Base, Ohio, ATTN: Mr. George L. Larr, WWKSC

AD_____

The University of Michigan, Electron Physics Laboratory, Ann Arbor, Michigan. THEORETICAL AND EXPERIMENTAL INVESTIGATION OF LARGE-SIGNAL TRAVELING-WAVE TUBES, by G.T. Konrad, R.W. Larson, J.G. Meeker, J.E. Rowe, H. Sobol, J.W. Ward, C.P. Wen, August, 1960, 221 pp. incl. illust. (Proj. No. 5573, Task No. 55253)

Analysis of Linear and Nonlinear O-Type Systems. The nonlinear O-Type backward-wave oscillator is analyzed using the modified large-signal amplifier equations. An analysis of the Crestatron amplifier is presented. A small-signal analysis of a premodulated electron stream interacting with a propagating circuit is treated. Phase Focusing in Traveling-Wave Tubes. A general nonlinear analysis of the phase focusing of electron bunches in growing-wave devices and beating-wave devices is presented. X-Band Traveling-Wave Amplifiers. Extensive design and experimental information on several models of a 1-watt X-band amplifier is given. Experimental Study of Crestatrons. Experimental results are given on several models of both cw and pulsed Crestatrons used in the S-band frequency regime. Analysis of Modulated O-Type Devices. A general analysis of beam-modulated O-type devices is given along with both low and high-frequency modulations. Disk and Helically Loaded Coaxial and Waveguide TWA Structures. Disk and helically loaded structures are analyzed and various possibilities are compared from the standpoint of impedance and operating bandwidth. UHF Crestatron. The design and initial experimental results are presented on a high-pulsed-power uhf Crestatron.

UNCLASSIFIED

1. Analysis of Linear and Nonlinear O-Type Systems
2. Phase Focusing in Traveling-Wave Tubes
3. X-Band Traveling-Wave Amplifiers
4. Experimental Study of Crestatrons
5. Analysis of Modulated O-Type Devices
6. Disk and Helically Loaded Coaxial and Waveguide TWA Structures
7. UHF Crestatron

I. Konrad, G. T.
II. Larson, R. W.
III. Meeker, J. G.
IV. Rowe, J. E.
V. Sobol, H.
VI. Ward, J. W.
VII. Wen, C. P.

UNCLASSIFIED

AD_____

The University of Michigan, Electron Physics Laboratory, Ann Arbor, Michigan. THEORETICAL AND EXPERIMENTAL INVESTIGATION OF LARGE-SIGNAL TRAVELING-WAVE TUBES, by G.T. Konrad, R.W. Larson, J.G. Meeker, J.E. Rowe, H. Sobol, J.W. Ward, C.P. Wen, August, 1960, 221 pp. incl. illust. (Proj. No. 5573, Task No. 55253)

Analysis of Linear and Nonlinear O-Type Systems. The nonlinear O-Type backward-wave oscillator is analyzed using the modified large-signal amplifier equations. An analysis of the Crestatron amplifier is presented. A small-signal analysis of a premodulated electron stream interacting with a propagating circuit is treated. Phase Focusing in Traveling-Wave Tubes. A general nonlinear analysis of the phase focusing of electron bunches in growing-wave devices and beating-wave devices is presented. X-Band Traveling-Wave Amplifiers. Extensive design and experimental information on several models of a 1-watt X-band amplifier is given. Experimental Study of Crestatrons. Experimental results are given on several models of both cw and pulsed Crestatrons used in the S-band frequency regime. Analysis of Modulated O-Type Devices. A general analysis of beam-modulated O-type devices is given along with both low and high-frequency modulations. Disk and Helically Loaded Coaxial and Waveguide TWA Structures. Disk and helically loaded structures are analyzed and various possibilities are compared from the standpoint of impedance and operating bandwidth. UHF Crestatron. The design and initial experimental results are presented on a high-pulsed-power uhf Crestatron.

UNCLASSIFIED

1. Analysis of Linear and Nonlinear O-Type Systems
2. Phase Focusing in Traveling-Wave Tubes
3. X-Band Traveling-Wave Amplifiers
4. Experimental Study of Crestatrons
5. Analysis of Modulated O-Type Devices
6. Disk and Helically Loaded Coaxial and Waveguide TWA Structures
7. UHF Crestatron

I. Konrad, G. T.
II. Larson, R. W.
III. Meeker, J. G.
IV. Rowe, J. E.
V. Sobol, H.
VI. Ward, J. W.
VII. Wen, C. P.

UNCLASSIFIED

AD_____

The University of Michigan, Electron Physics Laboratory, Ann Arbor, Michigan. THEORETICAL AND EXPERIMENTAL INVESTIGATION OF LARGE-SIGNAL TRAVELING-WAVE TUBES, by G.T. Konrad, R.W. Larson, J.G. Meeker, J.E. Rowe, H. Sobol, J.W. Ward, C.P. Wen, August, 1960, 221 pp. incl. illust. (Proj. No. 5573, Task No. 55253)

Analysis of Linear and Nonlinear O-Type Systems. The nonlinear O-type backward-wave oscillator is analyzed using the modified large-signal amplifier equations. An analysis of the Crestatron amplifier is presented. A small-signal analysis of a premodulated electron stream interacting with a propagating circuit is treated. Phase Focusing in Traveling-Wave Tubes. A general nonlinear analysis of the phase focusing of electron bunches in growing-wave devices and beating-wave devices is presented. X-Band Traveling-Wave Amplifiers. Extensive design and experimental information on several models of a 1-watt X-band amplifier is given. Experimental Study of Crestatrons. Experimental results are given on several models of both cw and pulsed Crestatrons used in the S-band frequency regime. Analysis of Modulated O-Type Devices. A general analysis of beam-modulated O-type devices is given along with both low and high-frequency modulations. Disk and Helically Loaded Coaxial and Waveguide TWA Structures. Disk and helically loaded structures are analyzed and various possibilities are compared from the standpoint of impedance and operating bandwidth. UHF Crestatron. The design and initial experimental results are presented on a high-pulsed-power uhf Crestatron.

UNCLASSIFIED

1. Analysis of Linear and Nonlinear O-Type Systems
2. Phase Focusing in Traveling-Wave Tubes
3. X-Band Traveling-Wave Amplifiers
4. Experimental Study of Crestatrons
5. Analysis of Modulated O-Type Devices
6. Disk and Helically Loaded Coaxial and Waveguide TWA Structures
7. UHF Crestatron

I. Konrad, G. T.
II. Larson, R. W.
III. Meeker, J. G.
IV. Rowe, J. E.
V. Sobol, H.
VI. Ward, J. W.
VII. Wen, C. P.

UNCLASSIFIED

AD_____

The University of Michigan, Electron Physics Laboratory, Ann Arbor, Michigan. THEORETICAL AND EXPERIMENTAL INVESTIGATION OF LARGE-SIGNAL TRAVELING-WAVE TUBES, by G.T. Konrad, R.W. Larson, J.G. Meeker, J.E. Rowe, H. Sobol, J.W. Ward, C.P. Wen, August, 1960, 221 pp. incl. illust. (Proj. No. 5573, Task No. 55253)

Analysis of Linear and Nonlinear O-Type Systems. The nonlinear O-type backward-wave oscillator is analyzed using the modified large-signal amplifier equations. An analysis of the Crestatron amplifier is presented. A small-signal analysis of a premodulated electron stream interacting with a propagating circuit is treated. Phase Focusing in Traveling-Wave Tubes. A general nonlinear analysis of the phase focusing of electron bunches in growing-wave devices and beating-wave devices is presented. X-Band Traveling-Wave Amplifiers. Extensive design and experimental information on several models of a 1-watt X-band amplifier is given. Experimental Study of Crestatrons. Experimental results are given on several models of both cw and pulsed Crestatrons used in the S-band frequency regime. Analysis of Modulated O-Type Devices. A general analysis of beam-modulated O-type devices is given along with both low and high-frequency modulations. Disk and Helically Loaded Coaxial and Waveguide TWA Structures. Disk and helically loaded structures are analyzed and various possibilities are compared from the standpoint of impedance and operating bandwidth. UHF Crestatron. The design and initial experimental results are presented on a high-pulsed-power uhf Crestatron.

UNCLASSIFIED

1. Analysis of Linear and Nonlinear O-Type Systems
2. Phase Focusing in Traveling-Wave Tubes
3. X-Band Traveling-Wave Amplifiers
4. Experimental Study of Crestatrons
5. Analysis of Modulated O-Type Devices
6. Disk and Helically Loaded Coaxial and Waveguide TWA Structures
7. UHF Crestatron

I. Konrad, G. T.
II. Larson, R. W.
III. Meeker, J. G.
IV. Rowe, J. E.
V. Sobol, H.
VI. Ward, J. W.
VII. Wen, C. P.

UNCLASSIFIED

AD_____

The University of Michigan, Electron Physics Laboratory, Ann Arbor, Michigan. THEORETICAL AND EXPERIMENTAL INVESTIGATION OF LARGE-SIGNAL TRAVELING-WAVE TUBES, by G.T. Konrad, R.W. Larson, J.G. Meeker, J.E. Rowe, H. Sobol, J.W. Ward, C.P. Wen, August, 1960, 221 pp. incl. illust. (Proj. No. 5573, Task No. 55253)

Analysis of Linear and Nonlinear O-Type Systems. The nonlinear O-Type backward-wave oscillator is analyzed using the modified large-signal amplifier equations. An analysis of the Crestatron amplifier is presented. A small-signal analysis of a premodulated electron stream interacting with a propagating circuit is treated. Phase Focusing in Traveling-Wave Tubes. A general nonlinear analysis of the phase focusing of electron bunches in growing-wave devices and beating-wave devices is presented. X-Band Traveling-Wave Amplifiers. Extensive design and experimental information on several models of a 1-watt X-band amplifier is given. Experimental Study of Crestatrons. Experimental results are given on several models of both cw and pulsed Crestatrons used in the S-band frequency regime. Analysis of Modulated O-Type Devices. A general analysis of beam-modulated O-type devices is given along with both low and high-frequency modulations. Disk and Helically Loaded Coaxial and Waveguide TWA Structures. Disk and helically loaded structures are analyzed and various possibilities are compared from the standpoint of impedance and operating bandwidth. UHF Crestatron. The design and initial experimental results are presented on a high-pulsed-power uhf Crestatron.

UNCLASSIFIED

1. Analysis of Linear and Nonlinear O-Type Systems
2. Phase Focusing in Traveling-Wave Tubes
3. X-Band Traveling-Wave Amplifiers
4. Experimental Study of Crestatrons
5. Analysis of Modulated O-Type Devices
6. Disk and Helically Loaded Coaxial and Waveguide TWA Structures
7. UHF Crestatron

I. Konrad, G. T.
II. Larson, R. W.
III. Meeker, J. G.
IV. Rowe, J. E.
V. Sobol, H.
VI. Ward, J. W.
VII. Wen, C. P.

UNCLASSIFIED

AD_____

The University of Michigan, Electron Physics Laboratory, Ann Arbor, Michigan. THEORETICAL AND EXPERIMENTAL INVESTIGATION OF LARGE-SIGNAL TRAVELING-WAVE TUBES, by G.T. Konrad, R.W. Larson, J.G. Meeker, J.E. Rowe, H. Sobol, J.W. Ward, C.P. Wen, August, 1960, 221 pp. incl. illust. (Proj. No. 5573, Task No. 55253)

Analysis of Linear and Nonlinear O-Type Systems. The nonlinear O-Type backward-wave oscillator is analyzed using the modified large-signal amplifier equations. An analysis of the Crestatron amplifier is presented. A small-signal analysis of a premodulated electron stream interacting with a propagating circuit is treated. Phase Focusing in Traveling-Wave Tubes. A general nonlinear analysis of the phase focusing of electron bunches in growing-wave devices and beating-wave devices is presented. X-Band Traveling-Wave Amplifiers. Extensive design and experimental information on several models of a 1-watt X-band amplifier is given. Experimental Study of Crestatrons. Experimental results are given on several models of both cw and pulsed Crestatrons used in the S-band frequency regime. Analysis of Modulated O-Type Devices. A general analysis of beam-modulated O-type devices is given along with both low and high-frequency modulations. Disk and Helically Loaded Coaxial and Waveguide TWA Structures. Disk and helically loaded structures are analyzed and various possibilities are compared from the standpoint of impedance and operating bandwidth. UHF Crestatron. The design and initial experimental results are presented on a high-pulsed-power uhf Crestatron.

UNCLASSIFIED

1. Analysis of Linear and Nonlinear O-Type Systems
2. Phase Focusing in Traveling-Wave Tubes
3. X-Band Traveling-Wave Amplifiers
4. Experimental Study of Crestatrons
5. Analysis of Modulated O-Type Devices
6. Disk and Helically Loaded Coaxial and Waveguide TWA Structures
7. UHF Crestatron

I. Konrad, G. T.
II. Larson, R. W.
III. Meeker, J. G.
IV. Rowe, J. E.
V. Sobol, H.
VI. Ward, J. W.
VII. Wen, C. P.

UNCLASSIFIED

AD_____

The University of Michigan, Electron Physics Laboratory, Ann Arbor, Michigan. THEORETICAL AND EXPERIMENTAL INVESTIGATION OF LARGE-SIGNAL TRAVELING-WAVE TUBES, by G.T. Konrad, R.W. Larson, J.G. Meeker, J.E. Rowe, H. Sobol, J.W. Ward, C.P. Wen, August, 1960, 221 pp. incl. illust. (Proj. No. 5573, Task No. 55253)

Analysis of Linear and Nonlinear O-Type Systems. The nonlinear O-type backward-wave oscillator is analyzed using the modified large-signal amplifier equations. An analysis of the Crestatron amplifier is presented. A small-signal analysis of a premodulated electron stream interacting with a propagating circuit is treated. Phase Focusing in Traveling-Wave Tubes. A general nonlinear analysis of the phase focusing of electron bunches in growing-wave devices and beating-wave devices is presented. X-Band Traveling-Wave Amplifiers. Extensive design and experimental information on several models of a 1-watt X-band amplifier is given. Experimental Study of Crestatrons. Experimental results are given on several models of both cw and pulsed Crestatrons used in the S-band frequency regime. Analysis of Modulated O-Type Devices. A general analysis of beam-modulated O-type devices is given along with both low and high-frequency modulations. Disk and Helically Loaded Coaxial and Waveguide TWA Structures. Disk and helically loaded structures are analyzed and various possibilities are compared from the standpoint of impedance and operating bandwidth. UHF Crestatron. The design and initial experimental results are presented on a high-pulsed-power uhf Crestatron.

UNCLASSIFIED

1. Analysis of Linear and Nonlinear O-Type Systems
2. Phase Focusing in Traveling-Wave Tubes
3. X-Band Traveling-Wave Amplifiers
4. Experimental Study of Crestatrons
5. Analysis of Modulated O-Type Devices
6. Disk and Helically Loaded Coaxial and Waveguide TWA Structures
7. UHF Crestatron

I. Konrad, G. T.
II. Larson, R. W.
III. Meeker, J. G.
IV. Rowe, J. E.
V. Sobol, H.
VI. Ward, J. W.
VII. Wen, C. P.

UNCLASSIFIED

AD_____

The University of Michigan, Electron Physics Laboratory, Ann Arbor, Michigan. THEORETICAL AND EXPERIMENTAL INVESTIGATION OF LARGE-SIGNAL TRAVELING-WAVE TUBES, by G.T. Konrad, R.W. Larson, J.G. Meeker, J.E. Rowe, H. Sobol, J.W. Ward, C.P. Wen, August, 1960, 221 pp. incl. illust. (Proj. No. 5573, Task No. 55253)

Analysis of Linear and Nonlinear O-Type Systems. The nonlinear O-type backward-wave oscillator is analyzed using the modified large-signal amplifier equations. An analysis of the Crestatron amplifier is presented. A small-signal analysis of a premodulated electron stream interacting with a propagating circuit is treated. Phase Focusing in Traveling-Wave Tubes. A general nonlinear analysis of the phase focusing of electron bunches in growing-wave devices and beating-wave devices is presented. X-Band Traveling-Wave Amplifiers. Extensive design and experimental information on several models of a 1-watt X-band amplifier is given. Experimental Study of Crestatrons. Experimental results are given on several models of both cw and pulsed Crestatrons used in the S-band frequency regime. Analysis of Modulated O-Type Devices. A general analysis of beam-modulated O-type devices is given along with both low and high-frequency modulations. Disk and Helically Loaded Coaxial and Waveguide TWA Structures. Disk and helically loaded structures are analyzed and various possibilities are compared from the standpoint of impedance and operating bandwidth. UHF Crestatron. The design and initial experimental results are presented on a high-pulsed-power uhf Crestatron.

UNCLASSIFIED

1. Analysis of Linear and Nonlinear O-Type Systems
2. Phase Focusing in Traveling-Wave Tubes
3. X-Band Traveling-Wave Amplifiers
4. Experimental Study of Crestatrons
5. Analysis of Modulated O-Type Devices
6. Disk and Helically Loaded Coaxial and Waveguide TWA Structures
7. UHF Crestatron

I. Konrad, G. T.
II. Larson, R. W.
III. Meeker, J. G.
IV. Rowe, J. E.
V. Sobol, H.
VI. Ward, J. W.
VII. Wen, C. P.

UNCLASSIFIED

UNIVERSITY OF MICHIGAN
3 9015 03023 1446